Investigating the role of rhomboid proteases in the development of *Dictyostelium discoideum*

Mehak Rafiq

School of Science

University of Greenwich

Thesis submitted for the degree of Doctor of Philosophy

March 2015

Declaration of Authorship

I, Mehak Rafiq, hereby declare that the work presented here was composed by me and is my own unless otherwise indicated, and that all published work has been acknowledged. Furthermore, I affirm that I have neither fabricated nor falsified the results reported herein.

Signed:

Date: 27th March 2015

Acknowledgments

Firstly, I would like to thank my supervisor Dr Elinor Thompson for her guidance, support, and encouragement. I am especially thankful for the freedom she gave me to explore a variety of research interests and for providing a research environment that fostered independent thought; providing an understanding of what real science is all about. Thank you for everything.

I would also like to thank my second supervisor at University of Sussex, Dr John Spencer, and my advisor at University of Greenwich, Dr Bruce Alexander for all their invaluable advice throughout the last three years.

A special thanks to Dr David Traynor (Dr Rob Kay's Lab, MRC-LMB) and Dr Steven Robbery (Dr Robin Williams Lab, Royal Holloway) for teaching me *Dictyostelium* techniques. All of your help is really unforgettable. Dr Ian Brown (University of Kent) for helping me with TEM experiments

Also, I would like to thank all the member of the Thompson lab past (Dr Amit Prabhakar, Dr Colin Batman and Dr Kevin Symth) and present (Dr Iskandar Ibrahim and Ph.D student Billy Ferrara) for their continued and invaluable help, support and discussions over the years; without you guys I may not have made it this far. A special thank you to "the girls" M.Sc student Tayo Alegbeji, B.Sc, students Fatima Mehmood, Maria Silvia and Rebecca Vestal for their help with my work and who were always cheerful.

I also owe my thanks to all the members of the Neslon labs, especially Atiya Reza and Samantha Lewis, for her friendship and willingness to help in any way possible and help.

I would also like to thank all my friends and family for ALL their constant encouragement, love and support throughout the last three years. Especially to my sister, Foha, and friend, Samia Asif, you have all provided me with endless encouragement, advice and laughter that I have needed throughout the years, moulding me into the person I am today. To my 'UK family', Ruchir Bhomia, Pham Thi Minh Hai and Johanna Mork, you guys have been my strength when I needed you to be and have made the last three years doable. I value your friendships more than words can express and am so thankful to have such amazing friends.

So to all of you, I would not have made it through without your help, encouragement and support so THANK YOU, it is because of you guys that I have got this far.

Abstract

Dictyostelium discoideum is a model eukaryotic organism with many equivalent cellular mechanisms to humans. In this project *Dictyostelium* has been used to help investigate the role of rhomboid proteins. Bioinformatics tools were used to identify four potential rhomboids encoded within the *Dictyostelium* genome that contain the residues necessary for proteolytic activity. To identify their functions, three null mutants *rhmA*$^-$, *rhmB*$^-$ and *rhmC*$^-$ have been constructed, and their growth and development observed. It was found that development was unaltered following deletion of *rhmC*, whereas attempts to knock out the putative mitochondrial *rhmD* were unsuccessful. *rhmA* and *rhmB* null mutants gave rise to pleiotropic effects, *rhmA* altering the response to chemoattractants and demonstrating decreased motility in general. It also showed altered mitochondrial morphology which is consistent with phototaxis defects in slugs. *rhmB* null cells had slower growth rates, reaching stationary phase at a reduced density; a delayed response to folic acid stimulation; larger cell size in the unicellular phase and altered stalks in the multicellular phase. These results correspond with qPCR analysis, in which RhmA and RhmB transcript levels are highest during the multicellular development phase.

Dictyostelium is also a useful non-animal eukaryote for testing novel compounds and dissecting cell regulatory molecular networks. In this thesis I have used this social amoeba to test the effect of a series of arylboronic acids and a novel compound, cardiosulfa, on development, chemotaxis and viability of *Dictyostelium*. The arylboronic acids were investigated previously by collaborators for serine protease inhibition and urokinase-type plasminogen activator (uPA) inhibition, both *in vitro* and *in vivo*. In those biochemical assays, three compounds, BC11, SR3 and BC57 displayed micromolar inhibition of uPA with an excellent selectivity profile over related proteases (Smith *et al.*, 2012). Previous studies suggested that cardiosulfa, disrupted heart development in the zebrafish. Gene expression profiling studies showed that cardiosulfa induces high transcription levels of members of the aryl hydrocarbon receptor (AhR) family (Ko *et al.* 2009). These test compounds reported to show effects *in vivo* also disturbed cell adhesion and migration, without having an effect on *Dictyostelium* viability. Networks of predicted activity were

constructed to establish molecular mechanisms for cardiosulfa and arylboronic acids analogues.

In conclusion this project provides the first insight into the molecular and cellular functions of rhomboid proteins, potential aryl hydrocarbon receptor and urokinase-type plasminogen activator by using *Dictyostelium* as an early biomedical model to study these effects in eukaryotes.

Table of Contents

List of Figures and Tables

Figures

Tables

List of Abbreviations

3D	Three-dimensional
AarA	*Providencia stuartii* Rhomboid
ACA	Aggregation stage adenylyl cyclase
ADP	adenosine 5’ –diphosphate
ATP	adenosine 5’ –triphosphate
ADAM	A Disintegrin And Metalloproteinase
Arp2/3	actin-related protein 2/3
Bsr	blasticidin resistance cassette
cAMP	Cyclic adenosine 3'-5' monophosphate
cAR1-4	*Dictyostelium* cAMP receptor sub-types 1-4
cDNA	complementary DNA
CRAC	cytosolic regulator of adenylyl cyclase
ddH_2O	double distilled water
DMSO	dimethylsulphoxide
DNA	deoxyribonucleic acid
DNase	deoxyribonuclease
dNTP	deoxyribonucleotide triphosphate
DTT	1,4-dithiothreitol
EDTA	ethylenediaminetetraacetic acid
EGTA	ethyleneglycol-bis(2-amino-ethylene)N ,N ,N -tetraacetic acid
EGF	Epidermal Growth Factor
EGFR	Epidermal Growth Factor Receptor
EhROM1	*Entamoeba histolytica* Rhomboid 1
ER	Endoplasmic Reticulum
*ec*GlpG	*Escherichia coli* Rhomboid
F-actin	Filamentous actin
GFP	Green fluorescent protein
G-protein	Guanine nucleotide binding protein
G418	Neomycin selection marker
HEPES	N-(2-hydroxyethyl) piperazine-N. -2-ethanesulphonic acid

*hi*GlpG	*Haemophilus influenzae* Rhomboid
iRHOM	Inactive Rhomboid
IPTG	iso-propylthio-galactopyranoside
kb	kilobase pairs
kDa	Kilodalton
L	Litre
L1	Loop 1
L5	Loop 5
LacYTM2	LacY Transmembrane Helix 2
LY294002	2-(4-morpholinyl)-8-phenyichromone
ml	Millilitres
ß-ME	beta-mercaptoethanol
mRNA	Messenger RNA
MS	Mass Spectrometry
MW	molecular weight
µg	Microgram
µM	Micromolar
µl	Microlitre
nM	Nanomolar
NBT	nitrobluetetrazolium
NP-40	nonylphenylpolyethyleneglyco
OD	optical density
*pa*GlpG	*Pseudomonas aeruginosa* Rhomboid
PARL	Presenilin-associated rhomboid like
Pcp1	*Schizosaccharomyces pombe* mitochondrial rhomboid
PCR	polymerase chain reaction
PfROM4	*Plasmodium faciparum* Rhomboid 4
PIP3	phosphatidyl inositol (3,4,5) tris phosphate
P13K	Phosphatidylinositol 3-kinase
PKB	Protein kinase B
PLC	Phospholipase C
PMSF	Phenylmethylsulphonylfluoride

PROD	PARLl-Rhomboid-Domain
PTEN	Phosphatase and Tensin homolog
REMI	Restriction enzyme mediated integration
RHBDL2	*Homo sapiens* Rhomboid 2
Rho-1	*Drosophila melanogaster* Rhomboid 1
Rho-2	*Drosophila melanogaster* Rhomboid 2
Rho-3	*Drosophila melanogaster* Rhomboid 3
Rho-7	*Drosophila melanogaster* Mitochondrial Rhomboid 7
RNAseA	Ribonuclease A
RNA	ribonucleic acid
Rnase	Ribonuclease
rpm	rotations per minute
SDS	sodium dodecyl sulphate
TatA	Twin Arginine Translocase
TEMED	N, N, N., N. -tetramethyl-ethylendiamine
TgROM5	*Toxoplasma gondii* Rhomboid 5
TM	Transmembrane
TMD	Transmembrane Domain
TMH	Transmembrane Helix
TRITC	tetramethylrhodamine isothiocyanate
SCAR	Suppresser of cAR
SDS-Page	sodium dodecyl sulphate polyacrylamide gel electrophoresis
uPA	urokinase-type plasminogen activator
UV	ultraviolet
vol	volume
v/v	volume by volume
WT	Wild-type
w/v	weight by volume
YqgP	*Bacillus subtilis* Rhomboid

Chapter 1

Introduction

1.1 Rhomboid proteases

Rhomboids are a recently discovered family of serine proteases which, along with the zinc metalloprotease family and two aspartyl proteases, form the collectively named intramembrane cleaving proteases (i-CLiPs). These proteases catalyse regulated intramembrane proteolysis (RIP), a precise and usually irreversible mechanism by which inactive membrane proteins are activated by cleavage of their transmembrane domains and release of their functional domains (Erez *et al.*, 2009). I-CLiPs are transmembrane multi-spanning proteins which, hydrolyse peptides using amino acid residues buried within or in close vicinity to their hydrophobic transmembrane domains.

1.1.1 Discovery of rhomboids proteins

Rhomboids are perhaps the most widely conserved membrane protein family across all domains of life (Urban, Schlieper, *et al*>, 2002), suggesting that they play important roles. All identified rhomboids show notable structural similarity but retain only 6% sequence identity at amino acid level between them (Koonin *et al.*, 2003).

The first rhomboid, Rhomboid-1 (Rho-1) was discovered as an embryonic patterning mutant of *Drosophila melanogaster*. Rho-1 absence was responsible for the embryonic skeleton having a pointed head, hence the name rhomboid (Jurgens *et al.*, 1984). The affected protein was later shown to be localised to the Golgi compartment and was an important component in epidermal growth factor receptor (EGFR) signalling. Rho-1 cleaves the transmembrane domains (TMDs) of membrane-anchored EGFR ligand, Spitz, to release soluble, active growth factor (Lohi *et al.*, 2004).

1.1.2 Biological functions of rhomboids

The biological role of a rhomboid, unlike its structural component, is not well conserved and depends on the system in which it is found. Rhomboids have been implicated in many processes, including quorum sensing, mitochondrial membrane fusion, stem cell differentiation, apoptosis, host-cell invasion and immune system evasion by parasites (Urban, 2006). Conservation of rhomboid proteins in all organisms suggests that these proteases must function in important biological processes. The study of their role in many species such as *Drosophila* and *Arabidopsis thaliana* is still at an early stage, thus there are few studies that are able to link rhomboid activity to a specific substrate. Several of the known examples are discussed below (Table 1-1).

Table 1-1 Known rhomboid protease substrates and functions across evolution

Rhomboid	Organism	Substrates	Function
Rho-1	*Drosophila*[1]	Spitz, Keren	EGFR signalling (embryo, most developing tissues, adult)
Rho-2/Stet	*Drosophila*[1]	Gurken*	EGFR signalling in oocyte, germline
Rho-3/Ru	*Drosophila*[1]	Spitz, Keren	EGFR signalling in embryo, eye disc
Rho-4	*Drosophila*[1]	Spitz, Keren*	EGFR signalling?
Rho-7	*Drosophila*[1]	DmOpa1-like DmPINK1	Mitochondrial fusion, mitophagy
CeROM1	*Caenorhabditis elegans*[2]	LIN-3L	Amplifying EGFR signaling (vulva)
AarA	*Providencia stuartii*[3]	TatA	Activating twin-arginine translocon, quorum sensing
GlpG	*Escherichia coli*[3]	*	Antibiotic resistance?
Pcp1	*Saccharomyces cerevisiae*[4]	Mgm1	Mitochondrial membrane fusion, pre-sequence removal
RBD2	*S. cerevisiae*[5]	*	Actin assembly during clathrin-mediated endocytosis?
PARL	*Homo sapiens*[4]	PINK1, others	Down regulating mitophagy, crista remodeling, anti-apoptosis
RHBDL2	*H. sapiens*[6]	EphrinB1,2,3, EGF	Blood clotting? Cell migration? Cancer?
PfROM4	*Plasmodium falciparum*[7]	EBA175, TRAP	Invasion
PfROM1	*P. falciparum*[7]	AMA1?	Invasion? Growth
TgROM1	*Toxoplasma gondii*[8]	?	Growth
TgROM4	*T. gondii*[8]	AMA1, MIC2, MIC6	Invasion
TgROM5	*T. gondii*[8]	AMA1, MIC2, MIC6	Invasion
EhROM1	*Entamoeba histolytica*[9]	Lectins	Phagocytosis, immune evasion

Only those rhomboid proteases whose proteolytic activity has been detected *in vitro* and have known cellular function are included in the table. * Model substrate cleaved i.e., catalytically active, *in vivo* substrate unknown. EGFR, epidermal growth factor receptor. [1]Urban, Lee, *et al*., 2002; [2]Dutt *et al*., 2004; [3]Urban & Wolfe, 2005; [4]McQuibban *et al*., 2003; [5]Cortesio *et al*., 2015; [6]Adrain *et al*., 2011; [7]Baker *et al*., 2006; 8Brossier *et al*., 2005; [9]Baxt *et al*., 2008.

1.1.2.1 Rhomboid-like proteins: Involvement in cell signalling

RIP is a simple, yet precise and irreversible strategy for signal transduction by the release of sequestered protein domains (Brown *et al.*, 2000). Associated substrates seem to be membrane-anchored proteins that are inactive in their membrane-tethered form, and are activated upon cleavage within the TMD, through release of their cytoplasmic or luminal/extracellular domains. In fact, rhomboids are the only iCLiPs that do not require a previous cleavage event in order to recognise the substrate. Rhomboid-mediated RIP is most commonly associated with intercellular signal transduction pathways.

Drosophila Rho-1 regulates signalling of the epidermal growth factor by mediating cleavage of Spitz, the EGFR ligand (Lee *et al.*, 2001). Full-length Spitz is trapped in the endoplasmic reticulum (ER) until Star chaperones it to the Golgi apparatus (Tsruya *et al.*, 2002), where it is activated by Rho-1-mediated cleavage. Rho-1 also cleaves Star to regulate the levels of secreted Spitz (Tsruya *et al.*, 2007; Figure 1-1). In *Caenorhabditis elegans*, an EGFR-like pathway also employs a rhomboid. *C. elegans* cells express an EGF-like signalling factor called LIN-3, which bears similarities to Spitz. When the LIN-3 signal is received by the EGFR-like receptor the RAS/mitogen-activated protein kinase (MAPK) pathway is activated. In this case, rhomboid cleavage only increases the range of the LIN-3 signal (Dutt *et al.*, 2004; Figure 1-1A).

Whereas it is generally accepted that rhomboids are involved in EGFR-mediated cell development in *Drosophila*, only recently did evidence of a similar role in mammals become available (Pascall & Brown, 2004). One reason for this delay is that membrane-tethered EGFR signalling factors are typically released by members of a disintegrin and metalloproteinase (ADAM) family of proteases. However, the Freeman group has identified epidermal growth factor (EGF) to be a substrate of the mammalian RHBDL2 rhomboid since it could be processed by RHBDL2, and EGFR signalling can occur in a metalloprotease-independent manner (Adrain *et al.*, 2011). These conclusions suggest that RHBDL2-mediated release of EGF could be important at specific stages of embryogenesis, with cleavage by ADAM potentially occurring at different stages. Also worth noting is the orthologous human rhomboid, RHBDD2, which has recently been shown to be overexpressed in carcinomas that are negative for the oestrogen receptor. Interestingly, breast cancer cell proliferation can be reduced by *in vitro* silencing of this

rhomboid, raising the possibility that RHBDD2 could be acting in cell proliferation or survival signalling pathways (Lei & Li, 2009; Pascall & Brown, 2004).

A different role in signalling was described for the bacterial AarA rhomboid from *Providencia stuartii* which is required for quorum sensing. In *P. stuartii*, cleavage of the substrate twin arginine translocase TatA by the rhomboid AarA activates the TatA component of twin arginine transport channel and allows quorum sensing to take place (Gallio *et al.*, 2002; Stevenson *et al.*, 2007). AarA activates a subunit of the TatA by removing an inhibitory sequence of TatA, allowing the transport of the unidentified signal for quorum sensing (Figure 1-1B). This appears to be a unique mechanism for rhomboid-mediated inter-cellular signalling, since *P. stuartii* is currently the only known species that requires processing of the TatA protein. It is still unclear what the function of other bacterial rhomboids might be even though nearly all bacterial genomes encode one or more rhomboids.

Although their functions remain unclear, bacterial rhomboids are shown to be amenable to a range of structural and functional studies, and are consequently the best characterised in the rhomboid family. The *Escherichia coli* rhomboid, *ec*GlpG, is currently the most extensively studied member of the rhomboid proteases, although its function has yet to be elucidated. A GlpG knockout *E. coli* strain has been shown to be viable, and does not display any obvious phenotypic abnormalities (Maegawa *et al.*, 2005). The *glpG* gene is located in the glpEGR operon of the glp regulon that contains genes responsible for glycerol-3-phosphate (g3p) catabolism (Zeng *et al.*, 1996). In the same operon as *glpG* is *glpE*, a gene that encodes a protein of unknown function, and *glpR* that encodes a DNA-binding repressor protein. GlpR negatively controls all glp operon transcription by binding to sequences close to or overlapping with *glp* operon promoters (Zeng *et al.*, 1996). This inhibition is relieved by GlpR binding to g3p, allowing g3p-dependent expression of glp genes. It was found that GlpE, GlpG and GlpR are co-transcribed since there are no internal terminators within the operon. However, the presence of multiple promoters also raises the possibility of differential expression of these genes (Yang & Larson, 1998). The little that is known about the function of *ec*GlpG is that it can cleave certain EGFR ligands such as Gurken (Urban, Schlieper, *et al*>, 2002) or substitute for AarA in *P. stuartii* mutant (Clemmer *et al.*, 2006, Gallio *et al.*, 2002).

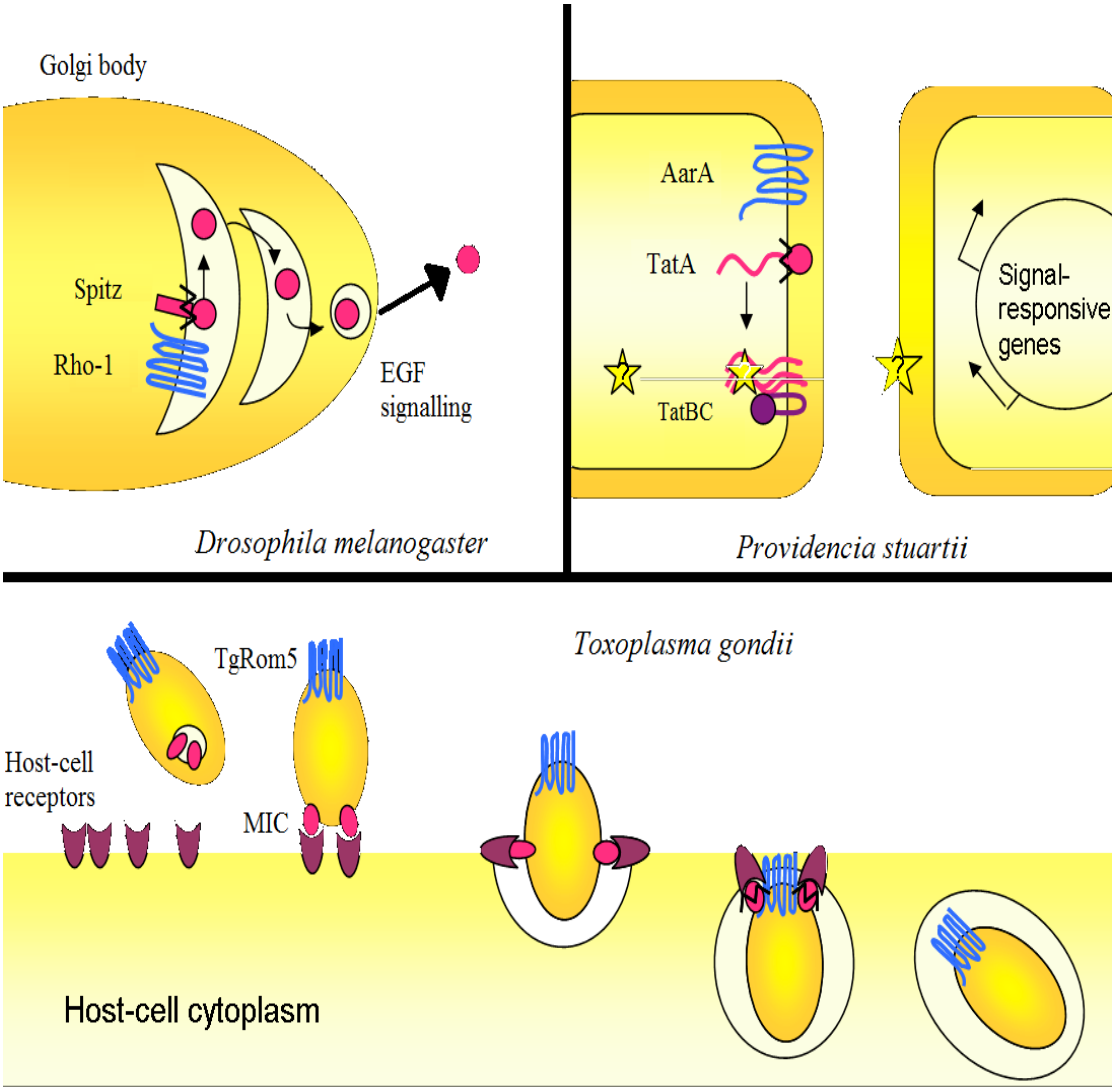

Figure 1-1 Examples of rhomboid function in biological systems. (A) In the *Drosophila* Golgi, Rhomboid-1 (blue) cleaves the luminal side of the Spitz transmembrane domain (pink) for release of the extracellular domain to be exported out of the cell for subsequent epidermal growth factor (EGF) signalling (Urban *et al.*, 2001). (B) The *Providencia stuartii* rhomboid, AarA (blue), is proposed to cleave TatA (pink) which can then bind the TatB/C complex (purple) to form a pore. This pore releases a signalling molecule that has not yet been characterised (shown as a yellow star), but is known to turn on signal-responsive genes for quorum sensing (Stevenson *et al.*, 2007). (C) Invasion of the protozoan parasite *Toxoplasma gondii* into host cells is mediated by the TgRom5 (blue). *T. gondii* Microneme proteins (MIC) adhesins (pink) bind to host-cell receptors (purple) and are cleaved during host-cell invasion to release the parasite (Dowse *et al.*, 2005).

1.1.2.2 Role in pathogenicity

Interest in rhomboid proteases has rapidly increased due to their role in invasion, growth and survival of protozoa parasites that infect a significant proportion of the human population, particularly in developing countries (reviewed in Rawson, 2008). This was first discovered in *Toxoplasma gondii*, the organism that causes toxoplasmosis, with cell-surface adhesins being identified as substrates of the rhomboid protease, which are cleaved during entry into the cell (Brossier *et al.*, 2005; Figure 1-1 C). Inhibition of this cleavage prevents host cell invasion without having a significant effect on parasite morphology, metabolism or gliding motility (Conseil *et al.*, 1999). Adhesins in *Plasmodium falciparum*, the causative agent of malaria, are also cleaved by a rhomboid; in this case PfROM4 (Baker *et al.*, 2006). While it appears that this cleavage is not directly linked to invasion of the host cell, it seems to be required for normal parasite growth. Another function for rhomboids has been described for *Entamoeba histolytica*, an extracellular parasite that can cause amoebic dysentery (Baxt *et al.*, 2008). In this case, the rhomboid EhROM1 appears to be required for immune system evasion, cleaving opsonised antigens that would normally target the parasite for phagocytosis by white blood cells. Evidence for this role includes the observation that EhROM1 localises to the region where opsonised antigens are typically shed from the parasite, and its cleavage of these antigens in cell culture based assays. The discovery of these roles for rhomboid proteases in parasite infection and survival has made them an attractive target for drug development.

1.1.2.3 Function of the PARL (mitochondrial) rhomboids

Mitochondrial rhomboids have evolved in eukaryotes to coordinate the regulation of mitochondrial membrane dynamics, a critical aspect of cell biology. This function appears to have required the emergence of a structural feature that is unique among all other rhomboids: an additional transmembrane domain positioned at the N-terminus of the six TMD that form the core proteolytic domain. This '1 + 6' structure is shared only by mitochondrial rhomboids. Members of the presenilin-associated rhomboid like (PARL) family are present in a number of eukaryotic systems, with yeast, mammalian and insect members being the best characterised. As the functions of these PARL

rhomboids were revealed, it became apparent that they do not associate with presenilin as was originally postulated. Instead mitochondrial rhomboids are thought to be the gatekeepers of mitochondrial dynamics, apoptosis and govern stress, signalling to the nucleus and other mitochondrial activities.

The yeast, *Saccharomyces cerevisiae* has only one mitochondrial rhomboid, Processing of Cytochrome c Peroxidase (Pcp1). The protease is inserted in the inner mitochondrial membrane, where it serves to cleave cytochrome c peroxidase protein (Ccp1p) and, perhaps more importantly, the dynamin-related protein Mgm1; a dynamin GTPase implicated in mitochondria fusion. Genetic ablation of Pcp1 results in fragmented mitochondrial shape, with cells not growing on non-fermentable medium and has a compromised ability to maintain their mitochondrial DNA content (Sesaki *et al.*, 2003).

Drosophila Rho-7 is a mitochondrial rhomboid. Deletion of the gene results in severely decreased viability of the flies, causing 90% of the flies to die before pupariation. The living flies show a wing position defect, and as a result are unable to fly and also have difficulty walking (Jeyaraju *et al.*, 2013).

The mammalian Parl mitochondrial rhomboid is inserted in the inner membrane of the mitochondrion. Interestingly homozygous deletion of $Parl^{-/-}$ mice develop normally and do not display the abnormal mitochondrial morphology seen in yeast and insects until the 4th postnatal week. After the fourth postnatal week, these mice start displaying severe growth retardation, with loss of muscle mass and postural defects. The animals die within 8 to 12 weeks possibly by aggravated feeding and breathing problems. It seems that the ablation of the mitochondrial rhomboid leaves the mice more susceptible to death inducing damage (Cipolat *et al.*, 2006).

1.1.3 Classification of the rhomboid proteins

The initial model from sequence analysis was that the rhomboids are classified into three distinct classes. The simplest class consists of six TMDs that form the core unit and contain the smallest catalytically active motif GxSx in TM4 and histidine (H) in TM6. This form is predominately present in prokaryotes, but is sometimes also present in eukaryotic organisms, including mammals. Added to this main core unit in eukaryotes, there is an additional seventh TMD. This usually follows the main core unit (6+1) TMD form (Freeman, 2008, Koonin *et al.*, 2003). It is rare to find an analogous seventh TMD form in bacteria, but several have been predicted (Urban, 2013). Lastly, there is the distinct form of rhomboid proteases usually present within the endosymbiotic organelle. As above it adds a seventh TMD, however it is before the main unit (1+6 configuration; Pellegrini *et al.*, 2001). Furthermore, there are rhomboid genes found that clearly lack the codons required for catalytic residues. These genes are considered rhomboid proteins or pseudoproteins but not proteases. They form two distinct clusters of the 6+1 configuration, called iRhom proteins, and six TMD form that is widely represented in eukaryotes by Derlin proteins (Figure 1-2).

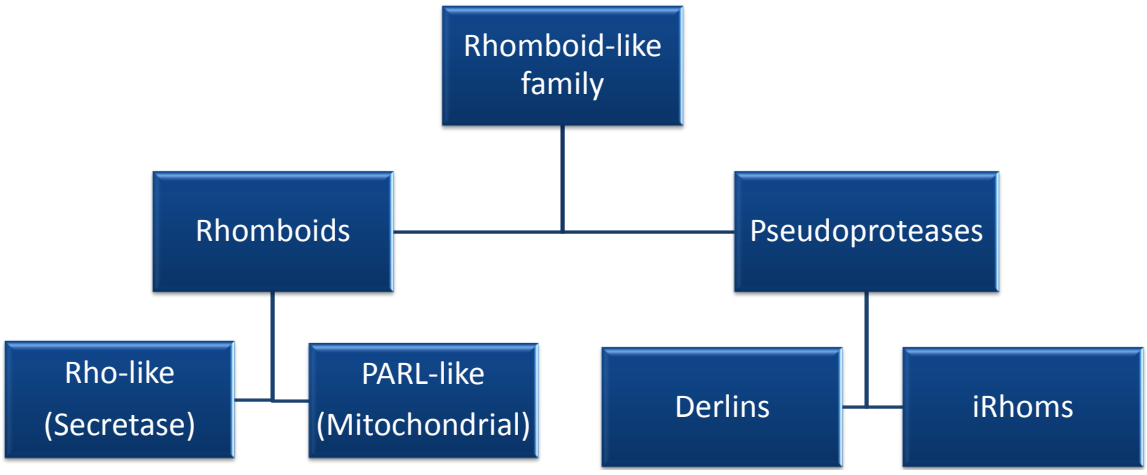

Figure 1-2 Subfamilies of rhomboids. Classification of rhomboid family of proteins reproduced from Urban & Freeman 2007b.

Both types of putative inactive rhomboid proteins have been suggested to work in endoplasmic reticulum-associated degradation (ERAD) pathways (Adrain & Freeman, 2012; Cao & Kaufman, 2011). Although some studies have found evidence of

oligomerisation, their potential to act as chaperones of rhomboid proteases should not be discounted as iClips have been hypothesised to work as monomers (Erez *et al.*, 2009).

1.1.4 Structure of the rhomboid proteases

Studies of bacterial rhomboid crystal structures from the *E. coli* and *Haemophilus influenza* ultimately revealed that the proteolytic reaction takes place within a water-filled cavity formed by its six TM helices. The serine (Ser) is within the GxSx (active site motif), characteristic of the oxyanion-binding pocket of classic serine proteases (Ben-Shem *et al.*, 2007; Lohi *et al.*, 2004, Russ & Engelman, 2000; Wang *et al.*, 2006). Most of the transmembrane helices are long and run perpendicular to the membrane, whereas the fourth TM is slanted relative to the others, and enters the centre of the protein more as an extended loop, converting it into an α-helix just at the catalytic serine. This cavity is lined with hydrophilic residues that surround the serine, approximately 1 nm below the membrane surface at the top of the short TM helix 4 (Vinothkumar *et al.*, 2010; Figure 1-3). The conserved histidine (His) of the catalytic dyad is found in TM5. The conserved GxSx motif also contains amino acids that stabilise interactions between TM3 and TM4 to maintain the structure. These interactions ensure that the catalytic dyad of His and Ser will remain accessible to both water and substrate. A conserved HxxGxxxG motif found on TM5 is responsible for ensuring that an active site histidine remains within hydrogen bonding distance of the serine nucleophile. This GxxxG motif is often found in interacting TM helices that, in the rhomboid, interacts with a matching motif in TM4 which ensures close contact between the active site histidine and serine (Lemberg, 2013; Russ & Engelman, 2000).

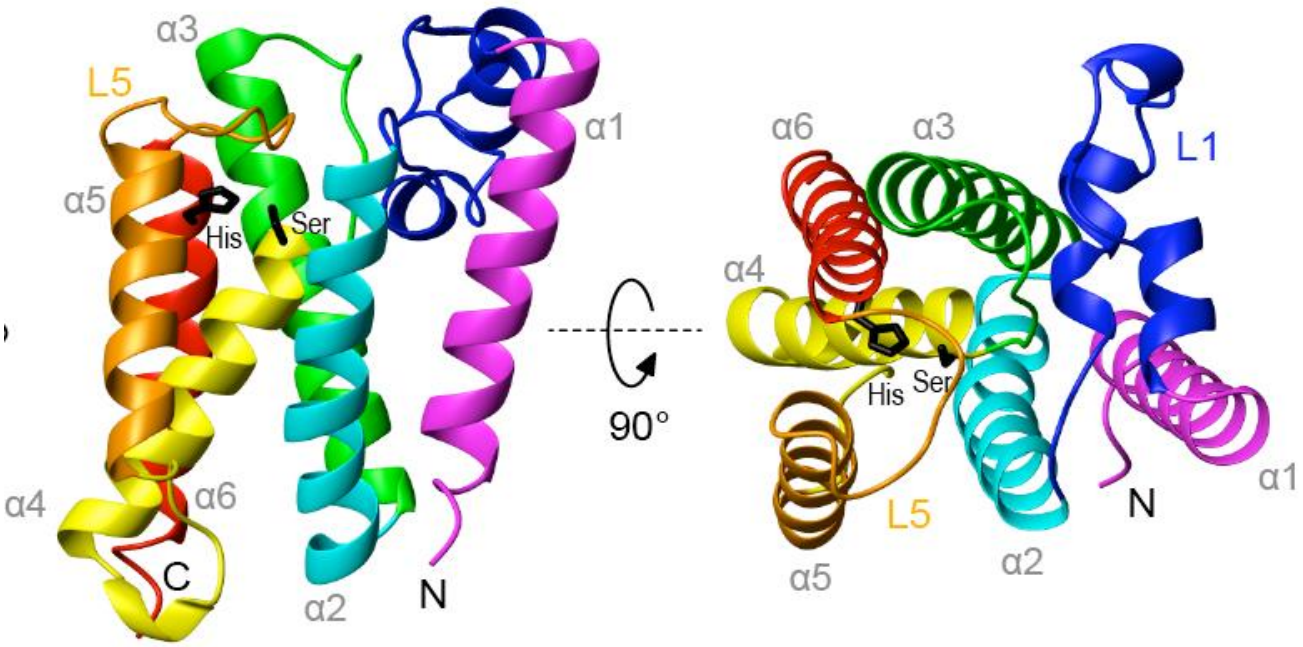

Figure 1-3 X-ray crystal structure of the *E. coli* GlpG rhomboid protease. The first published rhomboid structure is shown (PDB 2IC8), consisting of the C-terminal fragment (residues 91 – 272) isolated by limited proteolysis with chymotrypsin. Active site dyad side chains are shown in black with the L1 loop and six transmembrane helices distinguished by different colours reproduced from Vinothkumar *et al.* 2010.

Another feature of the GlpG rhomboid is the orientation of the extracellular L1 loop connecting the TM1 and TM2, which contains a tryptophan-arginine (WR) motif giving a highly asymmetric structure that, to some is extent, is able to regulate the catalytic activity of the rhomboids (Santos *et al.*, 2012). A number of residues (E/QxWRxxS/T) in this loop are highly conserved (Urban, 2010). Mutation of the arginine was found to reduce activity (Baker *et al.*, 2007; Wang *et al.*, 2007), whereas mutation of the tryptophan decreased activity in cell membranes, but not when the protein was reconstituted in detergents (Urban & Baker, 2008). The WR pair interacts within the L1 loop with the arginine alone forming five hydrogen bonds (Wang *et al.*, 2006). The functionally important L1 loop's unusual structure extends sideways, forming a lateral hairpin that lies half submerged in the membrane (Figure 1-3, side view). This feature had not been observed before publication of this crystal structure (Urban & Dickey, 2011; Figure 1-3). Recent thermodynamic analysis of the protein GlpG have shown that the L1 loop significantly stabilises the overall protein fold (Baker & Urban, 2012), which suggests that the main role of the L1 loop is to hold the substrate in place during catalytic reactions.

1.1.5 How are substrates recognised?

One issue that has not yet been resolved by the available library of rhomboid crystal structures is the mode of substrate entry into the active site from its lipid bilayer environment. Based on biochemical data, a membrane-integral rhomboid exosite has been proposed. This means that a secondary site can recognise the substrate without the need to fully translocate the substrate into the active site. There are two alternative modes proposed for the translocation (Wang *et al.*, 2006). The first model suggests that substrate entry may occur through a gap between TM2 and TM5. This hypothesis arose from the variation in the position of TM5 in the various structures published of GlpG, with some structures suggestive of a "closed" conformation, and others of a more "open" conformation. This has been supported by molecular and functional data generated GlpG gate mutants with increased spaces between the TM2 and TM5, which exhibited increased substrate cleavage rates (Baker & Urban, 2012; Baker *et al.*, 2007; Sherratt *et al.*, 2012).

The second, alternative model suggest the hydrophilic cavity is capped by flexible loop 5 (L5), and the gap between the opening of the helices is marginal at best. The flexibility is based on a crystal structure with the core exposed to the aqueous environment through an "open" conformation of this loop (Wang & Ha, 2007). The structure of the isocoumarin (a serine protease inhibitor) inhibited state also revealed significant displacement of the L5 cap away from the active site (Vinothkumar *et al.*, 2010). It is expected that a similar conformational change is involved in polypeptide substrate entry, although such data has yet to be shown experimentally.

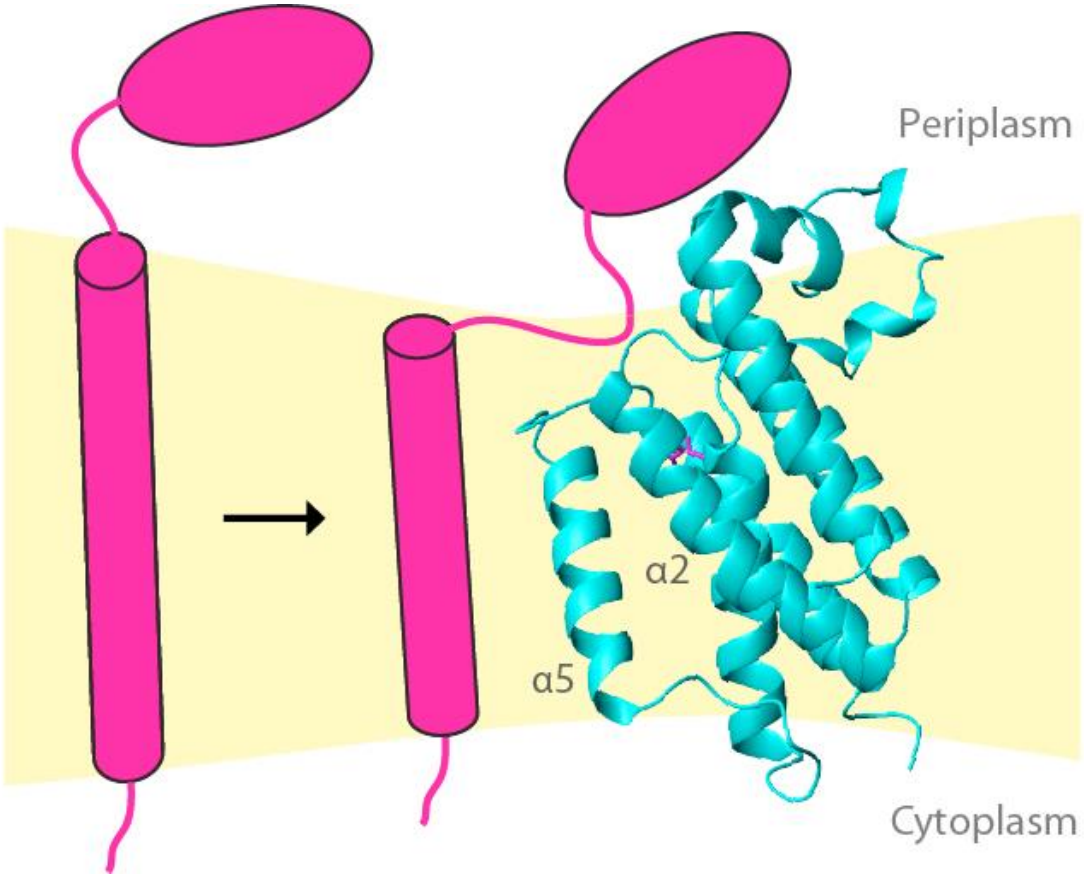

Figure 1-4 Proposed model of substrate entry to the active site. Analysis of detergent molecule localisation in GlpG structures (Wang *et al.*, 2007) and molecular dynamics simulations (Bondar *et al.*, 2009) suggest that the lipid bilayer is thinner in the region immediately surrounding the *ec*GlpG rhomboid protease (blue). Exposure of the end of the transmembrane substrate (pink) to this distorted membrane could induce a conformational change that exposes the peptide backbone to proteolytic attack. Active site entry is believed to occur between TM2 and TM5. Figure reproduced from (Sherratt *et al.*, 2012).

In addition, substrate entry may be assisted by membrane distortions around the rhomboid. Early evidence for this model was provided by crystal structures showing detergent molecules in a hydrophobic belt around the rhomboid that was narrower than the hydrophobic core of a regular lipid bilayer (Wang *et al.*, 2007; Figure 1-4). Molecular dynamics simulations also suggest that the membrane bilayer directly surrounding the protein is about 10% thinner than the bulk membrane (Bondar *et al.*, 2009).

1.1.5.1 Substrate specificity

Rhomboids typically cleave single-pass type I proteins (proteins that are anchored to the lipid membrane with a stop-transfer anchor sequence and have their N-terminal domains targeted to the ER lumen during synthesis) on the extracellular or luminal side, with the cleavage site usually being found near helix destabilising residues. Urban and

Freeman (2003), tested the activity of *Drosophila* Rho-1 with a series of chimeric Spitz-based substrates, allowing the identification of a seven residue substrate sequence (ASIASGA) required for cleavage. Moreover, the insertion of a non-native GA or GG motif in the N-terminal region of a TMD was found to convert a non-substrate TMD into a cleavable sequence, showing the importance of helix destabilising residues in the substrate. The presence of hydrophilic residues N-terminal to the cleavage site also appeared to be important, and was suggested to have a role in substrate entry to the active site (Urban & Freeman, 2003). Based on these findings it was possible to identify a similar motif in *Toxoplasma* adhesins, which were subsequently demonstrated to serve as substrates for three unrelated rhomboids (Brossier *et al.*, 2005).

The idea that helix-destabilising residues are required for substrate cleavage by rhomboids was further substantiated when the *E. coli* rhomboid, *ec*GlpG, was found to cleave a TMD segment originally meant to serve as a negative control. When Maegawa and coworkers created a large fusion protein consisting of the second transmembrane helix of LacY (LacYTM2) with β-lactamase at the N-terminus and maltose binding protein at the C-terminus (Maegawa *et al.*, 2005), this substrate was cleaved by *ec*GlpG *in vivo* and *in vitro* even though it was quite different from known rhomboid substrate sequences. The sequence features of LacYTM2 were then systematically analysed in GlpG mutant *E. coli* cells for their effects on cleavage. It was found that residues surrounding the cleavage site were only partially responsible for determining amount of substrate cleavage (Akiyama & Maegawa, 2007), and not completely dependent on a recognition motif. However, a three-fold increase in substrate cleavage could be obtained simply by the introduction of a helix-breaking glutamine-proline (QP) sequence into the middle of the TMD segment; approximately 17 residues away from the site of cleavage. Furthermore, it was possible to convert the Spitz TMD, that is not normally cleaved by this protease into a GlpG substrate by introducing the QP sequence seventeen residues from the cleavage site. The presence of destabilising residues around the cleavage site and midway through the transmembrane segment was hypothesised to bend the substrate into a favourable position for GlpG cleavage in the membrane (Akiyama & Maegawa, 2007).

To characterise the elusive rhomboid substrate specificity and in better detail, the Freeman group tested the ability of an extensive series of TatA; substrate mutants to be cleaved by the bacterial AarA rhomboid (Strisovsky *et al.*, 2009). Whereas the presence of helix destabilising residues in the TM substrate were an important determinant for cleavage *efficiency*, they did not seem to control *where* the substrate would be cleaved (Strisovsky *et al.*, 2009). These results were supported by analysis of other substrates that can be cleaved by AarA, and of substrates that are cleaved by various other rhomboids. These results indicate that diverse rhomboids recognise a general substrate recognition motif.

1.1.6 Regulation

While a number of aspects of rhomboid structure and function have become well understood over a relatively short period of time, little is still known about how these proteases are regulated. In the case of soluble proteases, regulation is often achieved by expression of a proenzyme form that must be proteolytically processed for activation. In contrast, rhomboids appear to be constitutively active, yet do not require any pre-processing of their substrates, raising questions about whether rhomboid activity is regulated in any way. Although a unified theme of rhomboid regulation has not been identified, partly due to the diversity in rhomboid function, some ideas regarding regulation have been forwarded for a small number of systems.

1.1.6.1 Regulation through expression and/or compartmentalisation

The best characterised mechanism of rhomboid regulation occurs at the level of rhomboid expression and/or compartmentalisation. Even before the rhomboid was identified as an intramembrane protease, expression patterns of Rho-1 in *Drosophila* embryogenesis were found to be complex, revolving around the EGFR pathway (Freeman *et al.*, 1992). Regulation through compartmentalisation in the cell was later uncovered with Rho-1 localising to the Golgi apparatus (Figure 1-1A) while its substrate, Spitz, is retained in the ER. Therefore, Spitz can only be processed when it is allowed to move from the ER to the Golgi, an event that requires the Star trafficking protein as an escort (Klämbt, 2002). Another example of regulation through compartmentalisation is seen in *T. gondii* parasite invasion mediated by TgROM5. The substrates for this rhomboid are adhesins that are normally localised to internal organelles. When these organelles fuse

with the cell surface, the adhesins localise to the plasma membrane where TgROM5 is also found, leading to the adhesin cleavage that is required for parasite invasion to proceed (Brossier *et al.*, 2005).

1.1.6.2 Modulation of PARL function

In a unique form of regulation, mammalian PARL can undergo two processing events (α and β-cleavage) in a long loop that connects the extra N-terminal helix to the core. Specifically, α-cleavage is constitutive and occurs during import into the mitochondria to produce mature PARL, whereas β-cleavage removes part of the N-terminus and depends on PARL phosphorylation. This β -cleavage event activates PARL and results in altered mitochondrial morphology (Jeyaraju *et al.*, 2006). When cells were transfected with truncated PARL with a sequence that started at the β-cleavage site rather than the full-length protein, it caused the cells to have a fragmented mitochondrial morphology. Surprisingly, the cleaved N-terminal peptide was also found to traverse the mitochondrial membranes and localise to the nucleus in what is described as mitochondrial retrograde signalling (MRS) (Sík *et al.*, 2004). MRS allows the nucleus to monitor and coordinate structural and functional events in the mitochondria; the possibility that the rhomboid is involved in signalling through release of part of itself is a very interesting concept that appears to be unique to PARL. The role of PARL in MRS requires further investigation to determine the requirements for this type of signalling, but it appears to provide one role for an extra rhomboid structure element outside the catalytic core.

1.2 *Dictyostelium discoideum* as a biomedical model

Dictyostelium discoideum is one of the most widely studied social amoebae or cellular slime moulds. Proteome-based eukaryotic phylogeny studies shows the divergence of *Dictyostelium* along the branch leading to the Metazoa soon after the plant animal split (Eichinger *et al.*, 2005; Figure 1-5). Despite the earlier divergence of *Dictyostelium*, many of its proteins are more similar to human orthologues than are those of *S. cerevisiae*, probably due to higher rates of evolutionary change along the fungal lineage.

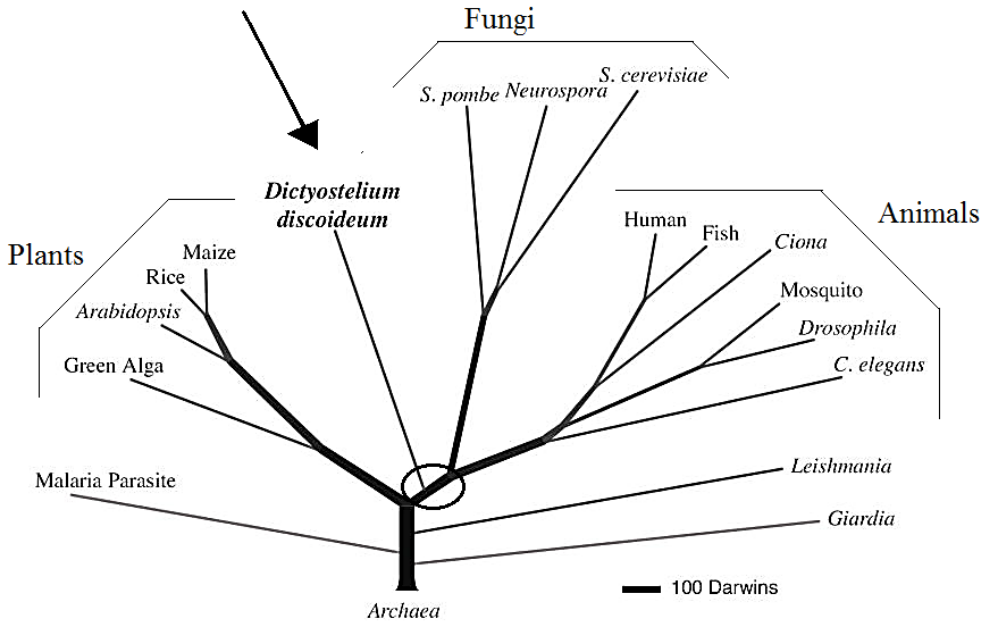

Figure 1-5 Proteome-based eukaryotic phylogeny. Relative lengths of branches are governed by Darwins, (1 Darwin representing 1/2000 of the divergence between *S. cerevisiae* and humans) (Eichinger *et al.*, 2005) S. = *Saccharomyces*, C. = *Caenorhabditis* **.**

When these amoebae deplete their food supply, they enter a starvation phase, which results in the aggregation of hundreds of thousands of cells into a hemispherical multicellular aggregate, the 'mound'. The mound undergoes complex morphogenesis to produce a multicellular slug that migrates in response to light and temperature gradients to the surface of the soil, where it forms a fruiting body consisting of a stalk supporting a mass of spores. In the mound, cells start to differentiate into prestalk and prespore cells; precursors of the stalk and spores that make up the fruiting body (Chisholm & Firtel, 2004; Weijer, 1999) (Figure 1-6). Upon the return of favourable conditions, spore cells

can germinate, thus allowing each spore to release an amoeba. The purpose of this developmental cycle in *Dictyostelium* is to allow cells to survive starvation conditions.

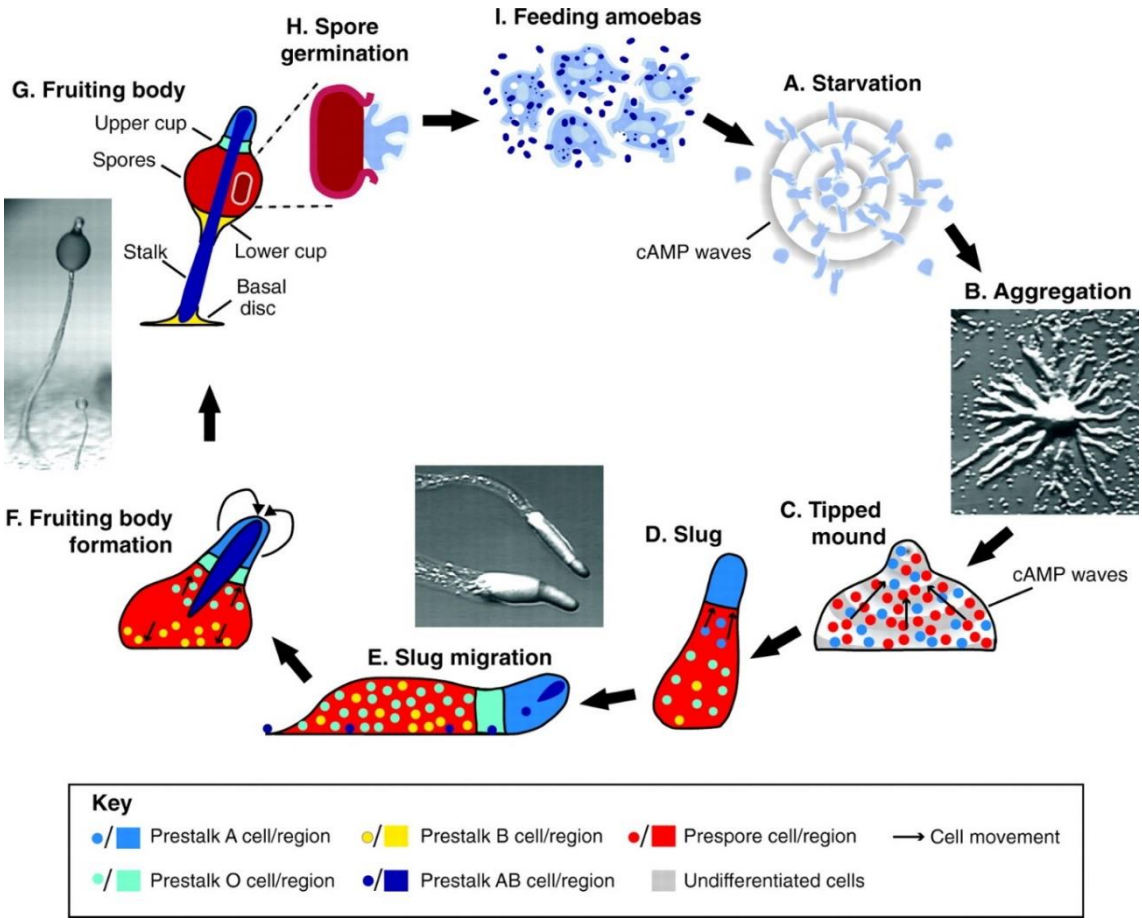

Figure 1-6 The life cycle of *Dictyostelium discoideum*. "(A) Starving *D. discoideum* amoebae secrete pulses of cyclic adenosine monophosphate (cAMP, indicated by grey rings) that (B) cause the chemotactic aggregation of cells into mounds. Cells in the mound move upwards in response to continued cAMP emission from its top, (C) causing the formation of a tipped mound. The differentiation of cells into two cell types, prespore and prestalk A, begins in these mounds. (D) A mound then forms a slug, in which further differentiation of cells into prestalk (O, B and AB) cells occurs. (E) The slug then falls over and starts to migrate. (F) Finally, it undergoes fruiting body formation, during which the different cell types migrate to specified locations in the fruiting body and (G) ultimately differentiate into spores, stalk cells and the structures that support the stalk and spore head. (H) After their dispersal to nutrient-rich habitats, spores germinate and (I) resume proliferation as individual amoebae. Modified with permission from Schaap, 2007" (Schaap, 2007).

Dictyostelium can be easily cultured in the laboratory, preying on bacterial lawns or modified laboratory strains in shaking culture in an axenic medium, hence the name of the control strains AX2, AX3 and AX4. Since many key cellular pathways are well conserved in *Dictyostelium*, most (if not all) of their components are present, however many of them have fewer paralogs in *Dictyostelium* species. Furthermore, there is often less redundancy in molecular pathways acting in *Dictyostelium*. Therefore, these two

features allow the unwinding of the complex molecular networks present in eukaryotic cells, and to define the functions of the proteins involved. Manipulation of genes can be achieved through highly efficient homologous recombination or Restriction Enzyme Mediated Integration (Kuspa & Loomis, 1992; Schiestl & Petes, 1991).

Dictyostelium has developed into a useful model for understanding aspects of certain pathologies because of the conservation of eukaryotic genes and molecular pathways, as well as its simplicity and manageability compared with mammalian systems (Boeckeler & Williams, 2001). Sequencing of the *Dictyostelium* genome has identified 22% of *Dictyostelium* genes sharing homology with human genes, which has made the organism a useful model for human drug targets and intracellular pathways involved in human disease (Eichinger *et al*., 2005). Many genes and targets expressed in *Dictyostelium* are lacking in other biomedical models such as *S. cerevisiae* and *Schizosaccharomyces pombe*, suggesting *Dictyostelium* may be a more advantageous non-sentient model (Eichinger *et al*., 2005).

In addition, *Dictyostelium* can be used as a model to study interactions with various important pathogens such as *Legionella, Mycobacterium* and *Pseudomonas* because it predates such bacteria in its natural environment. For example, *Dictyostelium* has been used to address mitochondrial dysfunction and secretory pathway diseases, such as Chediak Higashi Syndrome, a rare condition that arises from a mutation of a lysosomal trafficking regulator protein which affects multiple organs (Lima *et al.*, 2011; Steinert, 2011).

The mechanisms *Dictyostelium* cells use for motility and chemotaxis are similar to those of mammalian cells, specifically neutrophils. *Dictyostelium* contains all the classes of actin binding proteins that are typically found in eukaryotes and thus serves as a convenient model for the study of the actin cytoskeleton and its dynamics (Egelhoff & Spudich, 1991; Maniak, 2001; Neuhaus & Soldati, 1999; Rupper & Cardelli, 2001). There are on-going studies using *Dictyostelium* to help understand motility-related pathologies (Carnell & Insall, 2011). For instance, Lissencephaly, is a brain disease caused by defective neuronal migration and mutations in highly conserved genes: Isolated lissencephaly sequence 1 (*LIS1)* and doublecortin (*DCX)*, which are also present in *Dictyostelium* (Meyer *et al.*, 2011).

Dictyostelium has been a useful tool in pharmacogenomics as well; it has helped to unveil the mechanism of action of certain drugs as stated below, while reducing animal use in drug testing. *Dictyostelium* has increased our knowledge of the mechanism of two bipolar disorder treatments, namely valproic acid and lithium treatments (Ludtmann *et al.*, 2011; Terbach *et al.*, 2011; Williams *et al.*, 2002). Work in *Dictyostelium* has prompted further studies in human cells on the role of sphingolipids and ceramide in regulating the response to the chemotherapeutic drug Cysplatin (Alexander & Alexander, 2011). *Dictyostelium* also has the potential as a model in the analysis of emetic liability of novel chemical entities (Robery *et al.*, 2011).

1.2.1 Chemotactic movement

Dictyostelium is an advantageous tool to study chemotactic movement, which is fundamental to many physiological processes, such as angiogenesis and immune responses, as the mechanisms of motility in *Dictyostelium* cells are analogous to those of leukocytes (Hadjout *et al.*, 2001). The signalling pathways regulating chemotaxis in *Dictyostelium* have been studied extensively, all lines of evidence suggests that movement in this model eukaryote is a highly coordinated and regulated process, likely involving even more pathways that have yet to be identified. It is thought that these unidentified pathways may also involve redundant components (Insall & Andrew, 2007).

Cell movement also involves dynamic changes in the cytoskeleton of migrating cells. The cytoskeleton is present in the cytoplasm of both prokaryotic and eukaryotic cells and regulates cell shape and structure. In eukaryotic cells, the cytoskeleton is composed primarily of microfilaments (i.e. polymers of actin), intermediate filaments, and microtubules (i.e. polymers of tubulin). In addition, it interacts with a great diversity of cytoskeletal-binding proteins (e.g. myosin, talin, vinculin, α-actinin) that can coordinate cellular processes (e.g. cell movement) and mediate binding to cellular membranes (Doherty & McMahon, 2008). In *Dictyostelium*, actin polymerisation and myosin II heavy chain (MHC) assembly in the cytoskeleton are both required for efficient cell movement (Yumura, 1993). Dephosphorylation of MHC has also been shown to be necessary for actin polymerisation during *Dictyostelium* chemotaxis (Heid *et al.*, 2004).

Chemotaxis is a crucial process for *Dictyostelium's* developmental cycle in its natural environment. Chemotaxis begins with the detection of folate (released from bacterial cells) ensued by cAMP secreted by *Dictyostelium* during starvation. In addition to migration towards folate and cAMP, *Dictyostelium* has also been found to migrate towards ions such as calcium and magnesium as well as arachidonic acid (Fisher *et al.*, 1989). Upon detection of chemoattractive gradients, cells become polarised and initiate movement by the process termed 'blebbing'. This process is followed by the extension of pseudopodia at the leading edge which is attached to the substrate and directs the orientation of travel (Haupt *et al.*, 2007). The front of the cell generates a protrusive filamentous actin (F-actin) forward force, and the interaction between actin and myosin

II at the rear of the cell leads to a contractile force. In the case of cAMP detection, for example, the polarised leading edge and subsequent amplification process allows for greater sensitivity to cAMP then the rest of the cell resulting in migration towards a gradient as little as 2% cAMP difference between the front and the back of the cell (Firtel & Meili, 2000; Jin *et al.*, 2008).

1.2.1.1 cAMP chemotaxis

The chemotaxis of *Dictyostelium* amoebae towards cAMP begins with the binding of cAMP to a seven-transmembrane domain G-protein coupled cAMP receptor (cAR). Binding causes the dissociation of the Gα and Gβγ subunits from each other (Jin *et al.*, 1998; Lilly *et al.*, 1993; Zhang *et al.*, 2001). Gα or Gβγ then activate downstream effectors that interact with and activate phosphatidylinositol 3-kinase (PI3K). PI3K converts phosphatidylinositol 4, 5 bisphosphate (PIP2) to phosphatidylinositol 3,4,5 triphosphate (PIP3) on the inner plasma membrane (Funamoto *et al.*, 2001; Sasaki *et al.*, 2004). Elevation of PI3K results in the recruitment of several signalling components that control actin polymerisation such as cytosolic regulator of adenylyl cyclase (CRAC) and Protein kinase B (PKB) which ultimately drives the polarised migrating cell towards the chemoattractant source (Figure 1-7; Meili *et al.*, 1999; Parent *et al.*, 1998). In addition, Ca^{2+} and calmodulin (CaM)-mediated signalling via interaction with specific CaM-binding proteins (CaMBPs), have both been shown to be required for efficient cell motility and chemotaxis in *Dictyostelium* (Gauthier & O'Day, 2001, Lusche *et al.*, 2009).

Recent findings have shown that PI3K and phospholipase A2 (PLA_2) mediate cAMP chemotaxis in parallel compensatory pathways (Chen *et al.*, 2007; van Haastert *et al.*, 2007). PI3K controls F-actin polymerisation, which has been linked to pseudopod extension (Chen *et al.*, 2003; Takeda *et al.*, 2007), but the activation mechanism and the targets of PLA_2 are still unknown (Chen *et al.*, 2007; Veltman *et al.*, 2008). In *Dictyostelium*, LY294002 (2-Morpholin-4-yl-8-phenylchromen-4-one) and quinacrine have been shown to be effective inhibitors of PI3K and PLA2, respectively (van Haastert *et al.*, 2007). Studies have also shown that PLC and Ca^{2+} are essential for PI3K and PLA_2-mediated signalling, respectively (Lusche *et al.*, 2009). In mammalian cells, PLA_2 induces Ca^{2+} signalling through the release of arachidonic acid. This fatty acid may

therefore be a possible second messenger mediating the PLA_2-dependent chemotactic response (Chen *et al.*, 2007). These recent findings have identified a pathway independent of the PI3K mediated pathway, thus implying that more pathways may be involved in this complex cellular process (Insall & Andrew, 2007). In addition, a recent study described the ability of aggregation-competent *Dictyostelium* amoebae to directionally respond towards a gradient of Ca^{2+} (Scherer *et al.*, 2010), suggesting the existence of other motility regulatory components in *Dictyostelium* that have yet to be identified.

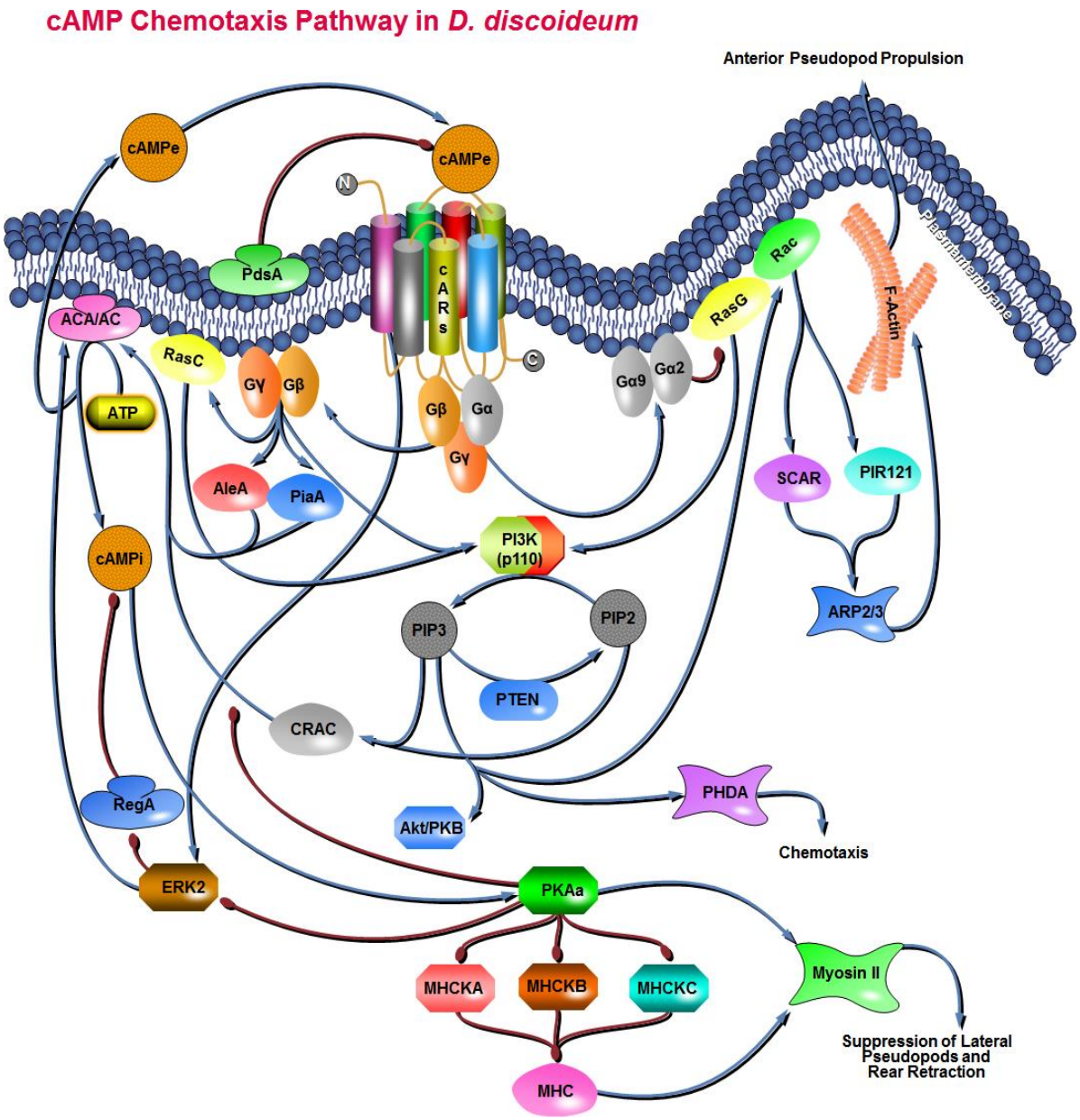

Figure 1-7 cAMP signal induction pathway. The activation of the cAMP receptor (cAR) receptors leads to the production of secondary messenger molecules such as phosphatidylinositol (3, 4, 5)-triphosphate (PIP3), cAMP and cGMP and activation of small G-proteins. The cAMP secreted by cells in starvation mode binds to cAR1 which activates extracellular regulated kinases (ERK). ERK2 suppresses phosphodiesterase2 - RegA, which is an inhibitor for internal cAMP. It also transmits signal to adenylyl cyclase (ACA). ACA secretes cAMP to the internal and external environment. It also secrets phosphodiesterase (PDE) to the environment, which destroys released cAMP signal up to a distance of 57 µm. The internal cAMP triggers activation of protein kinase A (PKA). High levels of PKA activate gene expression leading to the release of calcium and cell movement. It also acts as a feedback inhibitor for cAR1 and ERK2, hence regulating the amount of internal cAMP as ERK2 is no longer in large quantities to suppress RegA and thus cAMP is hydrolysed. Image reproduced from (Nash & Kalvala, 2009).

1.2.1.2 Folate chemotaxis

Although less extensively studied compared with cAMP chemotaxis, *Dictyostelium* can also chemotax towards folic acid, which is secreted by bacteria and allows *Dictyostelium* amoebae to find their food source. Within several hours of starvation, *Dictyostelium* cells develop cAMP receptors (cAR), losing their folic acid receptors and their sensitivity to folic acid (Nebl *et al.*, 2002). The signal transduction regulating folic acid chemotaxis is different from the signalling that mediates chemotaxis towards cAMP. For instance, tyrosine kinase activity has been shown to be required for chemotaxis towards folic acid but not cAMP, and unique CaM-dependent phosphoproteins have been shown to be linked solely to folic acid chemotaxis (Browning *et al.*, 1995; Gauthier & O'Day, 2001). It may activate many of the same intracellular pathways as cAMP to produce directed movement (Nebl *et al.*, 2002). However, experiments using SILAC showed that cAMP and folate share 18 phospoproteins between them. Individually, cAMP activates 108 and folate 29 phosphoproteins in their the signalling pathway (Gauthier & O'Day, 2001). The unknown folic acid receptors might be associated with the cytoskeleton, similar to cARs (Hadwiger & Srinivasan, 1999). Several proteins solubilised from *Dictyostelium* membranes bind to folic acid-derivative sepharose, amongst which might be folic acid receptors (Janssens & Van Haastert, 1987).

1.2.2 Slug formation

During mid-development, *Dictyostelium* can choose between two different pathways. After the tipped mound stage it can either proceed directly to culmination, or the organism can form a migratory slug. The migratory stage enables *Dictyostelium* to locate the best possible location to form fruiting bodies. Slug formation usually takes place in preferably low ionic strength medium and in the dark, approximately 16 h after onset of starvation (Fisher & Williams, 1981). The slug forms by the chemotactic aggregation of up to 10^5 starving cells. It is motile and migrates in response to light and temperature gradients to the surface of the soil to form a fruiting body consisting of a stalk supporting a spore head. Slug migration and behaviour result from the coordinated chemotactic movement of the individual cells in the slug. Undulations of the chemoattractant cAMP are

periodically initiated at the peak of the slug that propagate towards the rear of the slug, resulting in the periodic forward movement of individual cells as well as the whole slug.

The initial stages of slug formation involve the creation of an apical tip after movement of the prestalk cells to the apex of the mound. This prestalk domain then elongates to form a first finger, by which time, an anterior–posterior axis has been established, with prestalk cells at the front and prespore cells at the rear. The finger falls over to form a migrating slug, or pseudoplasmodium, that is both phototactic and thermotactic. In response to environmental signals, the slug undergoes culmination, resulting in the formation of a mature fruiting body containing terminally differentiated spores and stalk cells (Darcy *et al.*, 1994; Vasiev & Weijer, 2003). The multicellular *Dictyostelium* slug is able to move at an average speed of 0.2–2.0 mm/h aided by a secreted slime sheath composed of cellulose and protein that is synthesised as the cells progress, leaving a trail in its path (Fisher & Williams, 1981).

As well as demonstrating chemotaxis, slugs can sense and respond to differences in light and temperature gradients. Phototaxis relies on a lens effect; light refracted at the roughly cylindrical surface of the slug is focused onto its distal side, so that it turns away from its most intensely illuminated side and directs towards a light source. This slug behaviour is controlled by the slug tip (Fisher & Annesley, 2006). Signals from photoreceptors and thermoreceptors control the concentrations of intracellular second messengers such as cAMP, cyclic guanosine monophosphate (cGMP) or Ca^{2+}. These messengers, in turn, activate G proteins and the small GTP-binding proteins that are involved in transducing the signals. These help to adjust the tip activation and inhibition signal waves, which determine migratory speed and directionality. The tip activation signal is carried by 3-dimensional spiral scroll waves of cAMP emanating from the tip, analogous to the 2-dimensional cAMP waves that mediate aggregation (Figure 1-8). In the current model of phototaxis, light signals modulate the slug tip activation/inhibition system to cause slug turning by stimulating lateral shifts in the tip position (Fisher, 1997).

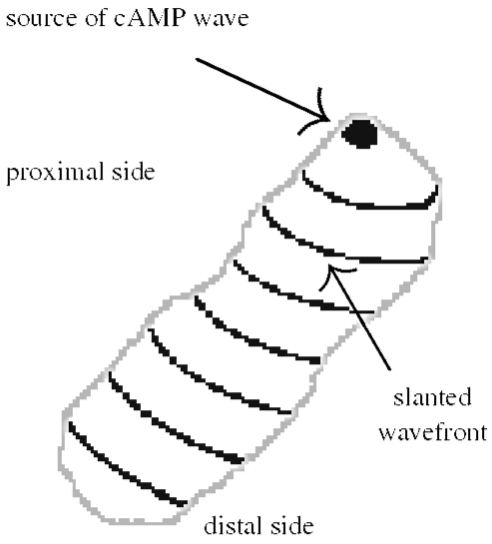

Figure 1-8 Signals during phototaxis. A diagram of the basic properties of the cAMP wave during phototaxis: the spiral lines show the wave shape at different locations in the slug (reproduced from Maree *et al.*, 1999).

The exact mechanism of the slug's motility is not known, but it is probably the communal effort of the entire cell community coordinated by the movement through the extracellular matrix of all the individuals (Figure 1-9) (Fisher & Annesley, 2006; Fisher, 1997; Maree *et al.*, 1999).

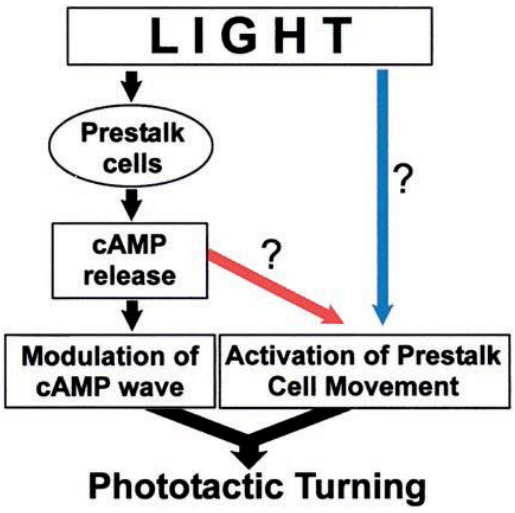

Figure 1-9 A scheme showing hypothesised light effects in slug phototaxis. Light induces cAMP release from pre-stalk cells modulating cAMP cell–cell signalling and may activate pre-stalk cell movement. These changes in multicellular coordination act to turn the slug tip. Whether light activates pre-stalk cell movement directly (blue arrow) or indirectly (red arrow) is not clear.

1.2.3 Chemical inhibitors of chemotaxis

Responses of *Dictyostelium* cells to various extracellular cues are less complicated than mammalian cells and thus environmental conditions and stimuli can be better controlled for these cells and the responses analysed. For this reason, *Dictyostelium* remains probably the most popular and powerful model for studying the features and molecular pathways of chemotaxis. It allowed identification of multiple genes involved in the process and improved an overall understanding of organisation and features of this phenomenon. It is important to understand chemotaxis as it is not only an integral part of the immune response, but cell motility is also an essential early event in metastasis of tumour cells and in angiogenesis of endothelial cells.

In the laboratory, *Dictyostelium* chemotaxis to cAMP can be studied after making cells' aggregation competent. This competency is achieved by a combination of starvation in a nutrient free buffer, and periodic pulses with cAMP; once every six minutes. After four to six hours of pulsing, cells are harvested and their response to chemoattractants can be analysed either by placing them in a gradient of cAMP, which can be generated in special devices, such as the Dunn chamber, gradient generating microfluidics device or a micropipette, or by uniformly stimulating the cells with a single dose of chemoattractant.

1.2.3.1 Channels and receptors in *Dictyostelium*

The *Dictyostelium* genome contains a wide variety of channels and receptors, many of which share homology with those found in chordates. Examples include the P2X receptors (Burnstock & Verkhratsky, 2009), which are ATP-gated ion channels involved in osmoregulation (Baines *et al.*, 2013) and calcium regulation (Ludlow *et al*., 2009). In addition, *Dictyostelium* contains a diverse range of seven-transmembrane receptors, which are the largest and most versatile family of receptors in eukaryotes (Eichinger *et al*., 2005; Pierce *et al*., 2002). These receptors and other proteins are the target of many therapeutic drugs in humans. For example pharmacological inhibition of PI3K in *Dictyostelium* amoebae and in a variety of mammalian cell types causes inhibition of chemotaxis and cell migration to varying degrees. LY294002, a PI3K inhibitor, has been reported to inhibit but not block chemotaxis in *Dictyostelium*, unless physiologically high concentrations are used (Funamoto et al., 2001). As in *Dictyostelium*, the PI3K/PIP3

pathway is important, but not essential for leukocyte chemotaxis. The role of the PI3K/PIP3 pathway in leukocytes, including neutrophils, T cells, and natural killer cells, was first examined using general PI3K inhibitors, wortmannin and LY294002 (Artemenko *et al.*, 2014). Although these inhibitors resulted in significantly reduced chemoattractant-induced migration, the inhibition was not complete. Thus screening for more potent and selective inhibitors are now needed as a starting point for the development.

1.2.3.2 Boronic acid as serine protease inhibitors

Boronic acids, as protease inhibitors, appeared for the first time 40 years ago as chymotrypsin (Philipp & Bender, 1971) and β-lactamase inhibitors (Koehler & Lienhard, 1971). The serine proteases chymotrypsin and subtilisin have been shown to be inhibited by aromatic boronic acids (Koehler & Lienhard, 1971; Lindquist & Terry, 1974). Since then, interest in these molecules increased continuously, and boronic acids with nanomolar affinity for proteases have been published or patented.

A boronic acid is an alkyl or aryl substituted boric acid containing a carbon to boron chemical bond belonging to the larger class of organoboranes (Smoum *et al.*, 2012). They are strong Lewis acids, their unique feature being that they are capable of forming reversible covalent complexes with sugars, amino acids, hydroxamic acids, etc. [i.e., molecules with vicinal[1], or occasionally substituted Lewis base donors (alcohol, amine, carboxylate)], meaning that with the appropriate substitution, boronic acids would have the right property making them ready for conversion from a neutral and triagonal planar sp2 boron (B−O bond length of 0.1361 nm) to an anionic tetrahedral sp3 boron (B−O bond length of 0.1469 nm; Figure 1-10). This essentially means that under the right physiological conditions, boronic acid compounds can make a transition state that bears a closer relationship to the structure of the true intermediate for the inhibition of hydrolytic enzymes.

[1] In chemistry vicinal (from Latin vicinus = neighbour) describes any two functional groups bonded to two adjacent carbon atoms.

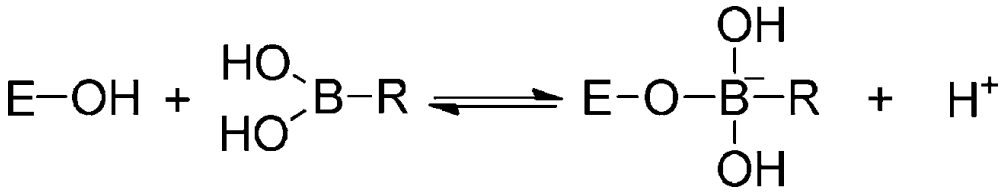

Figure 1-10 The reaction of the transition state analogue inhibitors (boronic acid derivatives) with serine peptidases (Smoum *et al.*, 2012)**.**

1.2.3.3 Cardiosulfa

The development of new treatments for a disease requires knowledge of the molecular target(s) of those treatments. *Dictyostelium* has recently been used in early drug development studies (Chang *et al.*, 2012) and to identify molecular pathways regulating drug action (Terbach *et al.*, 2011). Growth and development are controlled by a range of separate signalling pathways that can be probed at the molecular level by screening libraries of insertional mutants, constructed by REMI. This approach has provided new insights into how current therapeutic agents regulate cellular function (Williams *et al.*, 2006). For example, these screening techniques are being used in the identification of common signalling pathways targeted by lithium and valproic acid for the treatment of bipolar disorder, and increasingly being used to identify cellular mechanisms controlling drug targets using growth and development (Terbach *et al.*, 2011) or cell movement (Robery *et al.*, 2011) as phenotypic readouts.

A recent study by Ko *et al*. group (2009) investigated a library of sulfonamides and reported that cardiosulfa, a small molecule, disrupts heart development in zebrafish (*Danio rerio)* (Figure 1-11). In the study, fertilised zebrafish embryos were exposed to 5–30 µm cardiosulfa, which led to impaired heart morphology and function during development. Narrow and elongated ventricle and atrium were observed, accompanied by dramatic reductions in heart rates and peripheral blood flow as development proceeded, indicating impaired heart function. In the same study gene expression profiling in cardiosulfa treated embryos revealed increased transcription levels of members of the aryl hydrocarbon receptor (AhR) pathway including cytochrome P450 family (zfcyp1a, zfcyp1b1 and zfcyp1c1). In 2012 Ko *et al*. extended the study on the effects of cardiosulfa by using a zebrafish AhR (zfahr2) morpholino antisense oligonucleotide. The results concluded that heart deformation was protected by negative

regulators of AhR signalling pathway. However, the effects of cardiosulfa are not alleviated by using a morpholino antisense oligonucleotide for cytochrome P450 1A (zfcyp1a). In summary, cardiosulfa-induced heart deformation needs the zfahr2, but is not affected by zfcyp1a (Ko & Shin, 2012). This suggests that cardiosulfa functions through activation of the AhR signalling pathway in a cyp1a-independent manner.

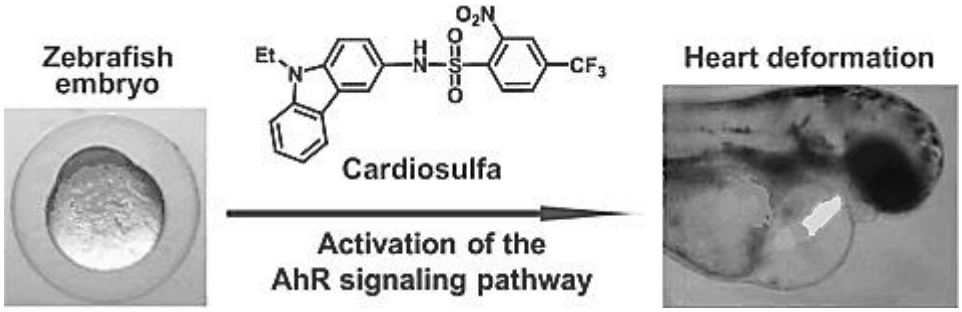

Figure 1-11 Cardiosulfa, causes aberrant heart formation and function in zebrafish embryos.

Dictyostelium can be used to provide an excellent model to study morphogenesis and more importantly possible cardiac defects. Previous studies have taken advantage of the genetics of *Dictyostelium* to study myosin mutations that cause cardiac myopathies in humans (Sasaki *et al.*, 1999). To study whether *Dictyostelium* had any similar pathways to zebrafish present, *Dictyostelium* cells were incubated with cardiosulfa and different cellular properties and phenotypes were tested in a variety of assays.

1.3 Rhomboids in *Dictyostelium*

Although the literature implicates rhomboid proteases in a wide range of functions from growth factor signalling to transport channel activation, specifics of rhomboid function in *Dictyostelium* is unknown and has not yet been studied. Analysis of the *Dictyostelium* genome database revealed at least four rhomboid proteases (RhmA, B, C and D) through their evolutionary conserved structure and catalytic domains. Given the important roles of rhomboids in fertility and development (Thompson *et al.*, 2012), cell signalling (Klämbt, 2002) and life cycle stage –specific expression (Brossier *et al.*, 2005), it seems reasonable to postulate that *Dictyostelium* rhomboids would act in regulating aspects of its unicellular to multicellular transition and/or its response to the environment.

The experiments related in this thesis therefore attempt to elucidate the role of rhomboids in regulation of cellular behaviour using reverse genetic studies in *Dictyostelium*.

From our studies of knockout mutants it was found that rhomboid mutant cells are defective in growth, pinocytosis, phagocytosis, chemotaxis and phototaxis. The experiments presented in this thesis have defined important roles for members of the rhomboid family in *Dictyostelium* in the control of cell behaviour during development.

Chapter 2
Methods

2.1 *Dictyostelium* methods

2.1.1 Cell culture

Cells were stored as spores in sterile horse serum (Sigma-Aldrich Co. Ltd. Poole, Dorset, UK) at -20 °C. Every 4 weeks a scraping from the frozen *Dictyostelium* stock was mixed with 300 µl of exponentially growing *Klebsiella aerogenes* culture and spread onto SM agar (ForMedium, Hunstanton, Norfolk, UK). This was incubated at 22 °C for 5-10 days. Liquid plates were then prepared by removing approximately 2 cm of the *Dictyostelium* growth zone (i.e. from the margin of a plaque of consumption of prey bacteria) from the agar plate and transferring it to HL5 (ForMedium) axenic medium, containing 50 µg/ml ampicillin and 100 µg/ml streptomycin (Sigma-Aldrich). The cells were maintained with shaking (180 rpm) at 22 °C and harvested in mid-log phase (10^6 cells/ml) for assays.

2.1.2 Solvent controls

0.01% v/v concentration of Dimethyl sulfoxide (DMSO) (Sigma-Aldrich) was used as control assays (see chapter 6 and 7) unless stated otherwise. The amount of DMSO present with test compound is in Table 2-1.

Table Error! No text of specified style in document.**-1 DMSO concentrations in assays.** The table denotes the calculated amount of DMSO added to a culture during treatment. 0.01% DMSO was used in the control assays

Concentrations of Compounds	***Equivalent concentrations of DMSO in control***
10 µM	0.001%
25 µM	0.0025%
50 µM	0.005%
75 µM	0.0075%
100 µM	0.01%

2.1.3 Determining the growth rate of treated cells

For growth curve assays, cells were seeded from mid log phase cultures at a density of 10^5 cells/ml in to fresh HL5 medium. Growth at various time points was than determined by counting using a Neubauer improved haemocytometer (Neubauer Bright Line); (Figure 2-1).

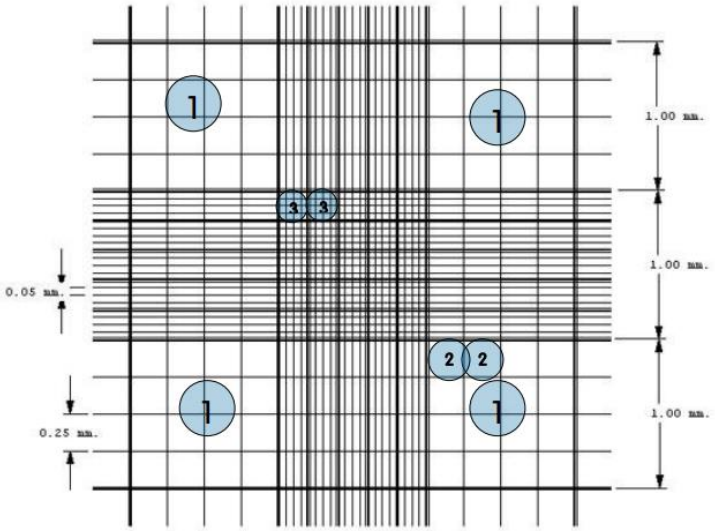

Figure Error! No text of specified style in document.**-1 Neubauer-improved chamber counting grid detail.** The maximum concentration for a cell count with Neubauer chamber is approximately 2.5 *10^6 cells /ml. The formula to calculate cells/ml is $C = \frac{NUMBER\ OF\ CELLS * 10{,}000}{No.of\ squares\ counted}$ where C is the cell count per ml.

To test effects on growth/doubling rate of the interested compounds, cells were diluted in fresh HL5 to a final concentration of 10^5 cells/ml with compound added. At intervals, approximately 0.1 ml aliquots were removed from the cell culture under sterile conditions and the cell concentration was determined using a haemocytometer under x400 total magnification. Solvent only controls were carried out for all experiments to ensure cell response resulted only from the treatment not the solvent.

The doubling time was calculated over a 3 day period, so a change of media was not required. The doubling time was calculated by taking two measurements of a growing culture, quantity q1 at time t1 and q2 at time t2 and, assuming a constant growth rate, doubling time was calculated as:

$$T_d = (t2 - t1) * \frac{\log(2)}{\left[\log\left(\frac{q_2}{q_1}\right)\right]}$$

2.1.4 *Dictyostelium* fruiting body development

Cells were grown at 22 ºC in shaking culture in HL5 medium to $5x10^6$ cells/ml. Effects on aggregation were analysed by plating cells on a 3.5 cm plates of phosphate (KK2) buffer (20 mM K_2HPO_4/KH_2PO_4 (Sigma-Aldrich) pH 6.2) and 1% bacteriological agar (Sigma-Aldrich) plates at $5x10^5$ cells/cm^2. The plates were kept in humid conditions and incubated at 22 °C for the desired time period. Development is observed within 6 – 9 h, depending on the strains used.

2.1.5 Determination of viability

Dictyostelium cells were washed and then re-suspended to $2x10^5$ cells/ml in KK2 buffer. Cells were incubated with the compounds of interest for 27 min and then stained with 0.4% trypan blue solution for 3 min (30 min total incubation with the compounds) prior to live counting. Dead cells were scored by distinctive blue staining as live cells with intact cell membranes are not stained.

2.1.6 Phagocytosis assay

Cells were washed and resuspended in Sorensen phosphate buffer (pH 6.1) at a cell density of 10^5 cells/ml, where appropriate incubated with a test compound was. At intervals, the compound was washed out by a 1:100 dilution aliquot of incubation solution in SM broth. The number of cells present in the culture was determined, and approximately 100 cells were inoculated onto a *K. aerogenes* lawn for plaque counting on a bacterial food source. Plaque diameters were recorded after incubation of plates for 4 days at 22 ºC, indicating growth of *Dictyostelium* from single cells. Under control conditions, the proportion of cells forming plaques – zones of phagocytosis - was enumerated at > 95%.

2.1.7 Adhesion assays

2.1.7.1 Cell to Substrate

Cell to substrate adhesion was analysed in HL5 medium in the presence or absence of 10 mM ethylenediaminetetraacetic acid (EDTA); (Sigma-Aldrich). Approximately 500 cells in 50 µl were deposited on a microscope slide and incubated at room temperature for 45 min. Excess liquid was removed and cells were counted (initial number N_0). Slides

were dipped 20 times in Phosphate buffered saline (PBS); (20 mM KH_2PO_4, 10 μM $CaCl_2$, 1 mM $MgCl_2$, pH 6.1), and the adhered cells photographed and counted (final number ***N***). Assays were repeated four times. Cell-substrate adhesion was defined as:

$$Adhesion\ rate = \left(\frac{N}{N_0}\right) \times 100\%$$

2.1.7.2 Cell – cell Adhesion

Assays were performed in triplicate as described (Geltosky *et al.*, 1979) with minor modifications. Cells were developed for various times, resuspended in PBS. The number of non-aggregated cells was the sum of single cells and two-cell aggregates (final count). The total number of cells was determined by disaggregating the cells by repeated pipetting (initial count). Cell-cell adhesion calculated from (initial count − final count)/(initial count).

2.1.8 Cell locomotion test

Cells were pulsed for 4 h with 30 nM cyclic adenosine monophosphate (cAMP) (Sigma-Aldrich) at 6 min intervals whilst shaking at 120 rpm. Cells were washed three times with cold KK2 solution, resuspended to a final concentration of 10^7 cells/ml and then sample was placed on a thin layer of agar. The sample was allowed to settle and the excess suspension was removed after 15 min. 10 cells were observed under a phase-contrast microscope for 2 – 3 h to trace their movements. Locomotion from point A to B was represented by the average speed of the cells in micrometres per h.

2.1.9 Cytokinesis defect assay

To investigate cytokinesis defects, cells were cultured in a shaking suspension for 24 h and fixed with 100% methanol at -20 ℃ for 15 min before being fluorescently labelled with 4', 6-diamidino-2-phenylindole (DAPI) (Sigma-Aldrich) to visualise and count the number of nuclei per cell.

2.1.10 Chemotaxis assay

2.1.10.1 Dunn chamber chemotaxis assay

Cells were pulsed for 4 h with 30 nM cAMP at 6 min intervals whilst shaking at 120 rpm. Cells were then washed in KK2 buffer and resuspended at the concentration of 10^7 cells/ml and used in the Dunn chamber assay, migrating toward 5 mM cAMP. A stable chemotactic gradient was allowed to form over a 30 min period, prior to recording cell shape and position. Cell images were recorded every 15 s over a 15 min period, with the initial 4 min period recorded prior to addition of test compounds to the outer well of the Dunn chamber. A minimum of three independent experiments for each drug/concentration and an average cell number of 10 cells quantified per experiment.

2.1.10.2 Cell behaviour assay

Cells were pulsed and resuspended at $2x10^5$ cells/ml, and 250 µl aliquots of cells were added to Lab-Tek 8-well chambered cover glass wells and allowed to adhere for 20 min. Cell movement was recorded as above at intervals of 20 s for a total of 20 min (in the absence of a chemotactic gradient).

In compound testing experiments cells were allowed to establish a baseline velocity for 5 min, prior to the addition of the test compounds to give required final concentrations. Following 5 min chemical exposure, cell buffer containing chemicals was aspirated from the chamber and replaced with 250 µl KK2 buffer and cells were monitored for a further 20 min. All experiments were performed in a minimum of triplicate individual assays.

2.1.10.3 Chemotaxis under agarose assay

Three troughs were cut in 1% SM agarose (Sigma-Aldrich) gel in the centre of a Petri dish. 0.1 mM folate was placed in the centre trough and incubated for 1 h to allow the gradient to develop. Cells were pelleted and resuspended in SM broth to a final concentration of $5 x10^6$ cells/ml. 150 µl of cell suspension was added to each trough and given 30 min to adhere. Speed of the cell population was determined by measuring the distance the leading cells had moved away from the trough edge at a particular time point. Data from 20 cells were used to calculate the mean distance the front-most cells had migrated. The time it took the cell front to travel to successive distance points was used to determine cell front speed (Figure 2-2).

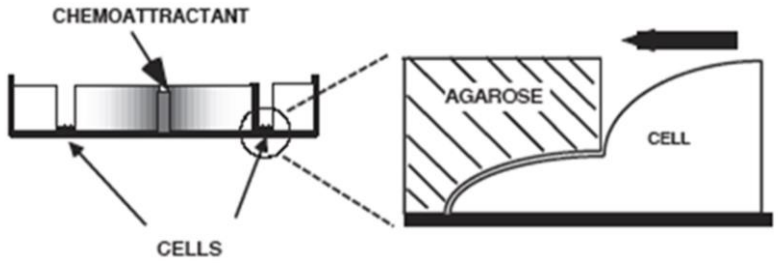

Figure Error! No text of specified style in document.**-2 The schematics of under agarose assasy.** Three 2 mm wide troughs are cut thorough the agarose 5 mm apart. The centre trough contains the chemoattractant with cells in the outer troughs. Cells migrate underneath the agarose to move towards the chemoattractant**.**

2.1.10.4 One drop chemotaxis assay

200µl cell suspension was spun down and the pellet resuspended in 20 µl KK2 buffer. Ten drops of 0.1 µl of the cells suspension were laid out as a line on 1% KK2 agar plates containing 10 nM cAMP. The drops were allowed to dry for 10 min and the results were scored every 20 min by inspection of the drops under a dissection microscope. For every time point the proportion drops showing a positive response is recorded for each strain (Figure 2-3).

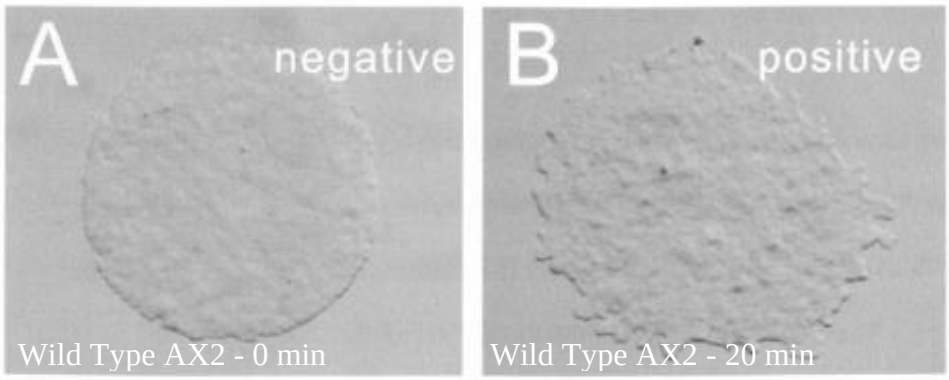

Figure Error! No text of specified style in document.**-3 Radial one drop assay positive response:** Response of wild type AX2 cells on a cAMP plate

2.1.10.5 Needle chemotaxis assay

Chemotaxis analysis was performed as described previously (Gerisch *et al.*, 1975). AX2 and mutant cell lines were grown to densities below $5x10^6$ cells/ml, harvested, washed, and resuspended in KK2 buffer to a density of 2×10^7 cells/ml and pulsed with 30nM cAMP for 5 hours at 6 min intervals. A 10 µl Hamilton needle (Hamilton company Reno, Nevada, USA) filled with $1x10^{-4}$M cAMP solution was brought into the field of

view of microscope. The response of the cells was recorded by taking photographs every 5 s for 3 min.

2.1.11 Phototaxis assay

$3x10^6$ cells were resuspended in 30 µl H_2O and inoculated into a petri dish containing 0.5% w/v activated charcoal in 1% w/v agar. The drops were placed 1 cm from the plate's periphery. The Petri dishes were incubated in a box with a small lateral hole, opposite the inoculation point, as a unidirectional light source. Temperature was kept constant at 22 °C. Approximately 48 h after inoculation, slime trails were blotted onto nitrocellulose filter paper (Fisher Scientific, Loughborough, and Leicestershire, England) and stained with Coomassie blue (Fisher Scientific) for 30 min followed by de-staining in 7% acetic acid.

2.1.12 Transmission electron microscopy

Cultures were grown in Petri dishes to 10^6 cells/ml. Fixation was carried out in nutrient rich media (HL5) with 2% glutaraldehyde (Sigma-Aldrich) and 1% paraformaldehyde (PFA) (Sigma-Aldrich) buffered in sodium cacodylate (Sigma-Aldrich) at pH 7.2 for at least 2 hours at 4 °C. After washing three times with 0.1 M sodium cacodylate buffer pH 7.2 (15 min incubation per change) cells were post fixed with 1% buffered osmium tetroxide (OsO_4) (Sigma-Aldrich) for about 30 min at room temperature. Cells were than washed three times with buffer (15 min per change). 1 ml of the buffer was added and cells were detached with a cell scraper. The cell suspension was transferred to a 1.5 ml microfuge tube and spun down for 5 min at 700 *g*. The pellet was than suspended in 2% agarose. The cells were spun down again at maximum speed for one minute and the agarose was left to solidify in the fridge for 30 min. The solidified pellet was cut with a razor blade into small pieces and dehydrated in alcohol series starting at 30% to 90 % (in 10% steps, 60 min per change). Alcoholic dehydration is finalised with leaving the sample overnight in 100% absolute alcohol. After this the sample was incubated for one 30 min change of (1:1) 100% ethanol (VWR International Ltd., Lutterworth, Leicestershire, England): propylene oxide (Sigma-Aldrich). Dehydration with propylene oxide is completed with three changes of propylene oxide at 4 °C (30 min per change). Embedding is also a step by step overnight process. Start with 2:1 propylenoxide to epon for 15 min then 1:1 for 30 min, 1:2 for an hour and pure Epon overnight. Next day samples were

embedded in freshly prepared Epon in gelatine capsules and left to polymerises at 60 °C overnight. Sections are placed on 300 mesh pioloform filmed grids.

2.1.12.1 Single grid staining

A piece of parafilm was placed in a covered Petri dish. Several drops of 0.5% uranyl acetate (UAc) were placed (one drop for each grid) on the film and the grids were placed upside down onto each drop, so that the tissue was in contact with the staining fluid (Figure 2-4). The dish was covered during staining time (15-25 min) to keep the samples dark. After the staining step is complete, the grid was removed with forceps and washed for about 3 min by moving the grid up and down in a beaker filled with distilled water (dH_2O). Then the grids were placed into another Petri dish with drops of lead citrate. It was important that several pellets of NaOH were positioned within the petri dish near the staining drops to prevent excessive precipitation of lead citrate. Again, the dish was covered during staining (10-15 min). The grids were rinsed drop wise with 0.01 M NaOH for 15-30 sec and then they were dipped in small beaker of dH_2O for several seconds, this is repeated with a second breaker. The remaining water is blotted off using filter paper triangles.

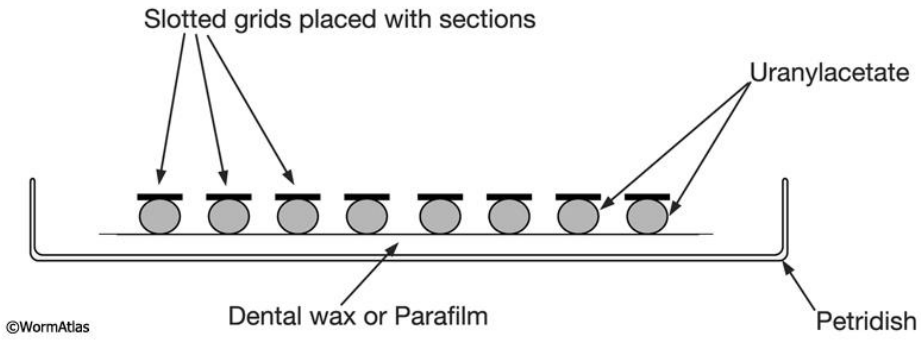

Figure Error! No text of specified style in document.**-4: Schematics of the staining procedure of single grids using uranylacetate or lead citerate.**

2.1.13 Succinate dehydrogenase assay

To assess the function of the mitochondrial system, the activity of the mitochondrial marker succinate dehydrogenase was measured in whole-cell lysates. Cells were washed in MES buffer, resuspended at 3 × 107 cells/ml, and lysed by forced passage through a 5-μm pore filter (Schleicher & Schüll). To measure succinate dehydrogenase activity, 10–

50 µl of whole-cell lysate were mixed with a buffer containing 40 mM sodium phosphate (pH 7.4), 250 µg/ml 2,6-Dichlorophenol Indophenol, (DCPIP; Sigma-Aldrich). 10 mM sodium succinate to a final volume of 500 µl and incubated at room temperature. After 30 min the reaction was stopped by the addition of 500 µl 2% SDS, and absorbance was measured at 600 nm.

The data were normalized with respect to total protein content of the cells, as determined with Bradford reagent (Bio-Rad) according to the manufacturer's instructions.

2.2 Molecular Biology methods

2.2.1 Polymerase chain reaction

DNA was amplified by polymerase chain reaction (PCR) under the following conditions: 1 µl of DNA, 12.5 µl Dream Taq (MBI Fermentas, Sunderland, Tyne and Wear, UK) 2x buffer and 1.5 µl of each primer (10 pmol) were used in a 20 µl reaction. The PCR was carried out under the following cycling conditions: initial denaturing 10 min at 95 °C, 30 cycles of denaturation for 30 sec at 95 °C, annealing at the appropriate temperatures for 45 sec and extension for 4 min at 68 °C (or 1 min at 72 °C depending on the primer), followed by a final extension of 10 min at 68 °C (or 72 °C). Samples were then stored at 4 °C.

2.2.1.1 Gel electrophoresis

Products were resolved on a 1% agarose (Sigma-Aldrich) 1x TAE gel. Generally used a 100 ml gel containing 5 µl of GelRed (10mg/ml stock; Sigma-Aldrich) with an 11-tooth comb. GeneRuler 100 bp plus and 1 kb DNA Ladder (MBI Fermentas, Sunderland, Tyne & Wear, England).

2.2.2 Preparation of competent cells

10 ml of Luria Bertani (LB); (Sigma-Aldrich) medium was inoculated with cells from a single colony of *E. coli* host strain in sterile condition and incubated at 37 °C overnight. 50 ml LB medium was inoculated with 1 ml of overnight culture. The culture was incubated at 37 °C in the shaker until OD_{600} 0.6 was reached. The culture was aseptically

transferred to a 50 ml sterile centrifuge tube and chilled on ice for 10 min. Cells were pelleted down and resuspended in 20 ml ice cold sterile 50 mM $CaCl_2$ solution and left on ice for 15 min. Cells were pelleted down again and resuspended in 2 ml of ice cold sterile 50 mM $CaCl_2$ Solution. The cells were stored at 4 °C for further use.

2.2.3 Transformation of competent cells

10 µl of ligation mix was added to 100 µl of competent *E. coli* cells. After the 30 min incubation on ice, the cells were heated at 42 °C in a heat block for 60 sec and then immediately transferred to ice for 2 min. 800 µl LB medium was added to the cells and incubated at 37 °C for 1 h. After incubation, cells were spun down in a centrifuge and the LB media was removed. The cells were resuspended in 100 µl fresh LB broth, plated onto LB agar plates with 100 µg/ml ampicillin, and incubated at 37 °C overnight.

2.2.3.1 Plasmid preparation

Plasmids used for cloning and sequencing were prepared using the Qiagen Plasmid Midi Kit (cat no. 12145, Qiagen, Hilden, Germany) as described by the manufacturers.

2.2.3.2 Restriction digests

All restriction digests were prepared according to the following conditions: in a 20 µl reaction, 10 µl of DNA was combined with 0.2 µl of restriction enzyme and 2 µl of the appropriate buffer. Reactions were incubated at desired temperature for specific time period as needed.

2.2.3.2.1 Restriction Enzymes

All restriction enzymes and the corresponding buffers (MBI Fermentas) and (New England Biolabs, Knowl Piece, Hitchin, UK).

2.2.4 Construction of the knockout (KO) vectors

PCR was used to amplify two fragments internal to the open reading frame of the gene of interest, using AX2 genomic DNA as a template (Figure 2-2). PCR products were purified using the GenElute PCR purification kit (Qiagen) protocol. The pLPBLP vector and gene fragments were double-digested with suitable restriction enzymes, and then each fragment was separately cloned into the pLPBLP vector backbone (Figure 2-7). The double digested PCR products were ligated into pLPBLP vector backbone using 1 µl T4

DNA ligase (MBI Fermentas) and it's appropriate buffer, at different ratios of insert**:**vector (10:1 and 100:1) and incubated at room temperature for 1 h. The constructs were transformed into chemically competent *E. coli* cells and the resulting colonies were prepared using Sigma GenElute Kit according to the manufacture's protocol. To confirm both vector and insert were present, the plasmid preparations were digested with the previously used restriction enzymes. The second fragment was inserted using the same method. After confirmation of the correct insertion of both gene fragments, the construct was transformed into *E. coli* and using the Plasmid Maxi Kit (Qiagen) purified according to the supplied protocol and used to transform *Dictyostelium* cells. A schematic of the knockout procedure can be seen in Figure 2-5.

2.2.4.1 Primers (Sigma-Aldrich) for gene knockout

Primer pair used to amplify regions upstream (5' end) and downstream (3' end) regions of the gene of interest. Restriction sites inserted are given in brackets

- ***rhmA* primers**

Upstream - Forward (*Apa*I)
AAAGGGCCCTATTAAAGGAGCGACAACAAGAATAAGGGATGGAGTTGG
Upstream - Reverse (*Hin*dIII)
ATGGAAGCTTTGGTTTCTTGCCATCTGTACGACCTCCACCACC

Downstream - Forward (*Not*I)
5'-CAGCGCGGCCGCTGCCATCATTAACACCAAAGAGAGAGCAATTGGAA-3'
Downstream - Reverse (*Sac*II)
5'-CAACCGCGGTAATACGCGAAAATCAGTTGCAAAACCATTGAC-3'

- ***rhmB* primers**

Upstream - Forward (*Apa*I)
TGTGGGCCCAAAGTGTATGACACTTGTCCCACCCTTTTTTTTAATTTCC
Upstream - Reverse (*Hin*d*I*II)
TAAAAGCTTCACTTGAAATACATGATCCGATTTTAGTTGTAAATGATGGTTG

Downstream - Forward (*Not*I)
GTTGCGGCCGCACTTTTGGTATCTGCCTATTTCGCATACGATTTATATAATG
Downstream - Reverse (*Sac*II)
AGGCCGCGGAAGTAATTTAGGAATAGCAACACTAAATAGGGAAAAGATCT

- ***rhmC* primers**

Upstream - Forward (*Kpn*I)
GAAGGTACCCGAACACTTGATCTATTCAAGA
Upstream - Reverse (*Hin*dIII)
RD59-5'1R CCAAAGCTTCCAAATATTGCTCCTACTATCCTG

Downstream - Forward (*Bam*HI)
CAAGGATCCCCACAACAACATCAAAGAGATAA
Downstream - Reverse (*Not*I)
RD59-3'1R CCAGCGGCCGCAGTCCATAAACATACAGATGGA

- ***rhmD* primers**

Upstream - Forward (*Kpn*I)
ATTGGTACCAGTATTATGTATAGTTTGGTGTCA
Upstream - Reverse (*Sal*I)
AAAGTCGACATATGATCACTAATCACAAGTGC

Downstream - Forward (*Bam*HI)
ATCGGATCCAAATAGAAAGAAGAAGTAGAAATTAA
Downstream - Reverse (*Spe*I)
ACTACTAGTACTGGATGAACCATCATACATATTC

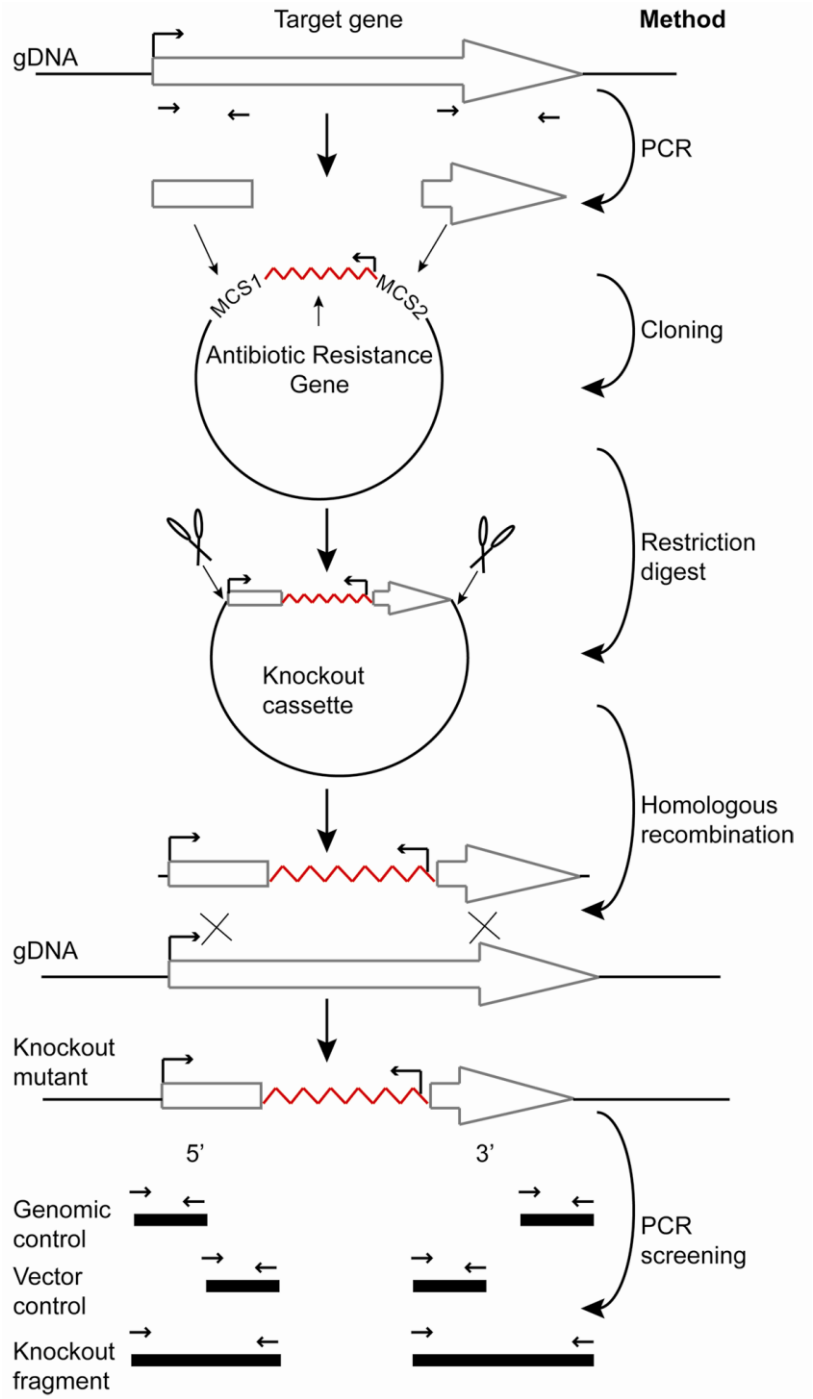

Figure Error! No text of specified style in document.**-5 A schematic showing the method used for cloning and screening of the knockout cell lines** Gene fragments were amplified from gDNA (5' and 3') using PCR and cloned into the pLPBLP vector to create a knockout cassette. The 5' and 3' fragments cloned into the vector at the multiple cloning site (MCS) 1 and 2, respectively, flanking a blasticidin resistance cassette. The orientation or the promoter for the genes or the blasticidin resistance gene is also shown. The knockout cassette was transformed into AX2 *Dictyostelium* cells and correct transformants were identified using PCR screening. The arrows show the primers used in the PCR screening, using a genomic (G) and a vector (V) control and a diagnostic knockout (KO) fragment (unique to homologous integrated transformants). Image reproduced from David Traynor (MRC-LMB, Cambridge) provided protocol for gene disruption in *Dictyostelium*

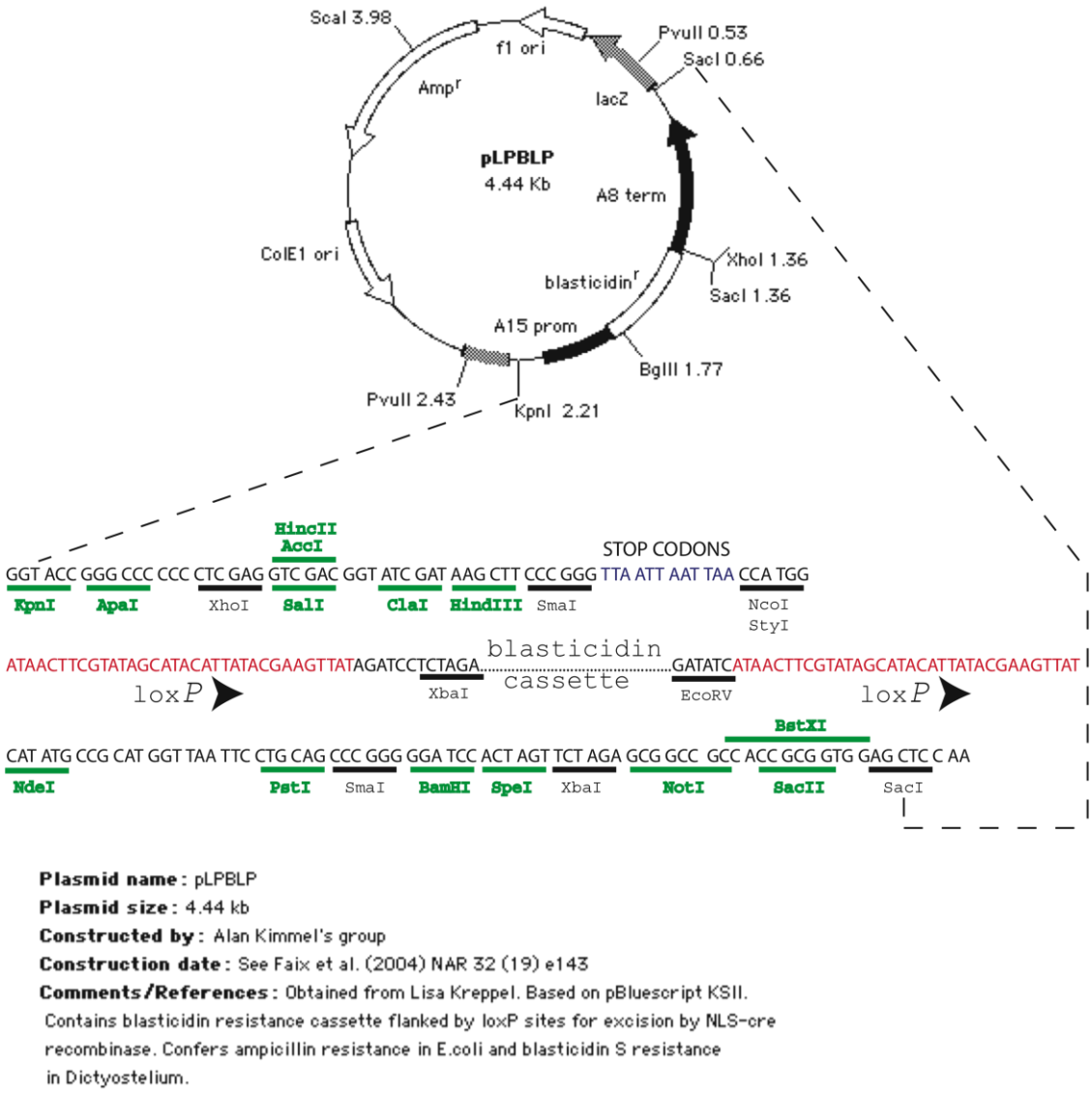

Figure Error! No text of specified style in document.**-6 pLBLP vector map.** This vector is used for gene disruption in *Dictyostelium*.restriction sites in green can be used to clone flanking regions of homology whereas sites in black cannot be used as they are wither not unique or will cut a critical part of the vector, the six stop codons for termination translation of truncated genes after excision of the floxed blasticidin cassette are shown in blue. The loxP sites are shown in red. Image reproduced from David Traynor (MRC-LMB, Cambridge) provided protocol for gene disruption in *Dictyostelium*

2.2.5 Transformation of *Dictyostelium* by electroporation

For the electroporation, 10^7 cells/ml were incubated on ice for 10 min before centrifugation at 800 *g* for 5 min at 4 °C. The cells were then washed once with 10 ml KK2 and then twice with 10 ml sterile filtered H50 (20 mM HEPES, 50 mM KCl, 10 mM NaCl, 1 mM $MgSO_4$, 5 mM $NaHCO_3$, 1 mM NaH_2PO_4 pH7.0). The cells were pelleted $3x10^7$cells/ml were resuspended in ice-cold sterile H50 and incubated on ice for

5 min. 105 µl of the chilled cell suspension and 15 µg of disruption cassette DNA was added electroporation cuvette (1 mm gap) without introducing air bubbles and then place the cuvette on ice for further 10 min. The cells were electroporated with a Bio-Rad GenePulser Xcell electroporator (Bio-Rad Laboratories, Hercules, CA, USA) using 2 pulses (0.75 kV, 25 µF and ∞ Ω). Immediately after the second pulse 500 µl of room temperature axenic medium containing (100 µg/ml streptomycin) was added to cuvette, mixed by inversion and return it to ice for at least 5 minutes. To obtain clones for analysis the entire contents of one electroporation cuvette was emptied into 14 ml of room temperature axenic medium containing antibiotics (100 µg/ml streptomycin) in a 50 ml sterile tube and mixed. The initial suspension was further diluted down by 1:10, 1:50, 1:100 and 1:200. 100 µl of the initial cell suspension was transferred into every well of a sterile flat bottomed 96 well plate using an electronic multichannel pipette with sterile tips. This was repeated for each dilution. After 24 h, 100 µl of fresh axenic medium (containing 100 µg/ml streptomycin) plus 20 µg/ml blasticidin (Sigma-Aldrich) was added to each well. After 3-4 days (at 22 ^{o}C) the medium was removed from each plate by inversion and shaking. 200 µl of fresh axenic medium (containing 100 µg/ml streptomycin) plus 10 µg/ml blasticidin to every well was added to every well. This procedure was repeated once more and by day 10-12 (at 22 ^{o}C) till semi or confluent wells were present in the least diluted plates.

2.2.5.1 Extraction of DNA from transformants

When cells were grown to confluence, 200 µl was removed and the DNA was extracted using the Zymo gDNA kit (Zymo Research, Irvine, CA, USA) protocol. The extracted DNA was then used in a PCR reaction to screen for transformants.

2.2.5.2 Screening for correct mutants

Screening primers were designed to detect via PCR whether the KO gene containing the blasticidin resistance cassette were inserted correctly into the *Dictyostelium* genomic DNA. For PCR analysis combinations of one or both primers corresponding to sequence that lies outside the gene disruption cassette (X and Y from Figure 2-7) and primers within the blasticidin resistance cassette (e.g. primer X with primer Y; primer X with BSR1B

and primer BSR2B with primer Y) were used. The primers that were used that correspond to sequence from within blasticidin resistance gene (Figure 2-7) are BSB1B and BSRB2.

BSR1B 5'-CAT TGT AAT CTT CTC TGT CGC TAC TTC TAC-3'

BSR2B 5'-GTG TAG GGA GTT GAT TTC AGA CTA TGC ACC-

Figure Error! No text of specified style in document.**-7 PCR analysis of the clones.** Primer X and Y lie outside the gene disruption cassett. Primers within the disruption cassette are; BSB1B [points towards Actin15 promoter (A15) of the blasticidin resistance cassette) and BSRB2 (points towards Actin8 terminator (A8) of the blasticidin resistance cassette]. Note that sequencing primers BSR1A and BSR2A can also be used for screening.

2.2.5.3 Sub-cloning of correct transformants

After confirmation of correct transformants using PCR, those colonies were selected for dilution in 200 µl exponentially growing culture of *K. aerogenes* in SM broth and spread onto a sterile SM agar plate. The plates were incubated at 21 °C for 3-4 days, and the resulting sub-cloned colonies were again screened using the same screening primers previously used.

2.2.6 Overexpression of fluorescently tagged protein

Overexpression plasmids containing c-terminal GFP fused to full length cDNA of RhmA and RhmB were made by using the pDT29 (Figure 2-8) kindly provided by D. Traynor (MRC-LMB, Cambridge, UK). The plasmids were transformed in to competent *E. coli* and prepared using Plasmid Maxi Kit (Qiagen). 1ng of each plasmid was transformed via electroporation in wild type AX2 or relevant mutant cell lines (as described above). After selection with 50 µg/ml G418 (Sigma-Aldrich) for approximately 2 weeks, correct transformants were selected and analysed using Nikon Fluorescence microscope.

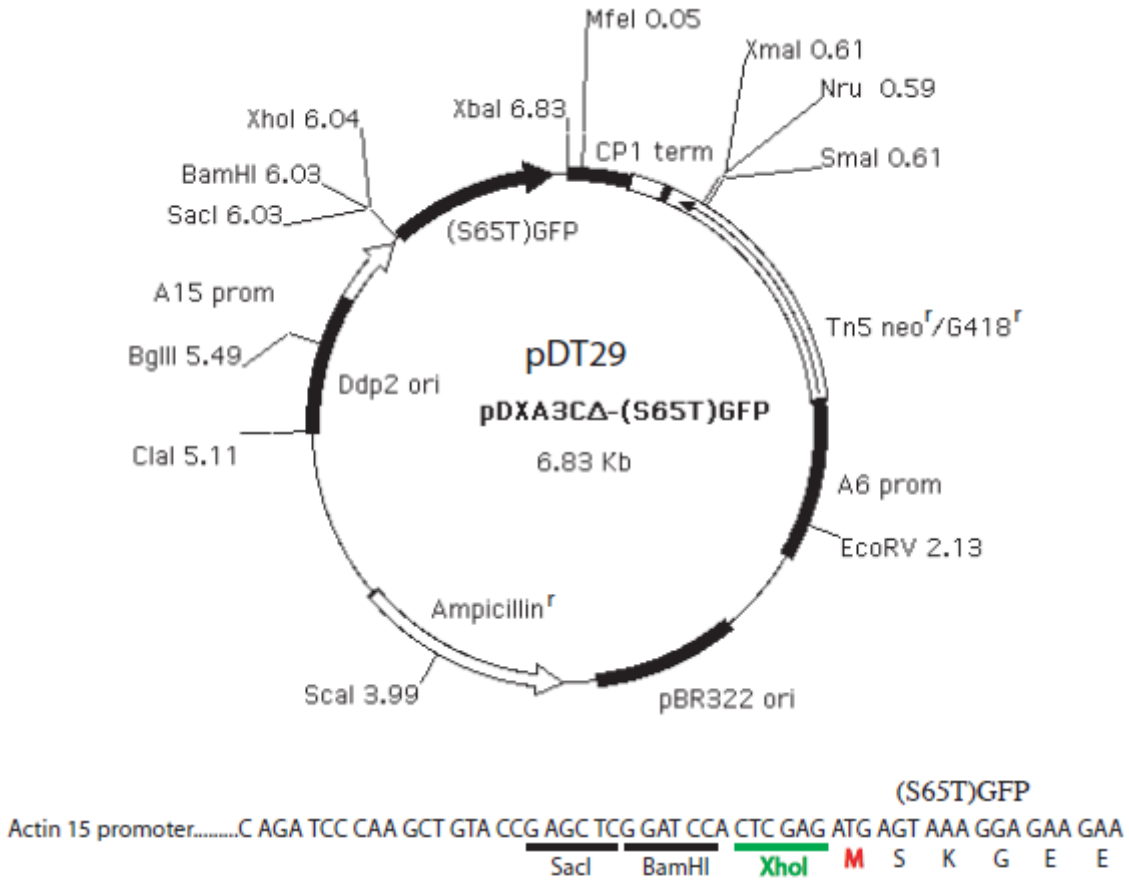

Figure Error! No text of specified style in document.**-8 Vector map of pDT29.** Genes to be expressed with (S65T)GFP fused at their C-terminus must contain an ATG and must not have a stop codon. The codon usage of the GFP is Jellyfish and was amplified by PCR as a *Xho*I/*Sal*I fragment from the cAR1-GFP plasmid (pZX2) and cloned, in the correct orientation, into the *Xho*I site of pDXA3C . Confers ampicillin resistance in *E.coli* and G418 resistance in *Dictyostelium*. The CP1 terminator contains sequences at both ends that act on the neomycin resistance transcript and the EGFP fusion transcript. This plasmid will be extrachromosomal in *Dictyostelium* strains expressing the Ddp2 ORF (ORF+ cells). In all other strains it will integrate.

2.2.6.1 Primers (Sigma-Aldrich) for GFP overexpression

*Sac*I restriction site was inserted in the forward primer, with *Xho*I in the reverse so the gene of interest could be in frame with the GFP.

- ***rhmA***

Forward – AAA GAGCTCATGTCCACATTAAAAAAGTT TTCTATTAAAGGA
Reverse – TTT CTCGAGGTCTTACACCAACTTAATACTTGA

- ***rhmB***

Forward – ATTTAAAGAGCTCATGAATAGAGGATTTAA
Reverse – ATTTCTCGAGGAATCTTCTTCTATTTGCT

- ***rhmC***

Forward – ACAGAGCTCATGATTTATGGTGATACAAGAG
Reverse – TCGCTCGAGTTTTGAGAAATCATATTCATC

- ***rhmD***

Forward - AACAAAAAAGAGCTCATGATAAGTTCGTCAA
Reverse - ATTCTCGAGATTTCTACTTCTTCTTTCTATTTGATC

2.2.7 RNA extraction

Cells were harvested at $2x10^7$ cells/ml before being washed with KK2 buffer at 4 °C. RNA was extracted using the RNAeasy kit (Sigma-Aldrich) according to the manufacturer's instructions.

2.2.8 Reverse transcriptase PCR

RNA was treated with the DNase I kit (New England Biolabs) to remove residual DNA contamination as described by the manufacturer. cDNA was synthesised from 1µg of RNA using the Fermentas First Strand cDNA synthesis kit Taq (MBI Fermentas) and Oligo. The 2 µl of the cDNA was used in a PCR reaction as previously described.

2.2.9 Quantitative real time PCR

Quantitative real time PCR, (qPCR) was carried out on Step one machine (Applied Biosystems, Waltham, Massachusetts, USA) using the SYBR Green method. This required a double-stranded DNA dye in the PCR reaction which bounds to newly synthesised double-stranded DNA and produces fluorescence. cDNA was amplified by

PCR under the following conditions: 0.5 µl of cDNA, 5 µl 2x QuantiFast Syber Green PCR master mix (Qiagen) and 1 µl of each primer (10 pmol) were used in a 10 µl reaction. PCR was carried out under the following cycling conditions: initial denaturing 10 min at 95 °C, 40 cycles of denaturation for 30 sec at 95 °C, annealing for 40 sec at 56 °C and extension for 50 sec at 61 °C. Samples were then stored at 4 °C.

2.2.9.1 Primers (Sigma-Aldrich) for qPCR

- ***H7 (Cycloheximide-INducible -1)* – Ref**

H7Q1_F: ATCCATCAGTACCACAAGCA
H7Q2_R: AAGAACAGCTTGACTTGGGA

- ***ecmA* (pstA cells*)***

ecmA_F: TGCGGAAACTGAAACCATAC
ecmA_R: TGGAATGTGAACTACACCAGT

- ***pspA* (Pre spore) Spore Cells**

pspA_F: GTCCGTTACATTCCTGATGC
pspA_R: ACTCCACTCCAATCAGAACC

- ***carA-1***

carA-1_F: GTATCCCATGGTTTTTGGGC
carA-1_R: CCAGAAGTACCACGACTTGA

- ***rhmA***

rhmA-2_F: GGTAGAGGTAGGGGTAGAGG
rhmA-2_R: GGATTGGTTTTCCATGGCTC

- ***rhmB***

rhmB-2_F: CTTAGGAGCATCAGGAGCAA
rhmB-2_R: GGCAGATACCAAAAGTGCAG

- ***rhmC***

rhmC-2_F: CTCGCAACCAAAGTGATTTCT
rhmC-2_R: AACCAAACATTGAAGGTGCT

- ***rhmD***

rhmD-2_F: CAGCATTGGCACTTTTCGAT
rhmD-2_R: ACCAACTAACGTTGAGCCTA

2.3 Proteomics

2.3.1 Pull down assays

GFP trap beads assays to pull down potential rhmA binding partners was performed using Chromotek- GFP trap beads (Chromotek, Germany) according to the protocol provided by the manufacturer. The only change was to double recommended concentration of the protease inhibitor cocktail to inhibit degradation of potential substrates by the rhomboids themselves. The eluted proteins were analysed using Coomassie blue stain of an SDS page gel.

2.3.2 SDS Page analysis

12 % SDS PAGE as described by Laemmli (1970) was used to analyse the protein expression using Mini-PROTEAN Tetra Cell (Bio-Rad). 12% resolving gel and 4% stacking gel was made (Table 2-2)

Table Error! No text of specified style in document.**-2 Recipes for making stacking and resolving gels**

Components (Sigma-Aldrich)	**Stacking Gel**	**Resolving Gel**		
	4%	8%	12%	X%
30% acrylamide/ bisacrylamide	1.98 ml	4 ml	6.0 ml	0.5 * X ml
0.5 M Tris-HCl containing 0.4% SDS, pH 6.8	3.78 ml	-	-	-
1.5 M Tris-HCl containing 0.4% SDS, pH 8.8	-	3.75 ml	3.75 ml	3.75 ml
dH_2O	9 ml	7 ml	5 ml	11-(0,5*X) ml
10% SDS	150 µl	150 µl	150 µl	150 µl
TEMED	15 µl	7.5 µl	7.5 µl	7.5 µl
10% APS	75 µl	75 µl	75 µl	75 µl
Total Volume	15 ml	15 ml	15 ml	15 ml

10% APS = ammonium prepared fresh, TEMED = Tetramethylethylenediamine, SDS = Sodium dodecyl sulfate, Tris-HCL = Trizma® hydrochloride

After polymerization, the gel plates were fixed in electrophoresis apparatus in placed in the gel tank (BIO-RAD, Singapore). Tank was filled with gel running buffer (1X Tris-Glycine) up to the marked area for 2 gels. Sample was loaded in the well run the gel at 40V till it enter into the resolving gel then the current was increased to 121V using power

supply, 5µL of protein standard ladder (MBI Fermentas) was run along with the sample in a separated well to compare the proteins sizes. Gel was run at a constant current supply 150 volts.

2.3.2.1 Coomassie staining and destaining

The gel was then stained in Coomassie solution prepared by dissolving 50mg dye in methanol: acetic acid: H_2O (45:9:45) and destained with a mixture of methanol (10%) and acetic acid (20%) in water. Gel was stored in destaining solution and photographed.

2.4 Image acquisition and microscopy

Cell were analysed using Nikon (Kingston Upon Thames, Surrey, UK) upright Eclipse 90i microscope or Nikon Eclipse Ti (inverted microscope) (10x 40x and 60x oil immersion objective used). Microscopy images were captured using image Nikon. Images taken were quantified using ImageJ (U. S. National Institutes of Health, Bethesda, Maryland, USA), Quimp11 plugin (University of Warwick, Coventry, UK) was used to analyses cell chemotaxis and movement. TEM images were captured using Gatan Digital Micrograph (Gatan, Pleasanton, CA, USA) and Hitachi SU8030 (Hitachi High-Tech, Tokyo, Japan).

2.5 Websites

http://dictybase.org/

http://dictyexpress.biolab.si/

http://dictybase.org/tools/blast

http://www.ncbi.nlm.nih.gov/BLAST/

http://www.ebi.ac.uk/Tools/msa/clustalw2/

2.6 Statistics

Statistical significant was calculated by using Paired student t-test method unless stated otherwise.

Chapter 3
Identifying *Dictyostelium* Rhomboids

3.1 Introduction

Homologues of rhomboids are found in all branches of life, but the amino acid sequence similarity is strikingly low, around 6% (Freeman, 2009). This may be partly because the proteins are widespread but also that proteins comprise of predominately transmembrane helices may experience different evolutionary pressures on those domains, than cytosolic domains. This chapter, describes approaches that were used to identify and predict location of rhomboids in *Dictyostelium*. To gain a more detailed understanding of the structural characteristics of these proteins and their evolutionary conservation throughout different kingdoms, protein BLAST analysis, sequence alignment, phylogenetic and domain structure analysis were performed.

3.1.1 The first rhomboids

The first rhomboid protease was identified by Mayer and Nusslein-Volhard, in 1988: it was the mutated protein Rho-1 in *Drosophila* embryo that led to an abnormally pointed (rhomboid-shaped) head skeleton (Lemberg & Freeman, 2007a). Rho-1 was found to be the primary regulator of EGF receptor (EGFR) signalling in *Drosophila* and a prototype of a widely conserved family of related membrane proteins (Wasserman *et al.*, 2000). Although proteolytic activity of *Drosophila* rhomboid Rho-1 is the most well studied of all. It was the transmembrane domains of prokaryotic rhomboids from *E. coli* and *H. influenzae* GlpG that was first structurally resolved. In 2006 Wang and colleagues published the first high-resolution structure of the *E. coli* rhomboid *ec*GlpG: the 0.21 nm (PDB ID: 2IC8) crystallographic structure (Wang *et al.*, 2006). Lemieux *et al.* (2007) solved the *H. influenzae* GlpG instead of the *E. coli* enzyme. Although crystallised in different detergents and by different groups, the architecture of all of these GlpG was very similar, which formed the basis for modelling rhomboids in other organisms.

3.1.2 Bioinformatics prediction of protein properties

Advances in technology have helped to increase the number of proteins for which the three dimensional (3D) structures can been determined. However, obtaining crystal

structures still remains a difficult and often unpredictable research path. Increasingly features and topological properties of proteins can be predicted by theoretical models. Such prediction software can be used to identify sequence domains specific for locations or activity, for example the zinc finger DNA binding domains that are typical of transcription factors or phosphotyrosine-binding (PTB) domain which are often found in signal transduction proteins.

To better understand the protein structure and localisation of *Dictyostelium* rhomboids, LocTree3 (ROSTLAB; Goldberg *et al.*, 2014), TargetP (CBS, Technical University of Denmark; O Emanuelsson *et al.*, 2000), and PSORT II (Nakai & Horton, 1999, Nakai & Kanehisa, 1992) were used. To predict N-terminal secretory or mitochondrial signals peptides, the prediction programmes SignalP (CBS, Technical University of Denmark; Petersen *et al.*, 2011) and MitoProt (Helmholtz Center Munich; Claros & Vincens, 1996) were employed.

Transmembrane domain predictors used in this study were HMMTOP 2.0 (Hungarian Academy of Sciences; Tusnády & Simon, 1998, Tusnády *et al.*, 2001), SOSUI (University of Nagoya; Hirokawa *et al.*, 1998), TMHMM 2.0 (CBS, Technical University of Denmark; Krogh *et al.*, 2001), TmPred 2.0 (Hungarian Academy of Sciences; (Tusnády *et al.*, 2001)) and Phobius (Stockholm Bioinformatics Center; Käll *et al.*, 2004), the latter being a combined predictor of transmembrane domains and signal peptides with a better discrimination between the two than SignalP (Käll *et al.*, 2004). SignalP 2.0 and 3.0 provides a more in depth analysis of the likelihood of a secretory signal peptide or a signal anchor, and additionally predicts cleavage sites for signal peptidase. Predictions are made using Neural Networks (SignalP-NN) or Hidden Markov Models (SignalP-HMM) trained on eukaryotic sequences (Bendtsen *et al.*, 2004).

A protein's 3D structure is always of great assistance in the study of protein function, and its interactions with ligands and other proteins. Homology modelling can provide low-resolution predicted structures, including information about the spatial arrangement of important residues in the protein and may guide the design of new experiments, for example, site-directed mutagenesis experiments. Homology modelling servers such as Phyre2 (Kelley & Sternberg, 2009), I-Tasser (University of Michigan; Zhang, 2008) and Swiss-Model Workspace (Arnold *et al.*, 2006) work on the observation that two proteins

belonging to the same family share similar amino acid sequences will have similar 3D structures. Chimera (Pettersen *et al.*, 2004) is a simple software program helpful in visualising the structures modelled.

Prediction programs can be powerful tools to gain an initial insight into a protein's likely solubility, anchoring and target compartment. Guidelines and information on the available prediction tools and their optimal usage have been collected and reviewed by Emanuelsson & von Heijne, (2001), and Emanuelsson *et al.*, (2000, 2007).

3.2 Identification of potential rhomboid proteins

Protein BLAST analysis of *Drosophila* Rho-1 against the *Dictyostelium* genome (taxis ID: 352472) generated a number of hits, when optimised for more dissimilar sequences (discontinuous megablast) within the protein collection of the 'non-redundant' database using the DELTA-BLAST (Domain Enhanced Lookup Time Accelerated BLAST (Altschul *et al.*, 1990)). Discontinuous megablast ignores some bases allowing mismatches and is intended for cross-species comparisons (Altschul *et al.*, 1990). Nine sequences produced significant alignments with E-value better than the threshold of E-04 or below. Using the prediction software for transmembrane domains, proteins were further eliminated if they contained fewer than six predicted transmembrane regions. This left only four potential homologues, which have been designated: Rhm A to D (Table 3-1).

Table 3-1 BLAST analysis results of the potential *Dictyostelium* homologues.

	Sequence ID (dictybase)	E-value to DmRho-1	Region
RhmA	DDB0266786|DDB_G0295849	2e-38	236-433
RhmB	DDB0238656|DDB_G0284937	2e-17	143-339
RhmC	DDB0204156|DDB_G0281359	1e-16	35-216
RhmD	DDB0308274|DDB_G0292430	6e-21	176-370

BLAST analysis of a protein orthologues present in the *Dictyostelium* genome, against the genomes of species across various biological kingdoms, revealed the degree of amino acid conservation of each potential homologue. Those with the highest degree of

homology coming from a range of species are presented in Table 3-2. A selection was made from the top results including species from the same genus and species with well-studied rhomboid proteins. The table lists protein size, percentage identity and similarity as well as the e-value.

Table 3-2 *Dictyostelium* protein with the smallest e-value was analysed in this BLAST search.

Dd RhmA	**Protein Length (aa)**	**Identity (%)**	**Similarity (%)**	**E-value**	**Genebank Accession**
Dictyostelium discoideum	489	100	100	0	XP002649151.1
Dictyostelium fasciculatum	490	53	100	1e-165	XP003292594.1
Arabidopsis thaliana	389	28	53	7e-50	NP_180469.3
Drosophila melanogaster	431	20	44	2e-38	AAK06752.1
Caenorhabditis elegans	356	26	47	1e-35	NP_498029.2
Homo sapiens	303	22	54	6e-33	NP_060291.2
Saccharomyces cerevisiae	262	14	43	5e-26	NP_015078.1
Dd RhmB	**Protein Length (aa)**	**Identity (%)**	**Similarity (%)**	**E-value**	**Genebank Accession**
Dictyostelium discoideum	341	100	100	0	XP_639942.1
Dictyostelium purpureum	326	50	62	1e-76	XP003292594.1
Arabidopsis thaliana	336	22	45	5e-29	NP_196342.1
Drosophila melanogaster	355	17	57	1e-29	CAA36692.1
Homo sapiens	383	12	60	9e-26	BAH11675.1
Saccharomyces cerevisiae	346	27	59	3e-24	EWG91070.1
Caenorhabditis elegans	861	17	43	1e-23	NP_503013.2
Dd RhmC	**Protein Length (aa)**	**Identity (%)**	**Similarity (%)**	**E-value**	**Genebank Accession**
Dictyostelium discoideum	344	100	100	0	XP_640745.1
Dictyostelium purpureum	382	38	65	1e-35	XP003288701.1
Arabidopsis thaliana	317	15	52	2e-33	NP_176500.1
Drosophila melanogaster	355	17	54	5e-28	CAA36692.1
Saccharomyces cerevisiae	346	17	52	3e-25	EWG91070.1
Caenorhabditis elegans	1203	16	42	3e-25	NP001041013.2
Homo sapiens	383	16	53	2e-23	BAH11675.1

Dd RhmD	Protein Length (aa)	Identity (%)	Similarity (%)	E-value	Genebank Accession
Dictyostelium discoideum	440	100	100	0	XP_629608.1
Dictyostelium purpureum	431	48	68	8e-74	XP003287798.1
Arabidopsis thaliana	343	21	57	1e-32	NP_173900.2
Homo sapiens	379	32	46	7e-25	NP_061092.3
Drosophila melanogaster	351	22	46	2e-21	NP_523704.1
Caenorhabditis elegans	325	28	41	4e-19	NP_491125.4
Saccharomyces cerevisiae	346	32	51	3e-15	EWG91070.1

The table shows the organism, protein length, % identity, % similarity and e-value. The Blast analysis used the *Dictyostelium* homologue protein sequence for comparison against all other genomes. A selection was then made from the top species results.

From the four proteins identified Rhm A – C were predicted to be part of the subfamily of the secretase group of rhomboids, whereas RhmD was predicted to be a mitochondrial PARL-like rhomboid. All these proteins were predicted to have the general configuration of seven TM and to contain residues characteristic of proteolytically active rhomboids (Chapter 1 for more details). The serine was within the active site of GxSx and the conserved histidine of the catalytic dyad was predicted. Detailed analysis of the *Dictyostelium* rhomboid homologues had not been previously carried out, nor had there been any studies published of ablation of *Dictyostelium* rhomboid homologues.

3.3 Phylogenetic analysis

Phylogenetic analysis of the rhomboid proteins was carried out to better understand the evolutionary conservation of the different subclasses of proteins within this family. As previously described, there are two main families of active rhomboids by structural analysis, and *Dictyostelium* rhomboids were likewise sub-classified as Rho-like and PARL-like secretases. Bootstrap analysis of the consensus tree clustered RhmB and RhmD with all the other PARL-type rhomboids, falling into one clade. This analysis however, also separated the non-PARL rhomboids into different subgroups, indicating a substantial diversification. RhmA and RhmC were both classified Rho-like secretase from other species.

The phylogenetic analysis (Figure 3-1), and alignment data (Figure 3-2) suggests and supports the assertion that homologues found in *Dictyostelium* can be analysed as rhomboid proteins. Characterising the signalling role of the *Dictyostelium* proteins can provide insight into the cellular roles and functioning in other higher eukaryotes.

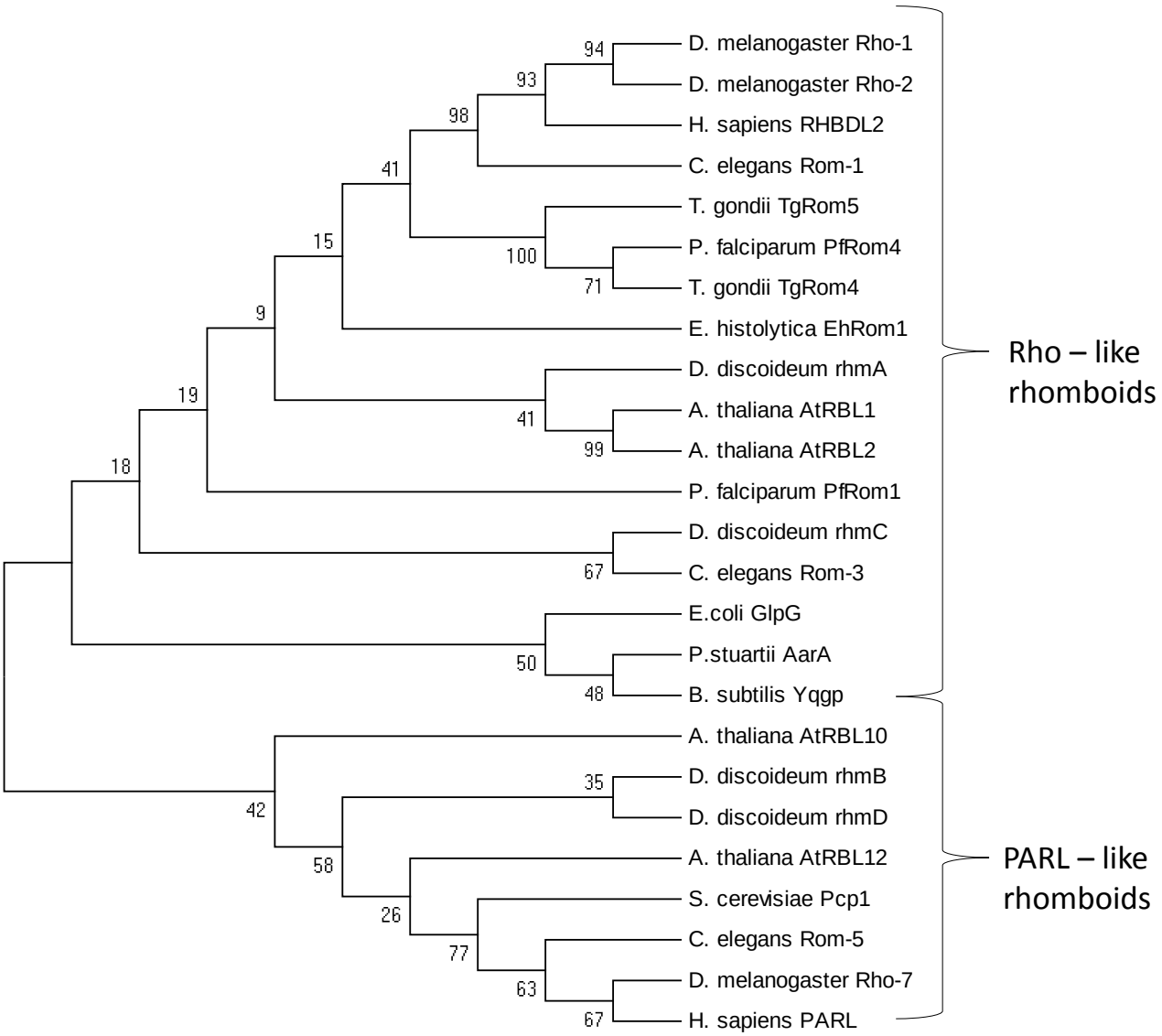

Figure 3-1 Phylogenetic analysis of rhomboid proteins across different kingdoms. The evolutionary history was inferred by using the Maximum Likelihood method based on the JTT matrix-based model (Jones *et al.*, 1992). The bootstrap consensus tree inferred from 500 replicates is taken to represent the evolutionary history of the taxa analysed (Felsenstein 1985). Branches corresponding to partitions reproduced in less than 50% bootstrap replicates are collapsed. The percentage of replicate trees in which the associated taxa clustered together in the bootstrap test (500 replicates) are shown next to the branches. Initial tree(s) for the heuristic search were obtained by applying the Neighbour-Joining method to a matrix of pairwise distances estimated using a JTT model. The analysis involved 25 amino acid sequences. There were a total of 983 positions in the final dataset. Evolutionary analyses were conducted in MEGA6 (Tamura *et al.*, 2013).

3.4 Rho like secretases

Multiple sequence alignments were carried out between the predicted *Dictyostelium* proteins identified above and those from a number of model animal systems, including predicted proteins from humans. Figure 3-2 shows the Clustal Omega (Larkin *et al.*, 2007) sequence alignment of the three Rho-like *Dictyostelium* rhomboid proteins, which serves to highlight the protein motifs conserved across species and with the *Dictyostelium* rhomboids.

The construction of the phylogenetic tree for the proteins across different kingdoms group the *Dictyostelium* homologues; RhmA – D amongst various eukaryotic rhomboid proteins. The inclusion of the *Dictyostelium* homologue in this clade has robust support, as shown by the obtained bootstrap values in the tree (Figure 3-1).

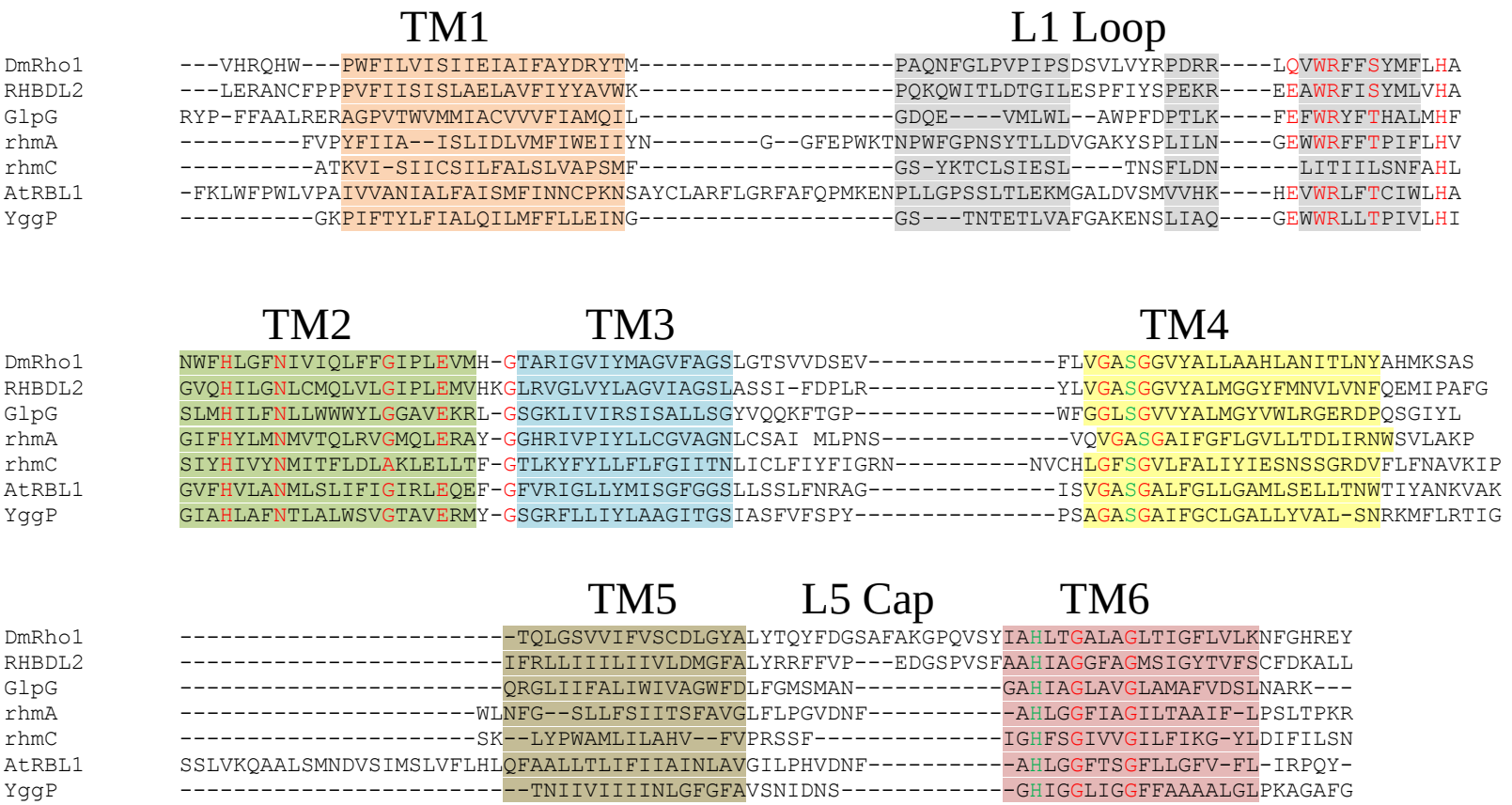

Figure 3-2 Sequence alignments of Rho-like rhomboids from representative species. *Dictyostelium* homologues RhmA and RhmC are shown aligned with the corresponding regions of three other well-studied rhomboid enzymes, GlpG from *E. coli*, DmRho1 (rhomboid-1 from *Drosophila melanogaster*), human RHBDL2, *Bacillus subtilis* YggP and *Arabidopsis thaliana* AtRBL1. N-terminal domains of all enzymes and TM7 and C-terminal domains of DmRho1, RHBDL2 and YqgP are deleted for formatting. Residues involved in nucleophilic catalysis (Ser and His) are shown in green, whereas conserved structural residues are shown in red.

3.4.1 *Dictyostelium* RhmA

Dictyostelium RhmA (Dictybase: DDB_G0295849) was predicted to form seven to eight transmembrane domain depending on the algorithm used (TMHMM used in Figure 3-3C). It was predicted to be positioned in the endoplasmic reticulum (ER) with the N-terminus facing the ER lumen, with a secretory peptide signal highly unlikely. Predictions using Mitoprot and TargetP agreed that there was a very low probability of mitochondrial import. Using E. coli GlpG (protein id: 2IC8) as the template, homology modelling was applied to assess the structural conservation (Figure 3-3A). Using Chimera, the model was visualised alongside with the GlpG (blue) and it can be seen that the model (brown) has high structural similarity to GlpG. Using Ramachandran plots, the quality of the models was assessed: 80% of the residues lie in the most favoured region (Figure 3-3B), i.e. this is predicted to be an appropriate model.

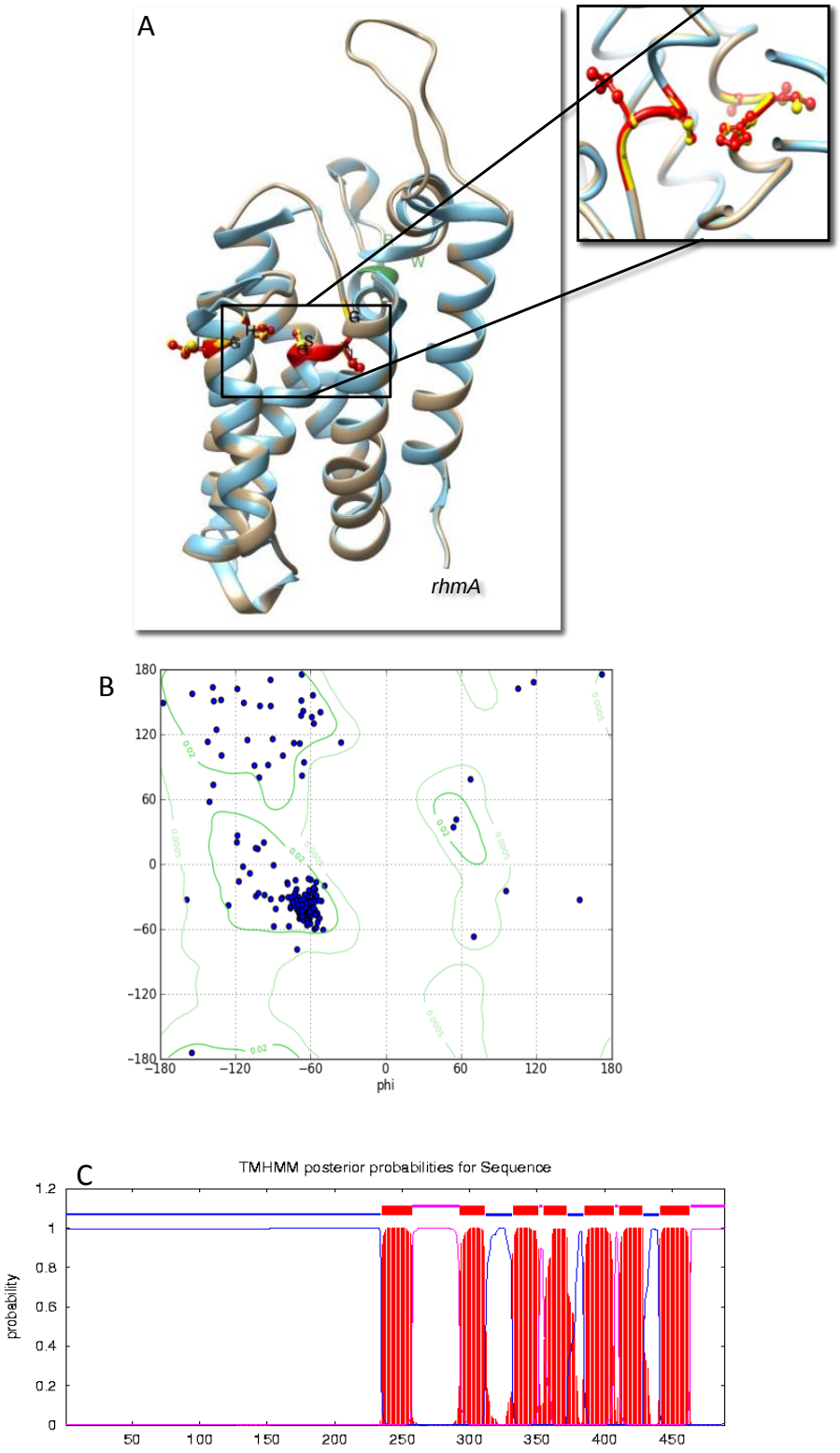

Figure 3-3 In silico analysis of RhmA. (A) Comparison of the crystallographically-determined 2IC8 (Blue) and predicted RhmA (Brown), the structures have been superimposed to see conservation of the motifs required for catalytic activity WR (green) and G*SG (red). (B) Ramachandran plot assessing the quality of the models. Most of the amino acids are found in the favoured region indicating that the model is of good stereochemical quality. (C) Transmembrane prediction plot for *Dictyostelium* rhomboid RhmA using TMHMM2.0. Numbers along the x-axis refer to the amino acids of the protein, with probability of internal (blue line), external (pink line) and transmembrane helix (red blocks) sequences on the y-axis.

Using STRING: functional protein association networks (Franceschini *et al.*, 2013; Snel *et al.*, 2000), proteins that might be associated with RhmA were scored (Figure 3-4 and 3-5). It is apparent from the database experiments data that rhmA could be associated with the dynamin family. The dynamin family and wdr61 (WD40 repeat, transcription factor). The association was concurred by transferring relevant information from *S. cerevisiae* with a probability of 0.706. Their association was later examined (Chapter 4) at transcriptional level in qPCR.

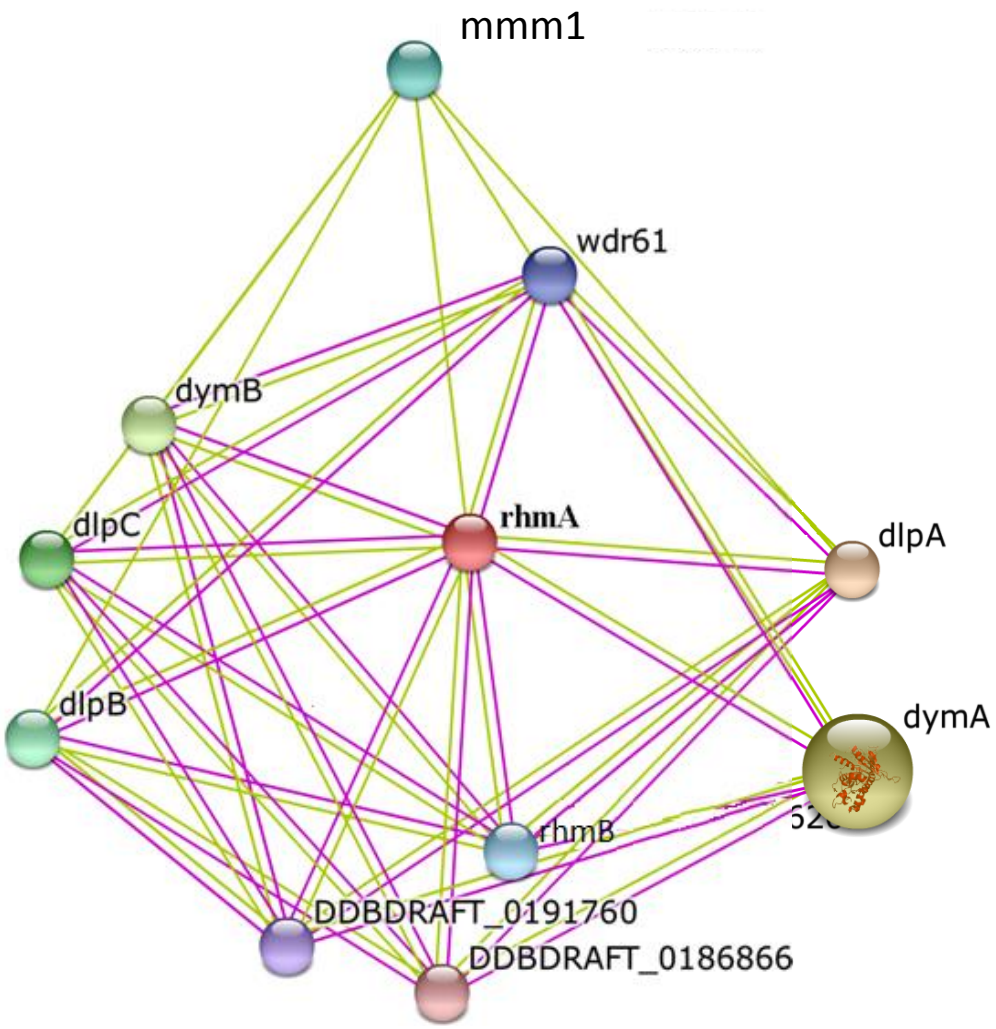

Figure 3-4 RhmA STRING Association network. The *rhmA* gene is shown to be associated with *rhmA* and the dynamin family of proteins not on the basis of just textmining but also through using hybridisation experiments in yeast. The different colour lines show different types of associations; experiments (purple), textmining (mustard). dlp, Dynamin like protein; dym, dynamin; mmm, Maintenance of Mitochondrial Morphology; mrpl, Mitochondrial Ribosomal Protein Large subunit;. wdr61, WD40 repeat- domain.

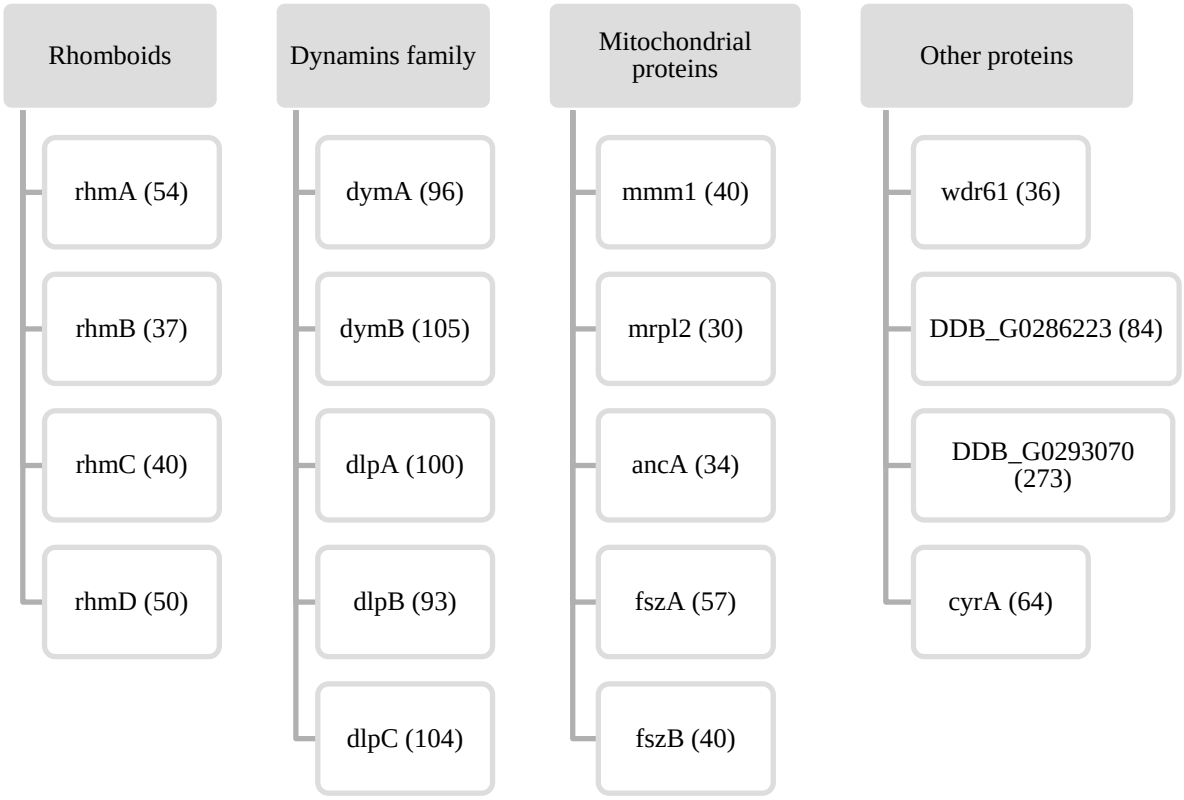

Figure 3-5 List of identified potential rhomboid binding partners. STRING network predicted related proteins or manually identified from the literature. Subdivided by either protein family or function. Sizes in kDa are given in brackets. anc, Adenine Nucleotide Carrier; cyrA, cysteine rich; dym, dynamin; dlp, dynamin-like protein; fsz, mitochondrial division protein; mmm, Maintenance of Mitochondrial Morphology; mrpl, Mitochondrial Ribosomal Protein Large subunit;. The signal transduction proteins all contain the WD40 repeat- domain.

3.4.2 *Dictyostelium* RhmC

Finally, the analysis of the last probable secretase-lie *Dictyostelium* protein, RhmC (Dictybase: DDB_G0281359) yielded the most varying and contradictory results. The software used to predict transmembrane domains gave results from none to at least seven. For example, SOSUI predicted it to be soluble with no transmembrane domains, whereas TMHMM and Phobius assigned four to seven transmembrane domains (Figure 3-6C). Nevertheless using Chimera the model was visualised alongside with the GlpG (blue) and it can be seen the model (brown) has high structural similarity to GlpG (Figure 3-6). Loctree3 predicted it to be a secreted protein with an accuracy of 89%. Even though there was no consensus between the transmembrane domain prediction software, the sequence analysis showed that RhmC had WR in the L1 loop with a catalytic dyad aligning (Figure 3-2) well with other known rhomboid proteins. Phylogenetic analysis clustered it with the TgRom5 of the *T. gondii*, a well-studied and characterized rhomboid protein.

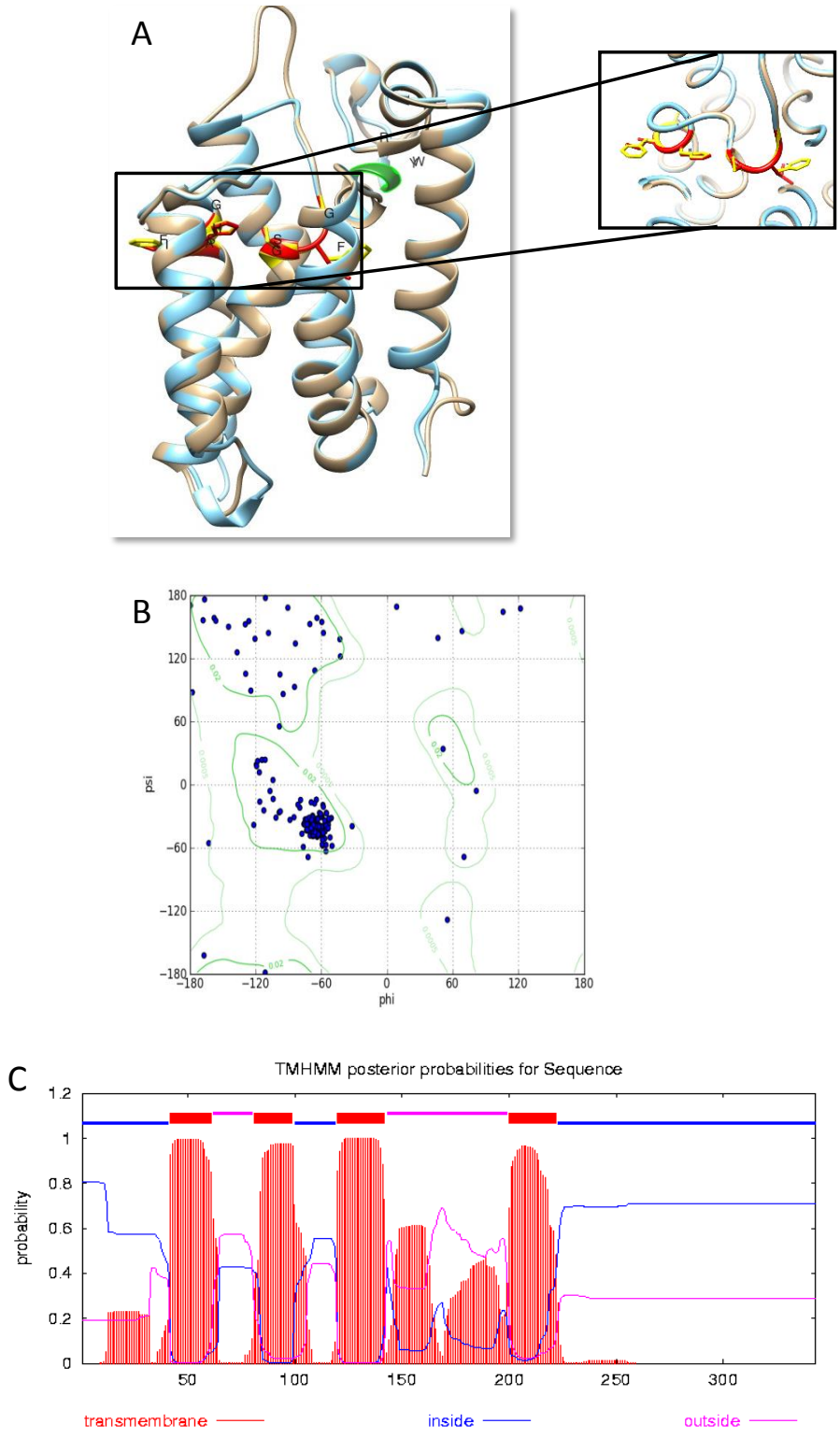

Figure 3-6 Insilco analysis of RhmC. (A): Comparison of the crystallographically-determined 2IC8 (Blue) and predicted RhmC (Brown) conserved motifs WR (green) G*SG (red). (B) Ramachandran plot assessing the quality of the models. Most of the amino acids are found in the favoured region indicating that the model is of good stereochemical quality (C) Transmembrane prediction plots for *Dictyostelium* RhmC using TMHMM2.0. Numbers along the x-axis refer to the amino acids of the protein, with probability of internal (blue line), external (pink line) and transmembrane helix (red blocks) sequences on the y-axis.

3.5 PARL – like proteins

The first mitochondrial rhomboid protein was found in yeast (Esser *et al.*, 2002, Herlan *et al.*, 2003), localised to the inner membrane of the organelle (McQuibban *et al.*, 2003). Soon afterwards it was reported that nearly all eukaryotes have mitochondrial rhomboids, based on sequences databases and prediction algorithms (Lemberg & Freeman, 2007a), which should be considered with caution, as later human RHBDL4 and yeast Rbd2, were predicted to localise to mitochondria using the same algorithms but were actually found in a compartment of the secretory pathway (Lemberg & Freeman, 2007b). This suggests multiple targeting routes which can be difficult to predict. Figure 3-6A shows the sequence conservation between Human PARL and *E. coli* GlpG rhomboids. In PARL like rhomboids there is a strict conservation of aspartic acid in TM5, which is not found in the rest of the rhomboids. This PARL specific Aspartic acid (D319) is critical for activity boxed in red in Figure 3-7 A. The residue points in towards the membrane layer and a rotation of TM5 would bring this residue adjacent to Histidine, where it could serve as a third catalytic residue (Jeyaraju *et al.*, 2013). It can also be seen from the figure that WR in the L1 loop thought to affect catalytic activity in the secretase like proteins (green box Figure 3-7A) is not present in the Human PARL protein.

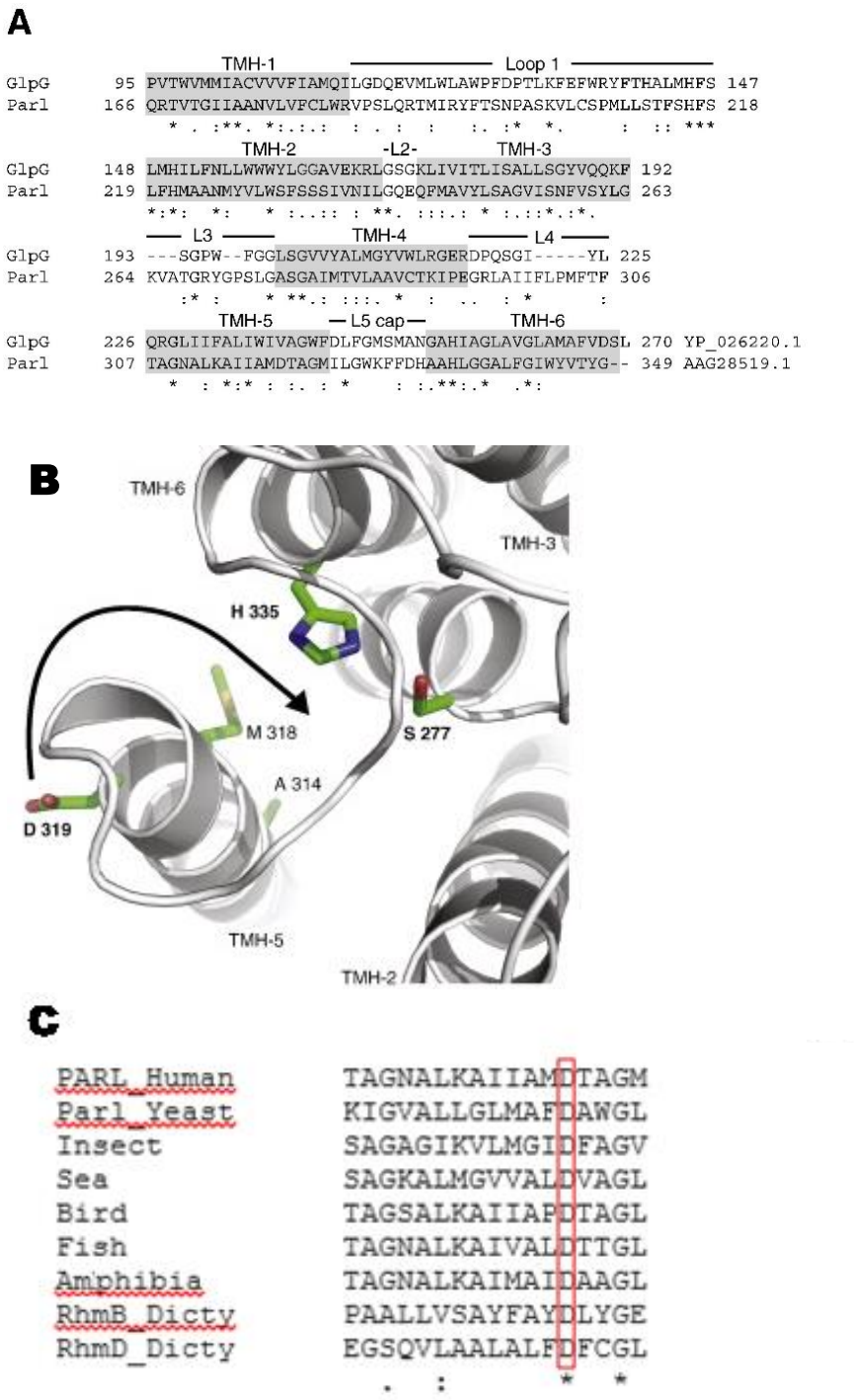

Figure 3-7 Characteristics of PARL-like proteins. (A) Sequence alignment of GlpG and PARL used to build homology models. GlpG is a bacterial rhomboid of known structure that served as a template for homology modelling of PARL rhomboid domain (PROD). (B) The PARL-specific D319 is required for PARL expression and activity, and might serve as a catalytic residue (Jeyaraju *et al.*, 2013). Reproduced from Jeyaraju *et al.*, 2013. (C) Sequence alignments of PROD in different species; *Dictyostelium* RhmB and RhmD contain the conserved aspartic acid (marked in red) in TMD5.

3.5.1 *Dictyostelium* RhmB

The second rhomboid-like serine peptidase RhmB (Dictybase: DDB_G0284937) was predicted to form five to eight transmembrane domains depending on the algorithm used (Phobius used in Figure 3-8C). It also had a very high probability values for import into the mitochondrion using LocTree3 (expected accuracy of 87%) and Mitoprot (probability of 0.9945). Mitpoprot also predicted a cleavage site after residue 65, but SignalP as well as Phobius did not predict a secretory signal peptide. Analysis of the protein sequences revealed conserved aspartic acid in TM5 typical for 'PARL type' rhomboids. The conserved residues E/QxWRxxS/T thought to influence proper catalytic activity are not found in the L1 Loop (see Chapter 1 for details). A 3D homology model based on *E. Coli* GlpG still showed conservation of the rhomboid structure (Figure 3-8A). The reconstruction of the phylogenetic tree of the rhomboid family proteins, across different representative taxa, (Figure 3-1) clustered RhmB in the same clade as the PARL–like protein suggesting that these proteins maybe evolutionarily derived from a common protein.

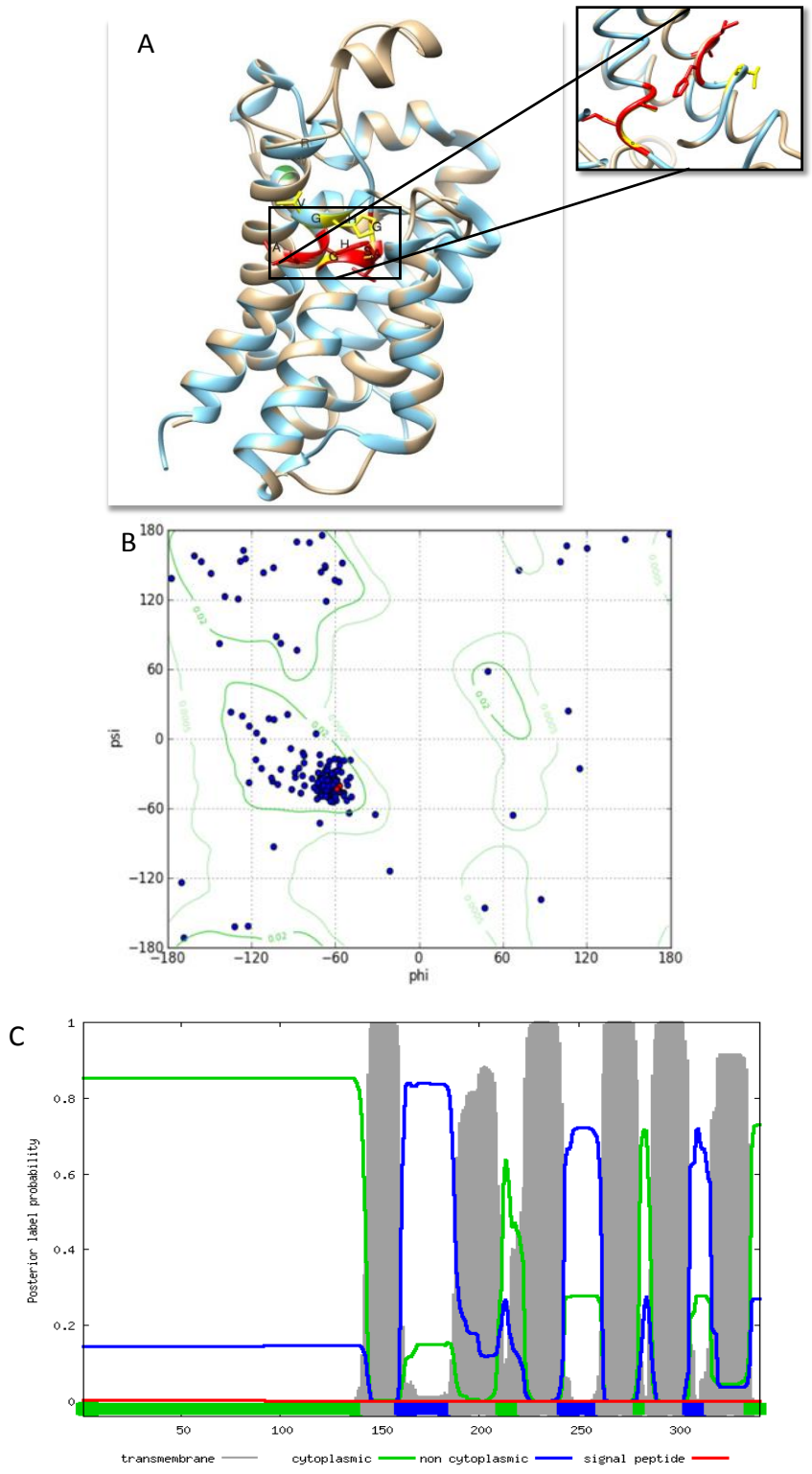

Figure 3-8 In silico analysis of RhmB. (A) Comparison of the crystallographically-determined 2IC8 (Blue) and predicted RhmB (Brown). Structures have been superimposed to visualise conservation of the motifs required for catalytic activity). (B) Ramachandran plot assessing the quality of the models. Most of the amino acids are found in the favoured region indicating that the model is of good stereochemical quality. (C) Transmembrane prediction plot for *Dictyostelium* rhomboid homologue RhmB using Phobius. Numbers along the x-axis refer to the amino acids of the protein, with probability of internal (blue line), and transmembrane helix (grey blocks) sequences on the y-axis.

Using STRING association network prediction (Franceschini *et al.*, 2013, Snel *et al.*, 2000), RhmB associated proteins were scored (Figure 5-13). As above different colour lines show different types of associations and as with RhmA again, RhmB was predicted to operate in networks containing dynamin protein family (Figure 3-7).

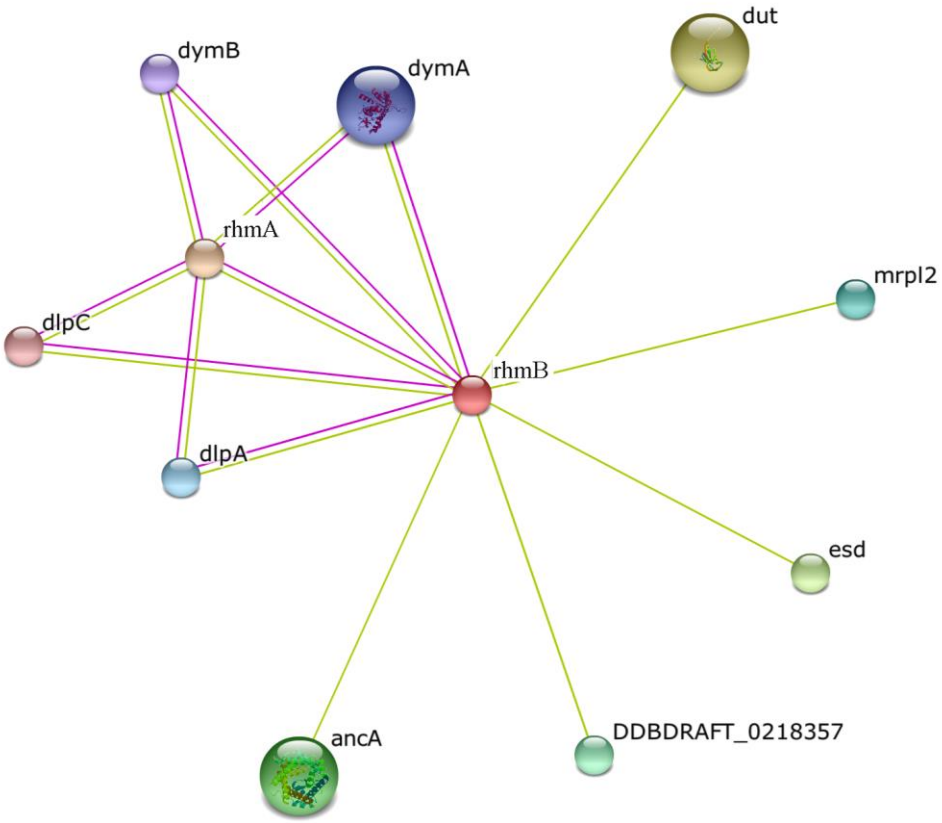

Figure 3-9 RhmB STRING Association network. The *rhmB* gene is shown to be associated with *rhmA* and the dynamin family of proteins not on the basis of just textmining but also through using hybridisation experiments in yeast. The different colour lines show different types of associations; experiments (purple), textmining (mustard). anc, adenine nucleotide carrier; dlp, dynamin-like protein;dym, dynamin; dut, DUTP pyrophosphatase; esd, esterase D**;** mrpl, mitochondrial ribosomal protein large subunit.

3.5.2 *Dictyostelium* RhmD

Alignment of the *Dictyostelium* RhmD (Dictybase: DDB_G0292430) protein with other members of the PARL–like family of proteins from various organisms show high conservation of the PARL rhomboid domain (Figure 3-7C). TMHMM and Phobius predicted RhmD to contain four to seven transmembrane domains (Figure 3-10), as well as predicting an extra TM helix before the N-terminus (1+6). The PARL-like protein rhmD received very high probability values for import into the mitochondrion by MitoProt (0.9835) and Loctree3 (82%) with a calculated cleavage site after residue 76. However PSORTII predicted it to be imported to the nucleus (21.7%) rather than to the mitochondria (17.4%).

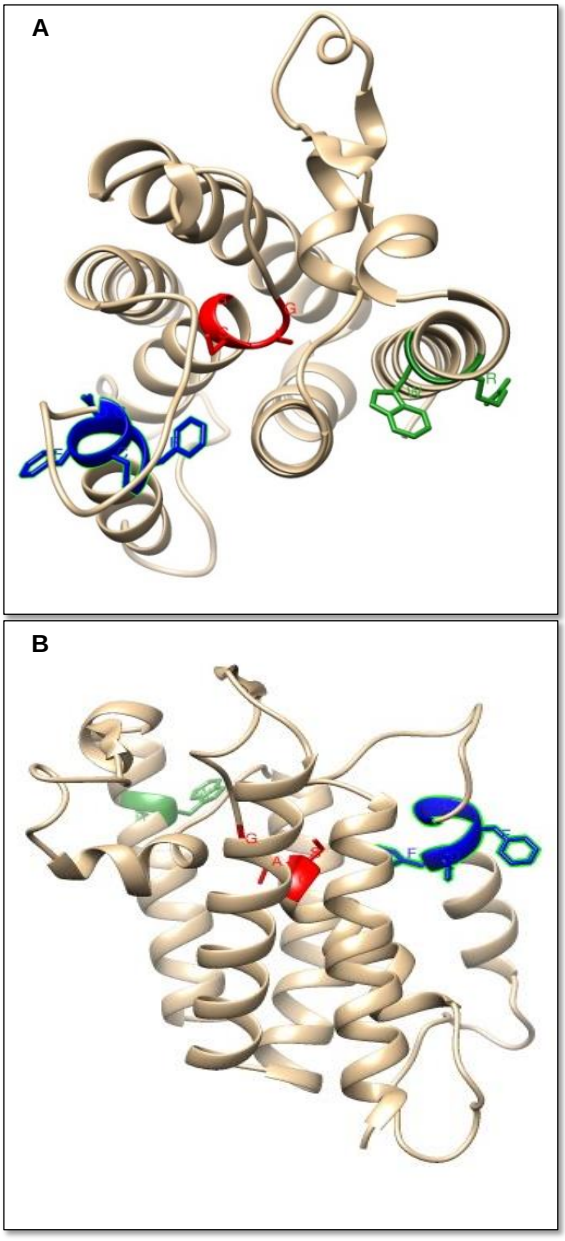

Figure 3-10 3D models of RhmD. (A) Top view probable *Dictyostelium* mitochondrial rhomboid rhmD. (B) Overall topology of rhmD. The catalytic Serine and Histidine residues lie on TMH-4 and -6, respectively (depicted as sticks in this figure). In PARL models, Aspartic acid is pointed into the membrane bilayer. Disruption of rhomboid proteins.

3.6 Summary

Rhomboids are intramembrane proteins that cleave other proteins within the membrane. The membrane lipid bilayer is an unusual site for proteolysis, but the active site of rhomboids contains a water-filled indentation which allows hydrolytic cleavage to take place in an otherwise hydrophobic environment. As previously mentioned in the introduction it is thought that eukaryotic cells contain at least two rhomboids, one of which is found in the mitochondrion. According to the bioinformatics carried out the *Dictyostelium* genome contains four predicted rhomboid-like serine peptidases. Range of bioinformatics tools predicted Rhm A–C belongs to the secretase subfamily of rhomboids and RhmD is a mitochondrial one. The *Dictyostelium* and other rhomboid proteins have a high degree of sequence and structural conservation and possess very similar active site conformations. The spacing between the key residues of the active site as well as the order in which they occur in the primary sequence is conserved between the *E. coli* and *Dictyostelium*, suggesting that the genes encoding them may have arisen from a common ancestor rather than via convergent evolution. The reconstruction of the phylogenetic tree for the rhomboid proteins across different kingdoms, groups the *Dictyostelium* homologues, amongst the other taxa. The inclusion of the *Dictyostelium* homologue in this clade has robust support.

Chapter 4
Role of RhmA

4.1 Introduction

Rhomboids are a family of polytopic serine proteases conserved through evolution. Using bioinformatics tools outlined in Chapter 3, it was found that *Dictyostelium* had four genes predicted to encode active rhomboid-like proteins targeted to a distinct subcellular compartment, which were named *rhmA, B, C and D*. To gain insight into the role of the rhomboid proteins especially RhmA and RhmB knockout mutants were generated

In this chapter, detailed characterisation of the phenotypes of *rhmA* null cells in *Dictyostelium* are described. The data from the study suggests that RhmA is involved in cell motility as the *rhmA* null cells show compromised chemotaxis to cAMP and folic acid and slug movement.

4.2 Results

4.2.1 Generation of *rhmA* null mutant by homologous recombination

To investigate a potential role for the rhomboids in *Dictyostelium*, *rhmA*, *rhmB* (Chapter 5) and *rhmC* (Appendix) were ablated using homologous integration of a Blasticidin resistance cassette. Knockout cassettes were designed to delete the active residues or full domains, thus ensuring only non-functional proteins could be produced following homologous integration of each cassette into the genome.

Knockout cassettes for each gene were created using PCR to amplify 5' (encoding Nterminus residue) and 3' (encoding C-terminus) regions from within each open reading frame. The 5' and 3' fragments for each gene were then cloned into the pLPBLP vector flanking the blasticidin resistance gene (Faix *et al.*, 2004). The *rhmA* and *rhmB* 5*'* fragments were cloned into the pLPBLP vector at the *Apa*I/*Hin*dIII. Subsequently; the 3' fragments were cloned at the NotI/SacII site. The construction of the *rhmA*$^{-}$ cells was done by Dr David Traynor (MRC-LMB, Cambridge).

This approach avoids reversion and transcription of partial gene products. The method deleted a large portion of the endogenous gene as opposed to the transposon technology method which inserts a resistance marker without deleting any regions of the target gene (Abe *et al*., 2003; Adley *et al*., 2006). Furthermore, the blasticidin resistance cassette was orientated within the pLPBLP expression vector such that transcription occurs in the opposite direction to that of the gene fragments; to avoid potential read through into the 3' region of the target gene.

Colony plating and selection of transformants enabled isolation of multiple independent colonies from a single electroporation. All these genes showed high transformation efficiency and rate of homologous integration. Although PCR confirmation on both sides of the cassette (followed by loss of transcription) provides proof of gene ablation, this approach could potentially give rise to additional integration events. However, multiple independent knockout cell lines were isolated from a single colony for each mutant, which enabled each of these independent clones to be analysed in parallel to each other. If multiple integration events had occurred, these colonies would behave in a dissimilar manner during development. Hence, independent isogenic cells lines lacking the rhomboid proteins were produced, and initially examined for altered development. From these studied cells lacking the *rhmC* gene did not show altered development compared to wild type cells (see Appendix for assay results). In contrast *rhmA* and *rhmB* (Chapter 5) null mutants demonstrated altered phenotypes versus wild type cells, hence these proteins were chosen for further analysis.

4.2.2 Loss of gene transcription

Subsequent to identifying knockout cell lines, reverse transcriptase PCR was used to confirm loss of gene transcription from the isogenic clones. cDNA derived from each clone was used to test for the presence or absence of the expressed target gene. Primers used to amplify diagnostic products from cDNA were located within the knocked out region of the gene. Successful amplification of a 308bp, a 341bp and 208bp fragment from the wild type derived cDNA indicated expression of a functional gene for *rhmA*, *rhmB* and *rhmC* respectively. Cycloheximide-Inducible (H7Q2) PCR product was used as an expression control, which has been shown to

be stably expressed throughout development (Zinda & Singleton, 1998). This control product gave rise to a 330bp fragment for cDNA and 500bp fragment for gDNA. This produced a second control for potential contaminating genomic DNA. Analysis of the three independent isogenic colonies for *rhmA, rhmB* and *rhmC* null mutants identified through the flanking PCR screening, confirmed the loss of the encoded RNA in each isolate, thus, independently confirming gene ablation (Figure 4-1).

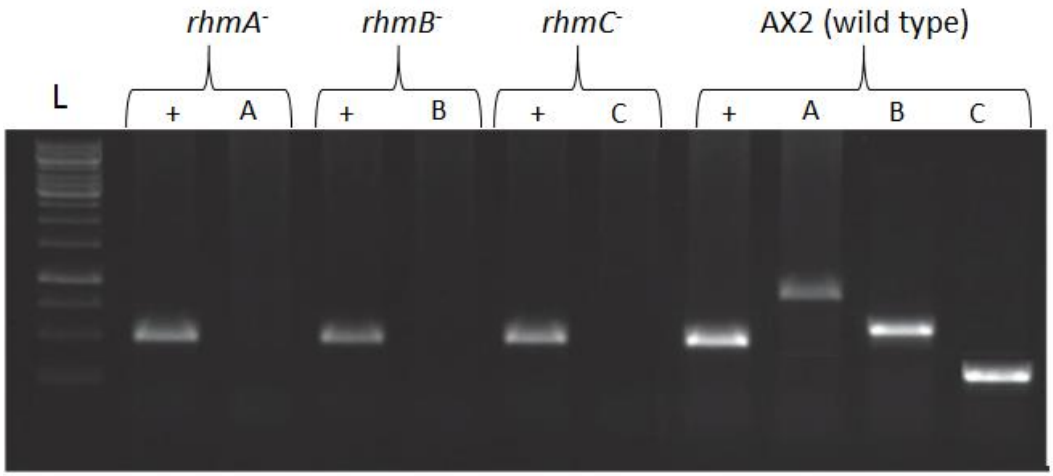

Figure 4-1 PCR analysis of gene transcription in wild type and putative null mutants. RNA was extracted from wild type, *rhmA*$^-$, *rhmB*$^-$ and *rhmC*$^-$ cell lines and converted to cDNA using reverse transcription PCR. H7Q2 (+) primers were used as a control, A: (rhmA), B: (rhmB) and C: (rhmC) were primers used for the specific gene. L = 1 kb ladder

4.2.3 Morphology of *rhmA* null cells

The disruption of *rhmA* did not result in obvious defects in the developmental morphology. The appearance of the *rhmA*$^-$ mutants grown on bacterial lawn was essentially the same as that of the wild type (WT) cells AX2 (Figure 4-2) visualised up to 20x magnification using Leica EZ4 stereo microscope (Leica Microsystems, Linford Wood, Milton Keynes, UK). The *rhmA*$^-$ cells grew as fast as the AX2-WT cells in axenic media (Figure 4-3).

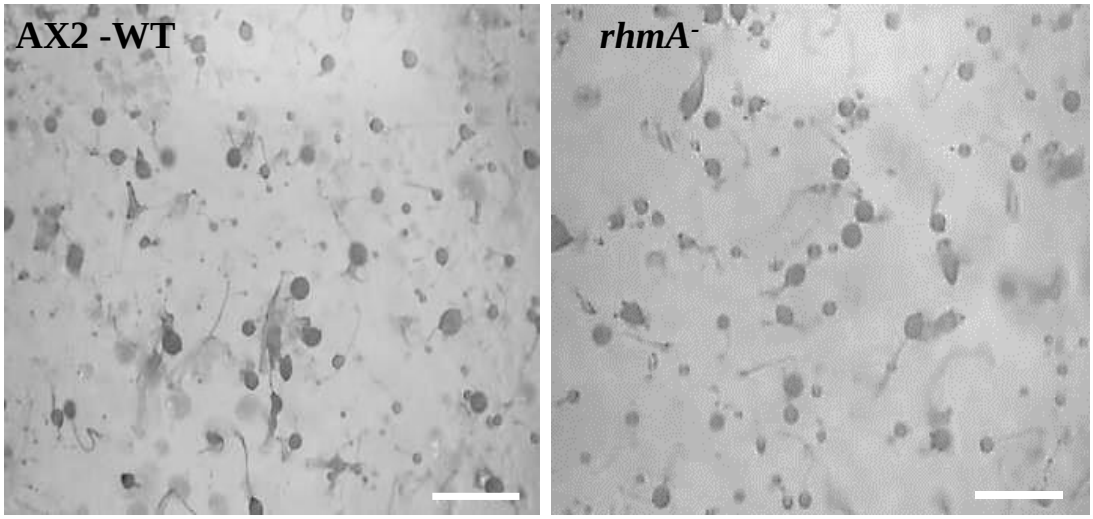

Figure 4-2 *rhmA*⁻ cell phenotype. The appearance of *rhmA* null aggregates on bacterial lawn plates were the same as that of the AX2 cells, including the size and shape during all the developmental stages. Scale bar = 0.5 mm

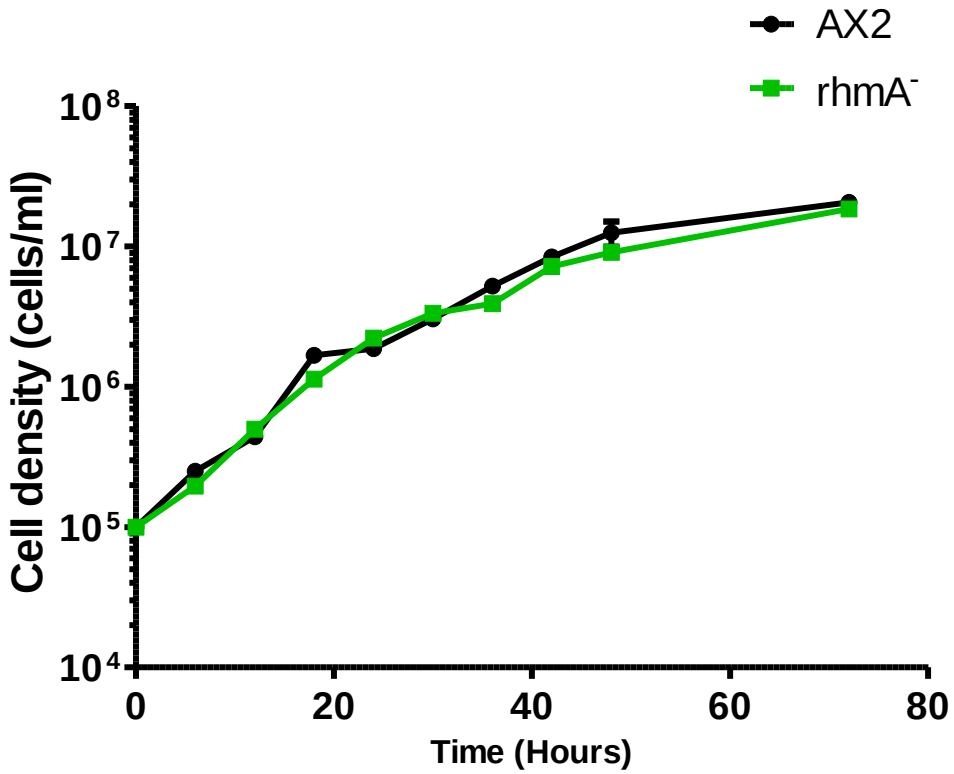

Figure 4-3 *rhmA* null cells growth curve. *rhmA*⁻ cells grew at a similar rate to the wild type cells (doubling time 6.54 ± 1.2 h). This data is the mean ± SEM of three independent experiments.

4.2.4 Expression profile of *rhmA*

The social life cycle of *Dictyostelium* is one of the most interesting aspects of the organism, and the relative expression of RhmA in its development was therefore examined. For initial analysis, wild type cells were allowed to develop over 24 h period, and RNA was extracted at specific time points. RNA was copied to cDNA, which was then used in qPCR to quantify the expression level of *rhmA* for each life stage. Expression levels were normalised using the standard ΔCt-method using the constitutively expressed H7Q2 control gene.

It can be seen (Figure 4-4) that *rhmA* is expressed during all the tested life stages but that the relative levels of expression vary, with *rhmA* expression elevated during aggregation and in slugs.

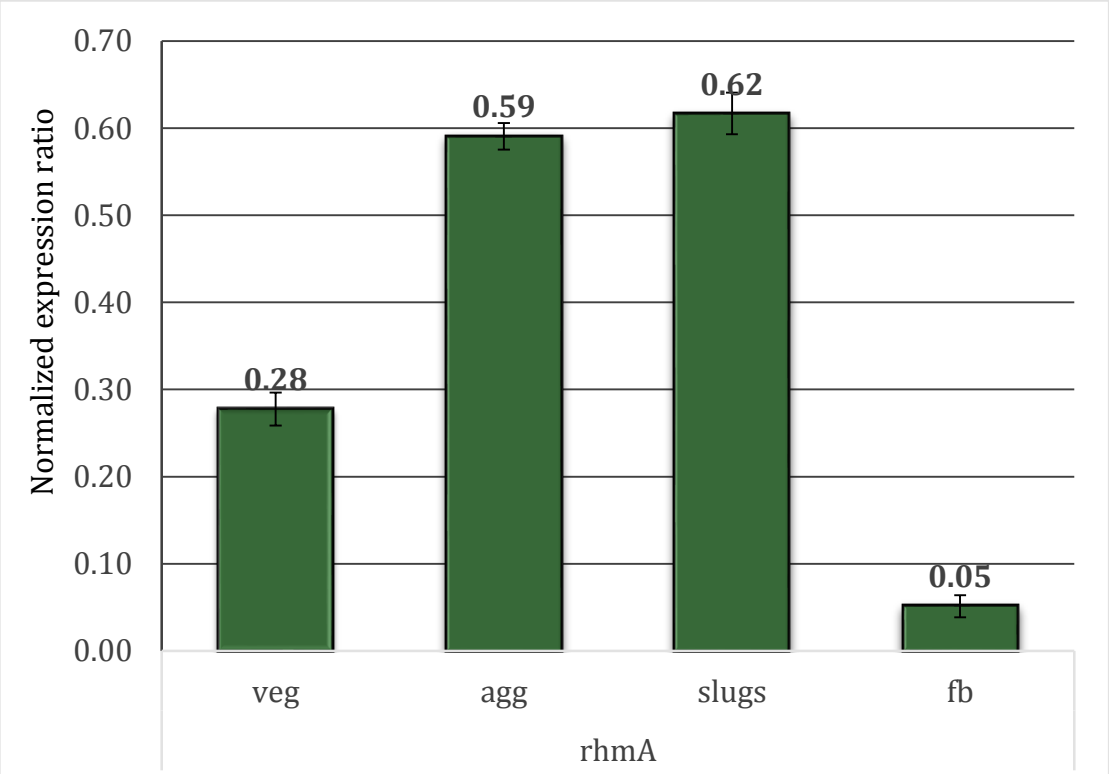

Figure 4-4 *Dictyostelium rhmA* gene expression during key life stages. RNA samples were prepared from *Dictyostelium* (grown axenically) during selected life stages with derived cDNA, and *rhmA* gene amplified. The transcription levels were quantified from four independent samples vs H7Q2 constitutive transcription.

The RNA-Seq database (http://dictyexpress.biolab.si) quantifies transcription, reports a peaks at 650 copies at 0 hr and 24 hr development , with a minor peak at 12 h of development (Figure 4-4).

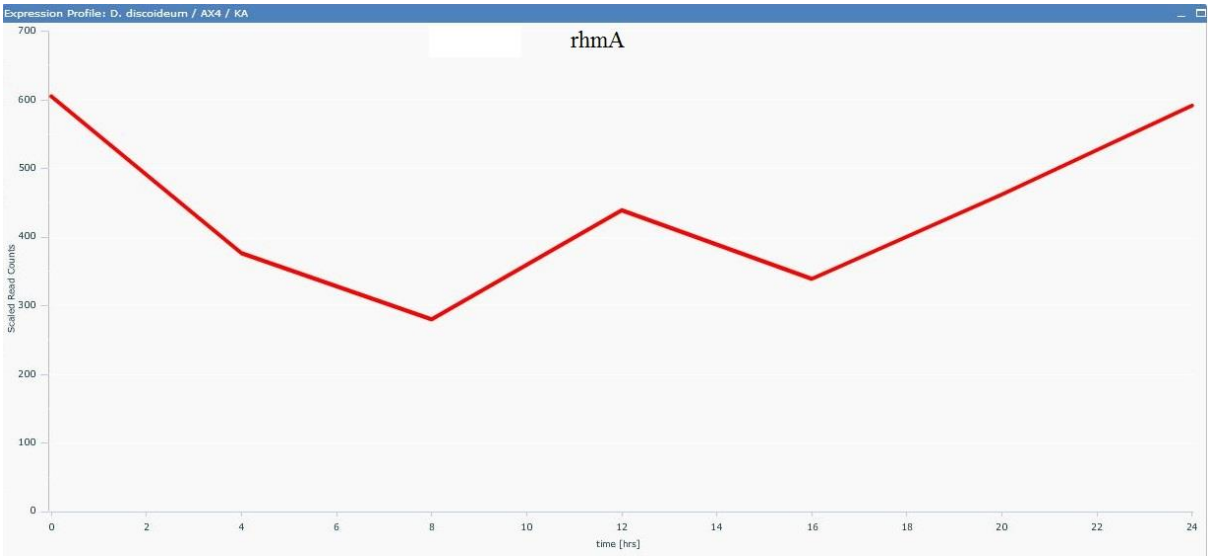

Figure 4-5 RNA-Seq data for RhmA from DictyExpress. The RNA-seq data were collected from *Dictyostelium* (grown in bacteria) at 4 h time intervals during development to monitor the expression profile of the *Dictyostelium rhmA* gene

4.2.5 RhmA affects cell movement

During early development, cells release the chemoattractant, cAMP stimulating cells to aggregate. As the expression profile showed the *rhmA* gene was highly expressed during aggregation, the response of the *rhmA* null mutants to cAMP was tested using one drop and under agarose assays of chemotaxis.

In the one drop assay, cells were spotted onto KK2 agar containing different concentrations of chemoattractant; 0.01 µM cAMP or 10 µM folate. A gradient forms around the perimeter of the spot if the cells are able to degrade the chemoattractant by extracellular membrane-associated phosphodiesterase in the case of cAMP, and by folate deaminase in the case of folate (Bernstein *et al.*, 1981). The forming gradient is detected by the cells which respond by migrating radially outwards (see Chapter 2). Counts were made of droplets showing a positive chemotactic response as a function of time (Figure 4-6). The results of the one drop assays indicate that *rhmA*$^{-}$ cells show a delayed response on plates containing 0.01 µM cAMP, in comparison with wild type cells.

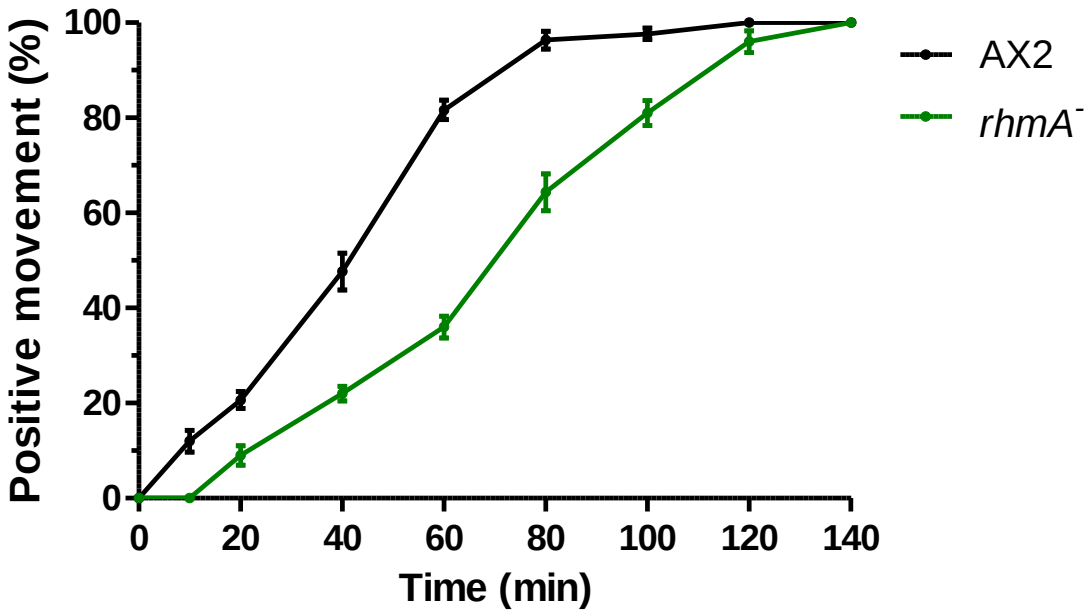

Figure 4-6 *rhmA*$^-$ one drop cAMP chemotaxis assay *rhmA*$^-$ cells showed a 20 minutes delay respectively on plates containing 0.01 µM cAMP in comparison to that observed for AX2 cells (measured as the time it takes 50% of the population to respond). These data show the mean ± SEM for results obtained in 3 independent experiments.

In the one drop assay a failure to move chemotactically could also result from a reduced ability of the cells to secrete the cAMP phosphodiesterase. To rule this out, another chemotaxis assay was performed in which the formation of the gradient does not depend on the action of phosphodiesterase but is formed by diffusion. In this assay, known as the under agarose assay, cells are challenged by a gradient of cAMP that forms by diffusion of cAMP from a localised source (see Chapter 2). In this assay, secreted cAMP phosphodiesterase will also degrade the gradient, but a lack of cAMP phosphodiesterase secretion would not affect the response to the chemoattractant. The *rhmA*$^-$ cells once again demonstrated a delayed response to 10 µM cAMP in under agarose chemotaxis assay (Figure 4-7). The effect was quite pronounced in the *rhmA*$^-$ cells, which covered nearly half the total distance seen of the wild-type cells.

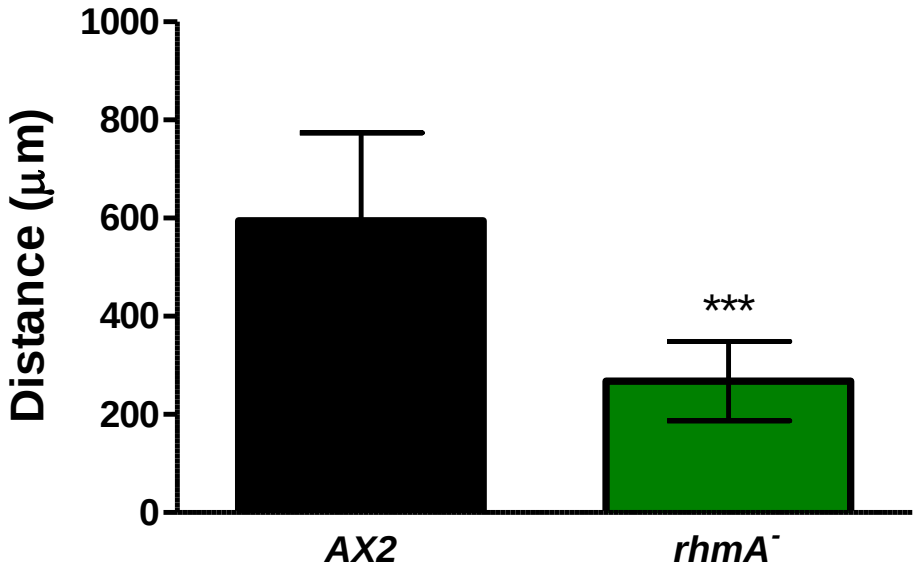

Figure 4-7 *rhmA*- cAMP under agarose chemotaxis assays. *rhmA*- cells in cAMP under agarose assay also show a delayed response after 4 h compared with wild type cells. These data shown are the mean ± SEM for results obtained in three independent experiments. *** = P ≤ 0.001

These results suggest that the cells are less sensitive to cAMP or need steeper gradients to detect them. However, it could also mean that cell motility is directly impeded by RhmA mutation, which would also result in a delayed chemotactic response.

To investigate if the cAMP alone was affected the same assays were repeated using folate as the chemoattractant on vegetative cells. Figure 4-8 and 4-9 show that there is a significant difference in the chemotactic response to 10 µM folate between *rhmA*- cells and wild type cells at vegetative stage. This indicates that there is an intrinsic difference in the ability of the *rhmA*- cells to move or direct movement in response to both stimuli. Nevertheless, it could also result from an effect of RhmA on signalling components involved in chemotactic signalling pathways for both cAMP and folate.

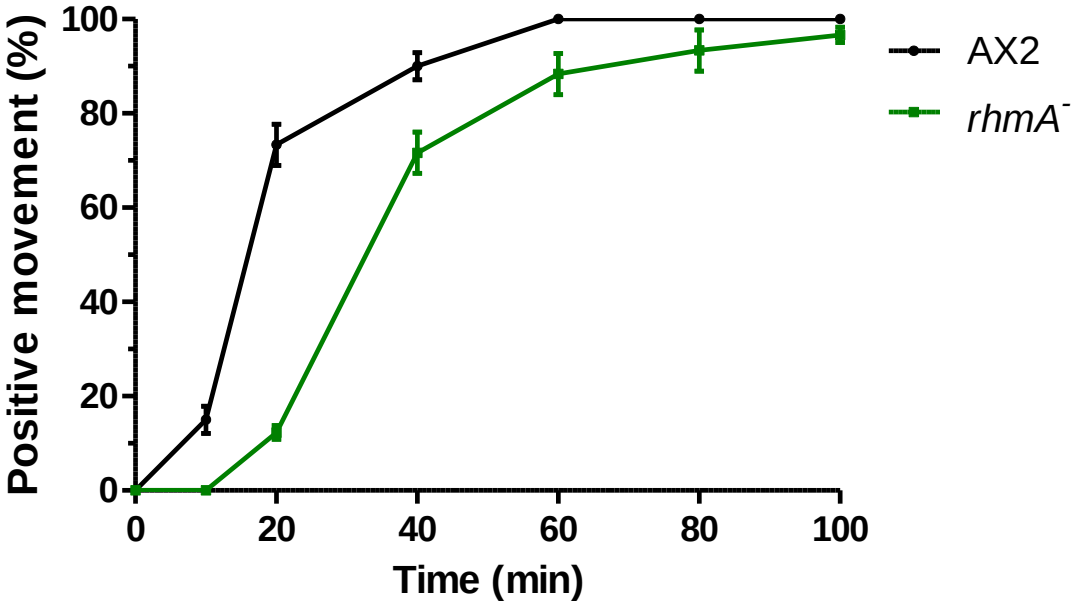

Figure 4-8 *rhmA*⁻ one drop folate chemotaxis assay. *rhmA*⁻ cells showed a 20 min delay on plates containing 10 µM folate in comparison with AX2 cells (measured as the time it takes 50% of the population to respond). Data are mean ± SEM for results obtained in three independent experiments.

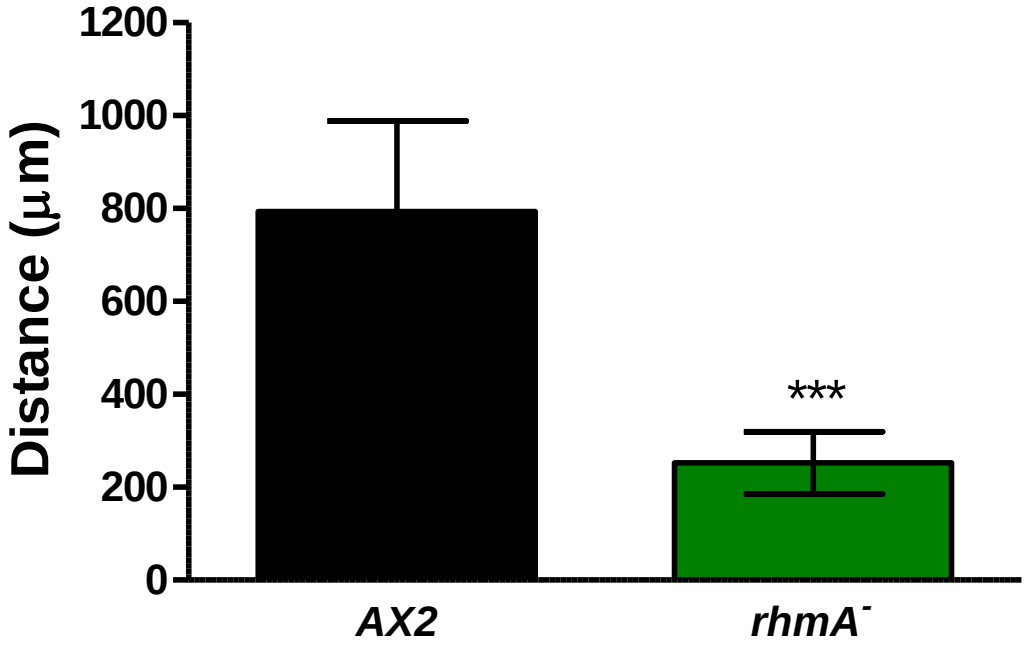

Figure 4-9 *rhmA*⁻ folate under agarose chemotaxis assays. *rhmA*⁻ cells exposed to folate show a delayed response compared with wild type cells. These data shown are the mean (after 4 h) ± SEM for results obtained in three independent experiments. *** = $P \leq 0.001$

To assess whether the responses seen are due to the reduced cell movement, the average locomotion was tested. The distance travelled from point A to B without any added chemoattractants was measured of cells pipetted down on agar layer on a slide. 40 cells in three different fields were observed for 20 min. The mean distance travelled over 2 h was significantly reduced for *rhmA*$^{-}$ cells, even though the difference between wild type and *rhmA*$^{-}$ mutant cell lines was only about 30 µm/h (Table 4-1). To quantify random cell movement, cells were added to 8-well Nunc™ chambered slides, individual cell movement was traced using ImageJ software, which also measure the formation of blebs and filopodia. While observing the cells, it was apparent that there were distinct changes in the cell shape; *rhmA*$^{-}$ cells formed many long filopodia and membrane ruffles at their anterior ends.

Table 4-1 Cell movement of *rhmA*$^{-}$ comapred to AX2 (wild type cells) 'with out any chemical stimuli

Strain	Locomotion (A →B) (µm/h)	Random cell movement (µm/min)
AX2	320.9 ± 3.7	3.15 ±0.02
rhmA^{-}	***288.7 ± 3.1 (P= 0.0057)***	3.08 ± 0.05 (P= 0.4463)
rhmA-GFP	315.6 ± 3.1 (P= 0.2677)	3.12 ± 0.08 (P= 0.7290)

4.2.6 Rapid cell movement response

To further characterise the chemotactic behaviour at the individual level, single cells were visualised to see how they responded to a relatively steep cAMP gradient produced by a point source of chemoattractant, i.e. cAMP, released by a micro needle. 50% AX2GFP transfected cells and 50% *rhmA*$^{-}$ cells were mixed in a microscope chamber containing KK2 buffer. Within minutes of exposure to the gradient, AX2-GFP cells become well polarised and started to migrate towards the tip of the needle. Comparatively, *rhmA*$^{-}$ cells exhibited a reduced/decreased response, 4.78 ± 2.31 µm/min versus to 8.02 ± 2.34 µm/min in AX2-GFP cells, (mean ± SEM, cell number = 40, P <0.05) and the cells were much less polarised. Although the *rhmA*$^{-}$ cells do eventually orient towards the tip of the micropipette, they displayed less directionality (0.43 ± 0.23) and were less elongated, compared with wild type cells (directionality 0.75 ± 0.21) (data

represents mean ± SEM number = 40, P <0.05), where the directionality value is the cosine alpha, the angle given in Figure 4-10.

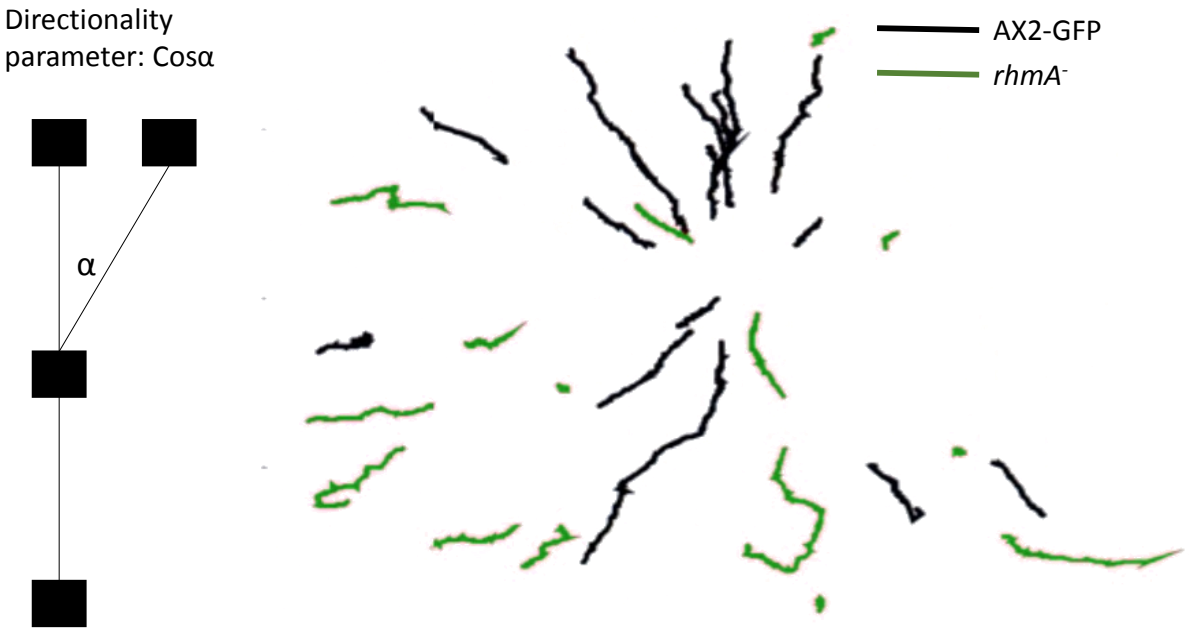

Figure 4-10 Needle chemotaxis assay. Aggregation competent cells were allowed to settle on a glass cover slip and stimulated with a micro-needle. Images of cells were captured every 5 sec. Cell movement was analysed using ImageJ (Quimp11 plugin). AX2-GFP cells were well polarised, migrate fast and oriented properly towards the cAMP source. Whereas *rhmA*$^{-}$ cells migrated with less directionality and less elongated compared with the control cells. Directionality is measured as the cosine alpha (cell moves toward the top).

To determine whether the *rhmA*$^{-}$ phenotype results from inability to reach full aggregation competence because of their failure to activate cAMP induced aggregation stage gene expression, the transcription of two aggregation-stage genes was monitored. The cAR1 and ACA genes were examined by qPCR. Both genes were expressed at similar levels in *rhmA*$^{-}$ cells and wild type cells (Figure 4-11).

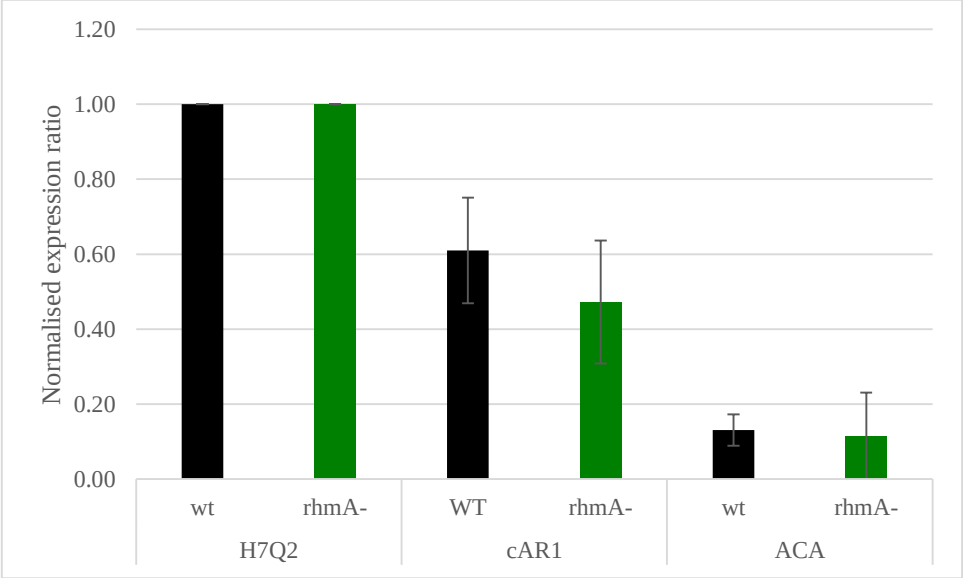

Figure 4-11 Transcription levels of aggregation-stage markers. Aggregation stage markers cAR1 and ACA were monitored for wild type and *rhmA*$^{-}$ cells. There was no significant difference between the wild type and *rhmA*$^{-}$ cells. Data is the mean ± SEM of three independent experiments.

4.2.7 *rhmA*$^{-}$ slugs show poor phototaxis

Genetic analysis has shown that a minimum of 20 genes are needed for wild type slug behaviour; that cAMP and cGMP function as secondary messengers, and that mitochondria and the actin binding protein ABP120 are involved (Fisher, 1997).

Dictyostelium slugs are sensitive to light, pH and even slight differences in temperature, which allows them to migrate towards the surface of the soil in their natural habitat; which provides an optimal location for fruiting (Fisher & Williams, 1981). When cells of wild type cells are grown in the presence of lateral light, they form slugs that move almost directly towards the light source. Actin cytoskeleton proteins and related regulators were found to be essential for proper phototaxis (Noegel & Schleicher, 2000) and therefore phototaxis was also investigated for *rhmA*$^{-}$ cells to see if their motility phenotype extened to this response too. Indeed, *rhmA*$^{-}$ slugs showed dramatically reduced movement, and were apparently unable to respond to light directionally, unlike wild type slugs (Figure 4-12).

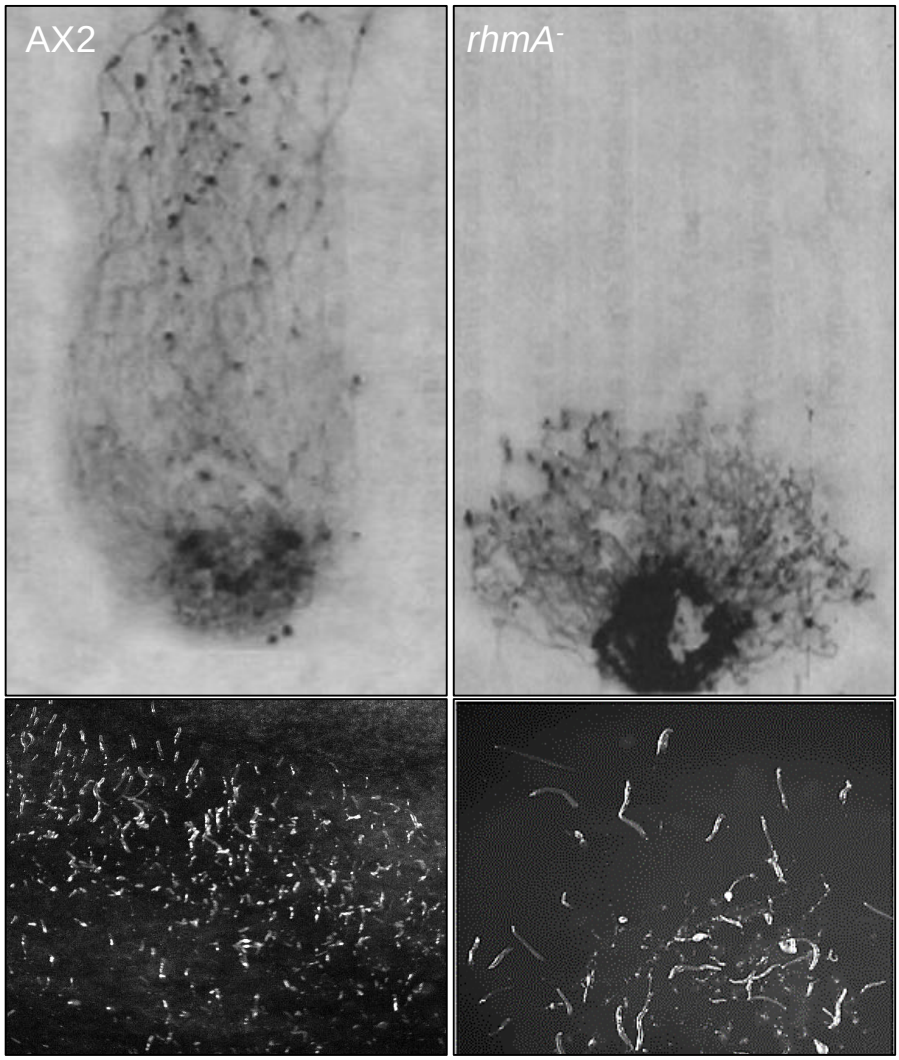

Figure 4-12 Phototaxis assay of *rhmA*$^-$ cells. There was a pronounced defect in phototaxis in *rhmA* null mutants. The wild type slugs move directly towards the light source. The *rhmA*$^-$ slugs move in a less directed manner and more slowly. Top panel, Coomassie stained tracks; bottom panel, light microscopy of slug formation. These results were reproducible in five independent experiments**.**

4.2.8 Mitochondrial morphology and function

Phototaxis and thermotaxis are both sensitive to defective mitochondrial function and various phototaxis mutants have been found to have aberrant mitochondrial morphology (Darcy *et al.*, 1994). Therefore, to determine whether mitochondrial dysfunction accounted for the *rhmA* null phenotype, mitochondria of the *rhmA*$^-$ cells were observed using transmission electron microscopy. It can be seen (Figure 4-13 and 4-14) that *rhmA*$^-$ mitochondria had unusual white spaces and protrusions. To confirm that these were not artefacts from fixing the cells, the experiment was repeated three times on independent lines and quantified (Figure 4-15).

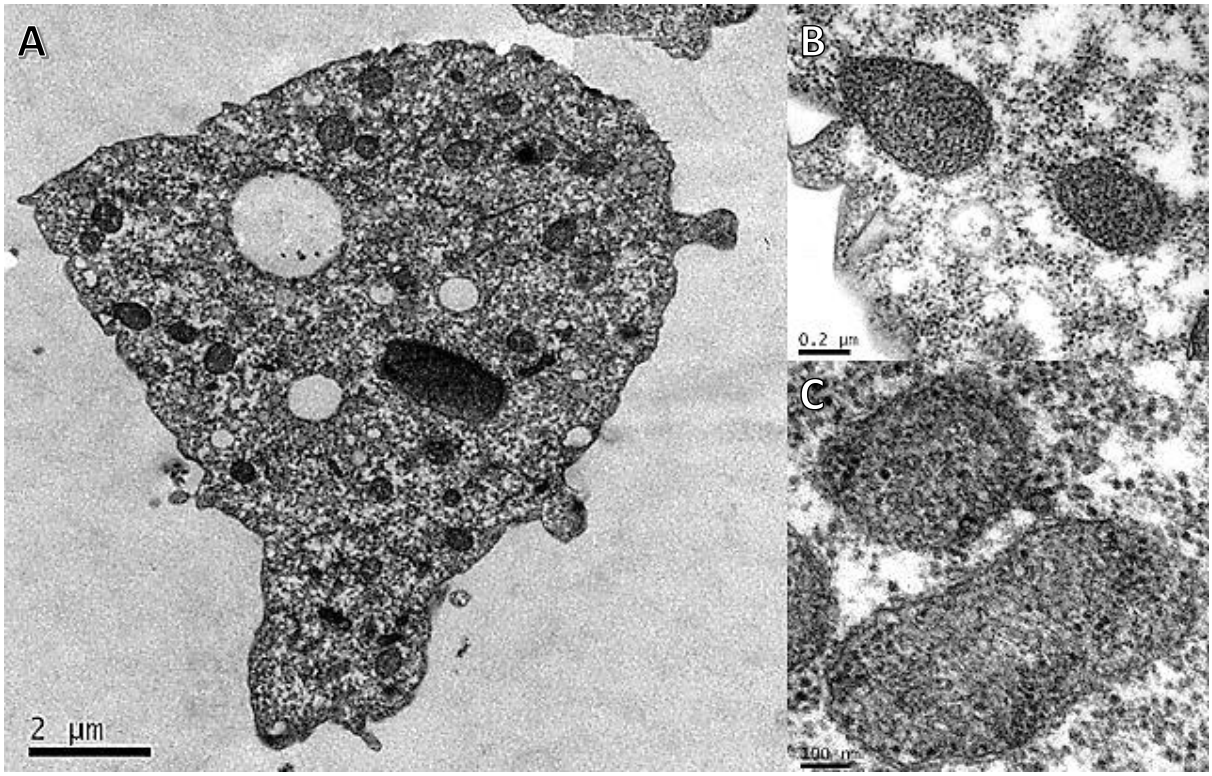

Figure 4-13 Transmission electron microscopic image of AX2 cell (A). Mitochondrial morphology of the wild type cells (B, C).

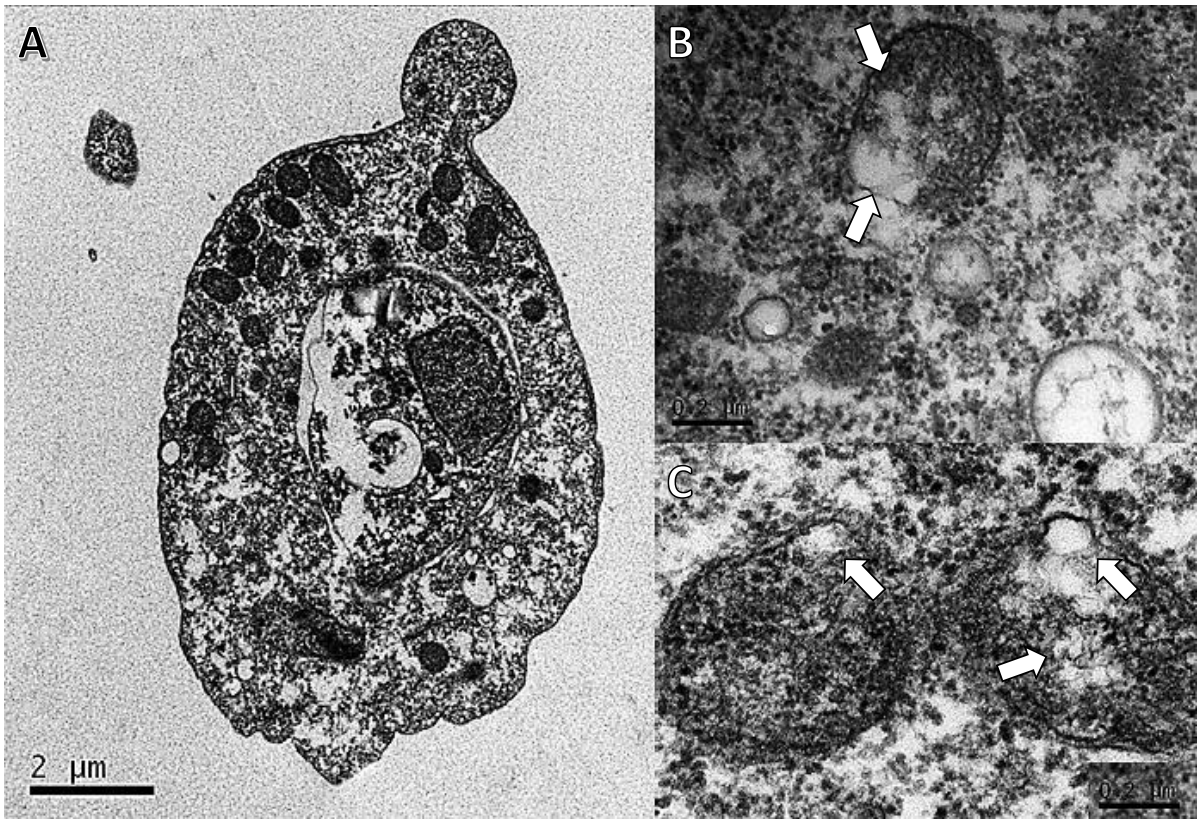

Figure 4-14 Transmission electron microscopic image of *rhmA*$^{-}$ cells (A) Mitochondrial morphology of the mutant cells (B, C). It can be seen that mitochondria of the null mutant have aberrant cristae and folds leading to unusual white space and protrusions (white arrows).

To determine whether there was a significant difference in the ultrastructure of wild type and *rhmA*$^-$ cells, the appearance of white space was quantified using ImageJ. Figure 4-15A-B shows that 70% of the mitochondria in *rhmA*$^-$ cells were defective compromising a mean of > 30% white space as a proportion of total area. There was no significant difference between the sizes of mitochondria in wild type cells (mean 10.06 ± 1.23 mm^2) versus *rhmA*$^-$ cells (mean 10.83 ± 2.89 mm^2). The diameter of the cells was significantly reduced by a mean of 10% (Figure 4-15C). The majority of the wild type cells had a mean diameter (at the cell's widest part) greater than 16 µm, whereas the majority of the mutant cells had a mean diameter of 12 µm.

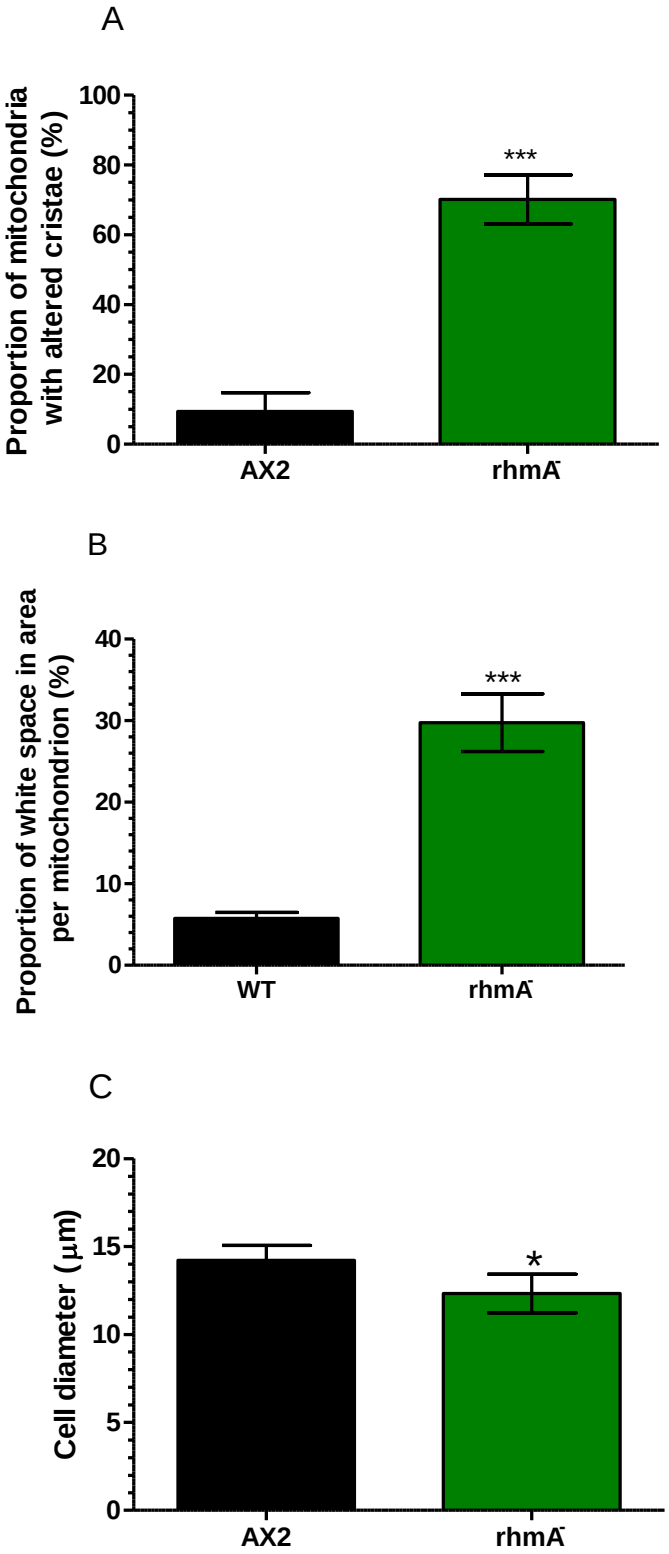

Figure 4-15 Mitochondrial morphology in *rhmA*$^-$ cells. (A) The proportion (%) of mitochondria affected in a single cell, at least 100 cells assessed for each strain. (B) Mean proportion (%) of white space per mitochondrion. 40 cells were analysed for each strain in three independent experiments. (C) Cell size measured by diameter was compared between AX2 and *rhmA*$^-$ cells. These data are mean ± SEM of independent experiments. * = $P \leq 0.05$, *** = $P \leq 0.001$

It has been reported previously that three distinct mitochondrial morphologies are found in *Dictyostelium*, namely spherical, which have even diameters, rod-like mitochondria, which have twice the length compared with the width, and lastly tubular mitochondrial, whose length is greater than threefold their width (Gilson *et al.*, 2003). Usually one shape is more prevalent in an individual cell. Mitochondria were scored and classified according to their dominant form (Figure 4-16), in the same cells examined when scoring white space. It is important to note here that there was no apparent clustering of the mitochondria in the mutant cells, which is observed in other mutants showing aberrant morphologies, such as *midA*$^-$ and *cluA*$^-$ (Schimmel *et al.*, 2012; Torija *et al.*, 2006). To make sure that the effect of development did not alter morphological results, cells were maintained in log phase vegetative cultures in axenic media. It was found that *rhmA*$^-$ mitochondria were found significantly less often in the spherical form, and more often in the tubular form.

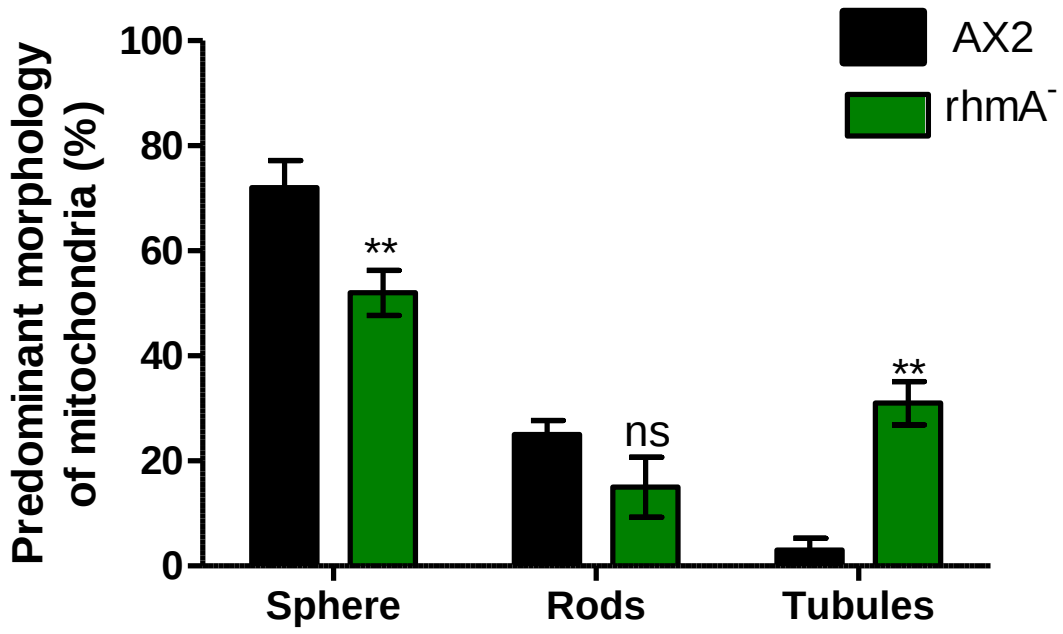

Figure 4-16 Mitochondrial shape in the *rhmA*$^-$ cells. In each strain the proportion of cells with predominantly spherical, rod-like (length twice times the width), and tubular (length more than three times the width) mitochondria are given. These data are mean ± SEM of 100 cells for each strain. ns = $P > 0.05$, ** = $P \leq 0.01$

Given the difference in morphology and ultrastructure, the fitness of the mitochondria was assessed via a simple succinate dehydrogenase activity assay. Succinate dehydrogenase is an enzyme of the tricarboxylic acid cycle and is found in mitochondria.

Because it is quite stable and found at high concentration only in the mitochondrion of eukaryotes, succinate dehydrogenase is useful as a marker enzyme for mitochondria. It was used to estimate the relative function of mitochondria in the wild type and mutant cell lines. After results were normalised for the protein content in cells (measured via Bradford assay) there was significant difference (P value = 0.046) in K_m[1] values for *rhmA*$^-$ (22.99 ± 2.75) and wild type cells (14.56 ± 1.16).

4.2.9 Subcellular localisation of RhmA

Although RhmA was not predicted to be transported to the mitochondrion, electron microscopy studies suggested a possible mitochondrial function. Subcellular location of RhmA was determined by expression of GFP fused to the C-terminus of the complete RhmA *Dictyostelium* protein. The expression of this construct was driven by an actin15 promoter (plasmid map in Chapter 2.2.6). After transfection into *rhmA* null cells the resulting clones demonstrated phenotype complementation, verifying the *rhmA*$^-$ was the cause of the mutant phenotype and also verifying function of the RhmA-GFP protein. Cell were able to respond to folic acid and cAMP in all assays (Figure 4-17).

[1] K_m gives an idea of the substrate binding affinity to an enzyme. In general, a high K_m value, the binding affinity is small and a low K_m means binding is strong. Thus lower K_m means that it requires less substrate to get the enzyme to work. A high K_m value means you need a lot of substrate to get the enzyme to act on it

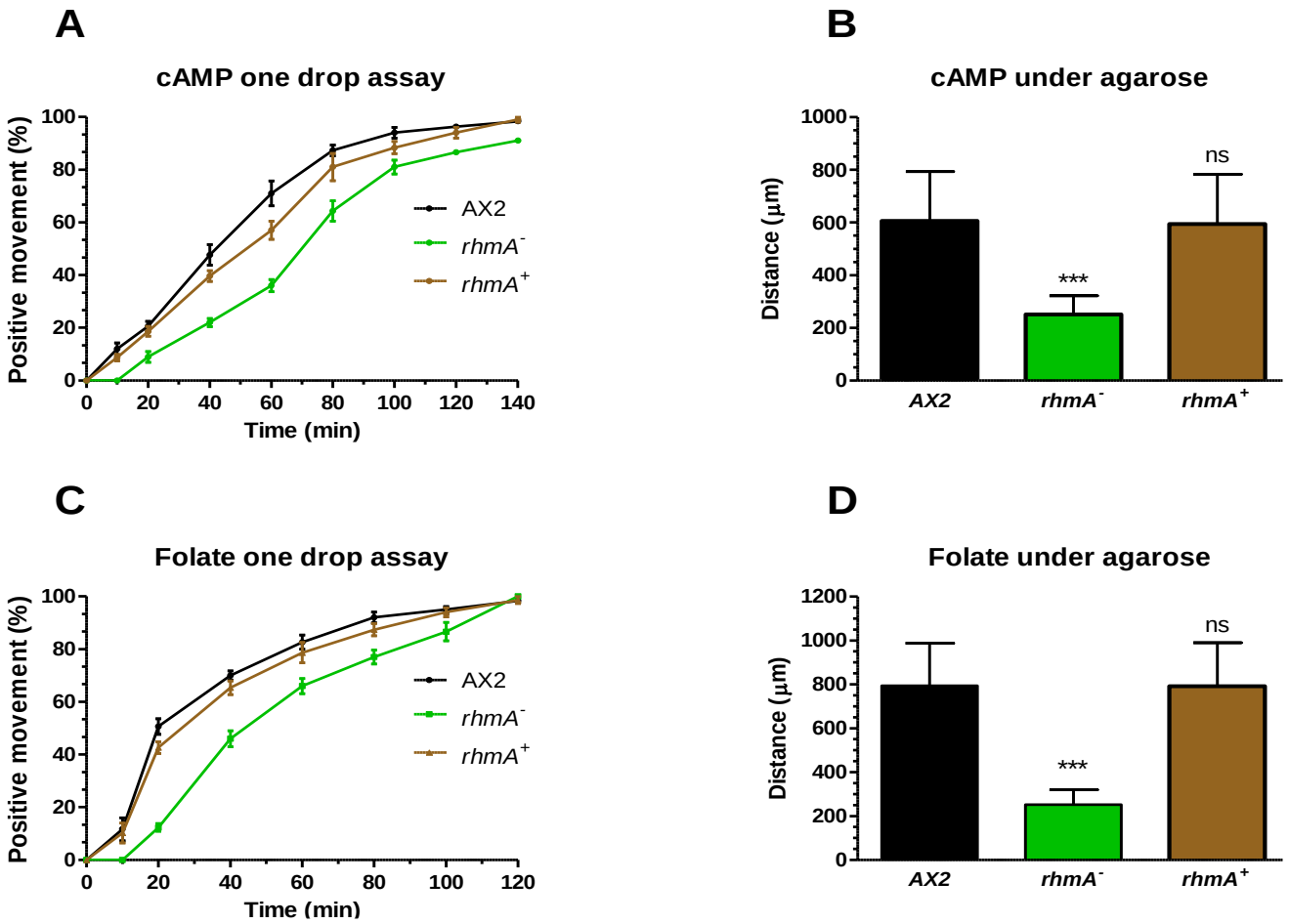

Figure 4-17 Rescue of the phenotype of *rhmA*⁻ using RhmA-GFP construct. After transfection with the RhmA-GFP construct cells were monitored for their response to folic acid and cAMP in one drop and under agarose assays. RhmA-GFP protein was able to rescue the defects seen in the null strain. Data are mean ± SEM of three independent experiments.

GFP fluorescence was examined in the complemented strains RhmA-GFP (*rhmA*$^{+}$). This revealed a punctate localisation, with greater fluorescence at the leading edge in moving cells (quantified by F. Mahmood, undergraduate student). Colocalisation experiments were carried out by with MitoTracker Red (CMXRos; Invitrogen), which showed, perhaps surprisingly, that RhmA-GFP did not colocalise with the mitochondrial dye (Figure 4-18).

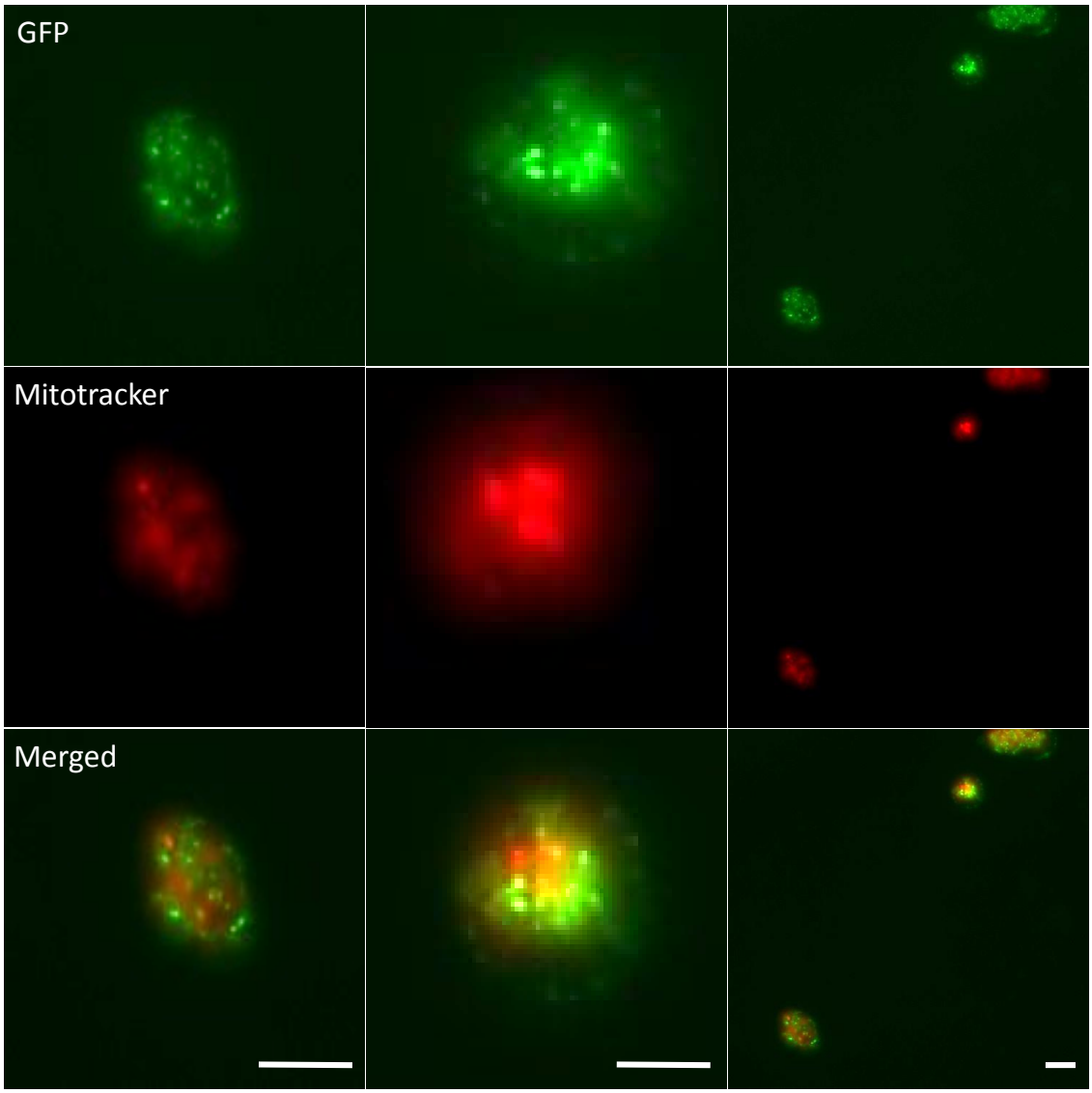

Figure 4-18 RhmA-GFP and Mitotracker red colocalisation studies. Cells expressing RhmA-GFP were incubated with mitochondrial tracker Mitotracker Red (CMXRos); live cells were visualised using a fluorescence microscope. GFP location, green; mitochondrial marker, red. It can be seen in merged images that the red and green are not colocalised. Scale bars 10 µM.

Further observations revealed that the fusion protein was localised more in the internal cell membranes; this was further confirmed from using FM4-64 dye (Invitrogen). FM4-64 is a lipophilic dye, which selectively stains the vacuolar membranes particularly the contractile vacuole (Figure 4-19).

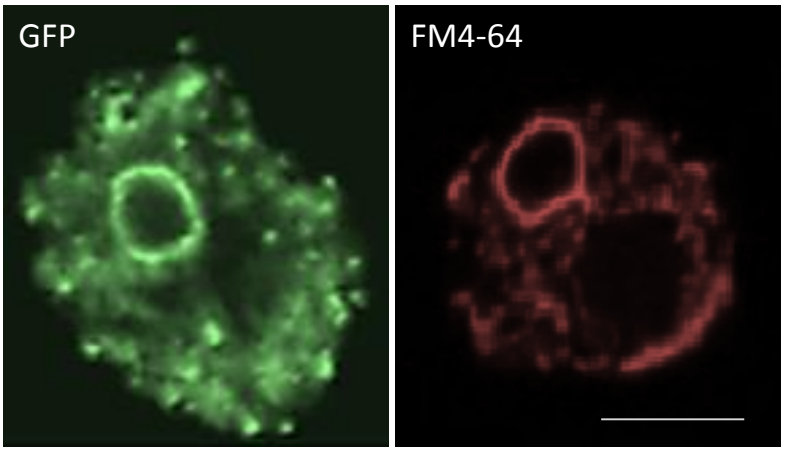

Figure 4-19 Localisation of RhmA in vegetative cells. Contractile vacuole membrane colocalisation of GFP-RhmA (green) and FM4–64 (red). Scale bar 10 µM

4.2.10 Testing potential RhmA partners

Rhomboids are known to interact directly and assemble into oligomers in bacteria (Sampathkumar *et al.*, 2012). Their interacting substrate proteins are usually type 1 single transmembrane proteins (Figure 4-20) *in vivo*, whose amino termini in the luminal or extracellular compartment. However, further studies suggested that type 2 membrane protein (i.e. with opposite topology: the amino terminus is cytoplasmic), or even multipass membrane proteins could act as rhomboid substrates (Tsruya *et al.*, 2007).

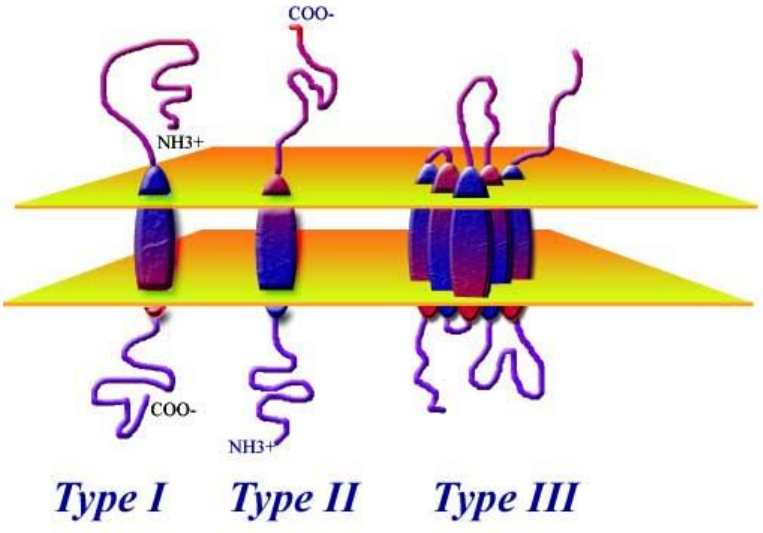

Figure 4-20 Classification method of transmembrane proteins. Type I proteins have a single TM stretch of hydrophobic residues, with the portion of the polypeptide on the N-terminus of the TM domain exposed on the exterior side of the membrane and the C terminus portion exposed on the cytoplasmic side. The proteins are subdivided into types Ia (cleavable signal sequences) and Ib (without cleavable signal sequence). Type II membrane proteins are similar to the type I class in that they span the membrane only once, but they have their N terminus on the cytoplasmic side of the cell and the C terminus on the exterior. Type III membrane proteins have multiple transmembrane domains in a single polypeptide chain.

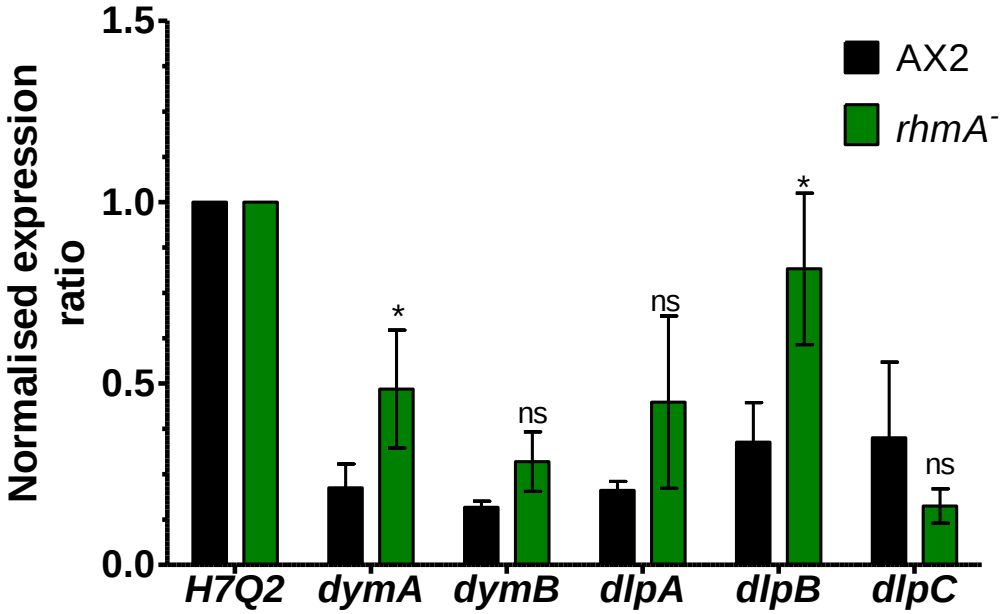

Figure 4-21 Transcription levels of dynamin related genes in vegetative cells. qPCR of *dymA, dymB, dlpA, dlpB and dlpC* in wild type vs *rhmA*$^{-}$ vegetative cells, relative to control H7Q2 constitutive transcription. Values are mean ± SEM. ns = $P > 0.05$; * = $P \leq 0.05$. dym = dynamin, dlp = dynamin-like protein.

There was a significant difference in transcription in vegetative cells for dynamin A (*dymA*) and dynamin-like protein B (*dlpB*) encoding gene ($P < 0.05$; Figure 4-21), confirming interactions predicted by STRING association networks (Chapter 3.4.1), although we cannot rule out a generalised up regulation of subset of genes at this stage in *rhmA*$^-$. To further evaluate any transcriptional level changes during *Dictyostelium* aggregation, qPCR analysis was performed on aggregating cells of *rhmA*$^-$ and compared with wild type cells. In this life cycle stage there was no differential regulation of the dynamin related family in the *rhmA* null mutants compared with the wild type (Figure 4-22), signifying the up regulation of *dymA* and *dlpB* seen in the vegetative *rhmA* null mutants was due to the deletion of the *rhmA* gene.

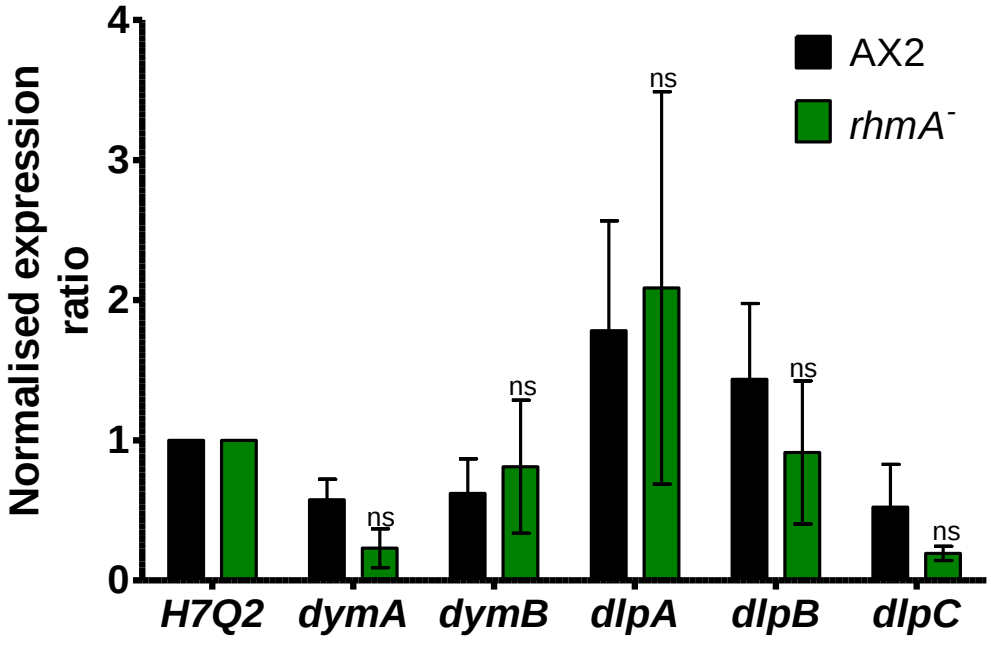

Figure 4-22 Transcription levels in aggregation competent cells. Gene expression the related genes; *dymA, dymB, dlpA, dlpB and dlpC* was compared between the wild type cells and *rhmA*$^-$ cells. Results are shown as comparison to the control (1.0) where $n \geq 3$ independent experiments ± SEM. H7Q2 was used as an expression control to normalise expression levels. ns = $P > 0.05$, dym = dynamin, dlp = dynamin-like protein.

To identify further potential binding partners for RhmA, a proteomic approach was employed to find protein-protein interactions in total cell lysate. Proteins were separated on an SDS-PAGE gel and visualised by Coomassie blue stain (Figure 4-23). It was hoped that anti-GFP beads would pulldown interacting substrates or proteins with RhmA-GFP protein in transformed cells (*rhmA*$^+$), but not in AX2 cells.

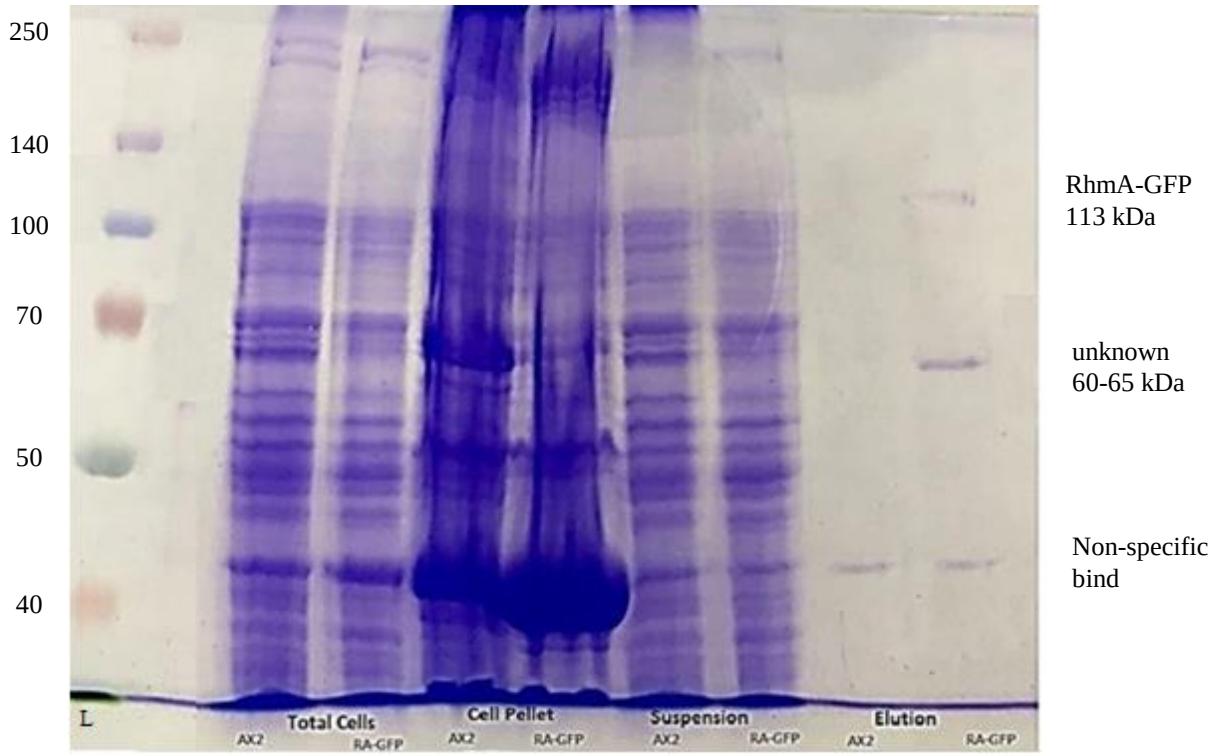

Figure 4-23 Total cell lysate immunoprecipation using anti-GFP coated beads. Extracts from wild type (AX2) and RhmA-GFP (RA-GFP) cell fractions from total lysate (Total cells), cell pellet, cells (containing RhmA-GFP) were used to identify protein bands specific to RhmA eluate absent in the wild type (control). The fraction from each cell total lysate (total cells), cell pellet, non-bound suspension (suspension) and elution pull down with anti-GFP beads. L, 10 - 260 kDa (Fisher Scientific)

One unique band was seen (around 65 kDa) in the *rhmA*$^{+}$ cells that was absent from the wild type cells. Mass spectrometry is ongoing to identify the protein, whose size did not match any of the STRING network associated proteins (Chapter 3.4.1). SDS PAGE gives an approximated molecular weight and many proteins behave atypically, and do not run according to size. For example, some proteins exhibited binding more than the expected amount of SDS, others less. This phenomenon is especially true for proteins with hydrophobic surface patches (Matagne *et al.*, 1991; Shi & Jackowski, 1998). Thus, the protein size of the unique band can be estimated at 65 ± 5 kDa, and, as most of the potential substrate proteins are largely hydrophobic in nature, this band awaits proper identification for conclusive data.

There was no evidence in the preliminary analysis for rhomboid oligomers although as with substrates, interactions may not have been maintained on the gel.

4.3 Discussion

Dictyostelium is one of the simplest model organisms that shares the important biological processes cell motility, phagocytosis, complex differentiation and multicellular development, amongst others with higher eukaryotic cells. Studies of these processes were made here to investigate whether RhmA is involved in function analogous in other eukaryotes, and to address the function of the conserved gene family in *Dictyostelium*.

In this chapter, the first *in vivo* experimental data for the protein RhmA is presented. It was shown using fluorescence microscopy that *Dictyostelium* RhmA is a protein associated with internal membranes that colocalises with FM4-64 dye and accumulating in the contractile vacuole. Bioinformatics predictions (Chapter 3.4.1) predicted it to have seven transmembrane domains and be located in the endoplasmic reticulum.

Deletion of *rhmA* had several interesting effects. *rhmA*$^{-}$ cells displayed a reduced chemotaxis response to cAMP. Although the *rhmA* null cells do eventually polarise and orient toward the tip of the micropipette in needle assay, they display less directionality and are less elongated than wild type cells. The *rhmA* mutant was also defective in chemotaxis towards folate, which implied a basic defect in motility or even in chemotaxis as a whole; a hypothesis supported further by the significantly reduced locomotion of *rhmA*$^{-}$ cells even in the absence of any chemoattractant.

Previous work showed that *Dictyostelium* mutants defective in chemotaxis can suffer impaired aggregation (Eichinger *et al.*, 2005; Firtel & Meili, 2000). Unexpectedly, however, *rhmA* null cells did not demonstrate noticeable impairment in aggregation. In *rhmA*$^{-}$ cells there was only a mild chemotaxis defect, and as aggregation does not solely rely on chemotaxis but on other mechanisms such as cell-cell adhesion differences (Ponte *et al.*, 1998), impaired aggregation was not observed.

To determine whether *rhmA* null cells were unable to demonstrate proper chemotaxis because of an inability to activate the cAMP-induced aggregation stage gene expression, qPCR of genes key to the aggregation was performed. It was found that *rhmA* null cells exhibit wild type transcription of cAR1 and ACA that are representative of genes expressed during aggregation required for chemotaxis (Iranfar *et al.*, 2003). Thus it was

concluded that the defects in cell movement observed were not a result of secondary effects on gene expression, although the possibility cannot be excluded that other genes required for both the folic acid and cAMP chemosensory response are not fully expressed.

Poor slug phototaxis was also observed in *rhmA*$^{-}$. The signalling during phototaxis is complex, and the basis for phototaxis is not well understood. It is known, however, that the first phenotypic effect of mitochondrial impairment in *Dictyostelium* is loss of slug phototaxis/thermotaxis (Darcy *et al.*, 1994, Francione *et al.*, 2011). Light affects cAMP signalling in the slug stage by speeding up the movement of prestalk cells and stimulating cAMP release (Fisher & Annesley, 2006). *rhmA* null slugs could move towards the light source but their movement was less directed in comparison with wild type slugs. As knocking out *rhmA* did not completely abate the slugs' ability to sense the light source, RhmA is presumably involved in slug migration coordination, not phototaxis directly.

Transmission electron microscopy revealed *rhmA*$^{-}$ mitochondria with altered ultrastructure, with white spaces and less compact cristae. It was also observed that the mutant cells had significantly fewer spherical mitochondria than the wild type, and a much higher proportion of tubular mitochondria present. At present, it is not known what determines the variation in morphology, but may relate to frequency of mitochondrial fission events. The change in the form is similar to that observed for the FtsZs, (*fszA* and *fszB)* knockout mutants (Gilson *et al.*, 2003). In bacteria, the protein FtsZ is the principal component of FtsZ cytokinetic ring (the Z-ring); a ring that constricts the cell at division. Null mutations in *fszA* and *fszB* resulted in a higher fraction of cells with tubular mitochondrial morphology (Gilson *et al.* 2003). Although the appearance of white spaces, was not observed in the FtsZs null mutants. It is interesting to note that FszA and FszB both have single transmembrane domains predicted by TMHMM and Signal P. Signal P and mitoprot also predict cleavage sites for FszA at 30 and FszB at 42 amino acids with the probability 0.9384 and 0.3487 respectively. Both proteins have been shown by GFP fusion to be located in the mitochondria. Hence these can be considered potential RhmA substrates.

The data from the succinate dehydrogenase assay also suggest that respiration in the mutant cell mitochondria is reduced vs wild type. This may explain the altered motility of the mutant cells. The fundamental role of succinate-coenzyme Q reductase in the

electron transport chain (ETC) of mitochondria makes it essential in most multicellular organisms. In mammalian cells, succinate dehydrogenase functions not only in mitochondrial energy generation, but also has a role in oxygen sensing and tumour suppression (Jones & Thompson, 2009). To verify an effect of RhmA on the ETC, the amount of ATP per cell needs to be measured.

Dictyostelium encodes two dynamin-like proteins, DymA and DymB (Wienke *et al.*, 1999). The inhibition of mitochondrial fission in *dymA*$^{-}$ mutants appears to be more severe than that in the *fsz* mutants, as the mitochondria of the former are not only tubular but are also clustered into interconnected sets of tubules (Wienke *et al.*, 1999). These proteins in *Dictyostelium* and their orthologues in *A. thaliana, S. cerevisiae* and *Cyanidioschyzon merolae* play key roles in mitochondrial outer membrane fission (Arimura & Tsutsumi, 2002; Bleazard *et al.*, 1999; Labrousse *et al.*, 1999). Dynamin proteins need to be processed in before they are imported to the mitochondria, which maybe analogous to cleavage of mitochondrial genome maintenance protein 1 (Mgm1), the yeast homologue of the mammalian protein optic atrophy protein 1 (OPA1). Mgm1 functions specifically in membrane fusion. It is the only one of the three dynamin family GTPases regulating mitochondrial membrane dynamics in yeast that has an aminoterminal signal peptide. Mgm1 is a dynamin-like large GTPase of the inner mitochondrial membrane which is essential for mitochondrial fusion and mtDNA inheritance (Zick & Reichert, 2013). The identification of Mgm1 as a key substrate of Pcp1 was able to explain the phenotype of mitochondrial fragmentation and impaired mtDNA inheritance that had previously been observed in *pcp1* null strains (Herlan *et al.*, 2003; Leroy *et al.*, 2010). Clearly, further studies are required on the post-translational processing of the potential mitochondrial division proteins FszA and B, and DymA in *Dictyostelium*.

Another likely candidate for RhmA potential substrate is CyrA, a novel cysteine-rich protein (63kDa) with four EGFL repeats is cleaved into two major C-terminal fragments, CyrA-C45 and CyrA-C40. One of the most well studied rhomboid, Rho-1 in *Drosophila*, is the main physiological regulator of EGF receptor signalling in the fly. It is required for development at multiple embryonic stages, during eye and wing disc development by mediating cleavage of Spitz, the EGF receptor ligand (Tsruya *et al.*, 2002). In mammals,

EGF binds to an EGFR to initiate intracellular signalling that regulates a diversity of cellular processes, including cell motility and chemotaxis. EGF is also known to enhance cell spreading and motility in normal and cancer cells via its regulation of the EGFR (Zandi *et al.*, 2007). CyrA is suggested to be analogous to the mammalian EGF, it needs to be cleaved by an unknown protease in the ER to be secreted in the ECM. A synthetic 18 amino acid peptide (DdEGFL1) of CyrA (EGFL1) that is present in both CyrA-C45 and -C40 has been shown to enhance both random cell motility and cAMP-mediated chemotaxis (Suarez *et al.*, 2011). Even though it is not a chemoattractant and doesn't enhance the folate mediate pathway, CryA is able to rescue chemotaxis towards folate when the pathway is blocked by commercial inhibitors. This suggest that the DdEGFL1 may activate a novel motility pathway (Nikolaeva *et al.*, 2012). Rhomboids in other eukaryotes such as *Drosophila* (Wasserman *et al.*, 2000), *C. elegans* (Dutt *et al.*, 2004) and humans (Adrain *et al.*, 2011) are known to regulate or enhance EGF signal, thus it is plausible that RhmA cleaves CryA to activate it (Figure 4-24). In *Dictyostelium*, this type of protein processing has previously been reported to occur in the acyl-CoA binding protein (AcbA), which is secreted and cleaved by the membrane bound serine protease TagC to generate the bioactive peptide Spore Differentiation Factor-2 (Anjard & Loomis, 2005).

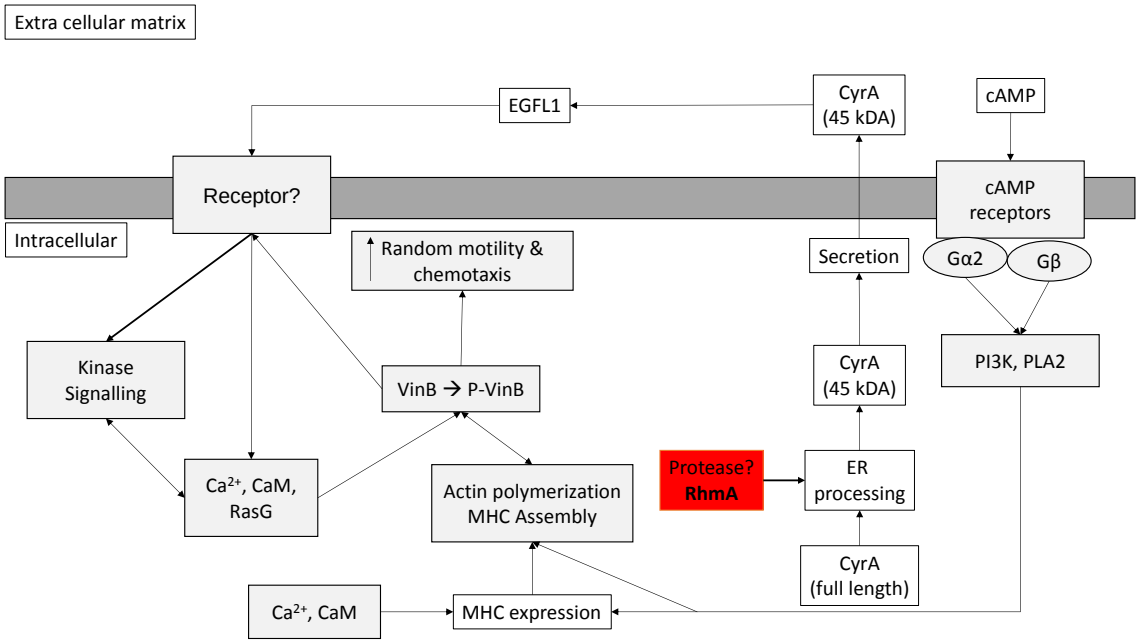

Figure 4-24 Proposed model of cleavage of CyrA by RhmA to induce EGFL repeat signal transduction in *Dictyostelium*.

In summary, Rhomboid A protein has a role in the maintenance of proper mitochondrial morphology and in cellular motility. The phenotype observed for the delay in response to chemical stimuli and movement could be attributed to a depleted energy source due to aberrant mitochondria since the succinate dehydrogenase assay showed that mitochondrial activity was significantly decreased. A role in cell motility is consistent with qPCR results which showed maximal *rhmA* transcription between aggregation and formation of slug. Nevertheless, more work is required to elucidate the potential substrate. Some mitochondrial proteins have been identified as potentially interacting with RhmA, but further work is ongoing using model-substrate assays in the group of K. Strisovsky (Institute of Organic Chemistry and Biochemistry AS CR, v.v.i., Prague, Czech Republic) while in our laboratory, fluorescence based colocalisation studies are in progress.

Chapter 5
Role of RhmB

5.1 Introduction

This chapter details the characterisation of the phenotype of the RhmB protein of Dictyostelium. The *rhmB* null cells described here showed compromised folic acid chemotaxis, micropinocytosis and significantly slower growth than wild-type cells. The phenotype reported here implicates RhmB in multiple possible cellular process. However, the *rhmA/rhmB*$^{-}$ double knockout interestingly was unable to phagocytose bacterial prey, and *rhmB* transcription levels are enhanced in the *rhmA*- null mutant suggesting some linked or redundant function.

5.2 Results

5.2.1 Deletion of *rhmB* gene

To better understand the role of RhmB in the regulation of cellular behaviour, an *rhmB* null strain in *Dictyostelium* was generated by homologous recombination. A construct was made consisting sequences 1.1 kb upstream of the start codon and 0.7 kb downstream of the end of the *rhmB* gene, with a blasticidin resistance cassette inserted in between the up- and downstream genes (Gaudet *et al.*, 2007). The cassette was inserted so that it was able to replace most of the active rhomboid. The construct was transfected into wild type cells and transformants were cloned following selection by using blasticidin (Chapter 2.2.4). All clones were checked to be *rhmB* null via RT-PCR (see Chapter 4.2.2 for figure).

5.2.2 Morphology of *rhmB* null cells

Cell diameter of 29 ± 0.5 μM and 19 ± 1.8 μM were measured for *rhmB*$^{-}$ and wild-type cells, respectively (mean ± SEM, n = 30 cells; Figure 5-1). In addition to significantly larger cells, *rhmB*$^{-}$ cells had a more rounded morphology.

rhmB null cells were able to complete their developmental life cycle and form fruiting bodies, but notably smaller aggregates, slugs and aberrant fruiting body morphology with thickened stalks and smaller spore heads. *rhmB*$^{-}$ spores had a mean maximum diameter

of 6.7 ± 0.2 μm compared with 8.5 ± 0.4 μm in AX2 cells. The spores remained viable even though they portrayed a smaller morphology.

The *rhmB* null cells growth rate was assessed on bacterial plates, on which 100 cells were mixed with an overnight culture of the *K. aerogenes* culture and plated on SM agar. Plaque size was then measured over time (Figure 5-2). Growth on SM agar plates was significantly slower for *rhmB* null cells than for wild-type cells.

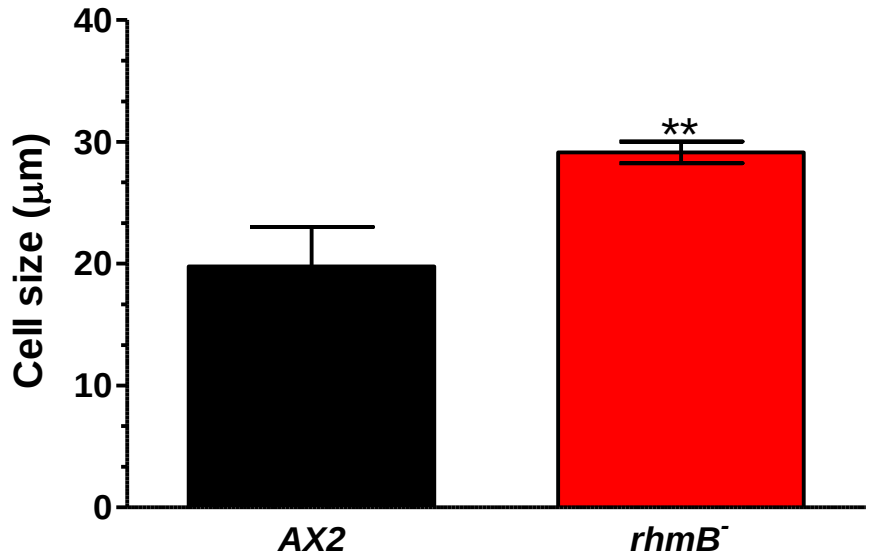

Figure 5-1 Size of *rhmB*$^-$ cells. Mean size ± SEM was calculated after 24 h incubation in HL5 at 22ºC (shaking). The cells were measured using the in-built Nikon Eclipse 90i tools. *rhmB*$^-$ cells were 54% larger than wild type. These experiments were repeated three times. ** = P ≤ 0.01

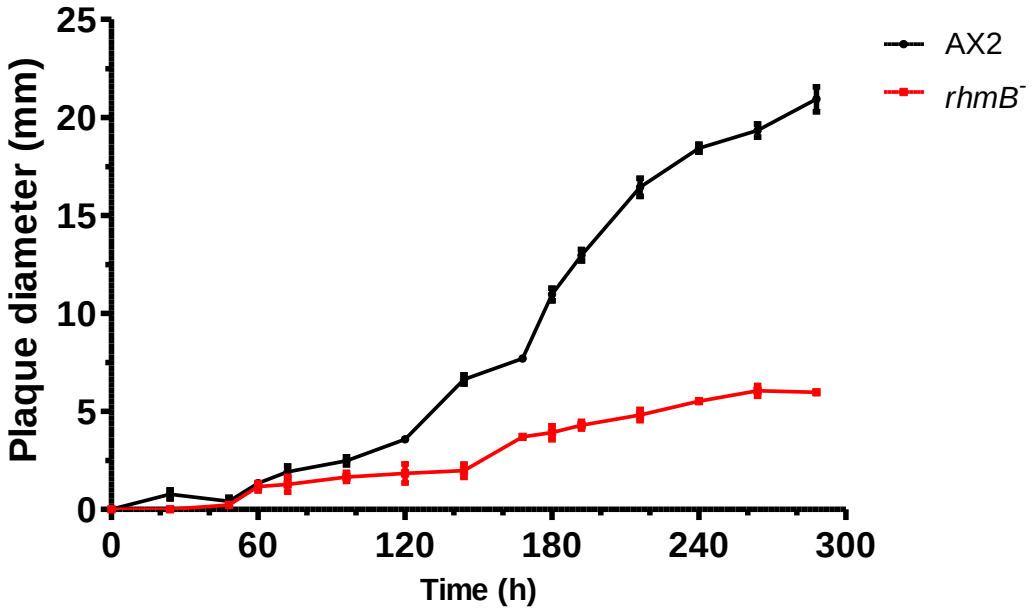

Figure 5-2 Reduced phagocytosis in *rhmB*⁻ cells. Plaque size: rhmB⁻ cells grew significantly ($P \leq 0.01$) slower on the *K. aerogenes* lawn than wild type cells. Data are means ± SEM of three independent experiments.

5.2.3 Disruption of *rhmB* results in slow growth

To check the growth kinetics of *rhmB*⁻ cells in axenic media, *rhmB*- and wild-type cells were cultured in HL5 medium supplemented with ampicillin/streptomycin at 22 °C. Cell growth was determined by measuring cell density at regular time intervals (Figure 5-3). The *rhmB*⁻ cells grew significantly slower than the wild-type cells. The doubling time (t_1 = 0 h, t_2 = 72 h; see Chapter 2.1.3 for details) of *rhmB*⁻ was approximately 24.6 ± 2.4 h, three times longer than that of wild-type cells (7.4 ± 1.2 h). The stationary phase for *rhmB*⁻ cells was reached when cells density was 10^5 cells, whereas for wild type cells the maximum cell density is 10^7 cells. This phenotype was rescued in the complemented strain (Section 5.2.8).

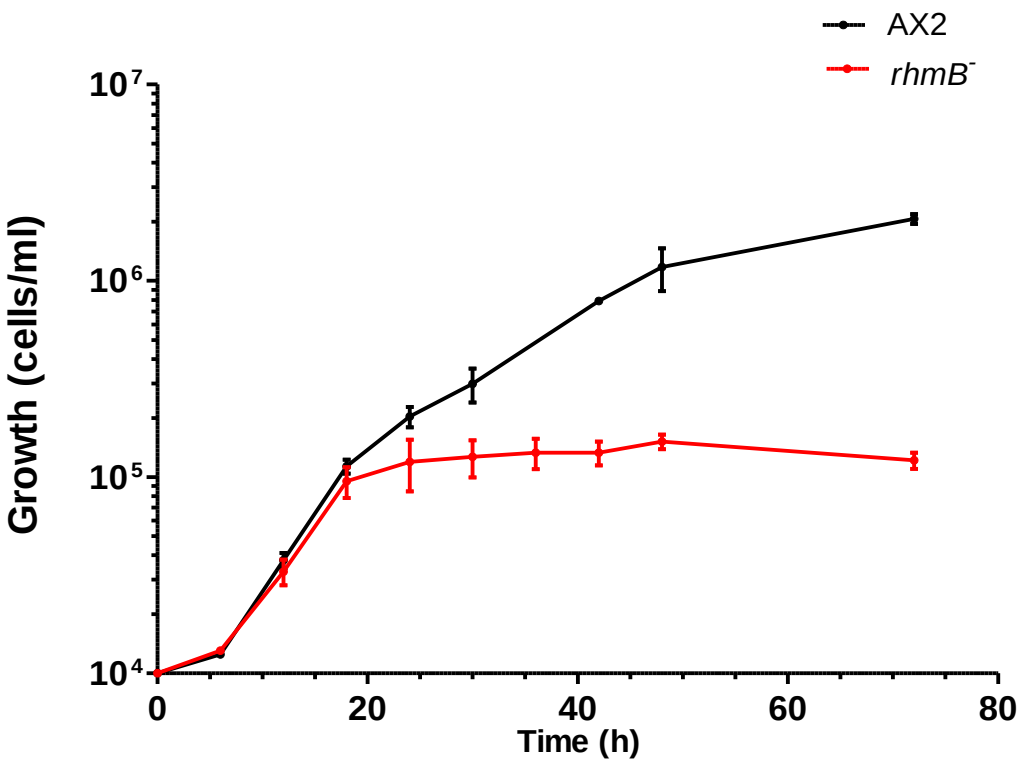

Figure 5-3 *rhmB*$^-$ growth in axenic media. *rhmB*$^-$ mutants grew significantly slower than wild type cells. The double time of *rhmB*$^-$ mutants is 24.6 ± 2.4 hours, three times longer than that of wild type cells (7.37 ± 1.2 hours). These data show the means ± SEM of three independent experiments, performed on different days.

It is known that many *Dictyostelium* mutants that grow slowly in axenic culture have defects in cytokinesis (Noegel & Schleicher, 2000). Defects in cytokinesis of cells grown in suspension culture typically result in large cell sizes as compared with wild-type cells because these cells become multinucleated. Since this defect is dependent on function of the actin cytoskeleton it was therefore investigated whether the slow growth and larger cell size of the *rhmB* null mutant was due to abnormal cytokinesis. Despite the defects in cell growth and cell size, results showed that there was no evidence of multiple nuclei/cell in *rhmB*$^-$ cells (Figure 5-4).

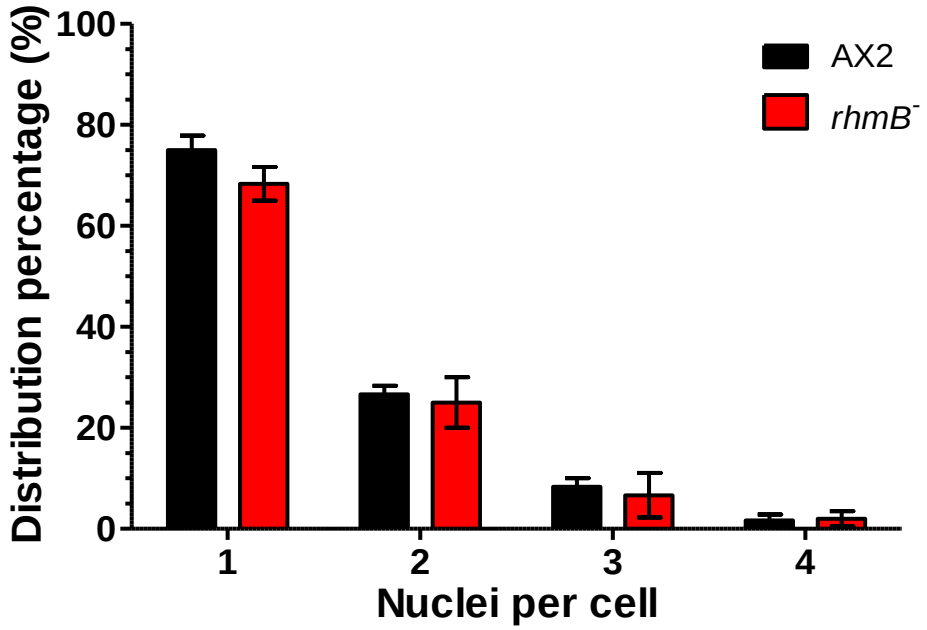

Figure 5-4 Nuclei per cell. Nuclei were stained by DAPI (4',6-diamidino-2-phenylindole) and visualised using fluorescence microscopy. The distribution of more than one nucleus per cell showed no significant difference between AX2 (69.4% ± 3.9%) cells and the *rhmB*$^-$ cells (65.7% ± 3.2); (mean ± SEM), in three independent experiments.

5.2.4 Inactivation of *rhmB* results in defective folate chemotaxis

Dictyostelium rhomboids resemble rhomboids in other unicellular eukaryotes, such as *Plasmodium* and T*oxoplamsma*, through their mediation of signals for cell movement during different life cycles (Buguliskis *et al.*, 2010, Ejigiri *et al.*, 2012). Therefore, as with *rhmA*-, chemotaxis assays were performed to examine whether *rhmB*$^-$ cells were defective in their ability to detect and respond to external chemoattractant gradient in both one drop and under agarose assays (Figure 5-5, 5-6). In one drop assay, *rhmB*$^-$ cells showed a 30 min delayed response to folic acid compared with the wild type cells (measured as the time for 50 % of the cell drops showed a response). Interestingly, there was no significant difference in chemotaxis to cAMP (Figure 5-7) between *rhmB*$^-$ and wild type cells. These results indicate that there is no direct effect of RhmB loss in the ability of *Dictyostelium* cells to move.

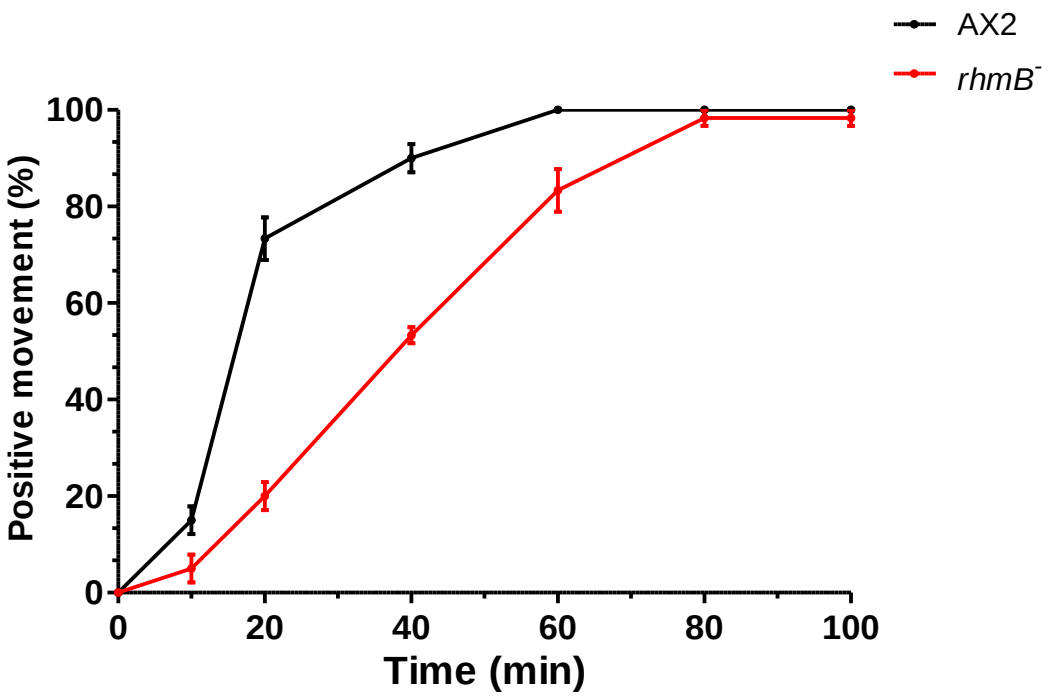

Figure 5-5 *rhmB*$^-$ response in folic acid one drop assay. *rhmB*$^-$ cells showed 30 min delay in response to 10 µM folate vs AX2 cells (measured as the time it took 50% of the population to respond). Data are the means ± SEM for results for three independent experiments.

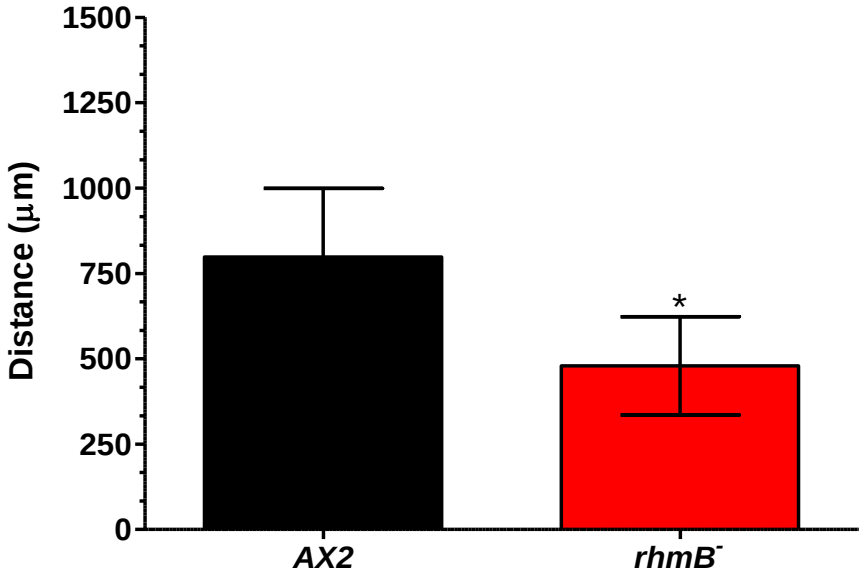

Figure 5-6 *rhmB*$^-$ folate under agarose chemotaxis assay. *rhmB*$^-$ cells exposed to folate show a delayed response compared with wild type cells. Data are the means ± SEM for results obtained in three independent experiments. * = $P \leq 0.05$

.

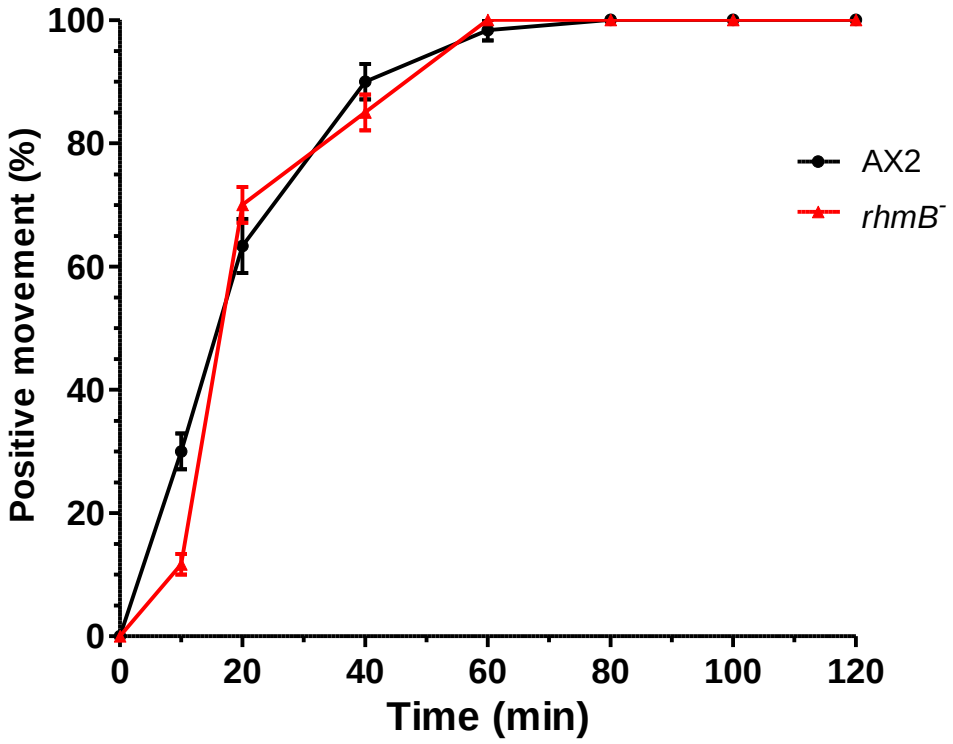

Figure 5-7 cAMP one drop chemotaxis assay. No significant different was seen between *rhmB*$^{-}$ and wild type cells response to cAMP. Data are the means ± SEM for results obtained in three independent experiments

5.2.5 RhmB affects cell adhesion

It is known that *Dictyostelium* have two different types of adhesion sites that differ in their sensitivity to cations (Ponte *et al.*, 1998). Contact site of type A (CsA) are stable in the presence of EDTA (up to the concentration of 10mM), whereas contact sites of type B (CsB) are easily disrupted by EDTA at the concentrations as low as 1-2 mM. The *rhmB* mutant cells adhere less effectively to substrate than the wild-type cells but, in the presence of EDTA, the difference was not significant (Figure 5-8), indicating that the effect observed was CsB dependent.

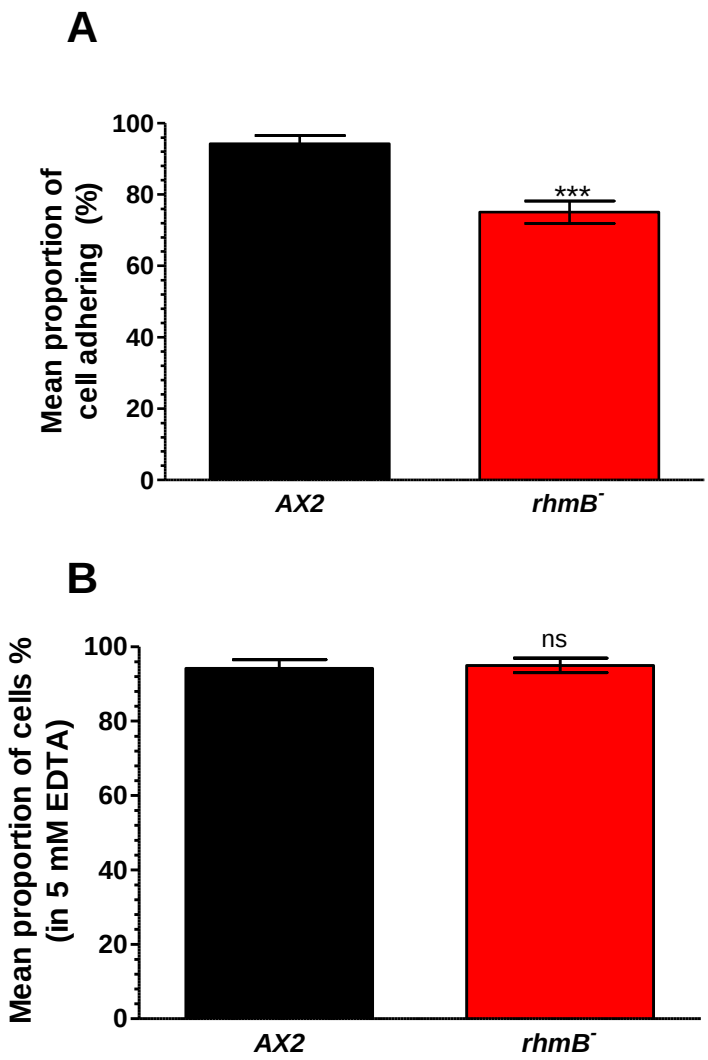

Figure 5-8 Changes in *rhmB* expression affect adhesion. Adhesion levels for wild-type, *rhmB*$^{-}$ are shown normalised for control measurements with wild-type cells. **A:** Substrate adhesion of wild-type, *rhmB*$^{-}$ cells was measured in the absence (total adhesion) and B: in the presence (cation-dependent adhesion) of EDTA. Data are means ± SEM in three independent experiments.

Cell to cell adhesion was measured as described in chapter 2 (Chapter 2.1.8.2). In *rhmB* null cells the difference in mean number cell aggregates was 15% (± SEM: 4%) lower than the wild-type cells at 28% (± SEM 5%), corresponding to an approximate 1.8 fold reduction. These results suggest that RhmB might regulate both the bivalent cation-sensitive cell-to-cell and cell-to-substrate adhesion.

5.2.6 *rhmA*/*rhmB* double knockout

rhmB cells demonstrated a delayed response to folate as did *rhmA* mutants. Therefore, *rhmA/B* null strains were generated to see if a more severe, additive, defect would be

observed. The double knockout was made using the *Cre-loxP* recombination system, which permits the recycling of the blasticidin cassette. Briefly, gene targeting the construct was made that had the cassette 'floxed' by the *loxP* sites with additional stop codons across all reading frames. Temporary expression of the *Cre* recombinase removes the cassette through intramolecular recombination, but retains the stop codons. This temporary expression creates nonsense mutations within the targeted gene. The blasticidin cassette can then be used for another gene construct (Faix *et al.*, 2004). Gene disruption was confirmed by PCR and lack of transcription using RT-PCR.

Interestingly, the *rhmA/B* null cells failed to grow on *K. aerogenes or E. coli* lawns. Growth in axenic media was also very slow. However, Trypan Blue staining assay showed drops in the viability to only be about 5 % (94 ±5 %; mean ± SEM, in three experiments).

5.2.7 Rescuing the developmental defects of *rhmB* deletion

To confirm that phenotypes observed were the results of *rhmB* deletion, a complementation strain was also constructed. The *rhmB* was modified to contain the *BamHI* and *XhoI* restriction sites which permitted directional cloning into the pDT29 plasmid vector (that was kindly provided to us by D. Traynor, MRC-LMB, Cambridge). The N-terminus was left unmodified to allow targeting of the protein through its N terminal secretory or mitochondrial signal, however part (8 AA) of its C-terminus truncated to facilitate cloning. This tagged the C-terminus of RhmB with GFP under actin 15 promoter. The RhmB-GFP construct was transformed into both the wild type lines and the *rhmB*$^{-}$ lines producing *rhmB*$^{+}$ and *rhmB*$^{-/+}$ complementation cell lines.

Developmental analysis of the RhmB-GFP expression employed wild type *rhmB*$^{+}$ and *rhmB*$^{-/+}$ cell lines, were used to determine if cells expressing RhmB-GFP showed altered morphology (Figure 5-9) As expected, complemented cells did not show altered development; axenic growth, cell size and defects in development were all restored by the re-expression of the protein, thereby confirming that the fusion protein was functional. The defects seen in *rhmB*$^{-}$ cells were caused by the ablation of the *rhmB* gene.

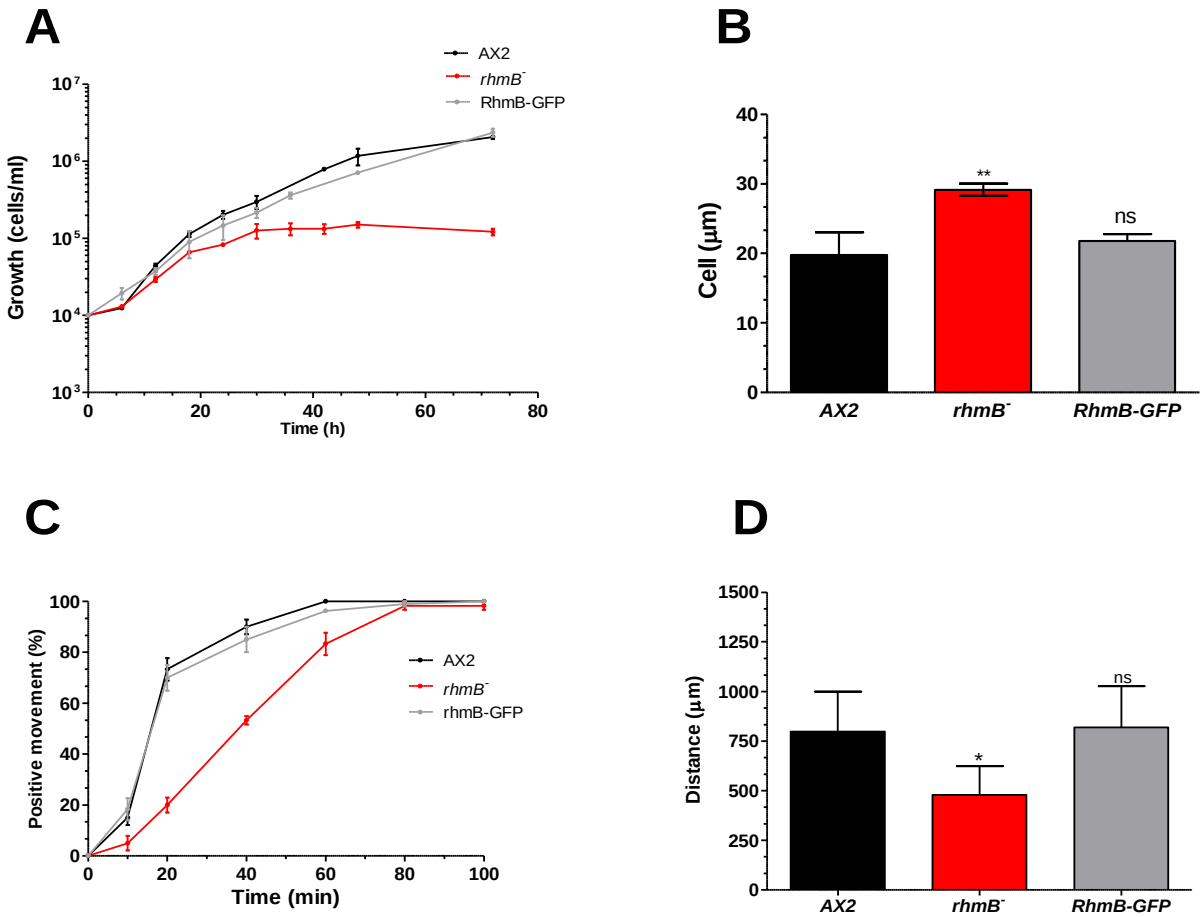

Figure 5-9 Developmental phenotypes of *rhmB*⁻ and RhmB-GFP cell lines (A) (B) Growth in axenic media and cell size (longest diameter), respectively after transfection of the construct A15::rhmB-GFP into *rhmB*⁻ cells. **(C) (D)** One drop folic acid chemotaxis assay and under agarose folic acid respectively. *rhmB*⁻ cells showed a delay that was rescued by introducing the GFP construct. Data ae mean ± SEM of three independent experiments.

5.2.8 Transcription levels: redundancy in rhomboids?

rhmB^{-} cells showed a defect only during their vegetative life cycle stages. Transcription levels of *rhmB* were analysed over a time period of 24 h of development (Figure 5-10), showing expression throughout, although relative levels varied, *rhmB* had the highest transcription levels during aggregation.

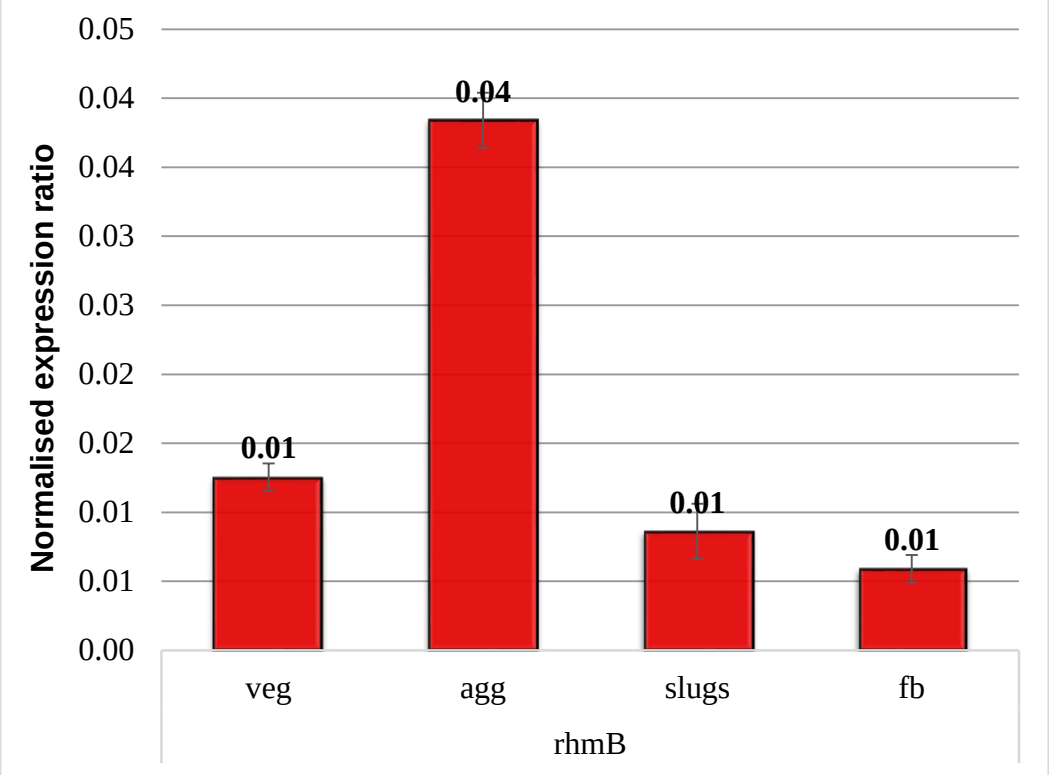

Figure 5-10 *rhmB* transcription throughout 24 h development. RNA samples were prepared from *Dictyostelium* cells during growth (Veg), Aggregation (agg) Phototactic Slug (slug) and Fruiting body (fb) with derived cDNA used to amplify genes. H7Q2 was used as a constitutively transcribed control. (B) Results are means ± SEM of three independent samples.

The data here were in agreement with the RNA-Seq databases (http://dictyexpress.biolab.si; Figure 5-11) in which, *rhmB* reached the highest expression level around 4 h, when cells entered the aggregation phase of their development. These levels remained steady until cells began to differentiate into pre-spore and stalk.

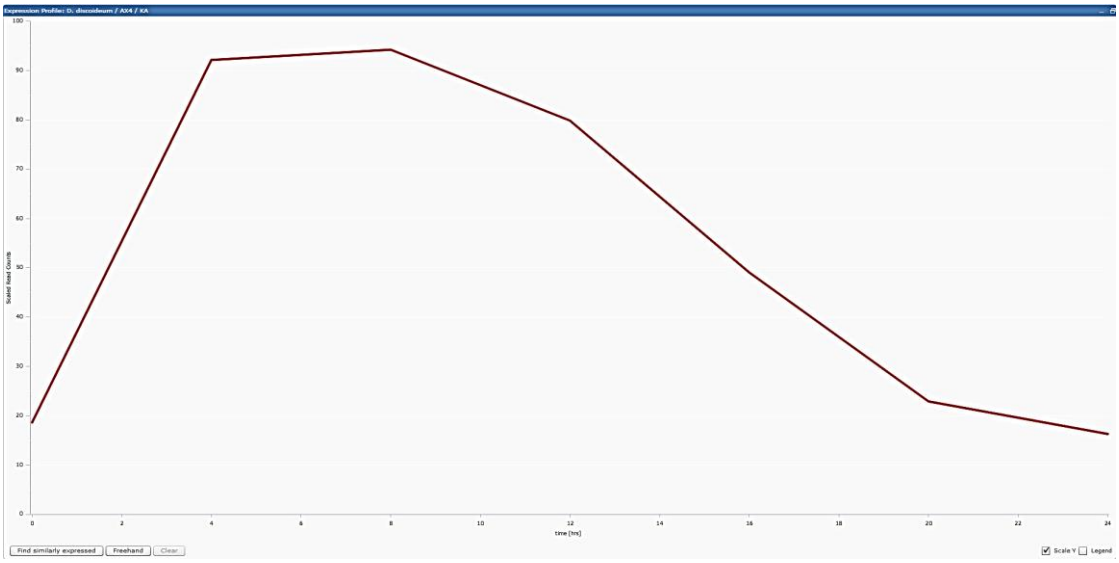

Figure 5-11 Expression profile of RhmB from RNA-Seq database. It was used to illustrate the expression profile of the *Dictyostelium* RhmB protein (http://dictybase.org). RNA-Seq data were collected from *Dictyostelium* at 4hr time intervals during development

To investigate whether the amount of *rhmB* transcript related to that of other rhomboids, transcriptional levels of the *rhmA* and *rhmC* were assessed in the *rhmB* null background. Indeed, *rhmA* had markedly increased transcript levels (Figure 5-12) in vegetative *rhmB* null cells ($P \leq 0.001$) and *rhmB* slugs ($P \leq 0.001$) vs wild type levels.

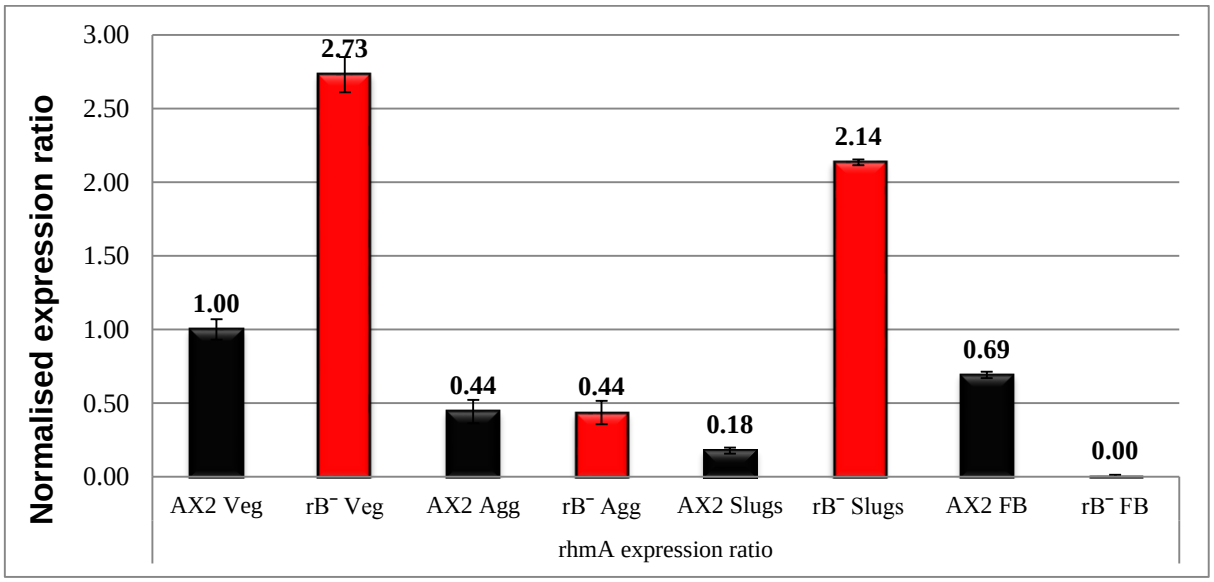

Figure 5-12 Transcription of *rhmA* in *rhmB*⁻ cells. *rhmA* expression was compared using qPCR in the wild-type and *rhmB* null cell lines, compared with the control gene H7Q2 (expression 1.0) in three 3 independent experiments ± SEM.

5.2.9 Subcellular localisation of RhmB

Cells expressing RhmB-GFP (*rhmB*$^{+}$) were used to visualise the localisation of the RhmB. Transcription of RhmB-GFP was confirmed by RT-PCR using GFP primers. Fluorescence imaging of RhmB-GFP agreed with RhmB bioinformatics that predicted that the protein might be localised in the mitochondrion: RhmB-GFP distribution co-localised with the mitochondrion specific plasmid pJSK543 (mitochondria outer membrane) kindly given to us by J. King (University of Sheffield, Sheffield, UK). Cells were analysed at different phases of growth, and throughout the *Dictyostelium* life cycle the RhmB-GFP showed unchanging pattern (Figure 5-13). These results strongly suggest that RhmB is targeted to the mitochondria and required there for its function. There was no other location of RhmB-GFP visible in other cell locations.

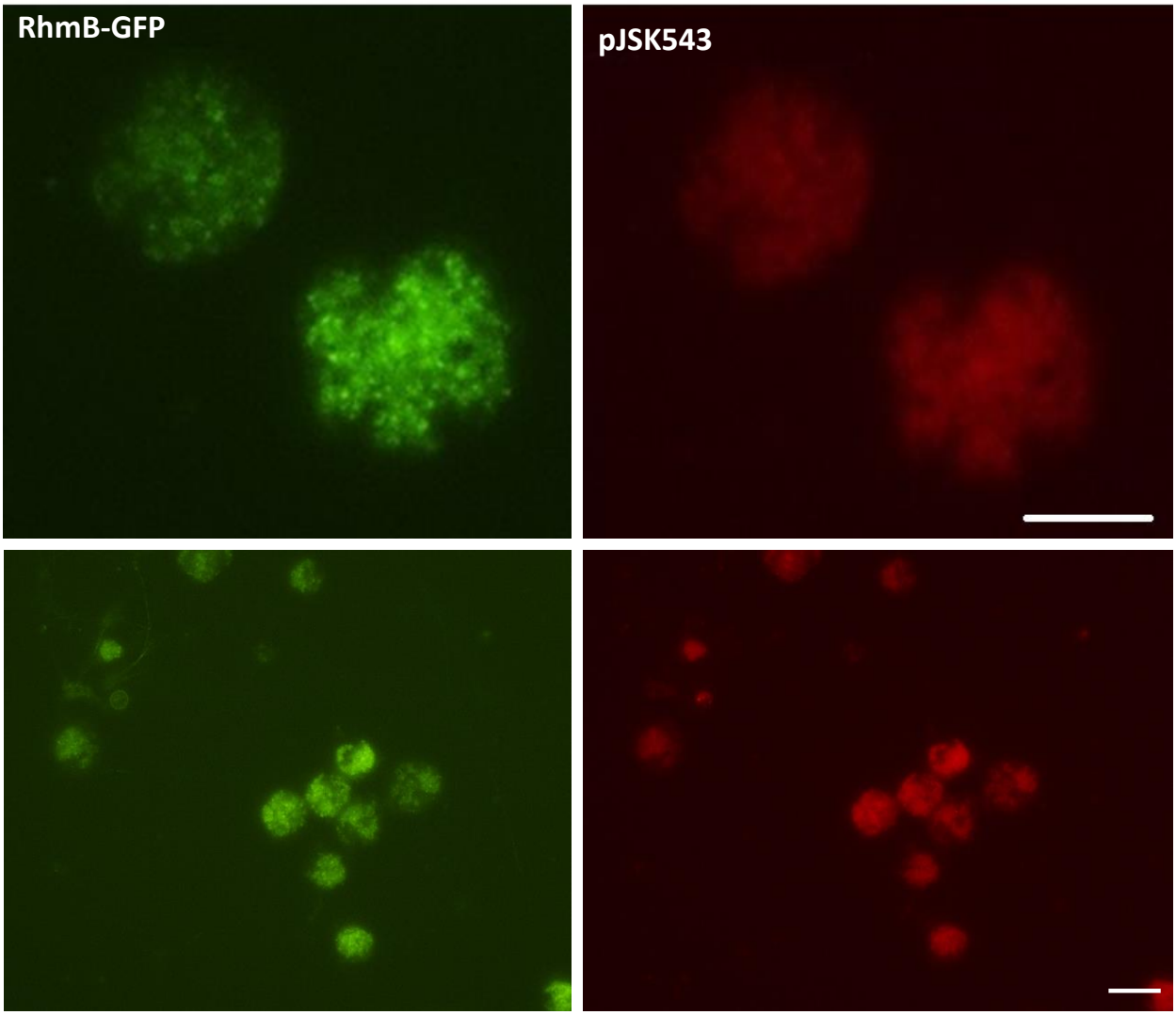

Figure 5-13 RhmB-GFP and pJSK543 colocalisation studies. Cells expressing RhmB-GFP were transfected with pJSK543 and live cells were visualised using fluorescence microscope. GFP location in green and the mitochondrial plasmid in red. Scale bars 10 µM.

5.2.10 Mitochondrial morphology and function

As the results of the fluorescence microscopy showing that RhmB-GFP was being targeted to the mitochondria, the possibility that loss of RhmB caused mitochondrial defects was tested by TEM of *rhmB*$^{-}$ cells. The resulting images did not display any obvious differences in cell or mitochondrial ultra-structure, despite their larger cell size (Figure 5-14, 5-15).

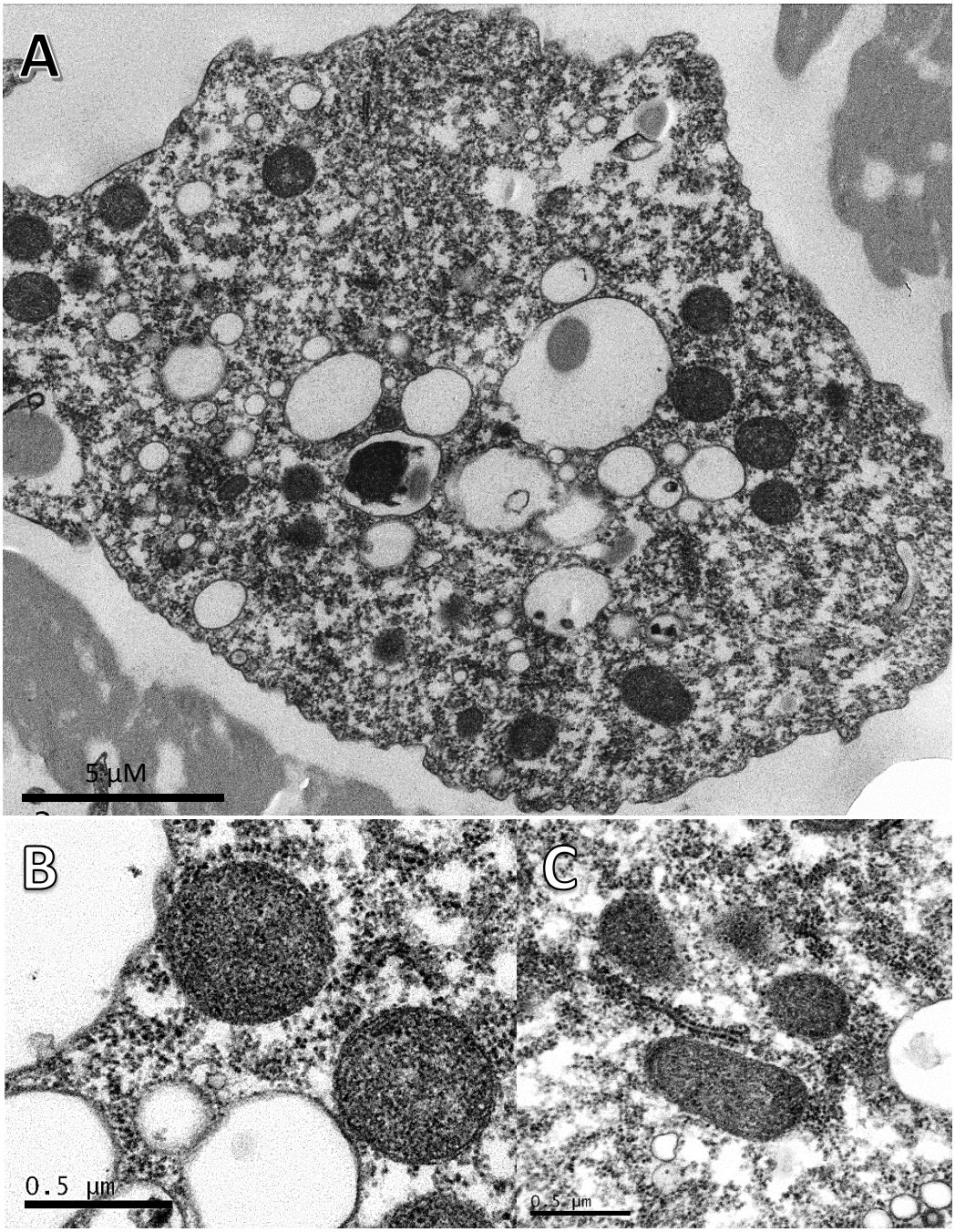

Figure 5-14 TEM of *rhmB*$^-$ cells. (A) Electron micrograph of *rhmB* null cell (B) (C) mitochondrial morphology of the cells.

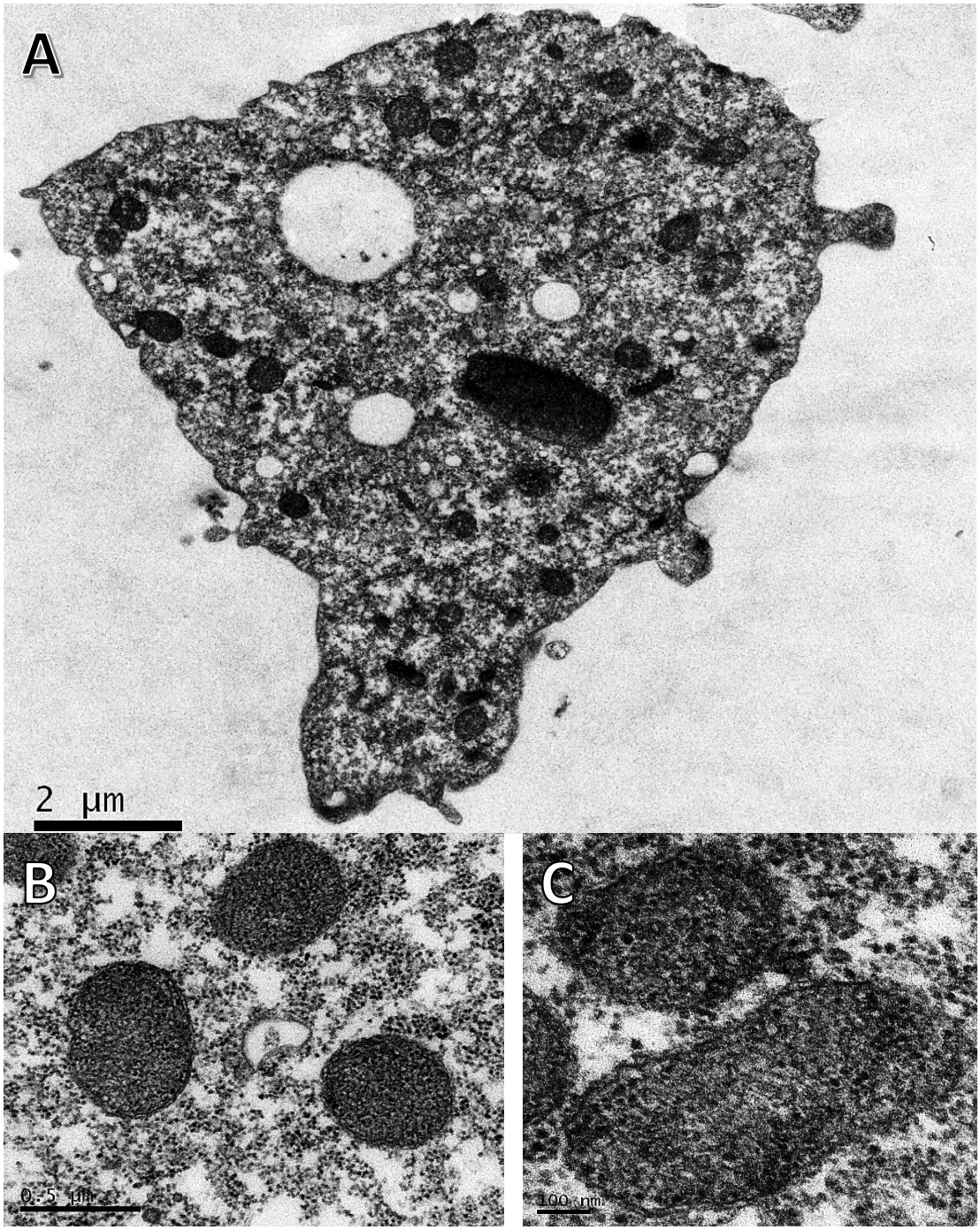

Figure 5-15 TEM of AX2 cells. (A) Electron micrograph wild type cell (B) (C) mitochondrial morphology of the cells

To assess the fitness of the mitochondria, a simple succinate dehydrogenase activity assay was performed with *rhmA*$^{-}$ cells (Chapter 4.2.8). After results were normalised for the protein content there was no significant difference in Km values for *rhmB*$^{-}$ cells (20.05 ± 2.23) and wild type cells (14.56 ± 1.16).

5.2.11 Potential substrates

Examples of notable proteins potentially associated with RhmB, are dynamin family (dymA), adenine nucleotide Carrier (ancA) and dUTP diphosphatase (dut). As there was experimental data to support association in STRING with the dynamin family, transcript level was examined using qPCR. Levels of dynamin family transcripts were quantified in the *rhmB* null mutant and wild type cells (Figure 5-16), as before with RhmA (Chapter 4.2.10).

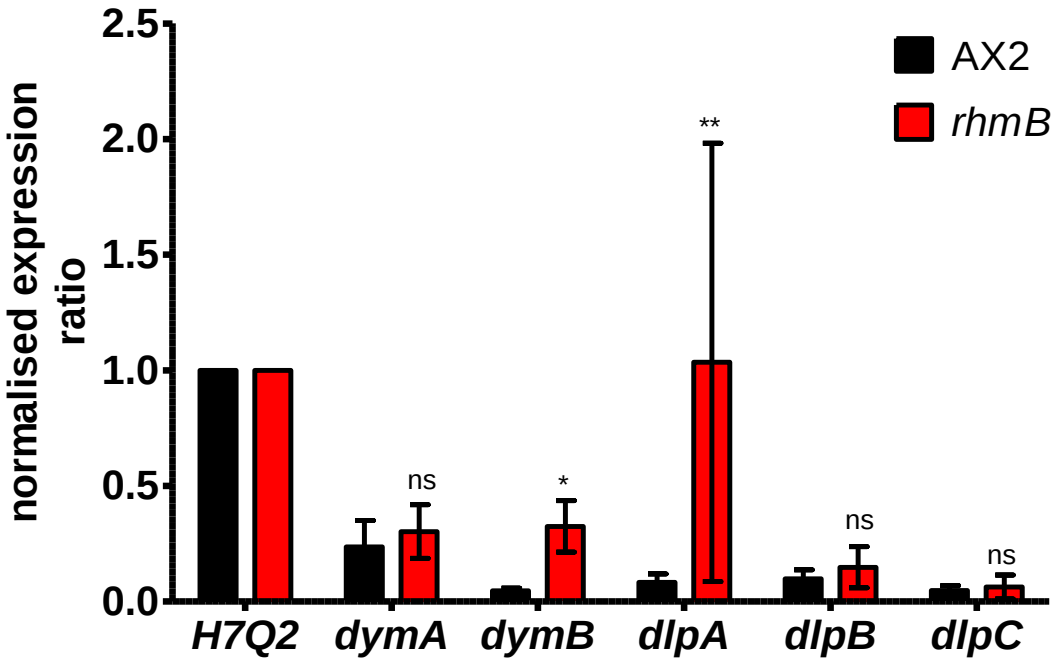

Figure 5-16 qPCR of in vegetative AX2 vs *rhmB*$^{-}$ cells. Comparison of related genes *dymA, dymB, dlpA, dlpB and dlpC* in the wild type and *rhmB*$^{-}$ vegetative cells. Results were standardised to constitutive H7Q2 gene transcription in three independent experiments ns = $P > 0.05$, * = $P \leq 0.05$, ** = $P \leq 0.01$

5.3 Discussion

The present study showed that the knockout of *rhmB* results in a consistent and marked phenotype, in which cells grow slower in axenic media, and show defects in their response to folic acid stimulation with poor adhesion to substrates and cells.

Localisation studies with GFP fused to the RhmB C-terminus showed that the protein is located in the mitochondria. This was indeed in accordance with bioinformatic predictions. However, despite being targeted to the mitochondria, RhmB does not play any obvious role in either the maintenance, division or the morphology of the organelle. This could be explained by the fission mechanism employed by *Dictyostelium*, which usually involves an extra-mitochondrial based system (Barth *et al.*, 2007). Also employed by plants and fungi, this system was inherited from bacterial ancestors which employed an ancient FtsZ-based fission process. However, FtsZ proteins have been functionally replaced by dynamin-like proteins in most eukaryotes. Although, FtsZ still functions in some lower eukaryotes, such as *Dictyostelium* (Nishida, 2003). In *Dictyostelium*, the deletion of dynamin A and the FtsZ orthologues FszA and FszB have shown to cause aberrant mitochondrial morphology (Gilson *et al.*, 2003).

Mitochondrial rhomboids are found in the genomes of all eukaryotes sequenced to date (Lemberg & Freeman, 2007). In humans, *Drosophila* and *S. cerevisiae*, PARL-like rhomboids are involved in mitochondrial fusion or in cristae remodelling (see Chapter 1). Many organisms contain orthologues of the *S. cerevisiae* PARL-like rhomboid-substrate, Mgm1 (OPA1 in metazoans), whose cleavage controls these processes but, a search thorough the *Dictyostelium* genome revealed that no equivalent of Mgm1 was encoded, nor of ccp1 – the second *S. cerevisiae* RBD1-substrate (Dowse, 2007). As mentioned earlier, however, deletion of *rhmB* does not affect the mitochondrial morphology. Furthermore, the absence of the Mgm1 orthologue suggests that RhmB may serve a different role in *Dictyostelium* compared with *S. cerevisiae*. It could also mean that its substrate is highly divergent in *Dictyostelium*. Substrates of intramembrane proteases, including rhomboids, have been shown to require TM helix-destabilizing residues; these are presumed to facilitate local helix unfolding into an open conformation conducive to cleavage (Akiyama & Maegawa, 2007; Brown *et al.*, 2000; Lemberg *et al.*, 2005; Urban

& Freeman, 2003). Beyond these conformational constraints, no sequence conservation in rhomboid substrates has been reported. Hence, it is very difficult to predict the substrates. Thus, identification of the substrate(s) of this protease would shed light on either of these possibilities, and reveal the likely networks in which RhmB operates.

As rhomboids are known to cleave dynamin like proteins (Shi *et al.*, 2011). The predictions from the STRING network and our qPCR results were interesting; showing a possible link between RhmB and the dynamin protein family. The dynamin family contains unique GTPases that are known to be involved in the fission and fusion process of the membrane throughout the cell. The first member of the family, Dynamin 1 (in humans) is crucial for endocytosis, synaptic membrane recycling and membrane trafficking within the cell, and is associated with filamentous actin. Additional dynamin family members such as DymA in *Dictyostelium* and Mgm1 in *S. cerevisiae*, have been implicated in a variety of fundamental cellular processes, including mitochondrial fission and fusion as above, antiviral activity, plant cell plate formation, and chloroplast biogenesis (van der Bliek & Koehler, 2003; Thompson *et al.*, 2012).

Furthermore the results here indicate that RhmB influences cell surface interactions, specifically adhesion, also similar to dynamin proteins. Rhomboids in other protozoa such as *Plasmodium* and *Toxoplasma*, also control surface adhesion in cells forming focal contacts (Sastry & Burridge, 2000). The aberrant growth seen on the *K. aerogenes* lawn could be attributed to lower adhesion. Mammalian Dynamin 1 affects the adhesion and the associated cytoskeleton. Also, depletion of Dynamin 2 in the fibroblasts inhibits migration of adherent cells. These findings link RhmB with the regulation of cell adhesion, thus strengthening the hypothesis that RhmB regulates a dynamin-like protein, and that the actin foci in *Dictyostelium* function analogous to the focal adhesion points of the mammalian cells (Uchida & Yumura, 2004; Wanders & Waterham, 2006).

The effect observed in the *rhmB* mutant was the opposite of that seen in the *dymB* null mutant (Rai *et al.*, 2011). DymB is made as a pre-protein of 105 kDa and is processed in the mitochondria by a two-step process similar to that of Mgm1. However, and intriguingly, unlike Mgm1 it is released back into the cytosol where it affects events at the cell adhesion sites, plasma membrane and components of the actin-based cytoskeleton. The opposing function and phenotypes of the *rhmB* and *dymB* null cells

makes it tempting to speculate that these two proteins interact, and possibly that RhmB is the protease in the mitochondria that processes DymB. Thus, the increase in the transcription of *dymB* is possibly due to a negative feedback loop. Other rhomboids are known to cleave their substrates after they have crossed minimum threshold levels (Tsruya *et al.*, 2002). In the *rhmB* null mutant, the cell hypothetically overproduces the dymB to effectively trigger its cleavage. However, as the protease in not present, there is an overabundance of the DymB long isoform, possibly leading to the *rhmB* null phenotype. Effects of overexpression of dynamin B of 105 kDa protein have not been studied.

A direct interaction between RhmB and DymB in *Dictyostelium* has yet to be established. This could be investigated by generating tandem affinity purification (TAP) tagged constructs of these proteins *in vivo* or *in vitro* by immunoprecipitation.

The other point of interest was the up regulation of *rhmA* transcript level in the *rhmB* null cells, suggesting that there may be redundancy in the rhomboids. Conversely, RhmA may be involved in the regulation of RhmB as *rhmA* null cells exhibit no transcriptional level changes of RhmB. It would be useful to determine which combinations of rhomboids proteins interact *in vivo* and if the different combinations of proteins produced subtle or pronounced differences in function. This type of regulation of proteolysis has been observed for other proteases such as FtsH (Nixon *et al.*, 2005)

In summary, it is clear that further investigation of RhmB is merited, as it seems to play a distinct and interesting role in several cellular processes.

Chapter 6

Elucidating the action of novel uPA inhibitors on *Dictyostelium*

6.1 Introduction

Collaborators at the University of Sussex, who have an interest in the synthesis and characterisation of arylboronic acids and their derivatives, have recently disclosed a synthetic route to thiouronium and guanidine substituted arylboronic acids (J Spencer, personal communication 2012). A library of compounds of regioisomeric arylboronic acids BC43, BC57 and BC11 were made, as well as their pinacol esters SR3 and JS62. *In vitro* assays showed BC11 to be a selective urokinase-type plasminogen activator (uPA) inhibitor (J. Spencer, personal communication, 2012). Therefore, a small library of bioisosteres [1]was synthesised, incorporating a potential hydrogen bond donor (e.g. AB4/5) or acceptor (e.g. JS65, JS66), and n-alkylated analogues (e.g. AB11 and derivatives). The purpose of this was to attempt to enhance the desired biological properties of a compound without making significant changes in chemical structure.

Previous work has used *Dictyostelium discoideum* to study chemotherapy drugs, with the aim of better understanding how they function and to combat the problem of drug resistance. To investigate whether these compounds would behave analogously in a range of organisms and to test their toxicity, standard assays in *Dictyostelium* were defined. It was found that the compounds produced interesting effects on wild type cells, with a decrease in directed chemotaxis without loss of viability. This was intriguing as some of the compounds were shown to be selective inhibitors of uPA, a trypsin like serine protease, particularly in tumour cells. It plays a role in regulating arterial remodelling, angiogenesis, cell migration and proliferation, as well as participating in various pathological processes, such as bacterial invasion, tumour cell invasion and metastasis (Figure 6-1; Blasi & Carmeliet, 2002). Hence, further work with the compounds was carried out to identify orthologues of the uPA in *Dictyostelium.*

[1] In medicinal chemistry, bioisosteres are substituents or groups with similar physical or chemical properties which produce broadly similar biological properties to a chemical compound.

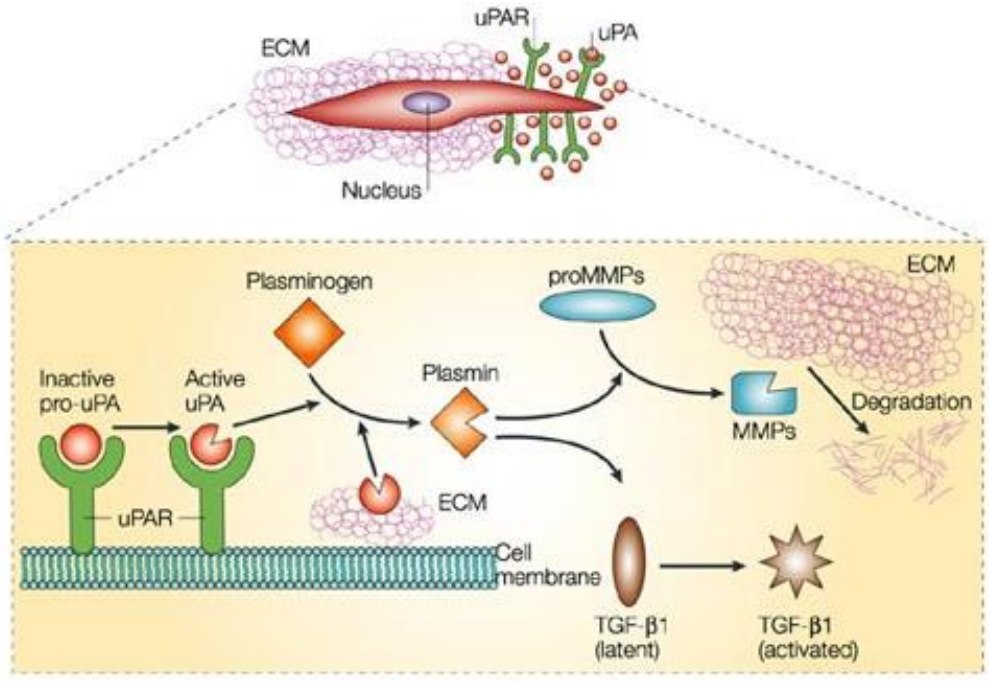

Figure 6-1 Fibrinolysis. In migrating mammalian cells, urokinase receptor (uPAR) binds to inactive urokinase (pro-uPA) at the leading edge, converting it to active uPA. Components of the extracellular matrix (ECM) might also bind to uPA to activate it. Active uPA converts the inactive zymogen plasminogen to active plasmin, which either breaks down ECM components or activates latent growth factors such as transforming growth factor beta1 (TGF-β1). Plasmin also degrades the ECM indirectly through activation of pro-matrix metalloproteinases (pro-MMPs), leading to cell migration in tumour cells. Image reproduced from Blasi & Carmeliet, 2002.

6.2 Optimisation of DMSO concentration

The boronic acids kindly provided by our collaborators were soluble in DMSO. Viability of the amoebae in DMSO was tested at a range of concentrations from 0 – 10%. The results showed that the viability of cells was not affected by any concentration (Figure 6-2), but there was a dose-dependent effect on cell adhesion and movement. *Dictyostelium* cells show a decrease in cell movement if exposed to concentrations more than 2% (Figure 6-2), and cell-to-substrate adhesion was disrupted at even 1%. Therefore, throughout the work, the proportion of DMSO in test solutions was kept to less than 0.01% v/v.

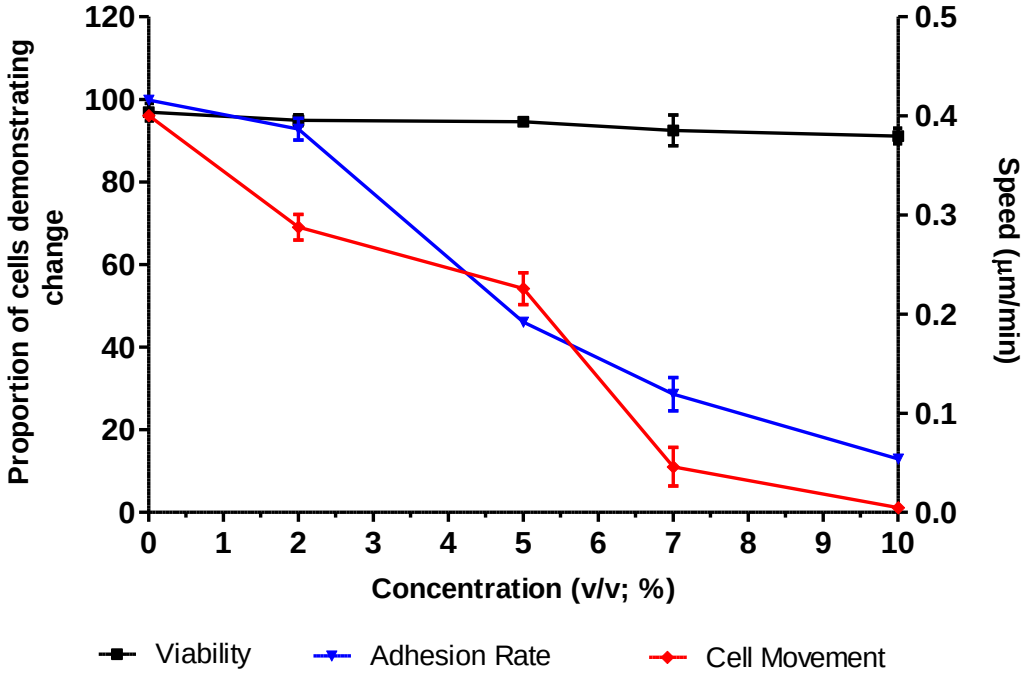

Figure 6-2 Optimisation of DMSO concentration. *Dictyostelium* is tolerant of up to 2% DMSO v/v. Adhesion > 92 ± 2.6 and Speed 0.29 ± 0.013; Data are the means ± SEM, of three independent experiments.

6.3 Development of a suitable motility assay

Dictyostelium cell behaviour when subjected to the inhibitor library was monitored by quantifying cell-to-substrate adhesion and assessing their chemotactic capability. Cells were visualised using phase contrast microscopy and their movement was recorded over a 15-min period (Figure 6-3), and controls were compared in 0.01% DMSO. To quantify *Dictyostelium* motility, Nikon NIH software was used to record the speed of the cells' motility and cell aspect, and data collected were then analysed and quantified using Quimp 11 (Image J plugin). Speed was defined as the distance travelled by the cell (measured from the centre) from time point 1 to time point 2 between each frame. Since individual cells migrated in slightly different directions, it is important to note that the mean velocity was actually a measurement for cell speed because a single direction for all cells could not accurately be determined. The cell aspect of the chemotaxing cells was defined as the ratio of the lengths of the y- and x-axes at each time point, where the value of 1 is a circle.

To quantify cell behaviour, a minimum of 15 cells were required to produce a comprehensive view of cell movement and aspect values (Robery *et al.*, 2011). Each assay was performed at least in triplicate to allow statistical evaluation of data.

6.3.1 Control assays

Images were recorded for 5 minutes prior to and 10 minutes after the addition of 0.01% DMSO (control) diluted in phosphate buffer, which served as a control solution. No significant changes were observed during the assay based on the 2 tailed student t-test (Figure 6-3). Phosphate buffer was used as a diluent in an attempt to neutralise any major pH changes that might occur due to the addition of the compounds. This standard assay enabled the analysis of compounds on *Dictyostelium* cell behaviour. The normality of the data was assessed using the D'Agostino and Pearson omnibus normality test and Kolmogorov-Smirnov test (Figure 6-4).

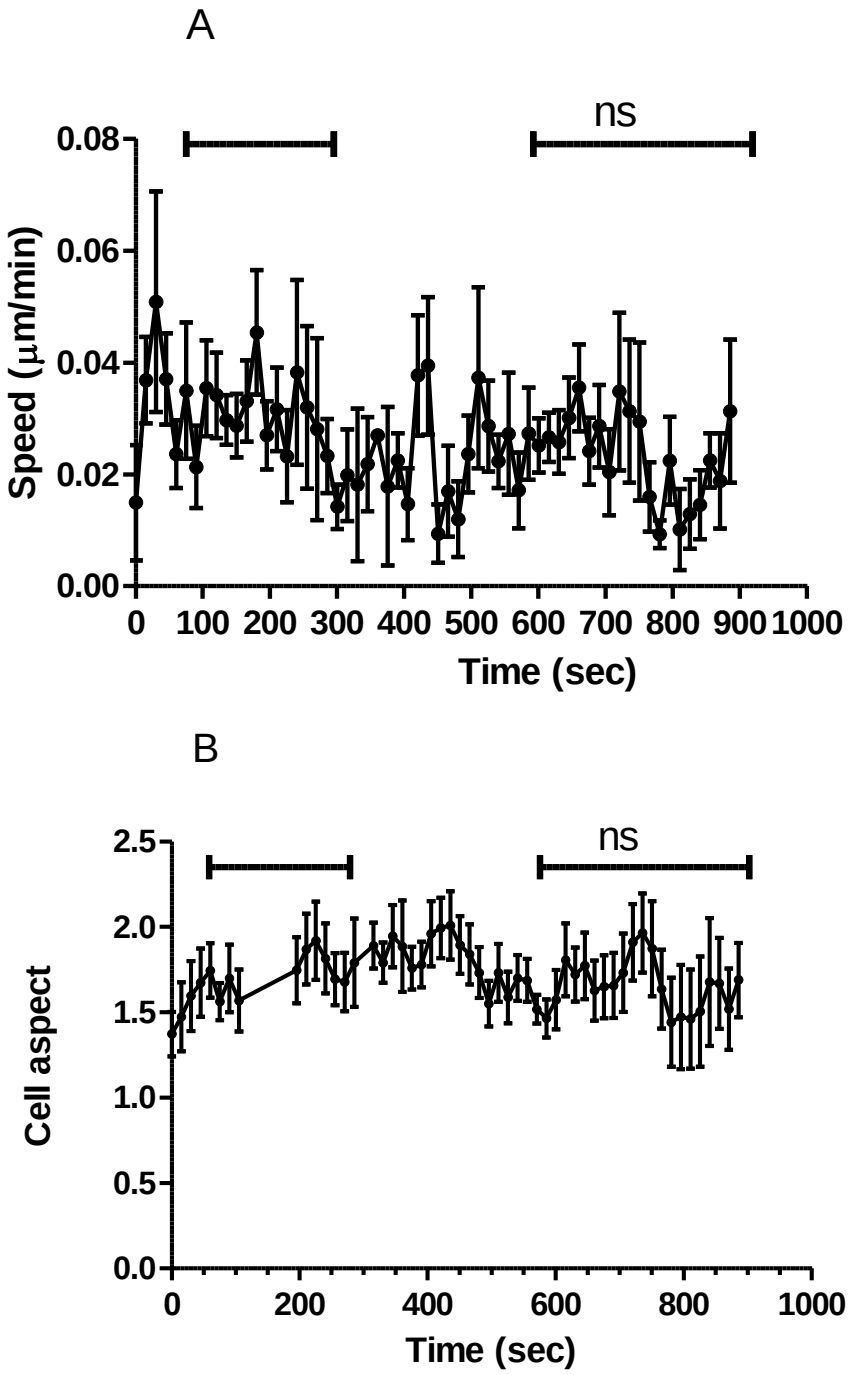

Figure 6-3 Analysis of *Dictyostelium* cell motility under control conditions (0.01% DMSO). (A) Cell velocity; (B) Cell aspect measured under a stable chemotactic gradient in a Dunn chamber; 25 cells evaluated every 6s over a 900s period with the addition of the DMSO at 300s.

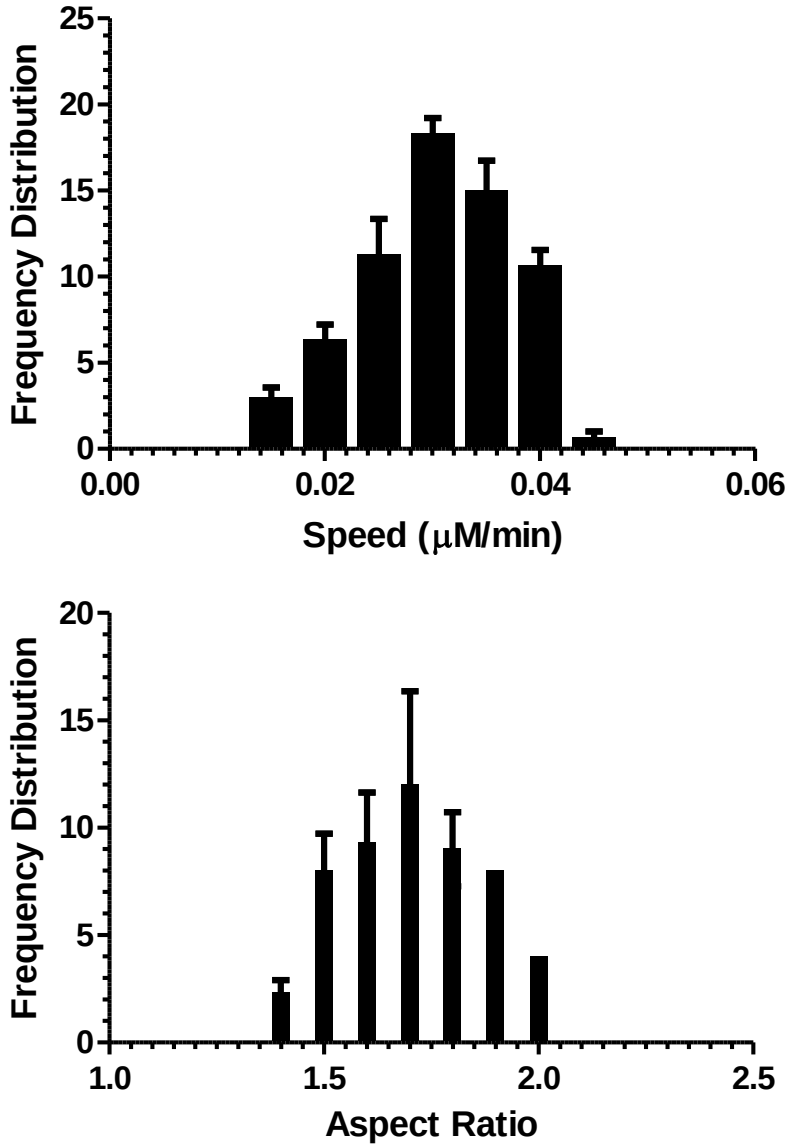

Figure 6-4 Histogram of *Dictyostelium* cell velocity and aspect. Mean cell velocity (speed) and the cell aspect was recorded for 15 cells for the duration of the motility assay. A D'Agostino and Pearson omnibus normality test showed that the data were normally distributed ($P < 0.05$).

6.3.2 Screening with test compounds

In the initial phase of testing, five concentrations of the test compound (10µM, 25µM, 50µM, 75µM and 100µM) in 0.01% DMSO were used. In this initial phase, viability was measured by using trypan blue staining. Viability was assessed after cells were incubated with the compounds for 10 min (acute) and 30 min (prolonged) to test the effect of exposure time (Table 6-1).

When using the Dunn chamber there was a delay of 3 minutes until the complete diffusion of the compound added to the outer chamber (Robery *et al.*, 2011). Cells were, therefore, monitored within the defined region of the chamber (Figure 6-6) to ensure constant exposure of cells to the compounds.

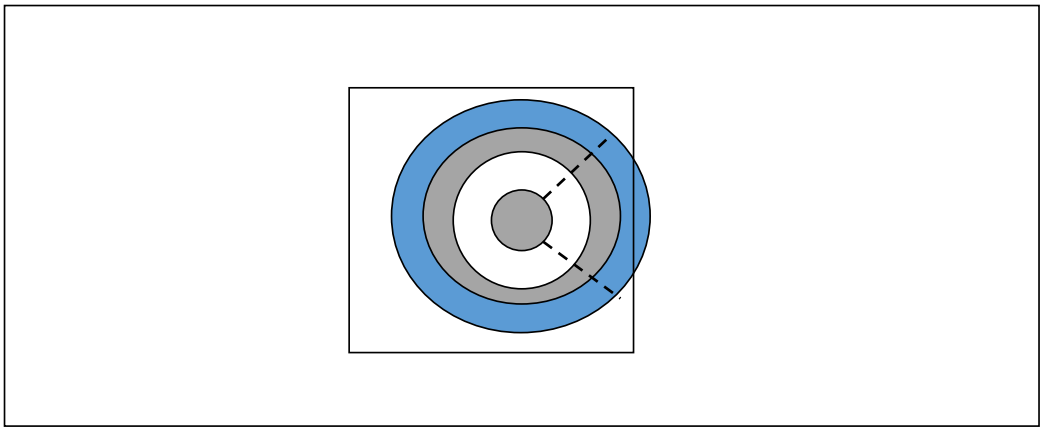

Figure 6-5 Dunn Chamber schematics. The dotted region on the diagram indicates the region within the Dunn chamber used for imaging and quantification to ensure consistent exposure to test compounds.

Table 6-1 *Dictyostelium* cell viability upon acute and prolonged exposure to test compounds showing the maximum and minimum concentrations used

Compound	Concentration (µM)	10 Min		30 Min	
		Viability ± SEM	P Value*	Viability ± SEM	P Value*
AB11	10	74.8± 0.83	P<0.001	26.2 ± 1.22	P<0.001
	100	43.3 ± 1.37	P<0.001	6.63 ± 1.17	P<0.001
AB5/4	10	50.3± 0.29	P<0.001	31.9 ± 0.95	P<0.001
	100	19.3± 0.24	P<0.001	12.9 ± 0.84	P<0.001
JS62	10	78.7 ± 0.19	P<0.001	22.2 ± 1.48	P<0.001
	100	30.6 ± 0.40	P<0.001	0.89 ± 0.33	P<0.001
JS67	10	88.1± 0.36	P<0.001	23.6 ± 0.47	P<0.001
	100	51.8± 0.23	P<0.001	2.2 ± 0.69	P<0.001
SR3	10	96.4 ± 0.83	ns	96.3 ± 1.06	P<0.001
	100	94.2 ± 0.14	ns	93.6 ± 1.83	P<0.001
BC11	10	98.0 ± 0.22	ns	92.4± 3.12	P<0.001
	100	94.5 ± 0.23	P<0.01	80.3 ± 1.91	P<0.001
BC57	10	98.3± 0.16	ns	89.9 ± 0.32	P<0.001
	100	94.2 ± 0.40	P<0.01	82.1 ± 0.12	P<0.001

* = student t test, ns > 0.05

Analysis of viability following acute exposure demonstrate that four out of the seven compounds (AB11, AB5/4, JS67 and JS62) showed a decrease (greater than 10%) in survival even at minimum concentrations. After prolonged exposure all of the compounds except SR3 provoked a decrease of ≥10% in viability.

Cells were incubated with the compounds for 30 min to test if the cells were able to recover from the exposure. The compounds affect was then terminated by a 1:100 dilution of the incubation solution into SM broth. Approximately 100 cells were then plated onto a *K. aerogenes* lawn on individual Petri dishes. After 2-3 days of incubation at 22 °C, the number of plaques formed were counted. The proportion of cells forming plaques was calculated using the following formula:

$$\frac{Dy}{Dx} \times 100\%$$

Where D_x is the number of plaques formed by control and D_y is the number of plaques formed by treated cells. It can be seen that most compounds that caused a decline in viability after acute exposure prevented *Dictyostelium* forming plaques on *K. aerogenes* except for BC11 and BC57 exposed cells. SR3 was the only compound that did not affect the viability or plaque formation after short or long incubation periods (Figure 6-6).

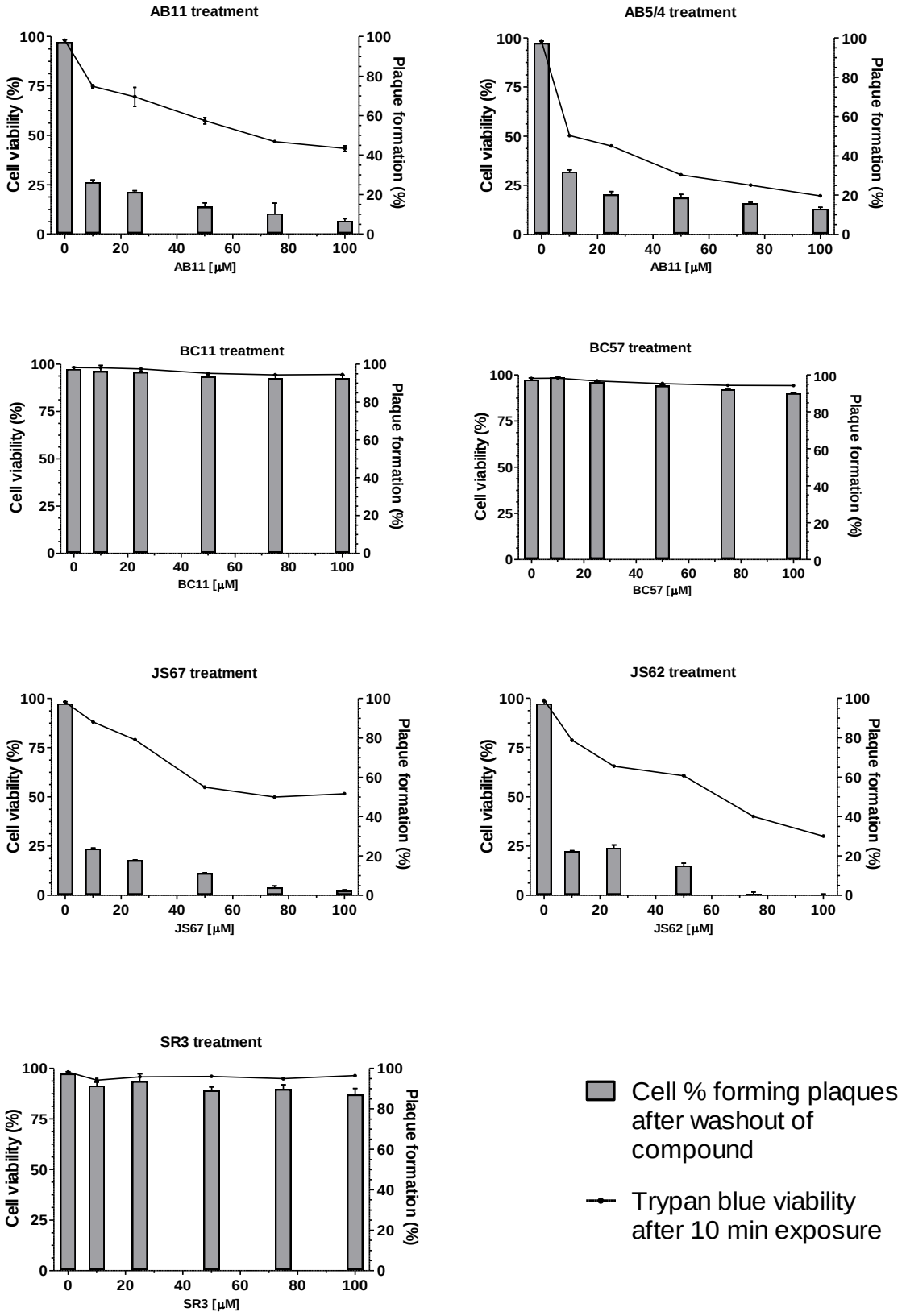

Figure 6-6 Cell viability after prolonged exposure. Proportion of cells able to form fruiting bodies on *K. aerogenes* lawn after prolonged exposure to the compounds in three independent experiments (means ± SEM).

A locomotion experiment (Chapter 2.1.9) was carried out for all the compounds. Each provoked a significant decrease in the cell motility (Figure 6-8), which could be caused by a variety of mechanism including toxicity, especially given viability results for AB11, AB5/4, JS67 and JS62.A modified locomotion assay was also used to quantify cell motility of chemotactically competent cells. After allowing time for adherence (approximately 20 min), slides were washed with phosphate buffer in order to remove dead cells. Table 6-2 shows the proportion inhibition of cell movement towards cAMP after treatment. Interestingly, compounds that had profound cytotoxic effects did not affect cell motility of remaining cells, with inhibition being < 20% at 100 µM.

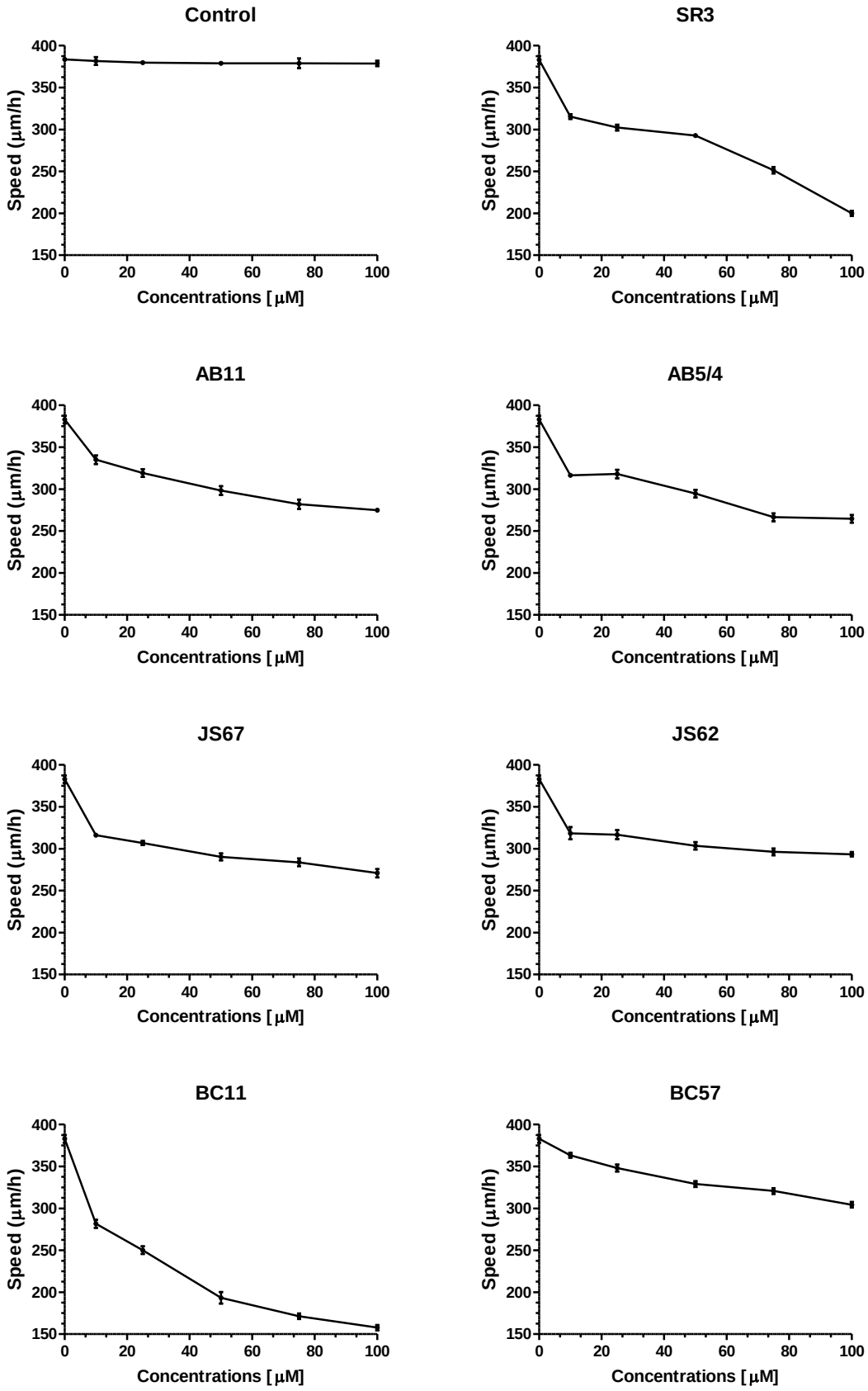

Figure 6-7 Locomotion assay Locomotion was measured by mapping cell movement of 10 individual cells on glass slides over a 2-hour period. The results are representative 3 independent repeats.

Table 6-2 Proportion of cells inhibited in chemotactic cell movement assays

Concentration (μM)	BC11	BC57	SR3	JS62	JS67	AB11	AB5/4
10	16.0	7.2	9.8	0.0	0.0	0.0	0.0
25	20.3	23.3	48.8	1.0	4.8	4.1	4.6
50	**60.2**	**45.2**	**63.4**	3.9	6.1	4.3	4.2
75	82.0	71.7	87.6	2.8	12.4	9.7	12.0
100	97.0	82.6	98.1	10.8	14.0	15.0	18.9

The results (Table 6-2) suggest that the effects seen in the general locomotion assay (Figure 6-6) for cytotoxic compounds, ABII, AB5/4, JS67 and JS62, were due to cell death. Therefore, only BC11, BC57 and SR3 were chosen for further investigations. Notably, the compounds identified here, affected motility specifically without cytotoxicity to *Dictyostelium* proved in concurrent experiments to provoke significantly decreased uPA activity in adult mice (J Spencer, personal communication, 2013). Collaborators' chromogenic assays (Figure 6-8; Smith *et al.*, 2012), BC11, BC57 and SR3 also reduced uPA activity by more than 50%.

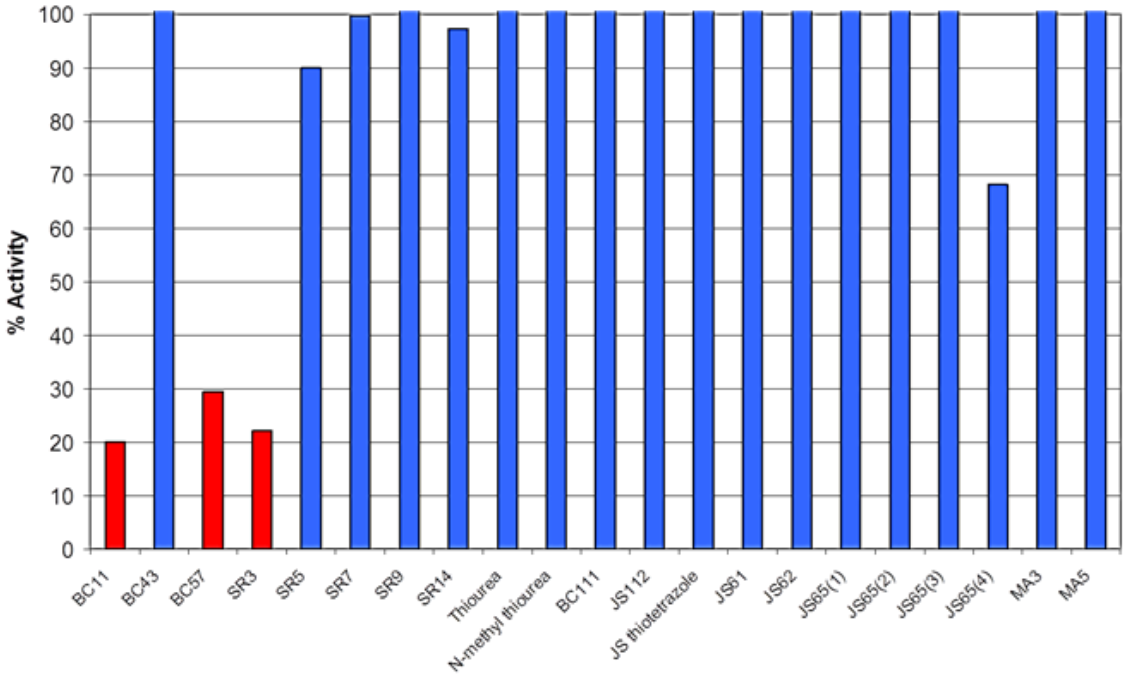

Figure 6-8 Three compounds showing selective inhibition of urokinase-type plasminogen activator (uPA). Initial screen of boronic acid library against uPA using chromogenic assay (Smith *et al.*, 2012)

6.3.3 Effect on development and chemotaxis

As SR3, BC57 and BC11 decreased cell motility, to about 50% at 50 µM concentration, a range of assays were performed caused to further investigate their effects.

Extending toxicological assays for longer exposure period, the effect of the compounds was observed for 30 h on *Dictyostelium* development on phosphate buffer agar plates (Figure 6-9).

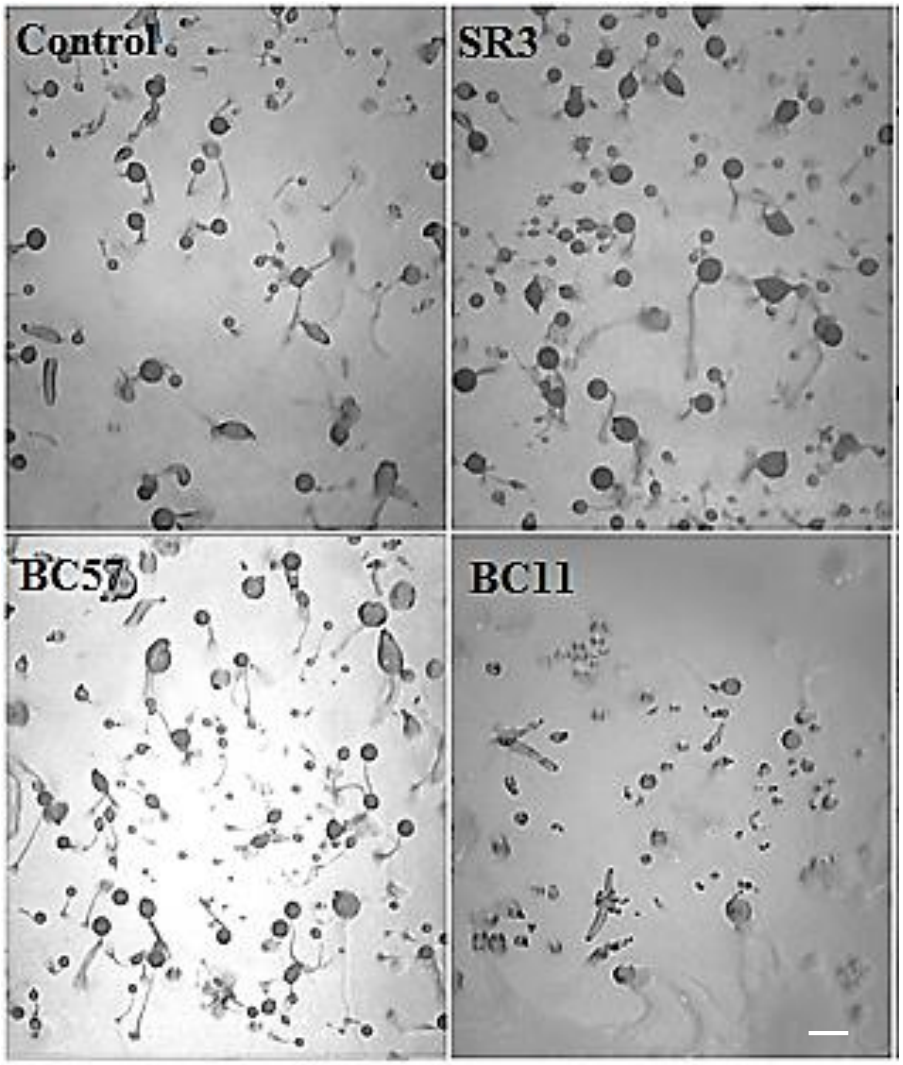

Figure 6-9 Development on KK2 agar plated. To test effects on development, cells were plates onto KK2 plates containing 50 µM of the compounds. SR3 and BC57, at 30 h formed fruiting bodies whereas most of BC11 cells remained at finger stage. Scale bar is 0.5 mm

Long-term exposure to BC57 and SR3 did not alter fruiting body morphology, whereas BC11 slowed development by a mean of 24 h ± SEM 3.5 h. Nevertheless cells were eventually able to develop into mature fruiting bodies with viable spores (data not

shown). These results, combined with cytotoxicological and developmental experiments, suggested that these three compounds did not block *Dictyostelium* behaviour via toxic or irreversible mechanisms.

Growth rate, cell size and doubling time was also measured with these three compounds (50 μM; Figure 6-1oA & B). Only BC11 caused a significant difference in growth, with doubling times nearly twice that of control and of the other two compounds. This phenotype was not apparently associated with defects in cell division as cell size was not affected (Figure 6-10C).

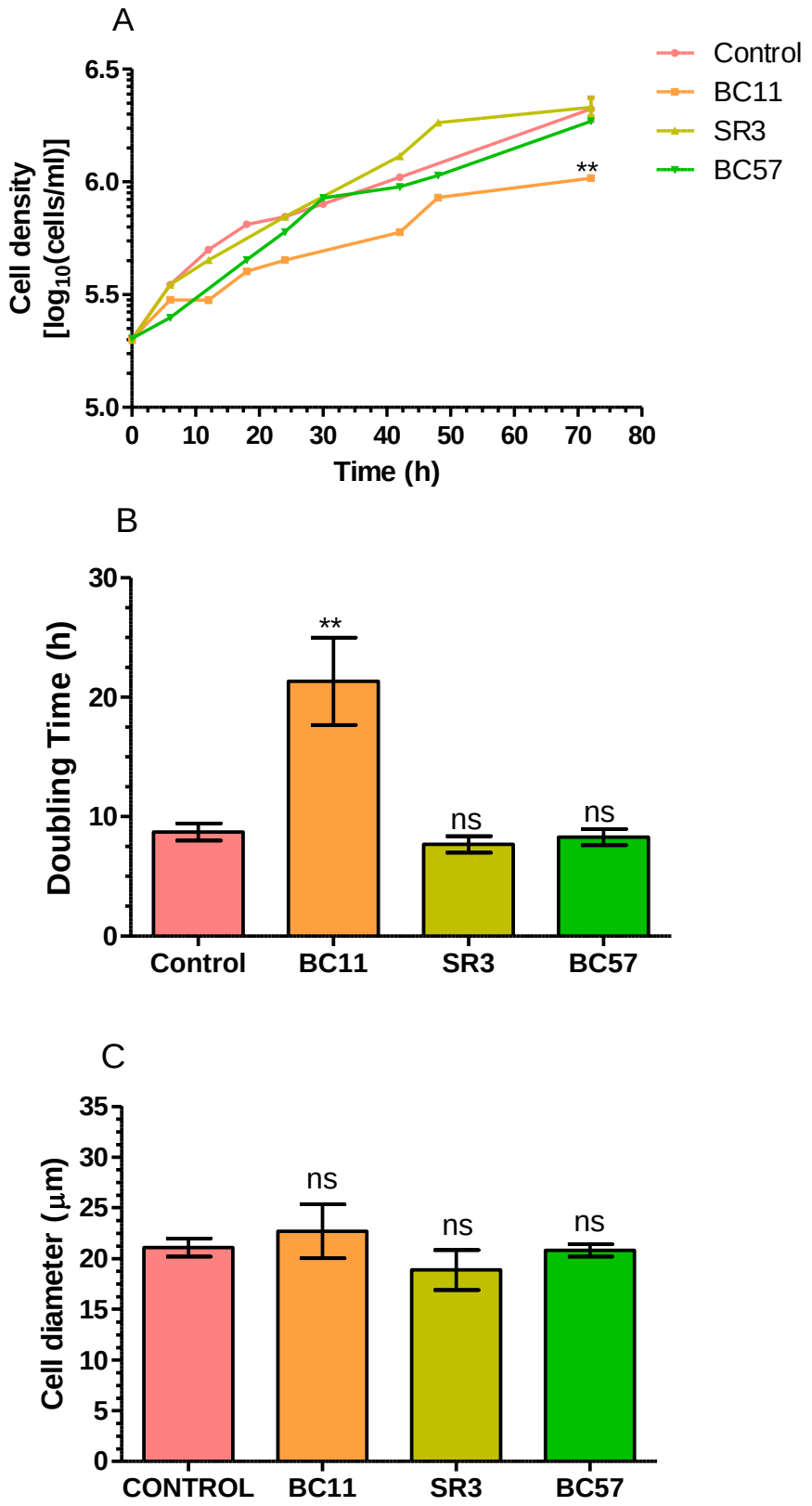

Figure 6-10 Phenotypes observed after incubation with 50 µM of test compounds (A) Growth rates of cells. (B) Doubling time from hourly readings. (C) Cell diameter 24 h; in viable cells (n= 15). Data are means ± SEM of three independent experiments, performed on different days. ns = $P > 0.05$; ** = $P \leq 0.01$

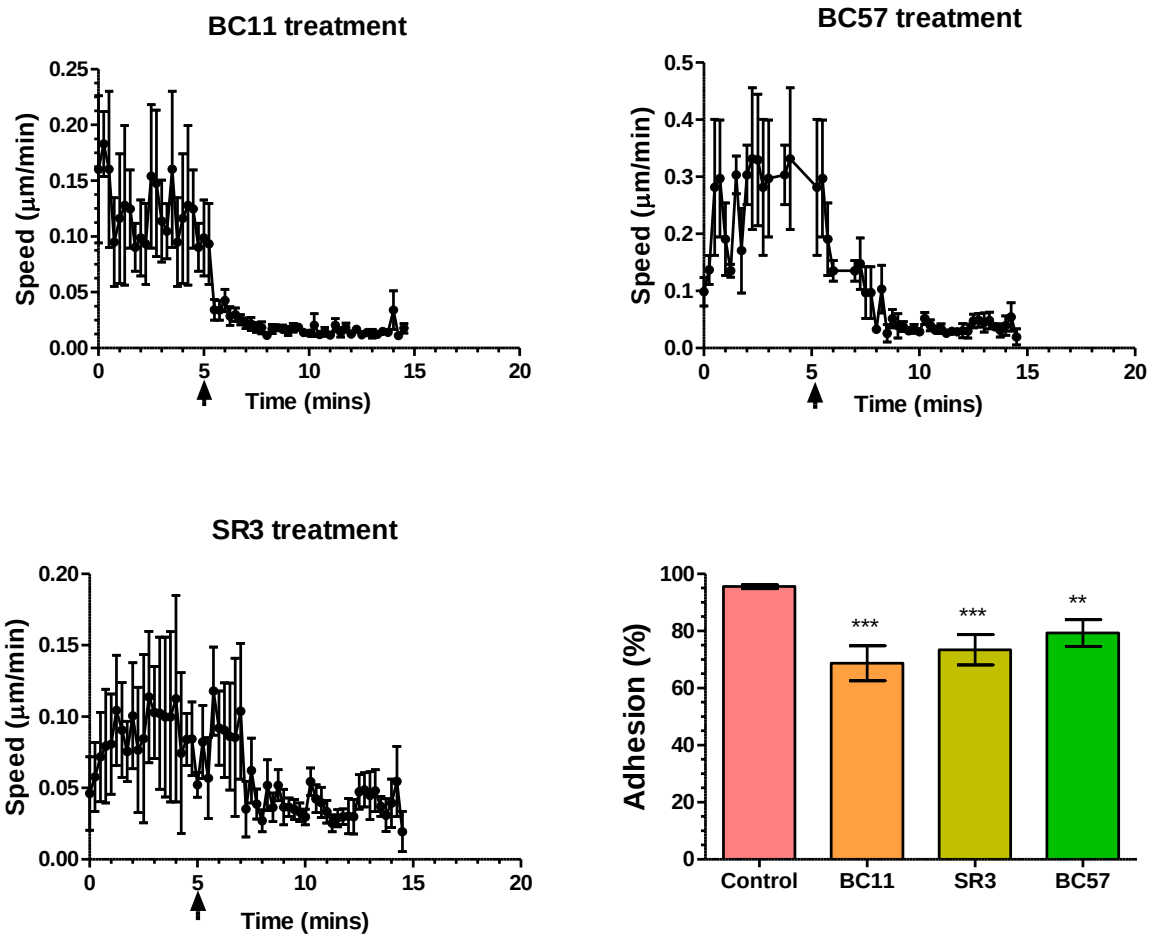

Figure 6-11 Cell behaviour after addition of 50 µM of the compounds. Speed measurements, mean ± SEM, from 15 cells. Adhesion (means ± SEM) to substrate was measured after washing coverslips twice with KK2 buffer and counting the number of cells remaining after the second wash. All experiments were reproducible different days. ** = P ≤ 0.01; ** = P ≤ 0.001;

Using 50 µM concentrations, chemotaxis assays were performed. In the Dunn chamber *Dictyostelium* cell behaviour was monitored by time-lapse photography every 15 s over a 15 min period under control conditions (Figure 6-11) within a chemotactic gradient, i.e. moving towards cAMP. Computer-generated outlines of 15 individual cells enabled the quantification of cell speed. It could be seen that the addition of the boronic acids restricted cell migration. BC11 has an immediate effect on the migration, whereas BC57 and SR3 both had a delayed effect. This would be consistent with BC11 acting on cell receptors or at the membrane, whereas BC57 and SR3 might need to be internalised by the cells for their effect to occur. All three compounds provoked decreased adherence to substrate in the absence of EDTA (Chapter 2.1.7.1 for detailed description).

6.3.4 Determination of inhibitory concentration of compounds

From results presented thus far, it can be seen that BC11, BC57 and SR3 affected cell behaviour without compromising cell viability. To discover if the potency of effect in *Dictyostelium* was analogous to that found in adult mice, uPA half maximal inhibitory concentration (IC50; provided by collaborators: BC11 8.2±1.7 μM > SR3 13.2 ±1.0 μM > BC57 15.9 ± 1.7 μM; Figure 6-12). The IC50 values were established for loss of cell movement, mean data from the last 5 min of random cell movement assays were used to calculate IC50 (Figure 6-13), i.e. the total reduction in velocity when compared to initial control conditions.

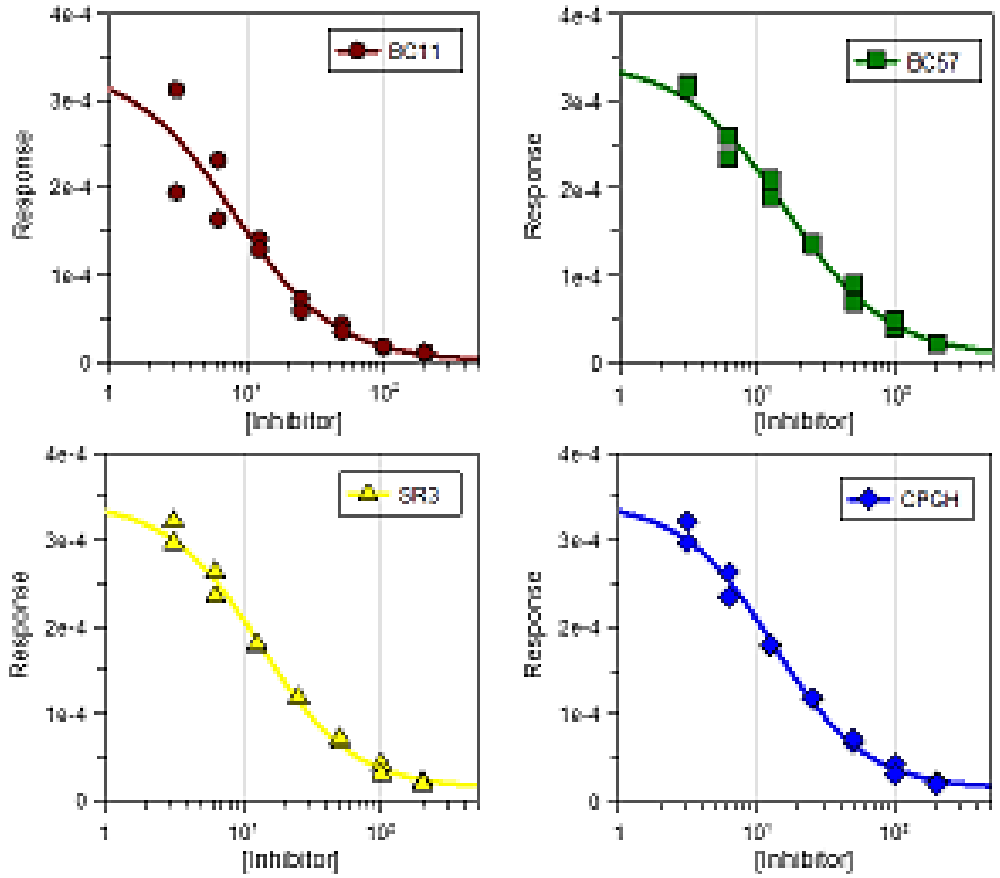

Figure 6-12 Collaborators' data on IC_{50} of compounds inhibiting uPA. CPGH is a known uPA inhibitor (J Spencer, personal communication 2013).

The compounds were ranked BC11 (IC50: 37±3.9 μM), SR3 (IC50=42 ±3.0 μM) and BC57 (IC50=50 ±2.0 μM; Figure 6-14), the potency ranking is similar to that for urokinase activity, although a higher dose was needed to block activity in *Dictyostelium* compared with the assays conducted by the collaborators. The concentration-dependent inhibition of *Dictyostelium* cell behaviour did however suggest direct activation or inhibition of cell components, which would result in greater inhibition of cell movement with a higher compound concentration.

Viability during these assays at concentrations higher than 250 μM, was less than 50%: at concentrations of 500 and 625 μM cells appeared to have lysed (Figure 6-13)

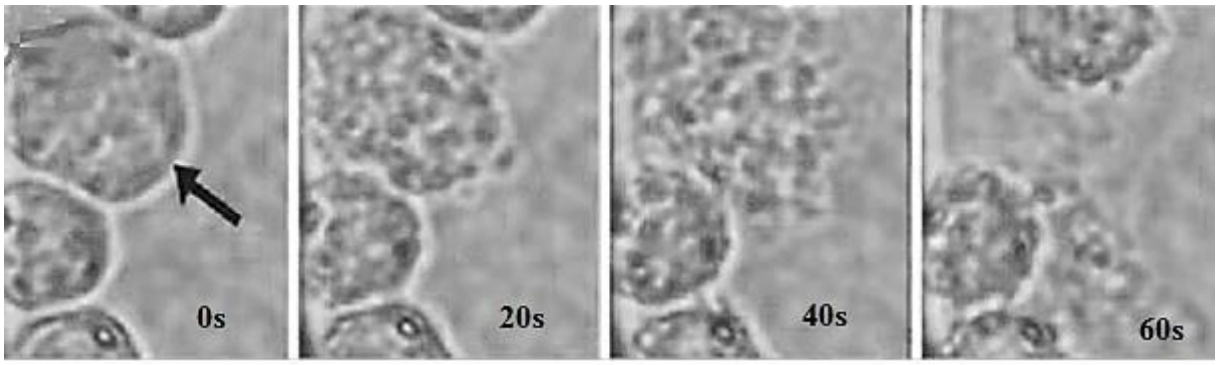

Figure 6-13 Time lapse images of *Dictyostelium* cell. One cell has been highlighted to show cell lysis after the addition off 500 μM BC11

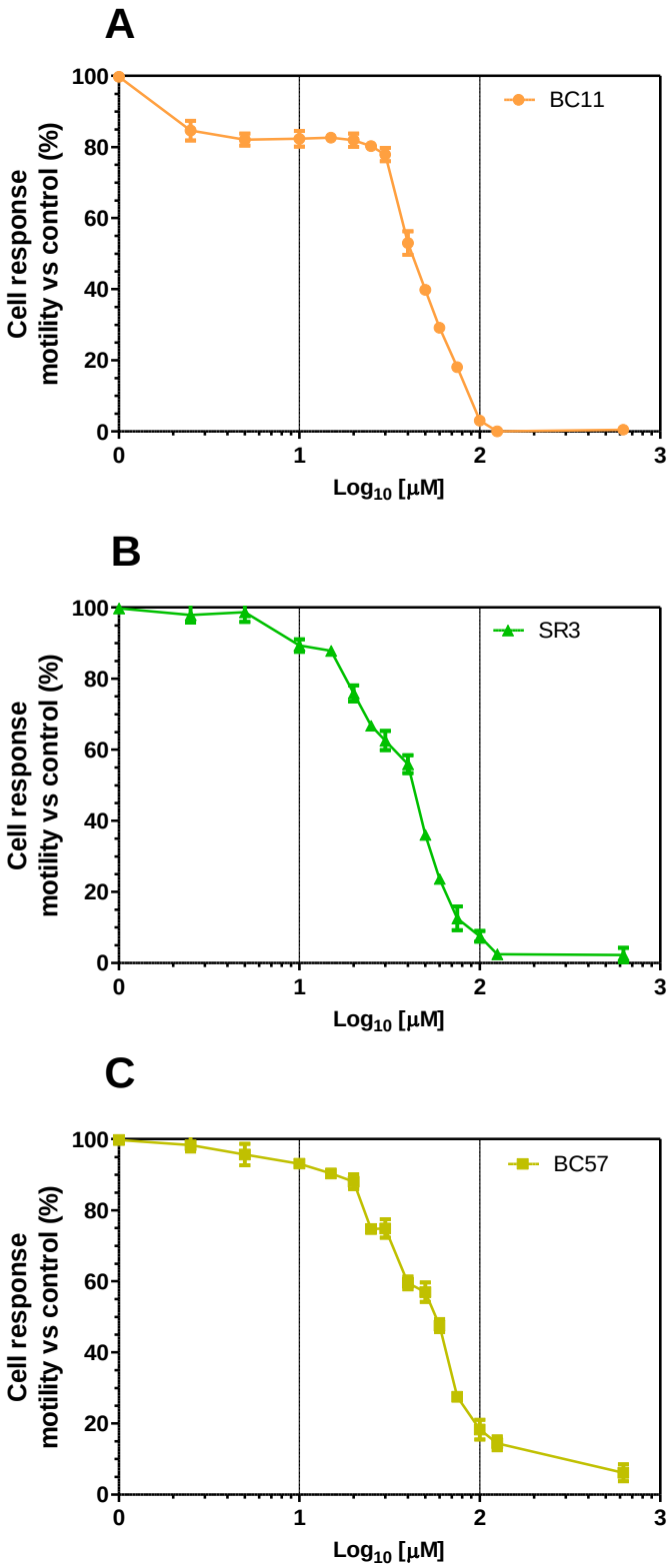

Figure 6-14 Concentration-dependent reduction of cell movement. (A) BC11 (B) SR3 (C) BC57: decrease in movement to control (0.01% DMSO) vs with 5 min treatment. Control taken as 100%, and reduction in movement subtracted to give the % of cell response at given concentrations. Data, mean ± SEM of triplicate experiments.

6.4 Is there an orthologue of uPA in *Dictyostelium*?

Novel applications of *Dictyostelium* are always of interest and activity of uPA inhibitors in the amoeba raises the question of orthologous cell migration and cell matrix regulators. Using protein Blast and domain Blast searches, similar proteins to the human urokinase receptor were sought, however no close matches were found. Searches for receptor proteins that might have a similar function to urokinase were also made. Urokinase, is a protease that degrades extracellular matrix. *Dictyostelium* proteins involved in degradation of extracellular proteins during chemotaxis, could be relevant: for example three phosphodiesterase (PDE) are predominantly responsible for degradation of extracellular cAMP, namely PdsA (DdPDE1), DdPDE7 and DdPDE4 (Bader *et al.*, 2007). To test whether the compounds affected any of these at transcription level, qPCR was performed before and after treatment (Figure 6-15). There was no significant effect at gene transcription level before and after treatment on any of the three genes.

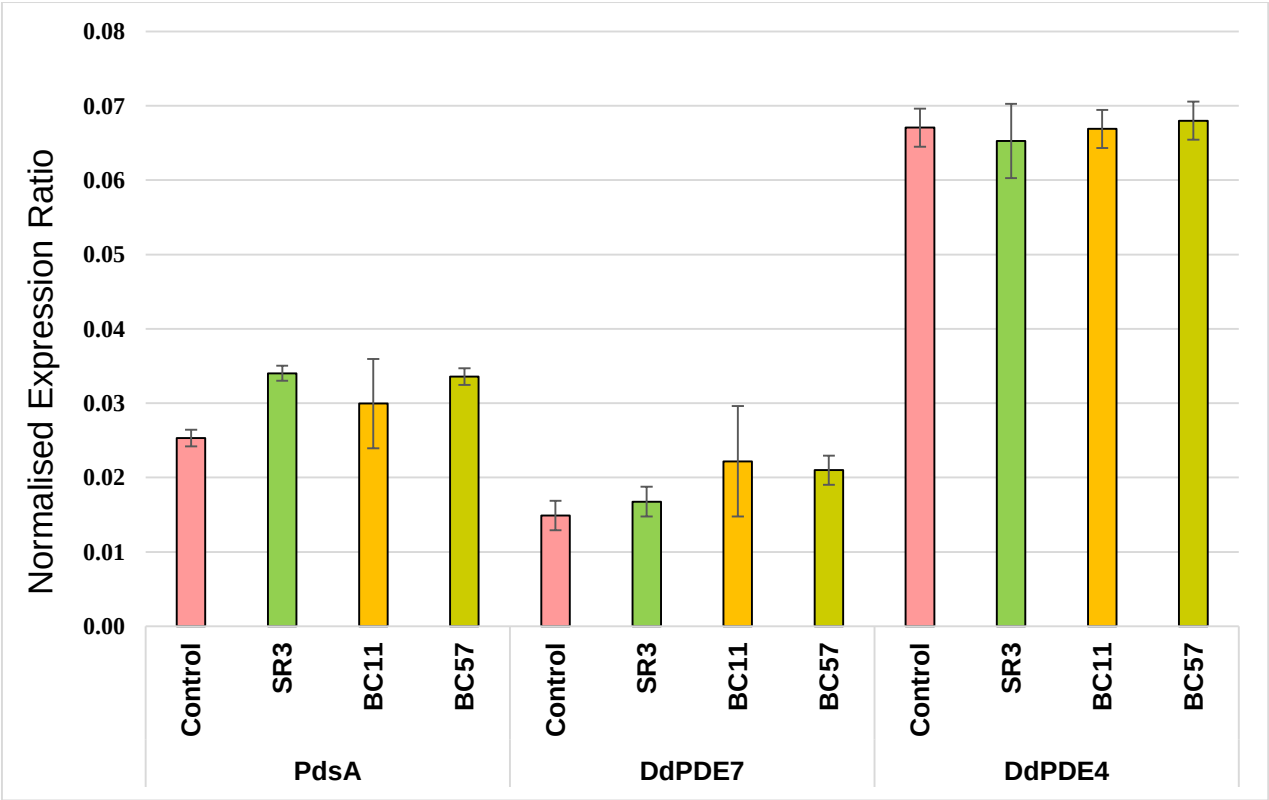

Figure 6-15 Transcription of phosphodiesterase (PDE) genes. Figure shows the relative transcription levels of 3 PDEs known to degrade extracellular matrix. The control is 0.01% DMSO (pink bars) and treatment was with 50µM test compounds. Data, mean ± SEM, Results were standardised to constitutive H7Q2 gene transcription in three independent experiment

6.5 Discussion

Urokinase is a trypsin-like serine protease, which plays an essential role in tumour cell invasion and metastasis. It has become an important therapeutic target for several cancer types. Studies from model systems show that uPA is involved in cancer propagation (Duffy, 2002). Consistent with its role in metastasis, multiple independent groups have shown that high uPA concentrations in primary breast cancers correlate with poor prognosis (Duffy *et al.*, 1999). One of the approaches to reduce uPA activity is to use synthetic non-peptide small molecule inhibitors. To be an effective drug, it is important that an uPA inhibitor is selective and does not inhibit other related serine proteases. It has been pointed out that Asp189, Ser190, Asp60A S1β and other sub sites are significant factors relating to the specificity and oral bioavailability (Harbeck *et al.*, 2004). The goal of this study was to explore whether *Dictyostelium* can be used as a model system for studying urokinase activity and inhibitors design, in order to better understand the metastasis signalling pathway of cancer.

The compounds BC11, BC57 and SR3 disrupted normal behaviour, affecting growth and movement of cells, ultimately leading to cell death at high concentrations. The response by *Dictyostelium* cells to the compounds BC57 and SR3 suggested that they might be internalised i.e., there was a delay before the observed decrease in cell velocity, whereas, but compound BC11 produced an immediate effect, which might relate to the compound acting on cell surface receptors.

To investigate the cytotoxicity of the compounds, short and long-term exposure experiments were carried out. It was seen that cells treated with compounds BC11**,** SR3 and BC57 could recover after termination of test compound effect and form plaques on *K. aerogenes* lawn. This suggested that inhibition of cell behaviour by these compounds was not through a toxic effect, confirmed by Trypan blue viability stain following 10 and 30 min exposure to these compounds. In all cases the pH was monitored (pH 6.5) to avoid significant alteration to pH levels, which could affect cell physiology.

Previous investigations of a wider range of arylboronic acids have also showed similar effects of uPA activity *in vitro* and *in vivo*. The ranking of the compounds on the basis of their effects on *Dictyostelium* cell movement showed a good correlation with the ranking

of the compounds BC11, SR3 and BC57 on the basis of their effects on uPA inhibition *in vivo*. Studies of the effects of these arylboronic acids on *Dictyostelium* motility may therefore aid understanding of the mechanism of action of these compounds.

A search for the molecular equivalents to uPA was not fruitful, but further investigations are required with no uPA receptor equivalent, *Dictyostelium* would provide a limited model for uPA inhibitor identification, but nevertheless may represent a new avenue for research into the molecular mechanisms of uPA inhibitors. These compounds had a rapid and marked effect on cell behaviour: as of yet uncharacterised molecular mechanism of action may still relate to facets of uPA activity. Future studies involving them would improve understanding of their mode of action and may indeed reveal an ancestral uPA cellular signalling pathway involved in cell movement. An understanding of how and where these compounds work in signalling pathways may also lead to an understanding of how other drugs, work such as the commonly used chemotherapeutic drug. This could lead to new advances to improve the effectiveness of chemotherapeutic drugs, improve the therapy or even lead to the development of new cancer diagnosis techniques.

Chapter 7
Cardiosulfa: Biological implications in D*ictyostelium*

7.1 Introduction

7.1.1 Role of Aryl Hydrocarbon Receptor in development

Organs are structures in an animal or a plant that are capable of performing some special action (termed its function), which is essential to the life or well-being of the whole. The heart and lungs are organs of animals, and the petal and leaf are organs of plants. One route to study developmental processes evolved in organ formation is to use synthetic molecules as probes, rather than the implementation of a conventional genetic approach. The utilisation of small molecules for probing biological events proved invaluable in a chemical-genetic study by Ko *et al.*, (2009). Treatment of zebrafish embryos with the small molecule cardiosulfa [N-(9-ethyl-9H-carbazol-3-yl)-2-nitro-4-(trifluoromethyl)-benzenesulfonamide] in micromolar concentrations resulted in narrow and elongated ventricles and atriums, accompanied by reductions in heart rates and peripheral blood flow (Figure 7-1; Ko *et al.*, 2009).

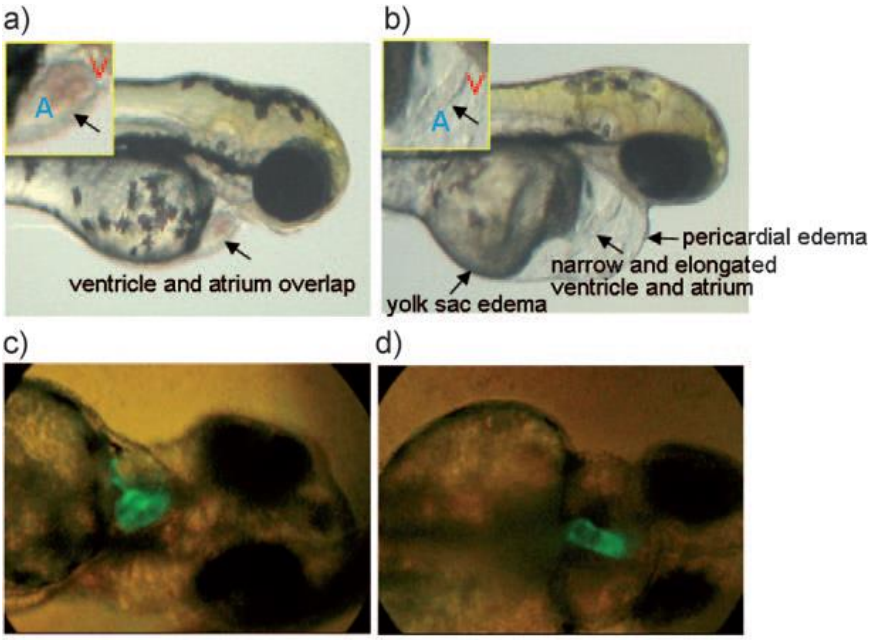

Figure 7-1 Effects of cardiosulfa on zebrafish heart development. (A) (B) Three-day-old zebrafish embryo untreated (a) and treated (b) with 20 mm cardiosulfa. Arrows in the insets indicate normal and abnormal heart morphology; V=ventricle, A=atrium. (C) (D) Tg (cmlc2: GFP) transgenic zebrafish embryo (three days old) untreated (c) and treated (d) with 20 mm cardiosulfa. Heart marked with green fluorescent protein (GFP). Image and description taken from Ko *et al.*, 2009

This observation was important because heart disease is one of the most common cause of human death and this study contributed to our understanding of the mechanism and pathways that are related to heart function. Interestingly, concomitant gene-expression profiling in cardiosulfa-treated embryos revealed increased transcription levels of members of the aryl hydrocarbon receptor (AhR) pathway, including cytochrome P450 (CYP) family genes (*cyp1a, cyp1b1* and *cyp1c1*). The AhR is a member of the family of basic helix-loop-helix transcription factors, the oldest physiological role of which is in development. AhR is presumed to have evolved from invertebrates where it served a ligand-independent role in development (Hahn *et al.*, 2006). The AhR orthologue in *Drosophila*, spineless (ss) is necessary for development of the distal segments of the antenna and leg (Duncan *et al.*, 1998). Ss dimerises with tango (tgo), which is the equivalent of the mammalian aryl hydrocarbon receptor nuclear translocator (Arnt), to initiate gene transcription. Evolution of the receptor in vertebrates resulted in the ability to bind 'ligands'. In developing vertebrates, AhR seems to play a role in cellular proliferation and differentiation (Tijet *et al.*, 2006). Indeed, despite lacking a clear endogenous ligand, AhR appears to play a role in the differentiation of many developmental pathways, including haematopoiesis (Gasiewicz *et al.*, 2010) lymphoid systems (Kiss *et al.*, 2011), T-cells (Quintana *et al.*, 2008), neurons (Akahoshi *et al.*, 2006) and hepatocytes (Walisser *et al.*, 2005). AhR has also been found to have an important function in hematopoietic stem cells: AhR modulation by Stem Regenin 1 protein promotes their self-renewal and ex-vivo expansion (Boitano *et al.*, 2010).

7.1.2 *Dictyostelium* use as a model organism

Organogenesis can be defined as the process of the initial formation of an organ from unspecified parts. The process begins with a series of organised integrated inductive events that transform progenitor undifferentiated cells into discrete structures, and ends when the fundamental structure of the organ is recognisable, such as a condensation of mesenchymal cells into the organ rudiment. *Dictyostelium* is a member of the Amoebozoa, a taxon that is basal to the Fungi-Metazoan branch. It is at the crux of unicellularity and multicellularity as unicellular amoebae upon starvation, aggregates to form mounds of 10^4-10^5 cells that organise into a multicellular migrating slug with anterior-posterior polarity. If food source is found, slug cells enters culmination/sporulation stage to form fruiting bodies. The latter are made of anterior (pre-stalk) cells which differentiate into stalk cells that elongate and die, whereas the posterior (pre-spore) cells differentiate into spores.

Development of *Dictyostelium discoideum* poses common questions for development of any multicellular organism: How do cells communicate with each other? How do cells adhere to each other together? How do cells know which end forms axes of development? How do cells in a multicellular organism form patterns?

Dictyostelium has been used to study many aspects of higher eukaryote function, including mammalian conditions such as epilepsy (Chang *et al.*, 2014; Terbach *et al.*, 2011), kidney disease (Waheed *et al.*, 2013) and even to investigate myosin mutations that cause cardiac myopathies in humans (Sasaki *et al.*, 1999). In this study, a chemical inhibitor approach was used to study whether *Dictyostelium* shares components of the molecular networks involved in tissue specialisation found in higher eukaryotes, which would further extend its utility as a model organism.

7.2 Results

7.2.1 Effects of cardiosulfa on viability and growth of *Dictyostelium*

To look into the utility of *Dictyostelium* as a model for the organ formation, developmental assays using cardiosulfa were carried out. Using *in vivo* concentrations effective in zebrafish, the viability of treated cells was determined to ensure that any difference observed in cell behaviour was not caused by cell toxicity and/or cell death. Viability was monitored following 30 min incubation with cardiosulfa at 10, 25, 50, 75 and 100 µM concentrations, and was determined using Trypan blue staining. In the presence of cardiosulfa, there was no significant decrease in the proportion of surviving cells (Figure 7-2). Viability was above 90% for all the concentrations.

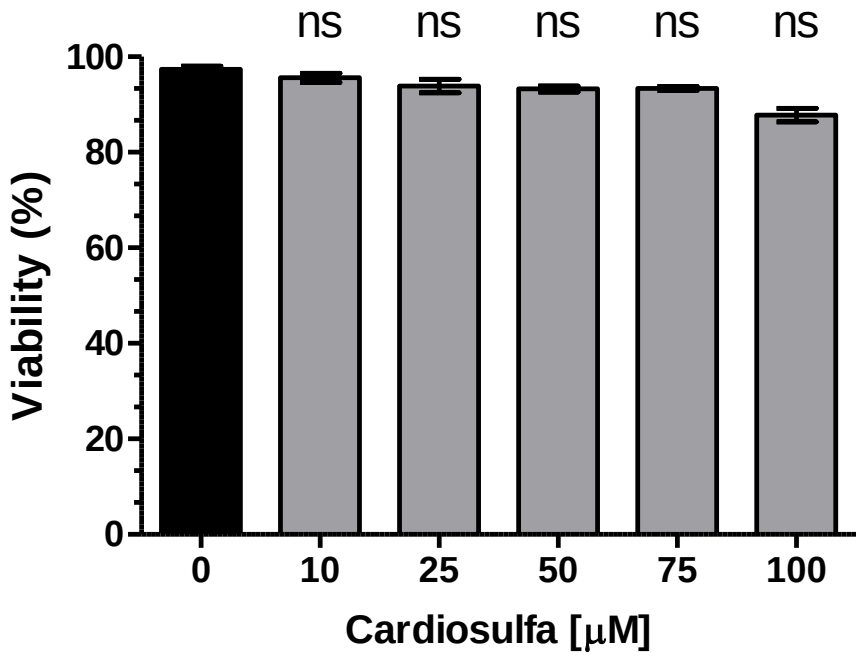

Figure 7-2 Viability of *Dictyostelium* cells. Trypan blue staining after 30 min incubation with cardiosulfa. Black bar, the control (0.01% DMSO). Data, mean ± SEM of three independent experiments, ns = P > 0.05.

The growth rate of *Dictyostelium* was then determined in axenic media and on bacterial lawns. *Dictyostelium* cells are relatively easy to grow, depending on lab strains and conditions, cells have a doubling time of 4-8 h (Eichinger & Rivero-Crespo, 2006). To examine the effect of cardiosulfa, cells were grown in shaking axenic cultures for 72 h at 22°C. Cell densities were measured at intervals and doubling time was calculated

(Figure 7-3). Cardiosulfa had a dose-dependent effect on the doubling time of the cells; the growth rate was significantly reduced by treatment with cardiosulfa.

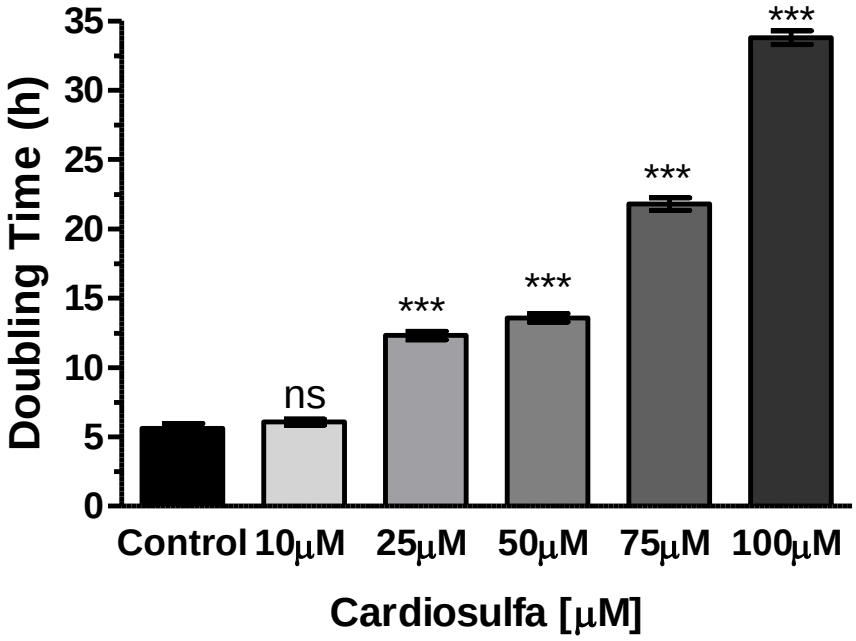

Figure 7-3 Doubling time of *Dictyostelium* cell. Cell densities measured over a 72-h period, from a starting concentration of all cultures of $1x10^4$ cells. Data are mean ± SEM of three individual experiments. ns = $P > 0.005$, *** = $P \leq 0.001$

The chronic effect that cardiosulfa may have on *Dictyostelium* cells was measured in an assay examining the recovery of cells after the inhibitor was removed. Using a range of concentrations as before, *Dictyostelium* vegetative cells were incubated with cardiosulfa in axenic media for 24 h. The drug effect was then terminated by a 1:100 dilution of the incubation solution into SM broth. Viability was measured simultaneously using Trypan blue staining. The number of cells present in the culture was determined, and approximately 100 cells were inoculated onto a *K. aerogenes* lawn for phagocytosis of this bacterial food source. Clones were observed after incubation for 5 days at 22°C, indicating growth of *Dictyostelium* from single cells. Under control conditions (0.01% DMSO), the proportion of cells forming plaques (zones of phagocytosis) was greater than 95%. In the cardiosulfa treated cells, a significant decrease was observed in the proportion of *Dictyostelium* forming plaques on a bacterial lawn (Figure 7-4), but there was no significant effect on the viability of cells.

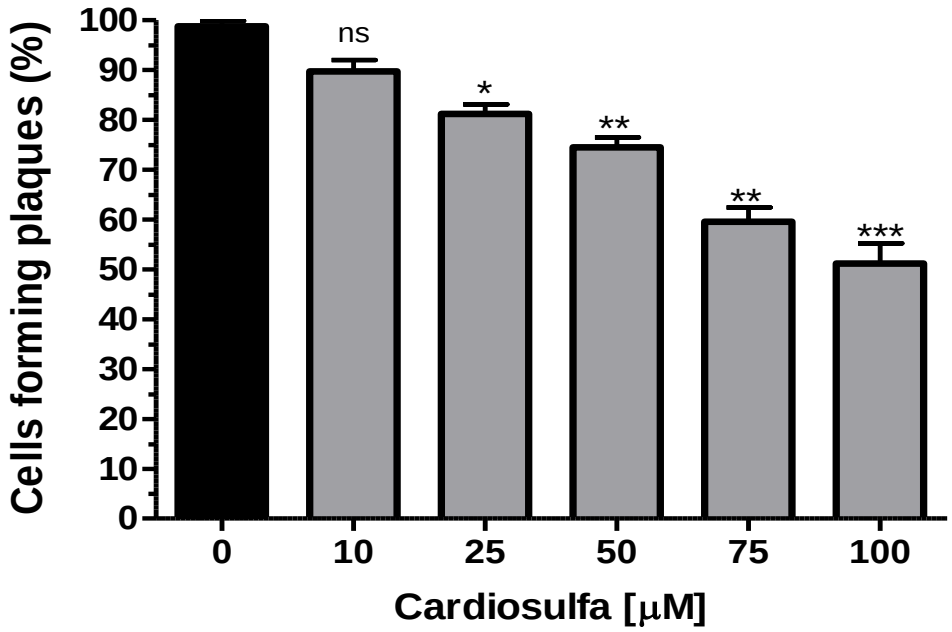

Figure 7-4 Cell survival. The proportion of cells able to form plaques on *K. aerogenes* lawns on agar plates. Black bar, untreated control. Data are mean ± SEM of three independent experiments, ns = P >0.05; * = P ≤0.05; ** = P ≤0.01; *** = P ≤0.001

7.2.2 Cardiosulfa treatment results in blocked chemotaxis

In a Dunn chamber chemotaxis assay *Dictyostelium* response to cAMP was examined. Cell behaviour in a chemotactic gradient was monitored by recording images every 15 sec over a 15 min period under control conditions. Computer-generated outlines enabled the quantification of speed and aspect of the cells. In the standard assay using 0.01% DMSO, cells displayed constant movement towards the cAMP without significantly deviating from their path. This standard assay allowed the analysis of the effect of addition of cardiosulfa on cell motility. Using the same range of concentrations, a minimum of three independent experiments were performed and an average of 20 cells quantified per experiment. Control behaviour was established for 4.5 min prior to the addition of cardiosulfa, the concentration used was based upon the *in vivo* concentration known to be effective in zebrafish (Ko *et al.*, 2009). In the chemotaxis assay (Figure 7-5A), 25 μM cardiosulfa treatment resulted in a significant and acute drop in the cell velocity, with the cells becoming nearly stationary. Figure 7-5B shows that the effect was concentration dependent and the dose of cardiosulfa was correlated with the speed change.

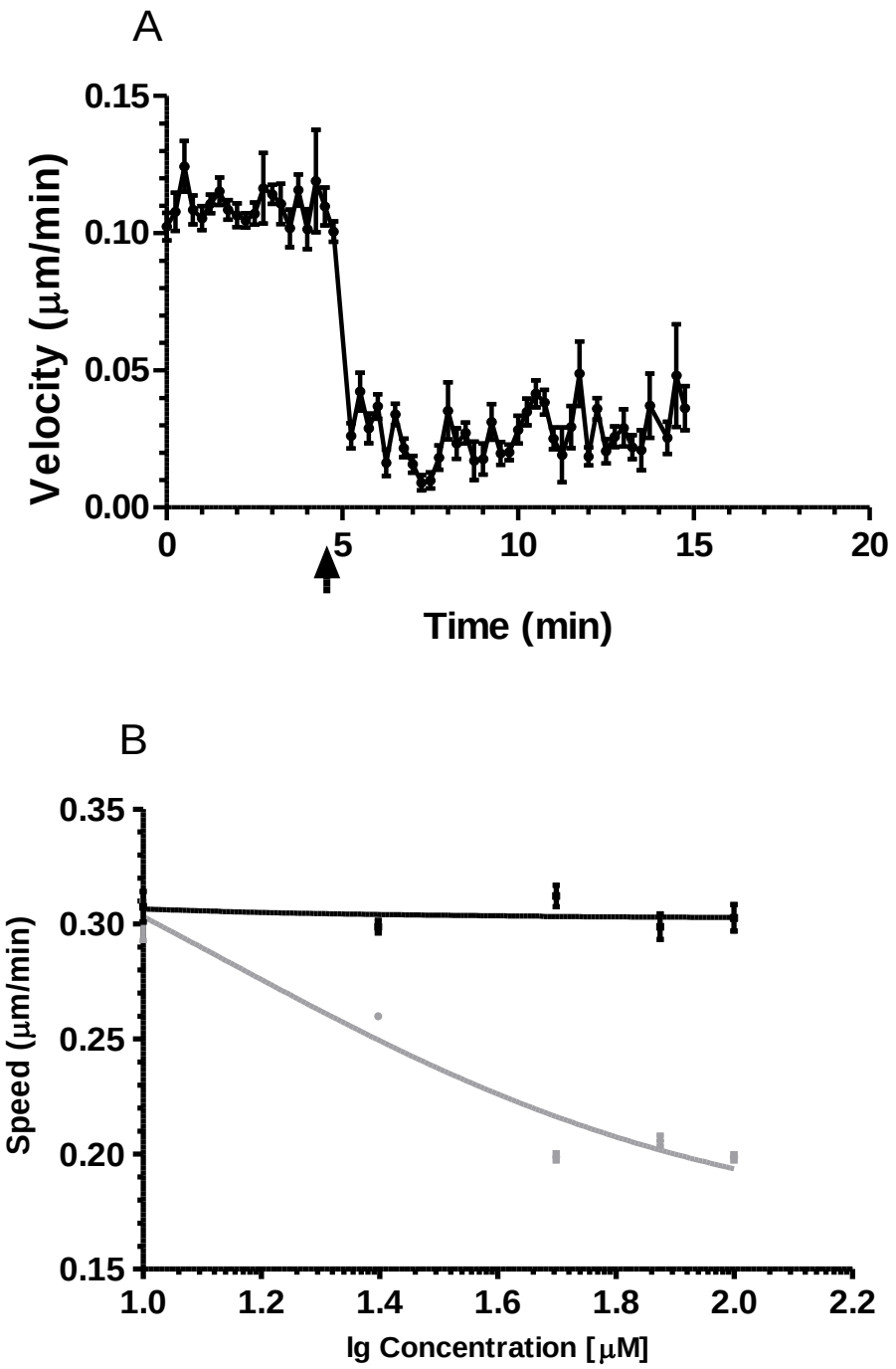

Figure 7-5 Analysis of *Dictyostelium* cell velocity. (A) Cells were allowed to migrate for 4.5 min toward 5 mM cAMP prior to the addition of 25 μM cardiosulfa (black arrow). Mean ± SEM represents 20 cells chemotaxis over a 15 min period. (B) *Dictyostelium* cell speed in random cell movement assay, each point represent mean speed ± SEM of 20 cells over 10 min after the addition of cardiosulfa, Black line, control, grey line, cardiosulfa

7.2.3 Reversibility of inhibition of cell movement

Despite cells shown to be viable after 30 min, the reversibility of the cardiosulfa effect on *Dictyostelium* cell behaviour was unknown. Using a separate cell movement assay, the block in *Dictyostelium* behaviour was assessed to see if the effects of cardiosulfa were reversible upon removal. Recovery of the cells was measured after a 5 min exposure to 25 µm cardiosulfa, a concentration chosen as it was the minimum required to elicit a response. Despite no loss of viability (93.9 ± 1.4%; Figure 7-2), after the removal of inhibitor, cells were not able to return to normal speeds (Figure 7-6).

7.2.4 Cardiosulfa causes delays in development and aberrant slug morphology

The effect of cardiosulfa on development was quantified. Under control conditions, cells undergo chemotaxis and eventually form multicellular fruiting bodies. Cardiosulfa-treated cells were significantly slower to form fruiting bodies than control, with a mean delay of 5.0 h (SEM ± 0.5 h; $P \leq 0.05$; Figure 7-7). To identify whether spores from treated cells remained viable, spores were isolated after the former developmental assays and inoculated onto *K. aerogenes* lawn. No development was seen on bacterial plates even after 10 days, whereas the control regenerated as expected.

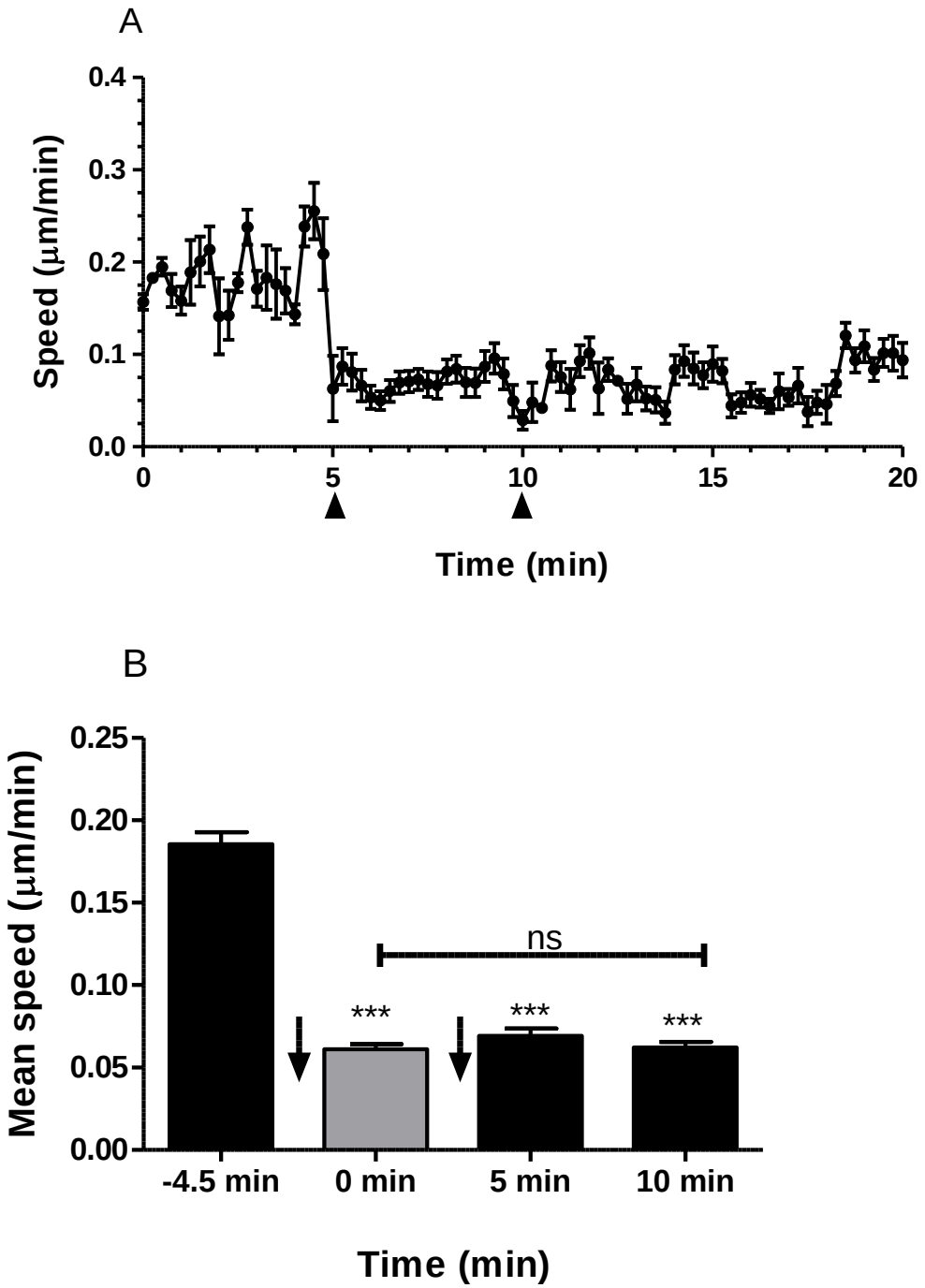

Figure 7-6 Recovery of cell movement after removal of cardiosulfa. (A) Cell behaviour after cardiosulfa (final concentration 25 µM) was added at 4.5 min (first arrow) and subsequently removed after 5 min incubation (second arrow). Data mean± SEM velocity of 15 cells. (B) Recovery following treatment was monitored by measuring velocity 4.5 min (-4.5 min) prior to the addition of cardiosulfa at 0 min (first arrow). Inhibitor was removed after 4.5 min incubation (second arrow) and recovery was recorded for 10 min. Data mean ± SEM; Grey bar presence of cardiosulfa. ns = $P>0.05$; *** = $P \leq 0.001$.

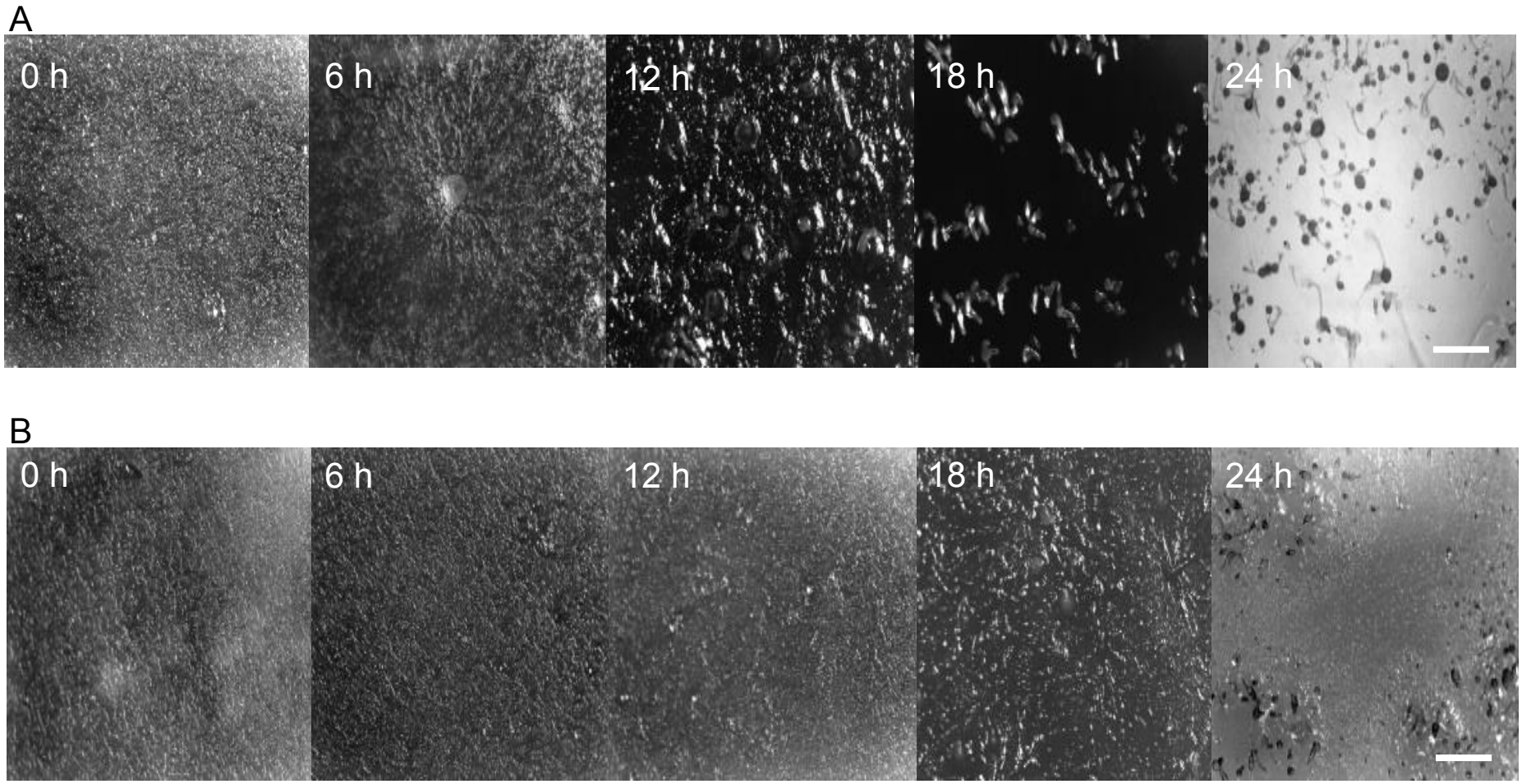

Figure 7-7 Development of *Dictyostelium* (A) Development of control at specific time intervals on KK2 plates. (B): Cardiosulfa treated cells. Cardiosulfa treated cells able to form proper fruiting bodies after approximately 28 -30 hours on KK2 plates. All size bars represent 0.5mm

To determine whether cardiosulfa affects a number of responses to the environment, phototaxis experiments were carried out which that lead to slug formation. Under control conditions 10^6 cells, incubated in the dark with a small lateral light opening, formed approximately 20-40 slugs. The motile slugs in control conditions moved constantly towards the light source without much deviation in their path. Repeating the experiment after cells had been incubated with cardiosulfa for 30 min prior to the assay, aberrant slug formation was observed including stationary aggregated cells. The few viable slugs that did develop moved slowly and were disoriented when tracks on a nitrocellulose paper were visualised using Coomassie blue staining (Figure 7-8).

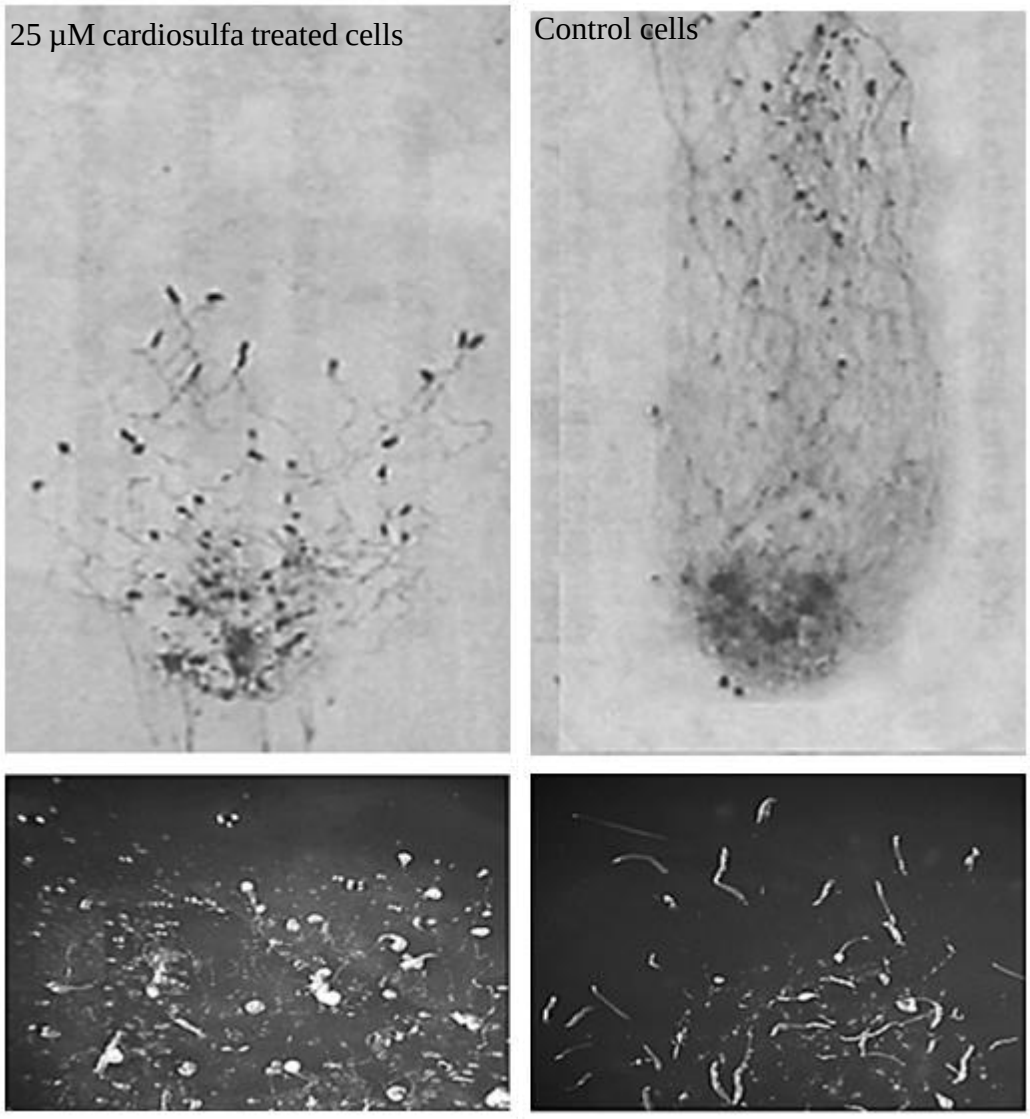

Figure 7-8 Phototaxis assay. A pronounced defect in phototaxis in cardiosulfa treated cells. The slugs were disoriented and moved more slowly. Top panel. Coomassie stained tracks; bottom panel, light microscopy of slugs formation.

The transition to multicellularity in *Dictyostelium* development is brought about by chemotaxis and cell-to-cell adhesion. Growth-phase cells are weakly cohesive, whereas aggregation-competent cells adhere strongly to each other (Eichinger & Rivero-Crespo, 2006). Cell adhesion molecules play an important physical role in shaping the structure of multicellular organisms (Kibler *et al.*, 2003). In *Dictyostelium* csA, a lectin like molecule that has homology to mammalian cell adhesion molecules (CAMs) that mediates EDTA-stable contacts. Ectopic expression of csA in vegetative cells causes cells to aggregate and initiate morphogenesis (Siu *et al.*, 2004). Therefore measuring EDTA-dependant stable adhesion can be a convenient way to help assess whether the delayed might be result of poor cell-to-cell adhesion. Cardiosulfa treated cells showed no significant reduction ($P > 0.05$) in the proportion of adherent cells rate (Figure 7-9) even at the highest concentration.

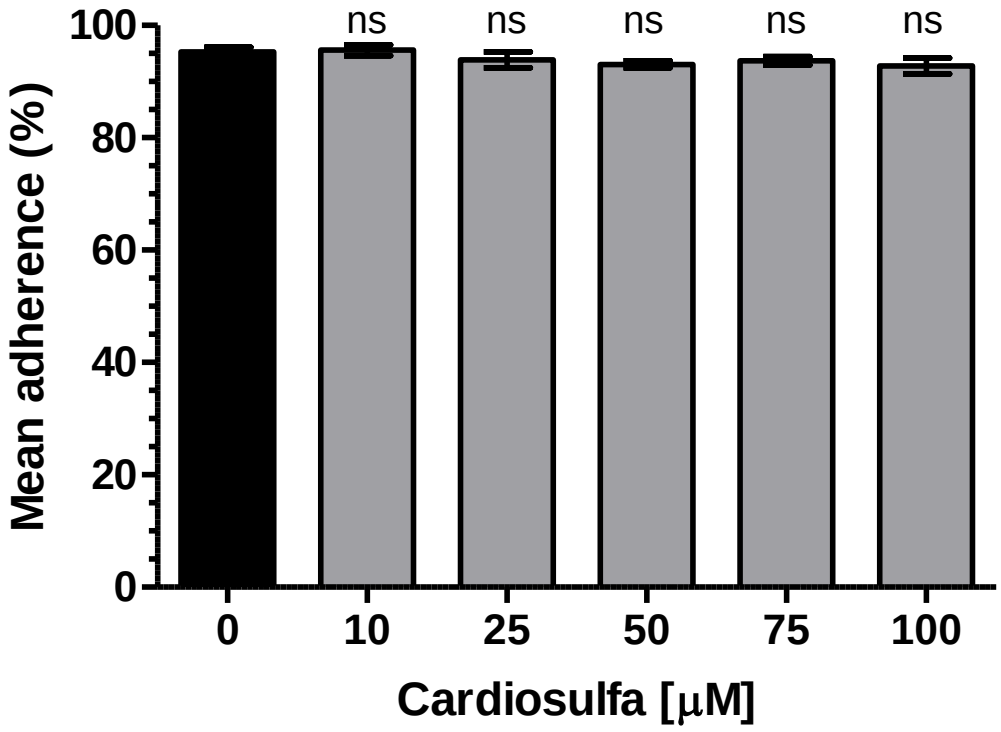

Figure 7-9 Cell-to-cell adherence. EDTA- resistant cohesiveness in 4 h starved cells. Black bar, control. Data, mean ± SEM representative of three independent experiments. ns = P >0.05.

7.2.5 Is there an AhR orthologue in *Dictyostelium?*

Results from cardiosulfa treatment of *Dictyostelium*, suggest that *Dictyostelium* may contain similar pathways to the molecular networks controlling zebrafish development. Using

well characterised AhR gene battery orthologues from the zebrafish proteome (Qin & Powell-Coffman, 2004; Scott *et al.*, 2011; Vasquez *et al.*, 2003), a domain BLAST search was carried out to identify possible *Dictyostelium* equivalents (Table 7-1).

Figure 7-10 illustrates the domain structure for the predicted protein encoded by DDB_G0280133 versus the functional domains of the AhR protein. The two PAS domains, PAS-A and PAS-B, are stretches of 100-200 amino acids that exhibit a high sequence homology to protein domains originally found in the *Drosophila* genes *period* (per) and *single-minded* (sim). The ligand binding site of AhR is contained within the PAS-B domain and contains several conserved residues critical for ligand binding. A Q-rich domain located in the C-terminus region of the protein, which in AhR is involved in co-activator recruitment and transactivation. This *Dictyostelium* protein, however, lacks the AhR basic helix-loop-helix DNA binding domain at the N-terminus, but instead has a Forkhead-associated (FHA) domain present at the C-terminus. FHA domains mediate relocation of these domain-containing proteins to DNA damage sites and facilitate the DNA damage response (Li *et al.*, 2013), acting as transcription factors.

Table 7-1 Potential AhR network proteins of *Dictyostelium* vs zebrafish

Zebra fish	***Dictyostelium***	**Identity (%)***
AhR	DDB_G0280133	12
AIP	DDB_G0278455	18
Arnt	DDB_G0274877; DDB_G0280193	14; 17
AhRR	DDB_G0282927	12
Hsp90	hspD; grp94; trap1	63; 40; 28
CYP1A1	cyp508A3; cyp508A2; cyp508A1	27; 23; 23

*, at amino acid level. AhR, Aryl hydrocarbon receptor; AIP, immunophilin-like protein; Arnt, AhR nuclear translocator; AhRR, AhR repressor; CYP, cyctochrome P450; grp, glucose-regulated protein; hsp, heat shock protein; trap, tumour necrosis factor (TNF) receptor-associated protein.

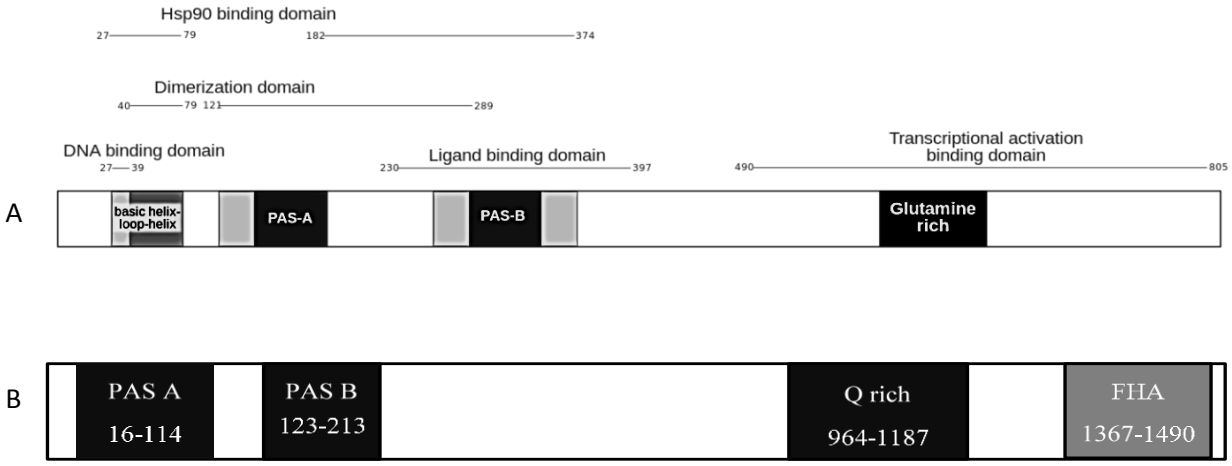

Figure 7-10 *Dictyostelium* putative protein (DDB_G0280133) containing the functional domains of an aryl hydrocarbon receptor. (A) Domains of aryl hydrocarbon receptor. (B) Putative orthologue domain structure in *Dictyostelium*. FHA, fork-head association domain; Hsp, heat shock protein; PAS; **P**er – period circadian protein, **A**rnt – aryl hydrocarbon receptor nuclear translocator protein, **S**im – single-minded protein, Q, Glutamine.

If cardiosulfa was acting in *Dictyostelium* on equivalent molecular networks to those in zebrafish, it is possible that the genes identified here would have altered transcript levels after treatment. Cells were incubated with cardiosulfa for 1 h. RNA extractions and first strand cDNA synthesis was carried according to the procedure outlined in methods and H7Q2, a putative helix-turn-helix transcription factor used as an internal control. Transcription levels for the genes identified were compared with and without cardiosulfa treatment (Figure 7-11) relative to the H7Q2 control.

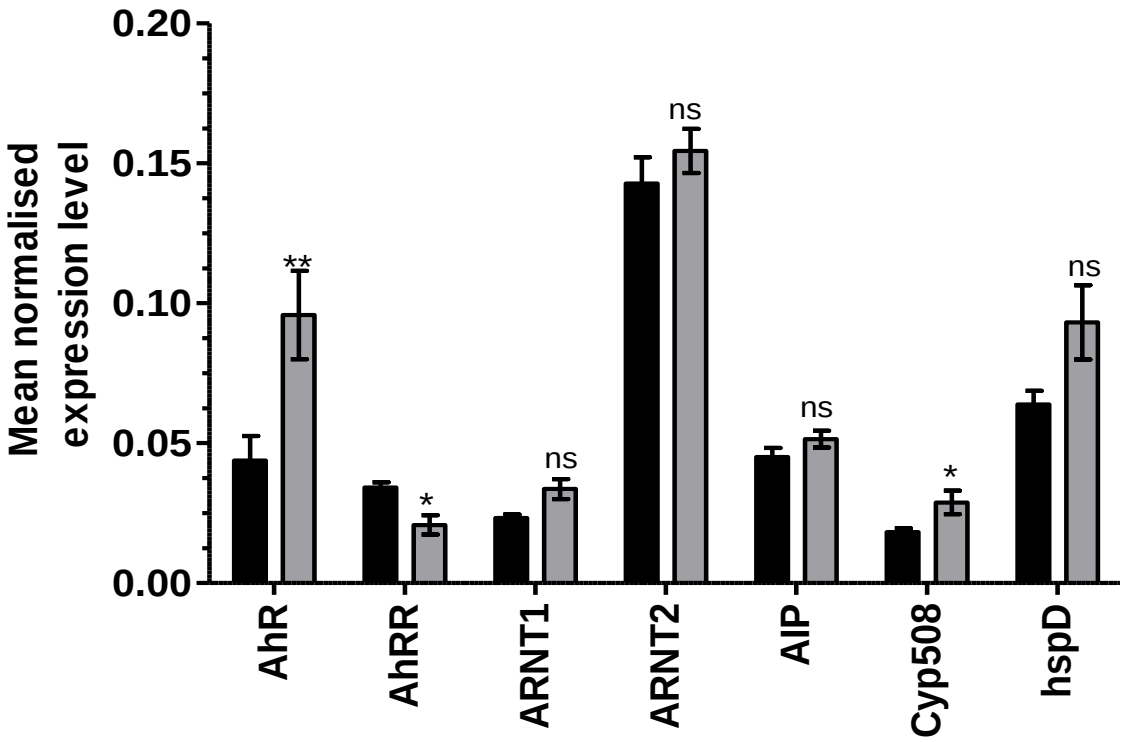

Figure 7-11 Relative transcription levels of possible AhR network genes. Control (0.01% DMSO; black bars) and after treatment (25 µM cardiosulfa; grey bars). Data, mean ± SEM, Results were standardised to constitutive H7Q2 gene transcription in three independent experiment. ns = $P > 0.05$; * = $P \leq 0.05$, ** = $P \leq 0.01$.

Putative AhR network genes transcription was indeed differentially regulated after cardiosulfa treatment. Notably this included putative AhR, AhRR and cytochrome P450 orthologues. In the case of AhR and cyp508 the transcription levels rose significantly and AhRR level decreased. This is what would be expected if cardiosulfa was activating transcription of the AhR protein, while blocking the negative feedback loop resulting in reduced transcription of AhRR (Figure 7-12).

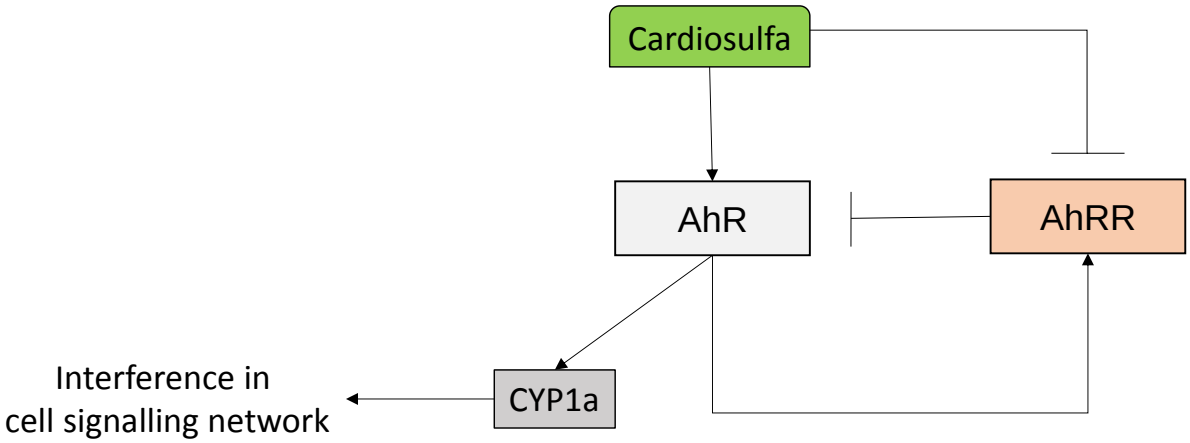

Figure 7-12 Proposed cardiosulfa effect on AhR signalling network. AhR, aryl hydrocarbon receptor; AhRR, aryl hydrocarbon receptor repressor; CYP, cytochrome P450.

7.3 Discussion

Organogenesis such as heart development is an elaborate process of pattern formation, migration and development. It requires communication between cells and depends on the recognition of the secreted signals produced by developing cells. Indeed wide range of molecules including proteins, small peptides, amino acids, nucleic acids, steroids and polylketides are used as intercellular signals in plants and animals. The similar molecules are also used by *Dictyostelium* to communicate when single cells aggregate to form multicellular structures.

One of the key objectives in the study of development is to map cellular processes such as division, differentiation, apoptosis and movement in space and time to give reproducible pattern formation and morphogenesis. Cells need to recognise each other and grow as a 'family' in the case of the heart for example mostly as cardiac muscle. *Dictyostelium*, can be used as a simple microbial model to study pattern formation and morphogenesis. *Dictyostelium* cells recognise when exogenous nutrients are limiting are thus initiate development, and also need to communicate among themselves to ensure there are enough cells to progress through development (Kim *et al.*, 2007; Poloz & O'Day, 2012). Within hours of establishing communication using pulses of cAMP, aggregates start to develop in harmony in relation to each other, differentiating into two major cell types prespore and prestalk cells. These then continue to signal each other to form well-proportioned fruiting bodies. Thus *Dictyostelium* cells can proceed through the stages of a necessary sequence in an orderly manner without cells being left out or

directed incorrectly (Sunderland, 2011; Vasiev & Weijer, 2001). Not all the components of these pathways have been identified, results from this study might help in elucidating those unidentified proteins, as well as any equivalent analogues to the AhR biology.

In zebrafish it was hypothesised that cardiosulfa was functioning via activation of the AhR signalling pathway in a CYP1a-independent manner (Ko & Shin, 2012). AhR is known to play a significant role in cardiovascular development and function in vertebrates. The receptor is highly expressed in the heart and vasculature of fish and birds (Andreasen *et al.*, 2002; Karchner *et al*., 1999; Walker *et al.*, 1997, 2000). AhR-null knockout mice manifest transient alterations in fetal and neonatal cardiac morphology, as well as progressive hypertension and angiotensin II mediated cardiac hypertrophy beginning soon after birth (Lahvis *et al.*, 2000; Lund *et al.*, 2002; Thackaberry *et al.*, 2002; Vasquez *et al.*, 2003). Hence, activation of AhR by which cardiosulfa elicits its response in zebrafish cardia muscles are not surprising. Nevertheless, results of two studies by this group showed that cardiosulfa-induced heart deformation was supressed by AhR antagonist and AhR morpholino knockdown, but not by CYP1A morpholino (Ko & Shin, 2012). Though induction of cytochrome P450 1A (CYP1A) gene expression is the single most sensitive molecular response to AhR activation and has been implicated in toxicity (Zhang, 2011). In the case of Tetrachlorodibenzo-p-dioxin (TCDD), a well-documented contaminant that causes direct impairment of the cardiac muscle in zebrafish and chicken embryos, CYP1A morpholino knockdowns have yielded contradictory results (Carney *et al.*, 2004; Teraoka *et al*., 2003). This is also observed for CYP1A1(−/−) and CYP1A2(−/−) knockouts in adult mice, the knockouts provided varying degrees of protection against TCDD toxicity (Zhang, 2011).

A possible mode for the adverse action induced by cardiosulfa can be through CYP1A mediated production of reactive oxygen species (ROS). ROS production by fish CYP1As has been clearly demonstrated and is associated with decoupling of the catalytic cycle (a possible causative mechanism) and enzyme inactivation (a possible consequence) (Schlezinger *et al*., 1999, 2000). There are multiple pathways via which reactive oxygen could exert cardiotoxic effects (Figure 7-13).

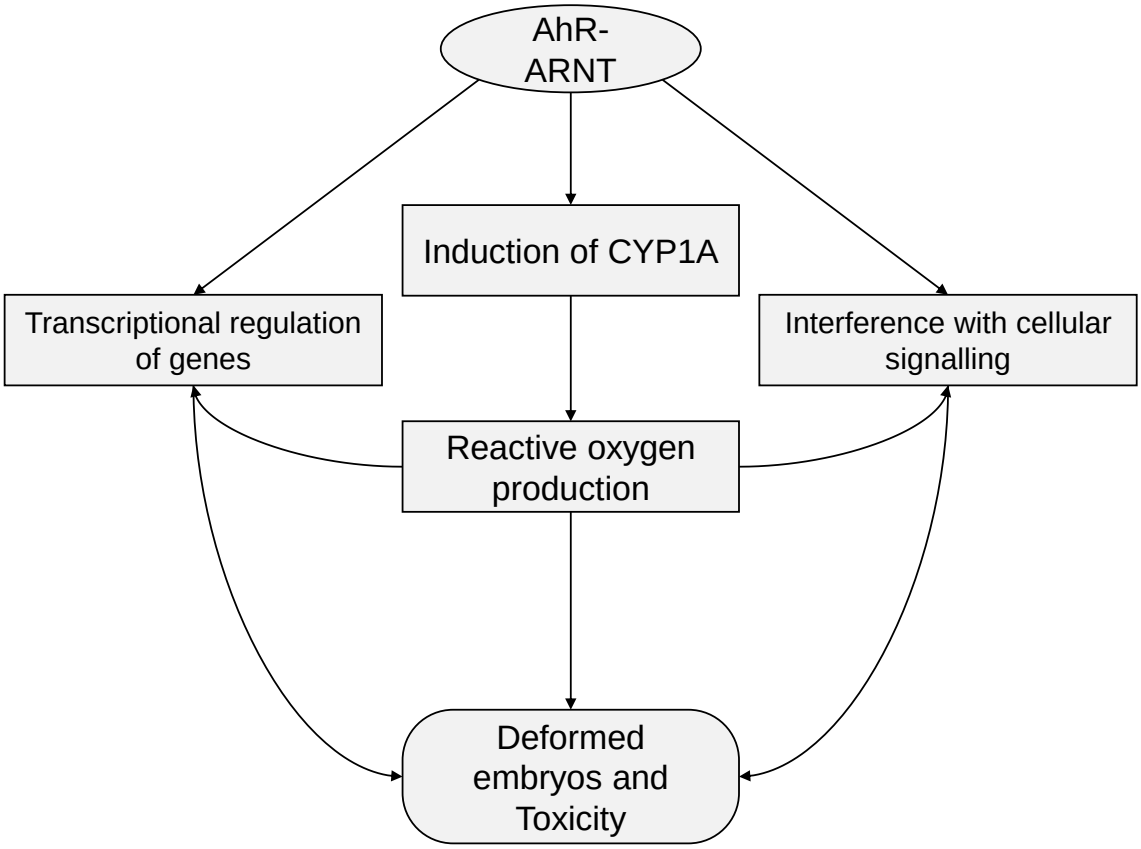

Figure 7-13 Reactive oxygen production pathways by which AhR activation and/or CYP1A induction could produce cardiovascular defects in zebrafish embryos

Processes of cardiovascular development and function are sensitive to intracellular oxygen conditions. There is evidence of a link between excess ROS production, particularly in the mitochondria, and cardiac pathologies (Dhalla *et al*., 2000; Hwang *et al*., 2002; Ide *et al*., 1999; Sorescu & Griendling, 2002). Though direct oxidative damage to DNA, proteins, or lipids may be particularly important in the heart deformation associated with cardiosulfa exposure.

However, previously, no known AhR or AhR-related proteins have been reported in *Dictyostelium,* although Kuramoto *et al.,* (2002) showed xenobiotic response element (XRE; TNGCGTG) binding in *Dictyostelium.* This probe was derived from the nuclear AhR from rat liver, indicated that mammalian AhR related proteins might exist in *Dictyostelium*: XRE binding was detected in cytosolic and nuclear fractions with different responsiveness in different developmental stages. This study did not identify potential *Dictyostelium* AhR or Arnt related proteins, however, and the immunoreactivity profiles of the binding proteins also had different molecular weights from those of the known AhR

proteins. Nevertheless, homologous genes encoding Hsp90 are found in *Dictyostelium* (Morita *et al.*, 2000) and other putative components of the AhR network have been reported here. Expression of novel AhR/Arnt family products in zebrafish have also been described with different molecular weights than previously reported (Tanguay *et al.*, 2000). It seems entirely possible, therefore that there may be unidentified AhR network proteins in *Dictyostelium* that are binding to the XRE.

Emerging data also indicate that proteins with PAS domain could act as the AhR in mammalian cells, as the ligand binding site of AhR is contained within the PAS domain. The PAS domains support secondary interactions so that heterozygous and homozygous protein complexes can form (Coumailleau *et al.*, 1995). DDB_G0280133 noted above (Table 7-1) contains the required functional domains and the conserved domain DNA binding. Orthologues of AhR target genes (*zfcyp1a*, *zfcyp1b1*, *zfcyp1c1*) in zebrafish organ formation (Figure 7-14) are also present in *Dictyostelium*.

qPCR revealed that transcription of *ahr* and *cyp508* genes in cells treated with cardiosulfa were elevated and *ahrr* was supressed. Development is difficult to separate from detoxification, however and the scenario in which cardiosulfa activates a xenobiotic enzymes because of a toxic effect cannot be excluded. AhR levels could in that case be elevated in response to the enzyme rather than a direct effect of cardiosulfa. Further work needs to be done to understand the detailed mechanism by which cardiosulfa elicits the response seen in *Dictyostelium*.

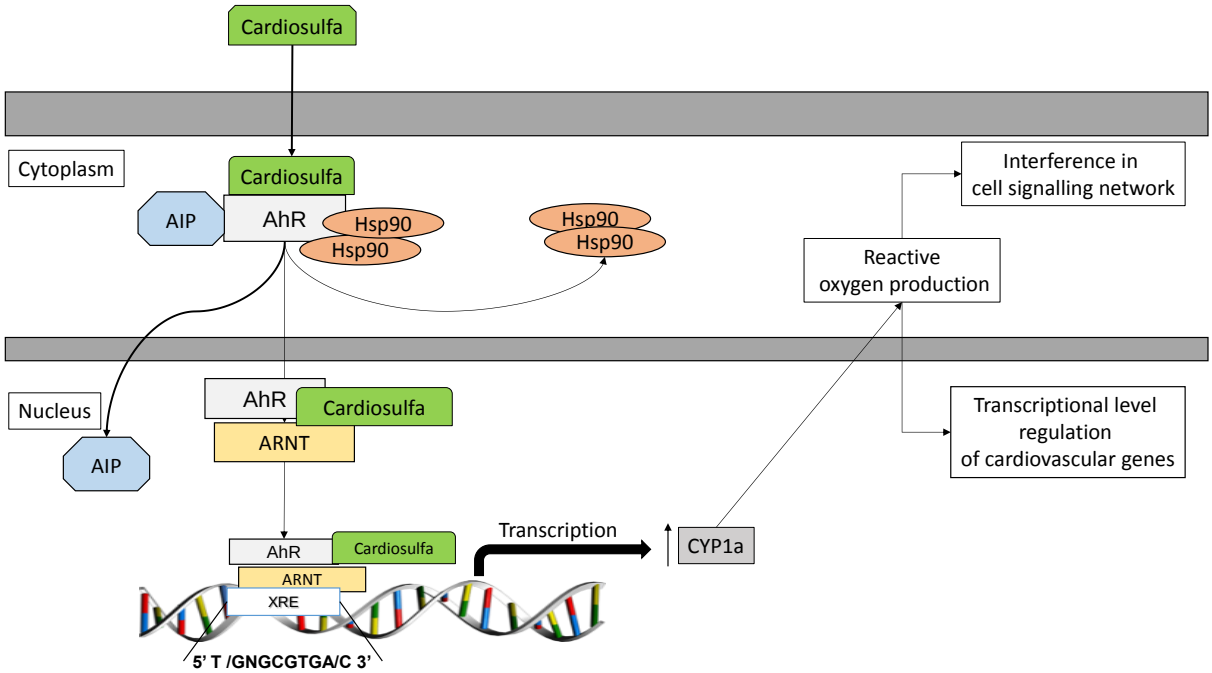

Figure 7-14 Aryl hydrocarbon receptor (AhR) signalling pathway implicated in organ formation. Non bound AhR is present in the cytoplasm as in active protein as a complex consisting of a dimer of heat shock protein (Hsp90) and immunophilin-like protein (AIP). Upon ligand (cardiosulfa) binding the AIP is released leading to import in the nucleus, and Hsp90 dissociates to allow binding of Aryl hydrocarbon receptor nuclear translocator (Arnt). The activated AhR/Arnt heterodimer complex is then capable of either directly interacting with DNA by binding to recognition sequences to activate transcription of different genes. Induction of cytochrome P450 1A (CYP1A) gene expression is the single most sensitive molecular response to AhR activation and has been implicated in toxicity.

In conclusion, putative AhR and AhRR proteins have been proposed in *Dictyostelium.* It remains to be seen whether these proteins are orthologues or arisen by convergent evolution. The observations augment the value of *Dictyostelium* as biomedical model in particular for the elucidation of differentiation and development. The presence of AhR type pathways is significant as it means *Dictyostelium* may have a further method of responding to its environment. Meanwhile soluble ligands and signals associated with ECM and important in directing morphogenetic movements(Darcy *et al.*, 1994) necessary to produce its multicellular life cycle stage could act as ligands for the putative.

CHAPTER 8
Conclusions and Future Work

8.1 Rhomboids

Rhomboid proteins, despite their ubiquity, are poorly characterised at the cellular level. In this work four previously unknown rhomboids, RhmA-D, were identified in *Dictyostelium* and their function investigated in parallel with work in the same laboratory on chloroplast orthologues. Bioinformatic analysis suggested these four putative proteins were proteolytically 'active' rhomboid proteases. Biological importance was confirmed for three of them via knockout lines: RhmA and RhmB were shown to have a role in development, I was unable to obtain a disruption of the *rhmD* gene which is consistent with RhmD being essential for viability. Phylogenetic analysis, sequence alignment and 3D structure analysis shows evolutionary conservation of the *Dictyostelium* rhomboid proteins; RhmA and RhmC appear to belong to the secretase subtype, whereas RhmB and RhmD are PARL like. *Dictyostelium* rhomboid proteins thus seem typical of eukaryotes and indeed mammalian proteins; therefore, analysing the cellular function of these proteins in this microbial model organism may help elucidate potential cellular roles in higher eukaryotes.

8.1.1 Role of RhmA

To understand the role of RhmA in *Dictyostelium*, the protein was both knocked out and overexpressed in the organism. Deletion of *rhmA* resulted in a reduced response in chemotaxis assays to both cAMP and folate, and *rhmA*$^-$ slugs were greatly impaired in phototaxis compared with wild type cells. The delay in chemotactic response does not rule out an inadequate chemotactic regulation, though could also result from cells moving more slowly. This latter hypothesis was substantiated by the significantly reduced speed of the random migration of *rhmA*$^-$ cells (although only 5% less than wild type cells). This was further supported by the fact that even though *rhmA*$^-$ cells show impaired chemotaxis, the *rhmA*$^-$ cells do eventually polarise and orient toward the chemokine source in a needle chemotaxis assay. Less directionality and less elongated *rhmA*$^-$ cells were seen in the latter, however.

Dictyostelium slugs form by aggregation of individual cells. Slugs then seek out optimal conditions for culmination by phototaxis and thermotaxis, during which the slugs move with great sensitivity towards sources of light and heat (Fisher, 1997). In *Dictyostelium* many mutants in components of the actin cytoskeleton show defects in

phototaxis (Noegel & Schleicher, 2000). A light signal is known to modulate the slug tip activation and inhibition system which provokes slug turning by stimulating lateral shifts in the tips' position (Fisher, 1997), but phototactic signalling pathways are complex and have not yet been fully delineated. A cytoskeleton defect in *rhmA*$^{-}$ cells cannot be excluded but the fact that numerous phototaxis defective mutants also display aberrant mitochondrial morphology (Francione *et al.*, 2011) is more compelling. Mitochondrial morphology and function of *rhmA*$^{-}$ cells was found to be impaired by TEM and succinate hydrogenase assays. *rhmA*$^{-}$ mitochondria displayed significantly altered ultrastructure and a reduced proportion of spherical mitochondria versus the wild type. The data from the succinate dehydrogenase assay also suggested that the mutant mitochondria were generating significantly less ATP. Reduced respiration because of mitochondrial defects would be consistent with the aberrant locomotion observed in *rhmA*$^{-}$ cells, although more detailed assays of the ETC are required to pinpoint the lesion in respiration.

Rhomboids such as the PARL in humans, Rho-7 in *Drosophila* and Pcp1 in *S. cerevisiae* are suggested to be responsible for the proteolytic processing of Opa1, the mammalian orthologue of Mgm1, which is linked to the regulation of mitochondrial morphology (Herlan *et al.*, 2003, Walder *et al.*, 2005). GFP tagging RhmA revealed punctate localisation in the cell, with enrichment in the vacuoles, suggesting RhmA is not only involved in the maintenance of the mitochondria but is presumably activating non organellar proteins that may affect function of, or be trafficked to, the mitochondrion after cleavage. This is further substantiated by the use of Mitotracker dye, with which RhmA-GFP did not colocalise. Using a GFP trap pull down assay, the binding partners of RhmA were investigated, but no conclusive results were obtained. The protein band pulled down with over expressed RhmA-GFP was not consistent with the size of *Dictyostelium* putative substrates (Chapter 3) identified from the literature and STRING association network. Although DymA and DlpB transcripts were differentially regulated in the *rhmA*$^{-}$ cells versus wild type cells. The RhmA constructs from this work are thus currently under exploration in cell based model substrate assays (K. Strisovsky, Prague) to confirm rhomboid activity and, in our laboratory, dynamin–GFP assays to confirm potential substrates. Final evidence for a direct substrate to protease relation is lacking even in well studied rhomboids such as Rho-7 and PARL (Zick & Reichert, 2013).

Nevertheless, CyrA, a cysteine-rich protein of 63kDa, is of similar size to the unknown band identified in the pull down assays. The protein has four EGFL repeats, and is cleaved into two major C-terminal fragments, CyrA-C45 and CyrA-C40. CyrA contains an 18 amino acid sequence (DdEGFL1) that has been reported to enhance both random cell motility and cAMP mediated chemotaxis. Even though it does not enhance folate chemotaxis, was able to rescue the movement when the pathway was blocked by commercial inhibitors (Nikolaeva *et al.*, 2012). One of the most well studied rhomboids, Rho-1 in *Drosophila* regulates signalling of the EGFR by mediating cleavage of Spitz, the EGFR ligand (Lee *et al.*, 2001). In mammals, EGF binds to an EGFR to initiate intracellular signalling that regulates a diversity of cellular processes including cell motility and chemotaxis. EGF is also known to enhance cell spreading and motility in normal and cancer cells via its regulation of the EGFR (Zandi *et al.*, 2007). Intriguingly *Dictyostelium* possesses more Epidermal Growth Factor-Like Repeats (EGFL) containing proteins than any other sequenced eukaryote, suggesting an important function for these domains in cellular and developmental processes (Glöckner *et al.*, 2002). This suggests there is a possibility that an EGFR-like protein exists in *Dictyostelium*. It is possible that the cleaved products CyrA-C45 and CyrA-C40 act as ligands to an ancestral EGFR. Bioinformatic analyses support the secretion of CyrA. SignalP, which predicts the presence and location of signal peptide cleavage sites in eukaryotic amino acid sequences (Petersen *et al.*, 2011), identified an N-terminal signal peptide with a cleavage site between residues 20 and 21 (89.2% probability). Similarly, TargetP, which predicts the subcellular localisation of eukaryotic proteins (Emanuelsson *et al.*, 2000), yielded a 93.9% probability that the destination of CyrA is the secretory pathway. In contrast, TMHMM, which predicts transmembrane helices in proteins (Krogh *et al.*, 2001), did not identify an appropriate transmembrane helix at any region within CyrA. As CyrA must be cleaved to release the DdEGFL1 to activate a novel motility pathway (Nikolaeva *et al.*, 2012), it is conceivable that this proteolytic processing might be carried out by RhmA.

For now, it is known that RhmA mediates cell motility in *Dictyostelium* by unknown means. RhmA may play a role in a number of signal transduction pathways, based on evidence presented here, but the principle cellular function of RhmA does seem most likely to involve the regulation of proteins needed in mitochondrial dynamics during development.

8.1.2 Role of RhmB

Ablation of *rhmB* caused slow growth, defects in early development, and aberrant morphology after 24 h, where sparse fruiting bodies were often collapsed with small spores. Overexpression of RhmB (using act15::RhmB-GFP fusion protein) did not cause a change in developmental morphology compared with wild type cells.

RhmB null cells also showed impaired growth in axenic media: efficient pinocytosis is required for cells to grow in liquid medium (Hacker *et al.*, 1997). The *rhmB* null cells were about 50% larger than wild type. Impaired axenic growth and increased cell size are phenotypes are often associated with defects in cytokinesis (Noegel & Schleicher, 2000). Defects in cytokinesis of cells grown in suspension culture typically result in large cell sizes compared to wild type cells, since these cells become multinucleated, however, multinucleated cells were not observed in *rhmB*$^-$ cells, there seemed to be no fault in cell division as compared with the wild type cells. *rhmB* null mutants were also monitored on *K. aerogenes* lawns, revealing slower growth compared with wild type cells. The aberrant growth seen on the *K. aerogenes* lawn could be attributed to lower cell-substrate adhesion. Additionally, The RhmA/B double mutant was unable to phagocytose prey bacteria at all and could only be grown axenically.

Endocytosis is an essential part of chemotaxis, and *rhmB*$^-$ cells showed a significant reduction in chemotaxis towards folate in one drop and under agarose assays. This potential involvement for RhmB in endocytosis, could be explained by defective cytoskeletal reorganisation, for example, *Dictyostelium* takes up fluid mainly by macropinocytosis, a process dependent on actin, coronin, and other actin-binding proteins. Macropinocytosis was also shown to be regulated by small GTPases of the Rac family and phosphatidylinositol 3-kinases (reviewed in Rupper & Cardelli, 2001). Although the observed rate of formation of macropinosomes is sufficient to account for all measured fluid phase uptake (Hacker *et al.*, 1997), coated vesicles are found in *Dictyostelium* and disruption of clathrin heavy chain leads to an 80% reduction in pinocytosis (O'Halloran & Anderson, 1992).

Interestingly, RhmB-GFP colocalised a mitochondrial outer membrane maker with, pJSK543. Despite being targeted to the mitochondria, there was no evidence for a role

for RhmB in either maintenance, division or the morphology in TEM or succinate dehydrogenase assay. Bioinformatics prediction did however suggest RhmB to be localised to the mitochondria and phylogenetic analysis grouped the protein with known PARL-like rhomboids. Although there is no orthologue of the Mgm1 in *Dictyostelium,* suggesting that RhmB may serve a different role compared with *S. cerevisiae,* humans and *Drosophila,* in which PARL-like rhomboids that are involved in mitochondrial fusion or in cristae remodelling.

Rhomboid proteases are known to cleave dynamin like proteins (Shi *et al.*, 2011), corresponding with the predictions from the STRING network and our qPCR results The experimental evidence shows a possible link between RhmB and the dynamin protein family specifically DymB. This may possibly explain the defective endocytosis observed in *rhmB*$^{-}$ cells. One of the best characterised functions of a dynamin family member is clathrin-mediated endocytosis, which was deduced from observations in *Drosophila* and mammalian cells. Initial studies of *D. melanogaster* mutants (Kosaka & Ikeda, 1983) and later mammalian cells expressing mutant forms of dynamin (Damke *et al.*, 1994) showed an increase in the presence of invaginations at the plasma membrane. Dynamin-1 localises to endocytic clathrin-coated pits and self-assembles into rings at the neck of clathrin-coated buds. This process is thought to be a key step in the mechanism by which vesicles are brought in at the plasma membrane as the dynamin rings constrict (Wienke *et al.*, 1999).

Furthermore the evidence presented here indicated RhmB influences cell adhesion, another role associated with the dynamin proteins. Rhomboids in other apicomplexan parasites, such as *Plasmodium* and *Toxoplasma,* also control surface adhesion as part of the process leading to host cell attachment and invasion by regulating microneme proteins (Urban & Freeman, 2003). Mammalian Dynamin 1 affects adhesion and the associated cytoskeleton, and depletion of Dynamin 2 in the fibroblasts inhibits migration of adherent cells. These findings, linked together with the fact that DymB is translated as a pre-protein, of 105 kDa, and that it is processed in a similar manner seen with Mgm1 in the mitochondria and then released back into the cytosol support the proposition that RhmB is could be involved in its regulation. TMPred and Phobius both predicted DymB to contain transmembrane domains (Käll *et al.*, 2004; Lao *et al.*, 2002)., consistent with

rhomboid substrates, but it should be mentioned that TMHMM did not predict any, suggesting the protein to be cytoplasmic (Käll *et al.*, 2004).

RhmB effects on cell to cell and cell to substrate adhesion and endocytosis could be mediated by events at the plasma membrane, components of the actin-based cytoskeleton, and cell adhesion sites. It should be noted that DymB is predicted to be a single transmembrane domain protein located in the mitochondria before its processing, which correlated with RhmB localisation and rhomboid proteases typical substrates (Cipolat *et al.*, 2006; Leroy *et al.*, 2010; Shi *et al.*, 2011). Again, although the substrate specificity of this protease is not yet clear, the possible association with classic dynamin and dynamin-related proteins is intriguing and merits further study.

8.1.3 Summary

From the data generated here it is seems that *Dictyostelium* rhomboids have evolved to possess different targeting signals. The different localisations of the rhomboids seems correspond to participation in different cellular functions. However, with the evidence from other systems suggesting that activity control is governed by compartmentalisation, it is possible that function and targeting have co-evolved (Arutyunova *et al.*, 2014; Tsruya *et al.*, 2002, 2007). Rhomboid proteins in *Dictyostelium* may interact with multiple targets not dissimilar to those seen with other rhomboids in various other taxa.

RhmA showed punctate localisation to cell membranes in the secretory pathway. It is known that rhomboids are ideally situated in organellar membranes to mediate roles in animal cell signalling by releasing growth factors from the membrane. This function emerged from genetic study of *Drosophila* (Tsruya *et al.*, 2007). Although the EGF signalling is seen in humans (Adrain *et al.*, 2011) and *C. elegans* (Dutt *et al.*, 2004), rhomboids main role is to set up a paracrine loop to amplify and spread the EGF signal rather than direct targeting. Interestingly, recent investigations that localised rhomboids to the secretory pathway uncovered increased expression in cancer cell with potential links to growth factor signalling (Adrain *et al.*, 2011; Lohi *et al.*, 2004). In yeast Pcp1 is localised in the mitochondria and is implicated in mitochondrial respiration and energy generation (Sesaki *et al.*, 2003). Subsequently, deletion of Pcp1 effects morphology and

development, similar to the aberrant slug development and dysfunctional mitochondria observed in *rhmA*$^{-}$ cells.

In contrast RhmB localises to the mitochondria without affecting mitochondrial morphology or function. The mammalian representative of the mitochondrial rhomboid PARL was initially suggested to be responsible for the processing of Opa1 (the mammalian orthologue of Mgm1). However PARL ablation did not itself induce any changes in the mitochondrial morphology or Opa1 processing (Cipolat *et al.*, 2006; Duvezin-Caubet *et al.*, 2007). The dephosphorylation-dependent β-cleavage of PARL has been associated with changes in mitochondrial morphology (Jeyaraju *et al.*, 2006). Rhomboids have been involved in cell adhesion, particularly in PfROM4, TgROM4 and TgROM5, where they dismantle the adhesive junctions on host cells following invasion by malarial parasite *P. falciparum* (Baker *et al.*, 2006) and *T. gondii* (Buguliskis *et al.*, 2010; Dowse *et al.*, 2005). Beyond invasion, roles in parasitic growth has also been observed (Srinivasan *et al.*, 2009), a phenotype similar to that seen in *rhmB*$^{-}$ cells.

To understand the role of RhmC and RhmD, both of these genes were subjected to attempted knockout. Knockout cell lines for *rhmC*$^{-}$ were successfully constructed, however no gross phenotypic changes were found during development or chemotaxis. One possible explanation for this might be the redundancy between rhomboid genes in *Dictyostelium.* However qPCR results (data not shown) did not reveal differential regulation of *rhmA* and *rhmB* transcripts in *rhmC*$^{-}$ null mutants. Further experiments are needed to dissect if RhmC has any role in *Dictyostelium* development. On the other hand, deletion of *rhmD* was unsuccessful even after multiple attempts, suggesting either the gene is essential for viability or a different approach is needed to silence the gene.

Apart from roles in chemotaxis, endocytosis and phototaxis discussed in this study for the rhomboid family (RhmA and RhmB), it is possible that the other rhomboids (RhmC and RhmD) have various other roles in the control of cell behaviour. The phenotype of these mutant cells needs to be investigated in much more detail.

8.2 Boronic Acids: Potential Inhibitors

8.2.1 Three novel compounds

In this study, three novel compounds have been shown to have a specific biological effect on *Dictyostelium* and how they inhibit uPA function is reported for the first time. BC11 in particular may serve as a lead compound for the development of novel uPA inhibitors: it was the most potent inhibitor of uPA in biochemical assays and caused an immediate yet reversible effect on the chemotaxis of *Dictyostelium.* Even though boronic acids derivates are not known to be synthesised in any organism, they are considered "green compounds" because of their low toxicity profile and they are tolerant in biological environments (Trippier & McGuigan, 2010), and ultimately degrade into the non-hazardous compound, boric acid. They are also relatively easy to synthesise. Boronic acids have the ability to form both hydrogen and covalent bonds in an enzyme's active site and to act as transition state analogues. Both biochemical assays performed by collaborators and our *Dictyostelium* cell behaviour assays suggest that these compounds can inhibit their targets in the micromolar range or lower.

Further work is required to elucidate the molecular targets of BC11, SR3 and BC57 in *Dictyostelium;* our collaborators are currently investigating their utility in tumour growth inhibition (J Spencer, personal communication, 2014).

8.3 Cardiosulfa

Cardiosulfa was identified as a novel small molecule inhibitor of zebrafish cardiovascular development and function, evoking a striking oedema response in the pericardial and yolk sac. Furthermore, cardiosulfa-exposed embryos exhibited dramatic reductions in heart rates and peripheral blood flow as development proceeded, thus indicating impaired heart function. According to gene expression profiling studies using zebrafish, cardiosulfa induces high expression levels of members of the AhR gene battery including *zfcyp1a*, *zfcyp1b1* and *zfcyp1c1*.

In terms of evolution, the oldest known physiological role of AhR is in development, for example AhR orthologue in *Drosophila*, spineless (ss), is necessary for development of the distal segments of the antenna and leg (Duncan *et al.*, 1998). AhR is thought to have evolved in invertebrates; invertebrates have single AhR that do not seem to bind typical ligands of vertebrate AhR (Hahn *et al.*, 2006).

Cardiosulfa treatment caused abnormal slug formation in *Dictyostelium* and decreased cell motility irreversibly, suggesting orthologous gene products to the zebrafish AhR exist. The *Dictyostelium* target binds cardiosulfa with lower affinity as higher concentrations are needed to elicit a response than in zebrafish. The AhR ligands' equivalents in the amoeba require investigation, as well as confirmation of the roles of putative AhR network in *Dictyostelium.* Nevertheless, intriguingly, cardiosulfa may unveil novel mechanisms and pathways relevant to heart disease, and shows that aspects of organogenesis may share evolutionary mechanisms even as with evolutionary distant eukaryotes as *Dictyostelium*.

The observations made in this investigation illustrate the value of *Dictyostelium* as biomedical model, suggesting utility in the study of differentiation and development processes. *Dictyostelium* could also be a good model for studying AhR function in cell detoxification, and aid understanding of AhR biology.

References

A

Akahoshi, E., Yoshimura, S. & Ishihara-Sugano, M., 2006. Over-expression of AhR (aryl hydrocarbon receptor) induces neural differentiation of Neuro2a cells: neurotoxicology study. *Environmental health : a global access science source*, 5(1), p.24.

Akiyama, Y. & Maegawa, S., 2007. Sequence features of substrates required for cleavage by GlpG, an Escherichia coli rhomboid protease. *Molecular microbiology*, 64(4), pp.1028–37.

Alexander, S. & Alexander, H., 2011. Lead genetic studies in Dictyostelium discoideum and translational studies in human cells demonstrate that sphingolipids are key regulators of sensitivity to cisplatin and other anticancer drugs. *Seminars in cell & developmental biology*, 22(1), pp.97–104.

Altschul, S.F. *et al.*, 1990. Basic local alignment search tool. *Journal of molecular biology*, 215, pp.403–410.

Arimura, S. & Tsutsumi, N., 2002. A dynamin-like protein (ADL2b), rather than FtsZ, is involved in Arabidopsis mitochondrial division. *Proceedings of the National Academy of Sciences of the United States of America*, 99(8), pp.5727–31.

Arnold, K. *et al.*, 2006. The SWISS-MODEL workspace: a web-based environment for protein structure homology modelling. *Bioinformatics*, 22(2), pp.195–201.

B

Bader, S., Kortholt, A. & Van Haastert, P.J.M., 2007. Seven Dictyostelium discoideum phosphodiesterases degrade three pools of cAMP and cGMP. *The Biochemical journal*, 402(1), pp.153–61.

Baker, R.P. *et al.*, 2007. Enzymatic analysis of a rhomboid intramembrane protease implicates transmembrane helix 5 as the lateral substrate gate. *Proceedings of the National Academy of Sciences of the United States of America*, 104(20), pp.8257–62.

Baker, R.P. & Urban, S., 2012. Architectural and thermodynamic principles underlying intramembrane protease function. *Nature chemical biology*, 8(9), pp.759–68.

Barth, C., Le, P. & Fisher, P.R., 2007. Mitochondrial biology and disease in Dictyostelium. *International review of cytology*, 263(07), pp.207–52.

Baxt, L.A. *et al.*, 2008. An Entamoeba histolytica rhomboid protease with atypical specificity cleaves a surface lectin involved in phagocytosis and immune evasion. *Genes & development*, 22(12), pp.1636–46.

Bendtsen, J.D. *et al.*, 2004. Improved prediction of signal peptides: SignalP 3.0. *Journal of molecular biology*, 340(4), pp.783–95.

Ben-Shem, A., Fass, D. & Bibi, E., 2007. Structural basis for intramembrane proteolysis by rhomboid serine proteases. *Proceedings of the National Academy of Sciences of the United States of America*, 104(2), pp.462–6.

Blasi, F. & Carmeliet, P., 2002. uPAR: a versatile signalling orchestrator. *Nature reviews. Molecular cell biology*, 3(12), pp.932–43.

Bleazard, W. *et al.*, 1999. The dynamin-related GTPase Dnm1 regulates mitochondrial fission in yeast. *Nature cell biology*, 1(5), pp.298–304.

Boeckeler, K. *et al.*, 2006. The neuroprotective agent, valproic acid, regulates the mitogen-activated protein kinase pathway through modulation of protein kinase A signalling in Dictyostelium discoideum. *European journal of cell biology*, 85(9-10), pp.1047–57.

Boeckeler, K. & Williams, R., 2007. Dictyostelium as a biomedical model. *Encyclopedia of Life Sciences*.

Boitano, A.E. *et al.*, 2010. Aryl hydrocarbon receptor antagonists promote the expansion of human hematopoietic stem cells. *Science*, 329(5997), pp.1345–8.

Bondar, A.-N., Val, C. del & White, S., 2009. Rhomboid protease dynamics and lipid interactions. *Structure*, 17(3), pp.395–405.

Brossier, F. *et al.*, 2005. A spatially localized rhomboid protease cleaves cell surface adhesins essential for invasion by Toxoplasma. *Proceedings of the National Academy of Sciences of the United States of America*, 102(11), pp.4146–51.

Brown, M.S. *et al.*, 2000. Regulated intramembrane proteolysis: a control mechanism conserved from bacteria to humans. *Cell*, 100(4), pp.391–8.

Browning, D.D., The, T. & O'Day, D.H., 1995. Comparative analysis of chemotaxis in Dictyostelium using a radial bioassay method: Protein tyrosine kinase activity is required for chemotaxis to folate but not to cAMP. *Cellular Signalling*, 7(5), pp.481–489.

Buguliskis, J.S. *et al.*, 2010. Rhomboid 4 (ROM4) affects the processing of surface adhesins and facilitates host cell invasion by Toxoplasma gondii. K. Kim, ed. *PLoS pathogens*, 6(4), p.e1000858.

C

Carnell, M.J. & Insall, R.H., 2011. Actin on disease--studying the pathobiology of cell motility using Dictyostelium discoideum. *Seminars in cell & developmental biology*, 22(1), pp.82–8.

Chang, P., Walker, M.C. & Williams, R.S.B., 2014. Seizure-induced reduction in PIP3 levels contributes to seizure-activity and is rescued by valproic acid. *Neurobiology of disease*, 62, pp.296–306.

Chen, L. *et al.*, 2007. PLA2 and PI3K/PTEN pathways act in parallel to mediate chemotaxis. *Developmental cell*, 12(4), pp.603–14.

Chen, L. *et al.*, 2003. Two phases of actin polymerization display different dependencies on PI(3,4,5)P3 accumulation and have unique roles during chemotaxis. *Molecular biology of the cell*, 14(12), pp.5028–37.

Claros, M.G. & Vincens, P., 1996. Computational method to predict mitochondrially imported proteins and their targeting sequences. *European journal of biochemistry*, 241(3), pp.779–86.

Clemmer, K.K.M. *et al.*, 2006. Functional characterization of Escherichia coli GlpG and additional rhomboid proteins using an aarA mutant of Providencia stuartii. *Journal of bacteriology*, 188(9), pp.3415–9.

Conseil, V., Soête, M. & Dubremetz, J.F., 1999. Serine protease inhibitors block invasion of host cells by Toxoplasma gondii. *Antimicrobial agents and chemotherapy*, 43(6), pp.1358–61.

Cortesio, C.L., Lewellyn, E.B. & Drubin, D.G., 2015. Control of lipid organization and actin assembly during clathrin-mediated endocytosis by the cytoplasmic tail of the Rhomboid protein Rbd2. *Molecular Biology of the Cell*, pp.1–42.

D

Darcy, P.K., Wilczynska, Z. & Fisher, P., 1994. Genetic analysis of Dictyostelium slug phototaxis mutants. *Genetics*, 137(4), pp.977–85.

Doherty, G.J. & McMahon, H.T., 2008. Mediation, modulation, and consequences of membrane-cytoskeleton interactions. *Annual review of biophysics*, 37, pp.65–95.

Duncan, D.M., Burgess, E.A. & Duncan, I., 1998. Control of distal antennal identity and tarsal development in Drosophila by spineless-aristapedia, a homolog of the mammalian dioxin receptor. *Genes & Development*, 12(9), pp.1290–1303.

Dutt, A. *et al.*, 2004. EGF signal propagation during C. elegans vulval development mediated by ROM-1 rhomboid. *PLoS biology*, 2(11), p.e334.

E

Eichinger, L. & Rivero-Crespo, F., 2006. *Dictyostelium discoideum protocols*, Springer.

Eichinger, L. *et al.*, 2005. The genome of the social amoeba Dictyostelium discoideum. *Nature*, 435(7038), pp.43–57.

Ejigiri, I. *et al.*, 2012. Shedding of TRAP by a rhomboid protease from the malaria sporozoite surface is essential for gliding motility and sporozoite infectivity. M. M. Mota, ed. *PLoS pathogens*, 8(7), p.e1002725.

Emanuelsson, O. *et al.*, 2007. Locating proteins in the cell using TargetP, SignalP and related tools. *Nature protocols*, 2(4), pp.953–71.

Emanuelsson, O. *et al.*, 2000. Predicting subcellular localization of proteins based on their N-terminal amino acid sequence. *Journal of molecular biology*, 300(4), pp.1005–16.

Emanuelsson, O. & von Heijne, G., 2001. Prediction of organellar targeting signals. *Biochimica et biophysica acta*, 1541(1-2), pp.114–9.

Erez, E., Fass, D. & Bibi, E., 2009. How intramembrane proteases bury hydrolytic reactions in the membrane. *Nature*, 459(7245), pp.371–8.

Esser, K. *et al.*, 2002. A Novel Two-step Mechanism for Removal of a Mitochondrial Signal Sequence Involves the mAAA Complex and the Putative Rhomboid Protease Pcp1. *Journal of Molecular Biology*, 323(5), pp.835–843.

F

Faix, J. *et al.*, 2004. A rapid and efficient method to generate multiple gene disruptions in Dictyostelium discoideum using a single selectable marker and the Cre-loxP system. *Nucleic acids research*, 32(19), p.e143.

Firtel, R. & Meili, R., 2000. Dictyostelium: a model for regulated cell movement during morphogenesis. *Current opinion in genetics & development*, pp.421–427.

Fisher, P., 1997. Genetics of phototaxis in a model eukaryote, Dictyostelium discoideum. *Bioessays*, 19(5), pp.397 – 407.

Fisher, P. & Annesley, S.J., 2006. Slug phototaxis, thermotaxis and spontaneous turning behaviour. In *Methods in molecular biology – Dictyostelium discoideum protocols*. Springer, pp. 128 – 162.

Fisher, P., Merkl, R. & Gerisch, G., 1989. Quantitative analysis of cell motility and chemotaxis in Dictyostelium discoideum by using an image processing system and a novel chemotaxis chamber providing stationary chemical gradients. *The Journal of cell biology*, 108(3), pp.973–84.

Fisher, P. & Williams, K., 1981. Bidirectional phototaxis by Dictyostelium discoideum slugs. *FEMS Microbiology Letters*, 12, pp.87–89.

Franceschini, A. *et al.*, 2013. STRING v9.1: protein-protein interaction networks, with increased coverage and integration. *Nucleic acids research*, 41(Database issue), pp.D808–15.

Freeman, M., 2008. Rhomboid proteases and their biological functions. *Annual review of genetics*, 42, pp.191–210.

Freeman, M., 2009. Rhomboids: 7 years of a new protease family. *Seminars in cell & developmental biology*, 20(2), pp.231–9.

Funamoto, S. *et al.*, 2001. Role of phosphatidylinositol 3' kinase and a downstream pleckstrin homology domain-containing protein in controlling chemotaxis in dictyostelium. *The Journal of cell biology*, 153(4), pp.795–810.

G

Gallio, M. *et al.*, 2002. A conserved mechanism for extracellular signaling in eukaryotes and prokaryotes. *Proceedings of the National Academy of Sciences of the United States of America*, 99(19), pp.12208–13.

Gasiewicz, T.A., Singh, K.P. & Casado, F.L., 2010. The aryl hydrocarbon receptor has an important role in the regulation of hematopoiesis: implications for benzene-induced hematopoietic toxicity. *Chemico-biological interactions*, 184(1-2), pp.246–51.

Gaudet, P. *et al.*, 2007. Transformation of Dictyostelium discoideum with plasmid DNA. *Nature protocols*, 2(6), pp.1317–24.

Gauthier, M.L. & O'Day, D.H., 2001. Detection of calmodulin-binding proteins and calmodulin-dependent phosphorylation linked to calmodulin-dependent chemotaxis to folic and cAMP in Dictyostelium. *Cellular signalling*, 13(8), pp.575–84.

Gilson, P.R.P. *et al.*, 2003. Dictyostelium orthologs of the prokaryotic cell division protein FtsZ localize to mitochondria and are required for the maintenance of normal mitochondrial morphology. *Eukaryotic cell*, 2(6), pp.1315–1326.

Goldberg, T. *et al.*, 2014. LocTree3 prediction of localization. *Nucleic acids research*, 42(Web Server issue), pp.W350–5.

H

Hadjout, N. *et al.*, 2001. Automated real-time measurement of chemotactic cell motility. *BioTechniques*, 31(5), pp.1130–8.

Hadwiger, J. a & Srinivasan, J., 1999. Folic acid stimulation of the Galpha4 G protein-mediated signal transduction pathway inhibits anterior prestalk cell development in Dictyostelium. *Differentiation; research in biological diversity*, 64(4), pp.195–204.

Hahn, M.E. *et al.*, 1997. Molecular evolution of two vertebrate aryl hydrocarbon (dioxin) receptors (AHR1 and AHR2) and the PAS family. *Proceedings of the National Academy of Sciences of the United States of America*, 94(25), pp.13743–8.

Hahn, M.E. *et al.*, 2006. Unexpected diversity of aryl hydrocarbon receptors in non-mammalian vertebrates: insights from comparative genomics. *Journal of experimental zoology*, 305(9), pp.693–706.

Harbeck, N. *et al.*, 2004. Urokinase-type plasminogen activator (uPA) and its inhibitor PAI-I: novel tumor-derived factors with a high prognostic and predictive impact in breast cancer. *Thrombosis and haemostasis*, 91(3), pp.450–6.

Haupt, B.J. *et al.*, 2007. Asymmetric elastic properties of Dictyostelium discoideum in relation to chemotaxis. *Langmuir : the ACS journal of surfaces and colloids*, 23(18), pp.9352–7.

Heid, P.J. *et al.*, 2004. The role of myosin heavy chain phosphorylation in Dictyostelium motility, chemotaxis and F-actin localization. *Journal of cell science*, 117(Pt 20), pp.4819–35.

Herlan, M. *et al.*, 2003. Processing of Mgm1 by the rhomboid-type protease Pcp1 is required for maintenance of mitochondrial morphology and of mitochondrial DNA. *The Journal of biological chemistry*, 278(30), pp.27781–8.

Hirokawa, T., Boon-Chieng, S. & Mitaku, S., 1998. SOSUI: classification and secondary structure prediction system for membrane proteins. *Bioinformatics*, 14(4), pp.378–379.

Huber, R. & O'Day, D.H., 2011. EGF-like peptide-enhanced cell motility in Dictyostelium functions independently of the cAMP-mediated pathway and requires active Ca2+/calmodulin signaling. *Cellular signalling*, 23(4), pp.731–8.

I

Insall, R. & Andrew, N., 2007. Chemotaxis in Dictyostelium: how to walk straight using parallel pathways. *Current opinion in microbiology*, 10(6), pp.578–81.

J

Janssens, P.M. & Van Haastert, P.J., 1987. Molecular basis of transmembrane signal transduction in Dictyostelium discoideum. *Microbiological reviews*, 51(4), pp.396–418.

Jeyaraju, D. V *et al.*, 2013. Rhomboid proteases in mitochondria and plastids: keeping organelles in shape. *Biochimica et biophysica acta*, 1833(2), pp.371–80.

Jin, T. *et al.*, 1998. Selection of gbeta subunits with point mutations that fail to activate specific signaling pathways in vivo: dissecting cellular responses mediated by a heterotrimeric G protein in Dictyostelium discoideum. *Molecular biology of the cell*, 9(10), pp.2949–61.

Jin, T., Xu, X. & Hereld, D., 2008. Chemotaxis, chemokine receptors and human disease. *Cytokine*, 44(1), pp.1–8.

Jones, R.G. & Thompson, C.B., 2009. Tumor suppressors and cell metabolism: a recipe for cancer growth. *Genes & development*, 23(5), pp.537–48.

Jurgens, G. *et al.*, 1984. Mutations affecting the pattern of the larval cuticle in Drosophila melanogaster. *Developmental Biology*, 193, pp.267 – 282.

K

Käll, L., Krogh, A. & Sonnhammer, E.L.L., 2004. A combined transmembrane topology and signal peptide prediction method. *Journal of molecular biology*, 338(5), pp.1027–36.

Kelley, L.A. & Sternberg, M.J.E., 2009. Protein structure prediction on the Web: a case study using the Phyre server. *Nature protocols*, 4(3), pp.363–71.

Kibler, K. *et al.*, 2003. A cell-adhesion pathway regulates intercellular communication during Dictyostelium development. *Developmental Biology*, 264(2), pp.506–521.

Kim, J. *et al.*, 2007. Stochastic noise and synchronisation during dictyostelium aggregation make cAMP oscillations robust. *PLoS computational biology*, 3(11), p.e218.

Kiss, E.A. *et al.*, 2011. Natural aryl hydrocarbon receptor ligands control organogenesis of intestinal lymphoid follicles. *Science*, 334(6062), pp.1561–5.

Ko, S.-K. *et al.*, 2009. Cardiosulfa, a small molecule that induces abnormal heart development in zebrafish, and its biological implications. *Angewandte Chemie (International ed. in English)*, 48(42), pp.7809–12.

Ko, S.-K. & Shin, I., 2012. Cardiosulfa induces heart deformation in zebrafish through the AhR-mediated, CYP1A-independent pathway. *Chembiochem : a European journal of chemical biology*, 13(10), pp.1483–9.

Koehler, K.A. & Lienhard, G.E., 1971. 2-phenylethaneboronic acid, a possible transition-state analog for chymotrypsin. *Biochemistry*, 10(13), pp.2477–83.

Koonin, E. V *et al.*, 2003. The rhomboids: a nearly ubiquitous family of intramembrane serine proteases that probably evolved by multiple ancient horizontal gene transfers. *Genome biology*, 4(3), p.R19.

Krogh, A. *et al.*, 2001. Predicting transmembrane protein topology with a hidden Markov model: application to complete genomes. *Journal of molecular biology*, 305(3), pp.567–80.

Kuramoto, N. *et al.*, 2002. Existence of xenobiotic response element binding in Dictyostelium. *Biochimica et biophysica acta*, 1578(1-3), pp.1–11.

L

Labrousse, A.M. *et al.*, 1999. C. elegans Dynamin-Related Protein DRP-1 Controls Severing of the Mitochondrial Outer Membrane. *Molecular Cell*, 4(5), pp.815–826.

Larkin, M.A. *et al.*, 2007. Clustal W and Clustal X version 2.0. *Bioinformatics*, 23(21), pp.2947–8.

Lee, J. *et al.*, 2001. Regulated Intracellular Ligand Transport and Proteolysis Control EGF Signal Activation in Drosophila. *Cell*, 107, pp.161–171.

Lei, X. & Li, Y.-M., 2009. The processing of human rhomboid intramembrane serine protease RHBDL2 is required for its proteolytic activity. *Journal of molecular biology*, 394(5), pp.815–25.

Lemberg, M.K. & Freeman, M., 2007a. Cutting proteins within lipid bilayers: rhomboid structure and mechanism. *Molecular cell*, 28(6), pp.930–40.

Lemberg, M.K. & Freeman, M., 2007b. Functional and evolutionary implications of enhanced genomic analysis of rhomboid intramembrane proteases. *Genome research*, 17(11), pp.1634–46.

Leroy, I. *et al.*, 2010. Processing of the dynamin Msp1p in S. pombe reveals an evolutionary switch between its orthologs Mgm1p in S. cerevisiae and OPA1 in mammals. *FEBS letters*, 584(14), pp.3153–7.

Li, M. *et al.*, 2013. The FHA and BRCT domains recognize ADP-ribosylation during DNA damage response. *Genes & development*, 27(16), pp.1752–68.

Lilly, P. *et al.*, 1993. A G-protein beta-subunit is essential for Dictyostelium development. *Genes & development*, 7(6), pp.986–95.

Lima, W.C., Lelong, E. & Cosson, P., 2011. What can Dictyostelium bring to the study of Pseudomonas infections? *Seminars in cell & developmental biology*, 22(1), pp.77–81.

Lohi, O., Urban, S. & Freeman, M., 2004. Diverse substrate recognition mechanisms for rhomboids; thrombomodulin is cleaved by Mammalian rhomboids. *Current biology*, 14(3), pp.236–41.

Ludtmann, M.H.R., Boeckeler, K. & Williams, R., 2011. Molecular pharmacology in a simple model system: implicating MAP kinase and phosphoinositide signalling in bipolar disorder. *Seminars in cell & developmental biology*, 22(1), pp.105–13.

Lusche, D.F., Wessels, D. & Soll, D.R., 2009. The effects of extracellular calcium on motility, pseudopod and uropod formation, chemotaxis, and the cortical localization of myosin II in Dictyostelium discoideum. *Cell motility and the cytoskeleton*, 66(8), pp.567–87.

M

Maegawa, S., Ito, K. & Akiyama, Y., 2005. Proteolytic action of GlpG, a rhomboid protease in the Escherichia coli cytoplasmic membrane. *Biochemistry*, 44(41), pp.13543–13552.

Matagne, A., Joris, B. & Frère, J.M., 1991. Anomalous behaviour of a protein during SDS/PAGE corrected by chemical modification of carboxylic groups. *The Biochemical journal*, 280 (Pt 2, pp.553–6.

Maree, A.F.M., Panfilov, A. V. & Hogeweg, P., 1999. Phototaxis during the slug stage of Dictyostelium discoideum: a model study. *Proceedings of the Royal Society B: Biological Sciences*, 266(1426), pp.1351–1360.

McQuibban, G.A., Saurya, S. & Freeman, M., 2003. Mitochondrial membrane remodelling regulated by a conserved rhomboid protease. *Nature*, 423(May), pp.537–541.

McQuibban, G.A. *et al.*, 2006. Normal mitochondrial dynamics requires rhomboid-7 and affects Drosophila lifespan and neuronal function. *Current biology*, 16(10), pp.982–9.

Meili, R. *et al.*, 1999. Chemoattractant-mediated transient activation and membrane localization of Akt/PKB is required for efficient chemotaxis to cAMP in Dictyostelium. *The EMBO journal*, 18(8), pp.2092–105.

Meyer, I., Kuhnert, O. & Gräf, R., 2011. Functional analyses of lissencephaly-related proteins in Dictyostelium. *Seminars in cell & developmental biology*, 22(1), pp.89–96.

Morita, T. *et al.*, 2000. Involvement of the glucose-regulated protein 94 (Dd-GRP94) in starvation response of Dictyostelium discoideum cells. *Biochemical and biophysical research communications*, 274(2), pp.323–31.

N

Nakai, K. & Horton, P., 1999. PSORT: a program for detecting sorting signals in proteins and predicting their subcellular localization. *Trends in biochemical sciences*, 24(1), pp.34–6.

Nakai, K. & Kanehisa, M., 1992. A knowledge base for predicting protein localization sites in eukaryotic cells. *Genomics*, 14(4), pp.897–911.

Nash, A. & Kalvala, S., 2009. A framework proposition for cellular locality of Dictyostelium modelled in π-Calculus. *CoSMoS 2009*.

Nebl, T. *et al.*, 2002. Multiple signalling pathways connect chemoattractant receptors and calcium channels in Dictyostelium. *Journal of muscle research and cell motility*, 23(7-8), pp.853–65.

Nishida, K., 2003. Dynamic recruitment of dynamin for final mitochondrial severance in a primitive red alga. *Proceedings of the …*, 100(4), pp.2146–51.

Noegel, A.A. & Schleicher, M., 2000. The actin cytoskeleton of Dictyostelium: a story told by mutants. *Journal of cell science*, 113(5), pp.759–66.

O

Osteryoung, K.W. & Vierling, E., 1995. Conserved cell and organelle division. *Nature*, 376(6540), pp.473–4.

P

Parent, C.A. *et al.*, 1998. G Protein Signaling Events Are Activated at the Leading Edge of Chemotactic Cells. *Cell*, 95(1), pp.81–91.

Pascall, J.C. & Brown, K.D., 2004. Intramembrane cleavage of ephrinB3 by the human rhomboid family protease, RHBDL2. *Biochemical and biophysical research communications*, 317(1), pp.244–52.

Pellegrini, L. *et al.*, 2001. PAMP and PARL, two novel putative metalloproteases interacting with the COOH-terminus of Presenilin-1 and -2. *Journal of Alzheimer's disease*, 3(2), pp.181–190.

Petersen, T.N. *et al.*, 2011. SignalP 4.0: discriminating signal peptides from transmembrane regions. *Nature methods*, 8(10), pp.785–6.

Pettersen, E.F. *et al.*, 2004. UCSF Chimera--a visualization system for exploratory research and analysis. *Journal of computational chemistry*, 25(13), pp.1605–12.

Philipp, M. & Bender, M.L., 1971. Inhibition of serine proteases by arylboronic acids. *Proceedings of the National Academy of Sciences of the United States of America*, 68(2), pp.478–80.

Poloz, Y. & O'Day, D.H., 2012. Colchicine affects cell motility, pattern formation and stalk cell differentiation in Dictyostelium by altering calcium signaling. *Differentiation; research in biological diversity*, 83(4), pp.185–99.

Ponte, E. *et al.*, 1998. Detection of subtle phenotypes: the case of the cell adhesion molecule csA in Dictyostelium. *Proceedings of the National Academy of Sciences of the United States of America*, 95(16), pp.9360–5.

Q

Qin, H. & Powell-Coffman, J.A., 2004. The Caenorhabditis elegans aryl hydrocarbon receptor, AHR-1, regulates neuronal development. *Developmental biology*, 270(1), pp.64–75.

Quintana, F.J. *et al.*, 2008. Control of T(reg) and T(H)17 cell differentiation by the aryl hydrocarbon receptor. *Nature*, 453(7191), pp.65–71.

R

Rai, A. *et al.*, 2011. Dictyostelium dynamin B modulates cytoskeletal structures and membranous organelles. *Cellular and molecular life sciences*, 68(16), pp.2751–67.

Rawson, R.B., 2008. Intriguing parasites and intramembrane proteases. *Genes & development*, 22(12), pp.1561–6.

Robery, S. *et al.*, 2011. Investigating the effect of emetic compounds on chemotaxis in Dictyostelium identifies a non-sentient model for bitter and hot tastant research. *PloS one*, 6(9), p.e24439.

Russ, W.P. & Engelman, D.M., 2000. The GxxxG motif: a framework for transmembrane helix-helix association. *Journal of molecular biology*, 296(3), pp.911–9.

S

Sampathkumar, P. *et al.*, 2012. Oligomeric state study of prokaryotic rhomboid proteases. *Biochimica et biophysica acta*, 1818(12), pp.3090–3097.

Santos, J., Graindorge, A. & Soldati-Favre, D., 2012. New insights into parasite rhomboid proteases. *Molecular and biochemical parasitology*, 182(1-2), pp.27–36

Sasaki, A.T. *et al.*, 2004. Localized Ras signaling at the leading edge regulates PI3K, cell polarity, and directional cell movement. *The Journal of cell biology*, 167(3), pp.505–18.

Sasaki, N. *et al.*, 1999. Deletion of the myopathy loop of Dictyostelium myosin II and its impact on motor functions. *The Journal of biological chemistry*, 274(53), pp.37840–4.

Scherer, A. *et al.*, 2010. Ca2+ chemotaxis in Dictyostelium discoideum. *Journal of cell science*, 123(Pt 21), pp.3756–67.

Scott, J. a *et al.*, 2011. AhR2-mediated, CYP1A-independent cardiovascular toxicity in zebrafish (Danio rerio) embryos exposed to retene. *Aquatic toxicology*, 101(1), pp.165–74.

Sesaki, H. *et al.*, 2003. Cells lacking Pcp1p/Ugo2p, a rhomboid-like protease required for Mgm1p processing, lose mtDNA and mitochondrial structure in a Dnm1p-dependent manner, but remain competent for mitochondrial fusion. *Biochemical and Biophysical Research Communications*, 308(2), pp.276–283.

Sherratt, A.R. *et al.*, 2012. Activity-based protein profiling of the Escherichia coli GlpG rhomboid protein delineates the catalytic core. *Biochemistry*, 51(39), pp.7794–803.

Shi, G., Lee, J. R., Grimes, D. a, Racacho, L., Ye, D., Yang, H., Ross, O. a, *et al.* (2011) Functional alteration of PARL contributes to mitochondrial dysregulation in Parkinson's disease. *Hum. Mol. Genet.* **20**(10), 1966–74

Shi, Q. & Jackowski, G., 1998. One-dimensional polyacrylamide gel electrophoresis. In B. D. Hames, ed. *Gel electrophoresis of proteins: A practical approach*. Oxford: Oxford Press.

Siu, C.H. *et al.*, 2004. Regulation of cell-cell adhesion during Dictyostelium development. *Seminars in Cell and Developmental Biology*, 15, pp.633–641.

Smith, E. *et al.*, 2012. Elucidating novel urokinase-type plasminogen activator inhibitors. In *Journal of Thrombosis and Haemostasis*. pp. e10–e24.

Smoum, R. *et al.*, 2012. Boron containing compounds as protease inhibitors. *Chemical reviews*, 112(7), pp.4156–220.

Snel, B. *et al.*, 2000. STRING: a web-server to retrieve and display the repeatedly occurring neighbourhood of a gene. *Nucleic acids research*, 28(18), pp.3442–4.

Steinert, M., 2011. Pathogen-host interactions in Dictyostelium, Legionella, Mycobacterium and other pathogens. *Seminars in cell & developmental biology*, 22(1), pp.70–6.

Stevenson, L.G. *et al.*, 2007. Rhomboid protease AarA mediates quorum-sensing in Providencia stuartii by activating TatA of the twin-arginine translocase. *Proceedings of the National Academy of Sciences of the United States of America*, 104(3), pp.1003–8.

Strisovsky, K., Sharpe, H.H.J.H. & Freeman, M., 2009. Sequence-specific intramembrane proteolysis: identification of a recognition motif in rhomboid substrates. *Molecular cell*, 36(6), pp.1048–1059.

Sunderland, M.E., 2011. Morphogenesis, Dictyostelium, and the search for shared developmental processes. *Studies in history and philosophy of biological and biomedical sciences*, 42(4), pp.508–17.

T

Takeda, K. *et al.*, 2007. Role of phosphatidylinositol 3-kinases in chemotaxis in Dictyostelium. *The Journal of biological chemistry*, 282(16), pp.11874–84.

Tamura, K. *et al.*, 2013. MEGA6: Molecular Evolutionary Genetics Analysis version 6.0. *Molecular biology and evolution*, 30(12), pp.2725–9.

Tanguay, R.L. *et al.*, 2000. Identification and expression of alternatively spliced aryl hydrocarbon nuclear translocator 2 (ARNT2) cDNAs from zebrafish with distinct functions. *Biochimica et biophysica acta*, 1494(1-2), pp.117–28.

Terbach, N. *et al.*, 2011. Identifying an uptake mechanism for the antiepileptic and bipolar disorder treatment valproic acid using the simple biomedical model Dictyostelium. *Journal of cell science*, 124(Pt 13), pp.2267–76.

Thompson, E.P., Smith, S.G.L. & Glover, B.J., 2012. An Arabidopsis rhomboid protease has roles in the chloroplast and in flower development. *Journal of experimental botany*, 63(10), pp.3559–70.

Tijet, N. *et al.*, 2006. Aryl hydrocarbon receptor regulates distinct dioxin-dependent and dioxin-independent gene batteries. *Molecular pharmacology*, 69(1), pp.140–53.

Tsruya, R. *et al.*, 2002. Intracellular trafficking by Star regulates cleavage of the Drosophila EGF receptor ligand Spitz. *Genes & development*, 16(2), pp.222–34.

Tsruya, R. *et al.*, 2007. Rhomboid cleaves Star to regulate the levels of secreted Spitz. *The EMBO journal*, 26(5), pp.1211–20.

Tsruya, R. *et al.*, 2007. Rhomboid cleaves Star to regulate the levels of secreted Spitz. *The EMBO journal*, 26(5), pp.1211–20.

Tusnády, G.E. & Simon, I., 1998. Principles governing amino acid composition of integral membrane proteins: application to topology prediction. *Journal of molecular biology*, 283(2), pp.489–506.

Tusnády, G.E., Simon, I. & Tusnady, G.E., 2001. The HMMTOP transmembrane topology prediction server. *Bioinformatics*, 17(9), pp.849–850.

U

Uchida, K.S.K. & Yumura, S., 2004. Dynamics of novel feet of Dictyostelium cells during migration. *Journal of cell science*, 117(Pt 8), pp.1443–55.

Urban, S., 2013. Bacterial and Protozoan Rhomboid Proteases. In N. Rawlings & G. Salvesen, eds. *Handbook of Proteolytic Enzymes*. Elsevier, pp. 3581–3593.

Urban, S., 2006. Rhomboid proteins: conserved membrane proteases with divergent biological functions. *Genes & development*, 20(22), pp.3054–68.

Urban, S., 2010. Taking the plunge: integrating structural, enzymatic and computational insights into a unified model for membrane-immersed rhomboid proteolysis. *The Biochemical journal*, 425(3), pp.501–12.

Urban, S. & Baker, R., 2008. In vivo analysis reveals substrate-gating mutants of a rhomboid intramembrane protease display increased activity in living cells. *Biological chemistry*, 389(8), pp.1107–1115.

Urban, S. & Dickey, S.W., 2011. The rhomboid protease family: a decade of progress on function and mechanism. *Genome biology*, 12(10), p.231.

Urban, S. & Freeman, M., 2003. Substrate specificity of rhomboid intramembrane proteases is governed by helix-breaking residues in the substrate transmembrane domain. *Molecular cell*, 11(6), pp.1425–34.

Urban, S., Schlieper, D. & Freeman, M., 2002. Conservation of intramembrane proteolytic activity and substrate specificity in prokaryotic and eukaryotic rhomboids. *Current biology*, 12(17), pp.1507–12.

V

Van der Bliek, A.M. & Koehler, C.M., 2003. A Mitochondrial Rhomboid Protease. *Developmental Cell*, 4(6), pp.769–770.

Van Haastert, P.J.M., Keizer-Gunnink, I. & Kortholt, A., 2007. Essential role of PI3-kinase and phospholipase A2 in Dictyostelium discoideum chemotaxis. *The Journal of cell biology*, 177(5), pp.809–16.

Vasiev, B. & Weijer, C.J., 2003. Modelling of Dictyostelium discoideum slug migration. *Journal of Theoretical Biology*, 223(3), pp.347–359.

Vasquez, A. *et al.*, 2003. A role for the aryl hydrocarbon receptor in cardiac physiology and function as demonstrated by AhR knockout mice. *Cardiovascular toxicology*, 3(2), pp.153–63.

Veltman, D.M., Keizer-Gunnik, I. & Van Haastert, P.J.M., 2008. Four key signaling pathways mediating chemotaxis in Dictyostelium discoideum. *The Journal of cell biology*, 180(4), pp.747–53.

Vinothkumar, K.R. *et al.*, 2010. The structural basis for catalysis and substrate specificity of a rhomboid protease. *The EMBO journal*, 29(22), pp.3797–809.

W

Waheed, A. *et al.*, 2013. Naringenin inhibits the growth of Dictyostelium and MDCK-derived cysts in a polycystin-2 (TRPP2)-dependent manner. *British journal of pharmacology*, 2.

Walisser, J. a *et al.*, 2005. Aryl hydrocarbon receptor-dependent liver development and hepatotoxicity are mediated by different cell types. *Proceedings of the National Academy of Sciences of the United States of America*, 102(49), pp.17858–63.

Wanders, R.J.A. & Waterham, H.R., 2006. Biochemistry of mammalian peroxisomes revisited. *Annual review of biochemistry*, 75, pp.295–332.

Wang, Y. *et al.*, 2007. The role of L1 loop in the mechanism of rhomboid intramembrane protease GlpG. *Journal of molecular biology*, 374(4), pp.1104–13.

Wang, Y. & Ha, Y., 2007. Open-cap conformation of intramembrane protease GlpG. *Proceedings of the National Academy of Sciences of the United States of America*, 104(7), pp.2098–102.

Wang, Y., Zhang, Y. & Ha, Y., 2006. Crystal structure of a rhomboid family intramembrane protease. *Nature*, 444(7116), pp.179–80.

Wasserman, J.D., Urban, S. & Freeman, M., 2000. A family of rhomboid-like genes: Drosophila rhomboid-1 and roughoid/rhomboid-3 cooperate to activate EGF receptor signaling. *Genes & development*, 14(13), pp.1651–63.

Wienke, D.C. *et al.*, 1999. Disruption of a dynamin homologue affects endocytosis, organelle morphology, and cytokinesis in Dictyostelium discoideum. *Molecular biology of the cell*, 10(1), pp.225–43.

Williams, R. *et al.*, 2002. A common mechanism of action for three mood-stabilizing drugs. *Nature*, 417(6886), pp.292–5.

Y

Yang, B. & Larson, T.J., 1998. Multiple promoters are responsible for transcription of the glpEGR operon of Escherichia coli K-12. *Biochimica et biophysica acta*, 1396(1), pp.114–26.

Yumura, S., 1993. Reorganization of actin and myosin II in Dictyostelium amoeba during stimulation by cAMP. *Cell structure and function*, 18(6), pp.379–88.

Z

Zeng, G., Ye, S. & Larson, T.J., 1996. Repressor for the sn-glycerol 3-phosphate regulon of Escherichia coli K-12: primary structure and identification of the DNA-binding domain. *Journal of bacteriology*, 178(24), pp.7080–9.

Zhang, N., Long, Y. & Devreotes, P.N., 2001. Ggamma in dictyostelium: its role in localization of gbetagamma to the membrane is required for chemotaxis in shallow gradients. *Molecular biology of the cell*, 12(10), pp.3204–13.

Zhang, Y., 2008. I-TASSER server for protein 3D structure prediction. *BMC bioinformatics*, 9(1), p.40.

Zinda, M.J. & Singleton, C.K., 1998. The hybrid histidine kinase dhkB regulates spore germination in Dictyostelium discoideum. *Developmental biology*, 196(2), pp.171–83.

Appendix

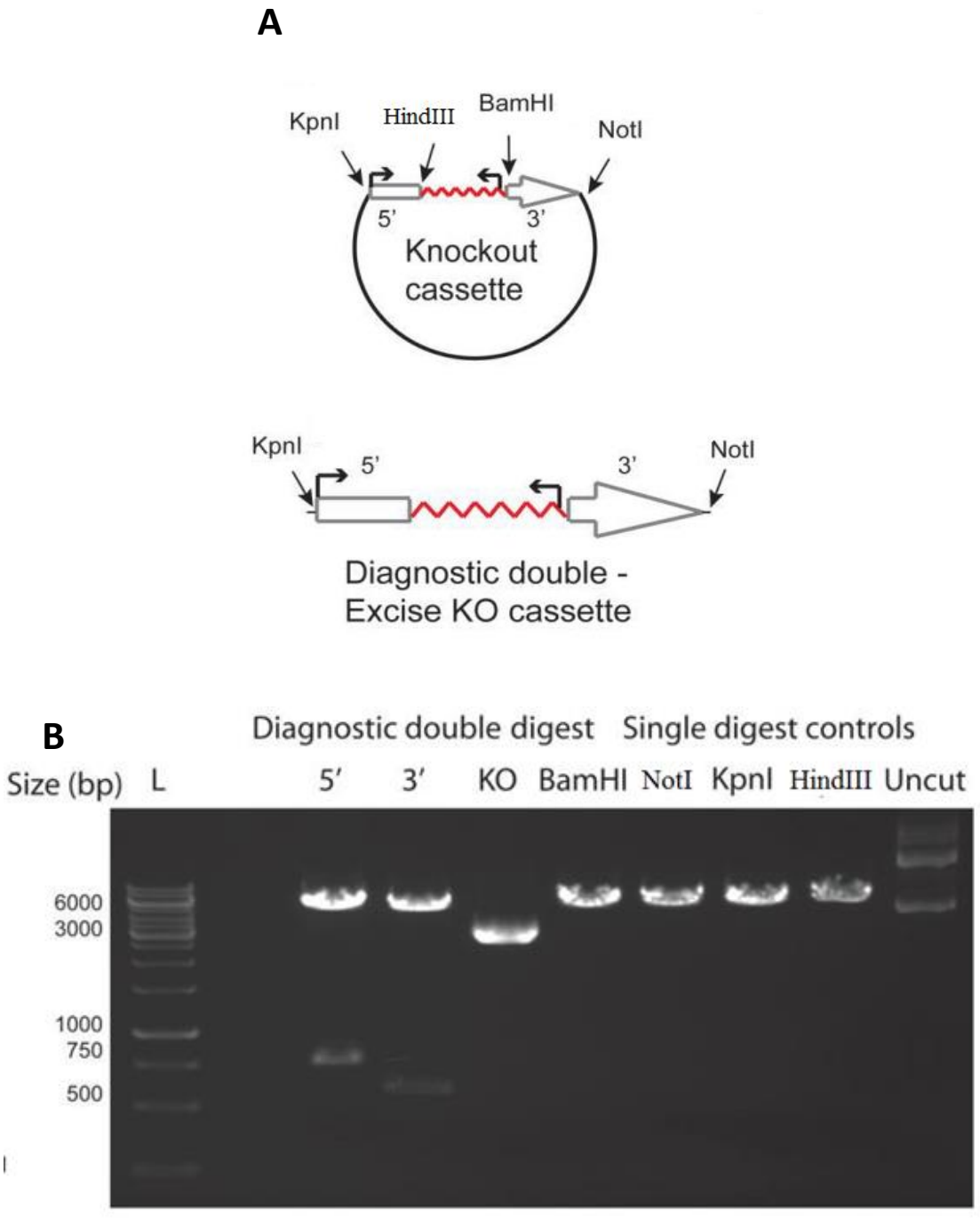

Figure 1 The *rhmC* 5' and 3' fragments were cloned into the pLPBLP vector backbone using specific restriction enzymes KpnI/HindIII and BamHI/NotI, respectively. The whole knockout cassette (KO) incorporating the blasticidin resistance cassette was excised with the KpnI and NotI (2806bp) restriction enzymes. The empty pLPBLP vector was used as a control to show undigested plasmid and the single digest for each different restriction enzyme to confirm the enzymes were cutting in a single place. The uncut lane indicates the undigested pLPBLP vector. L, a 1kb molecular ladder.

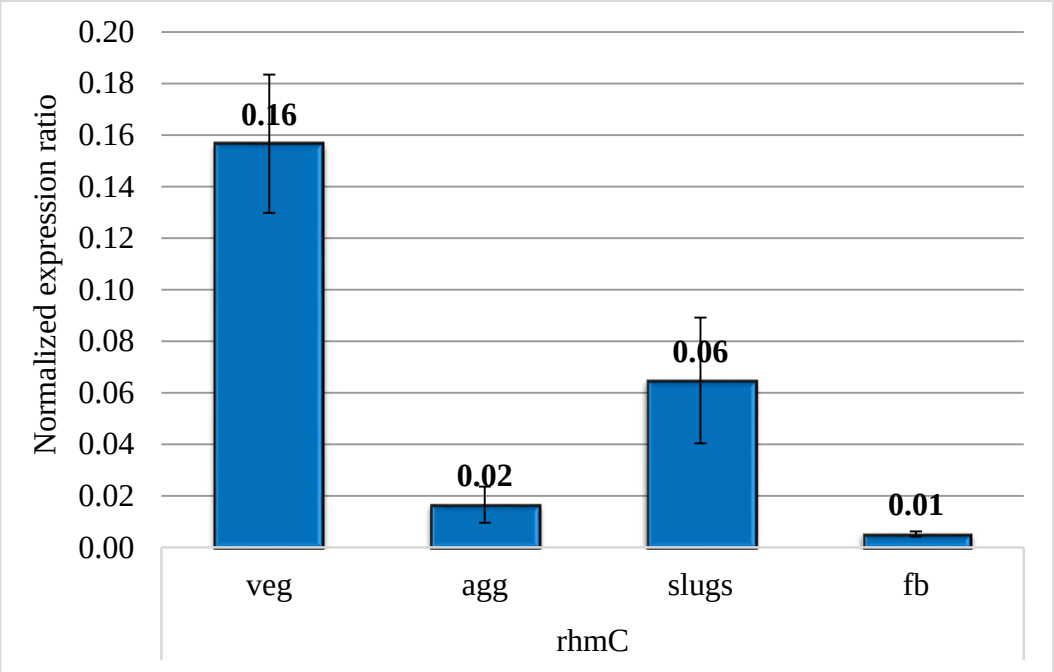

Figure 2 *Dictyostelium rhmC* gene expression during key life stages. RNA samples were prepared from *Dictyostelium* during selected life stages with derived cDNA, *rhmC* gene was amplified. The expression levels were quantified from four independent samples.

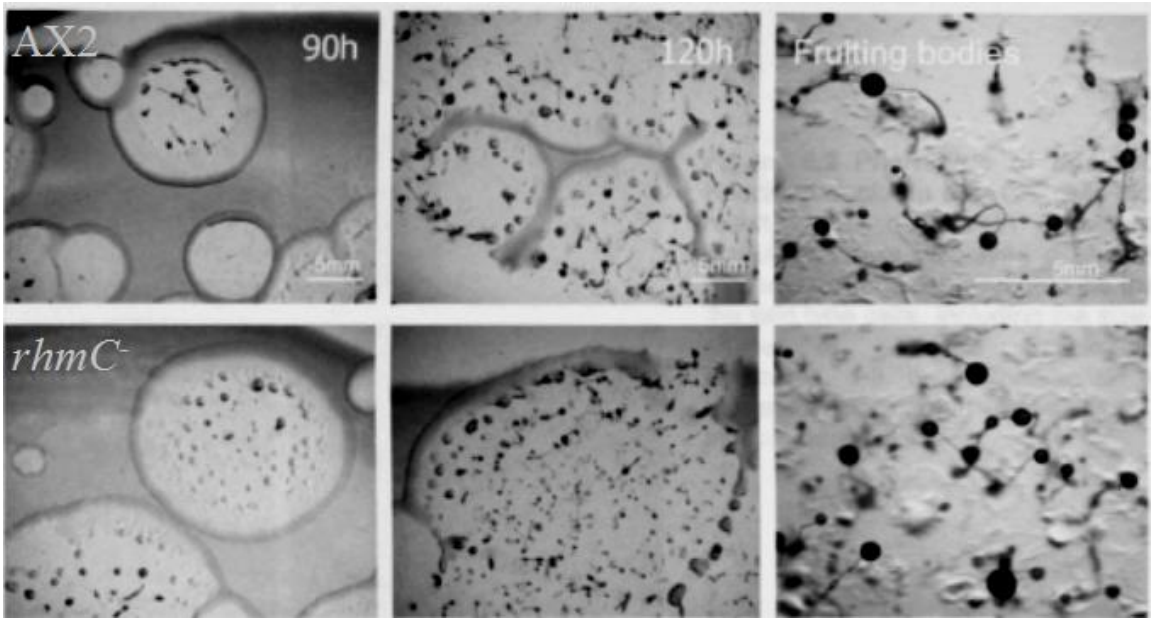

Figure 3 **Mutant Growth on SM Agar *rhmC* null cells had no significantly germination time than the wild type AX2. All experiments were repeated more than three times on independent days**

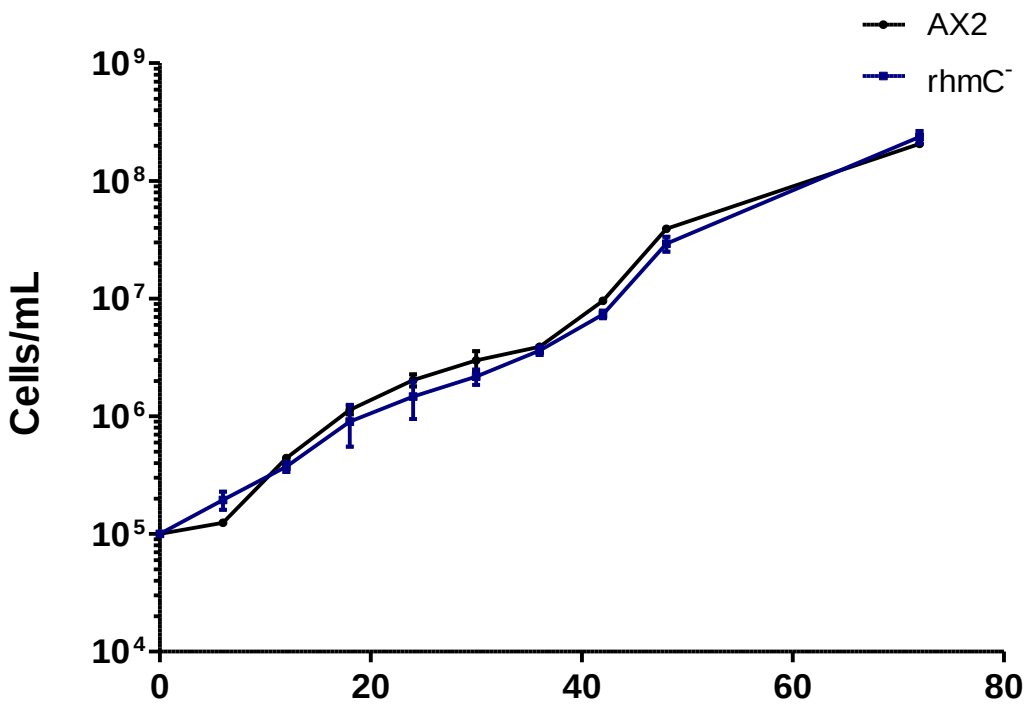

Figure 4 *rhmC* mutants grew at the similar speed to wild type cells, This data show the means and SEM of 3 independent experiments, performed on different days

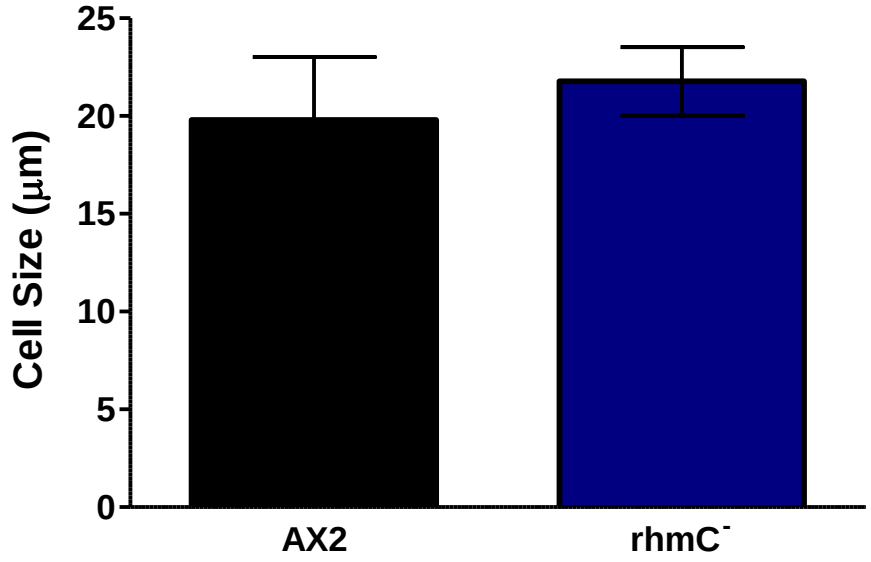

Figure 5 Cell size was calculated after 24 hours in HL5 at 22ºC shaking. The cells were measured using in-built tools in Nikon Eclipse 90i. The distribution of cell size one nucleus showed no significant difference between AX2 cells *rhmC* mutant cells. These experiments were repeated three times on different days

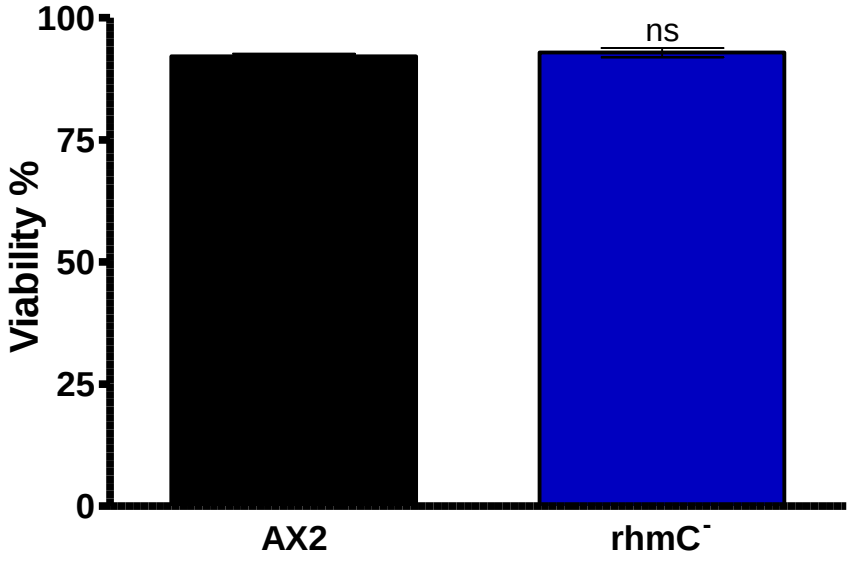

Figure 6 Cell viability was determined by trypan blue staining was calculated after 24 hours in HL5 at 22ºC shaking. There is no significant difference between AX2 cells and *rhmC* mutant cells. These experiments were repeated three times on different days

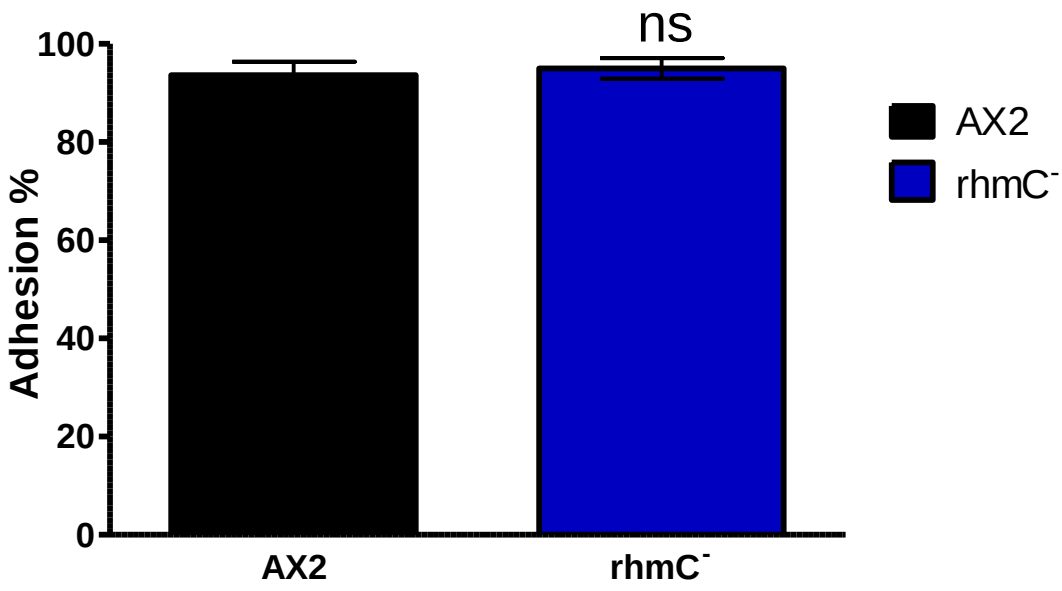

Figure 7 Cell adhesion was measured by proportion of cells remaining attached to glass surface after 2 washes. The cell to surface adhesion showed no significant difference between AX2 cells and *rhmC* mutant cells. These experiments were repeated three times on different days

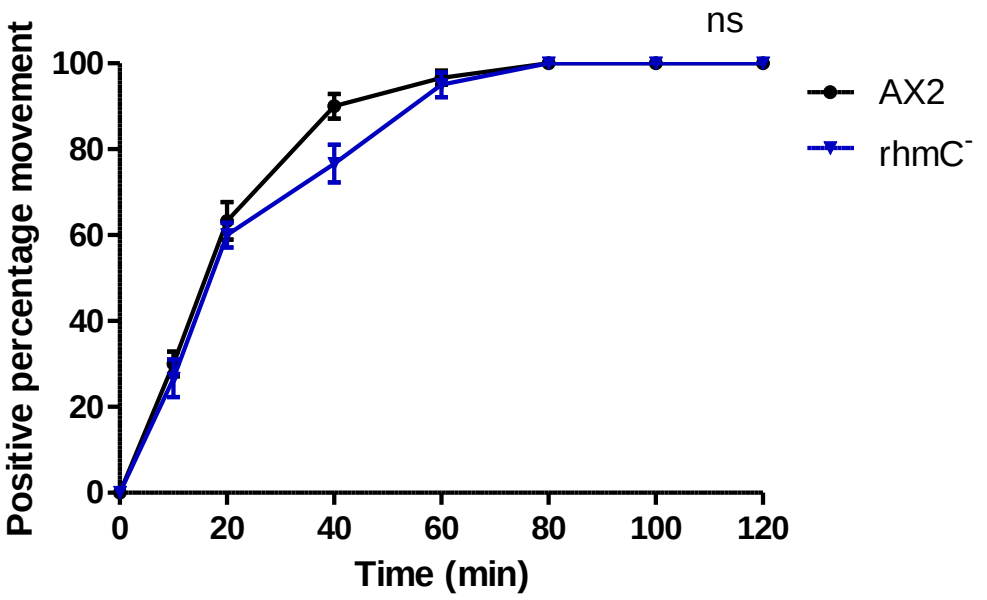

Figure 8 The One Drop Chemotaxis assay indicated that the *rhmC*- cells showed no difference in response to 10^{-8}M cAMP in comparison to that observed for AX2 cells (measured as the time it takes 50% of the population to respond). These data shown are the means ±SEM for results obtained in 3 independent experiments

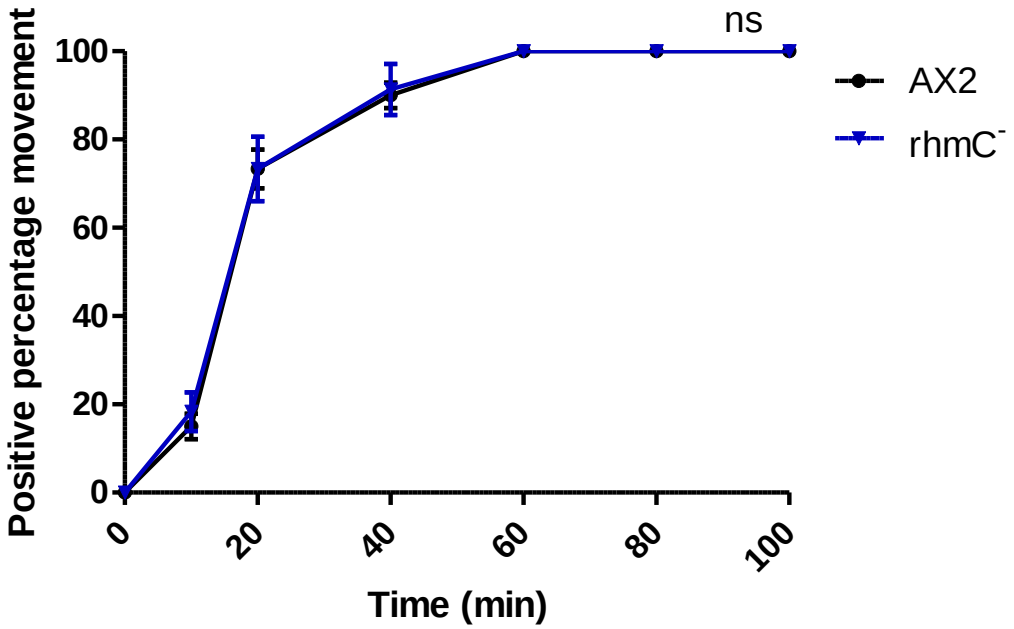

Figure 9 Folate One drop chemotaxis assay (10^{-5}M) *rhmC*- cells in folate one drop assay were similar in response compared to wild type cells. These data shown are the means and SEM for results obtained in 3 independent experiments.

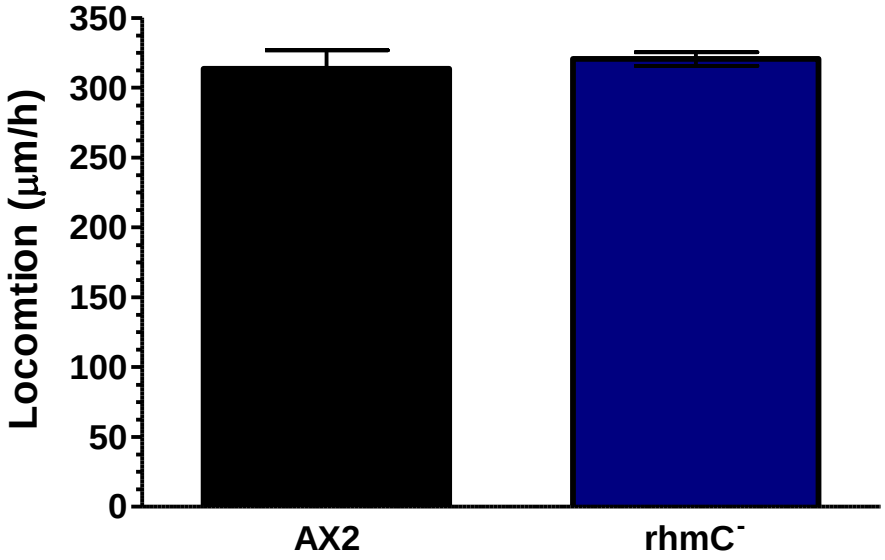

Figure 10 **Locomotion is the cell movement on agar slides without any chemoattractant or pulsing. *rhmC*- cells were similar in response compared to wild type cells. Data represents the mean of distance travelled by the cells in 2 hours ± SEM, number=5**

To make the *rhmD* knockout cassettes, 5' fragments were cloned into the pLPBLP vector at the KpnI/SalI, this was followed by the cloning of the 3' fragments at the BamHI/NotI restriction sites.

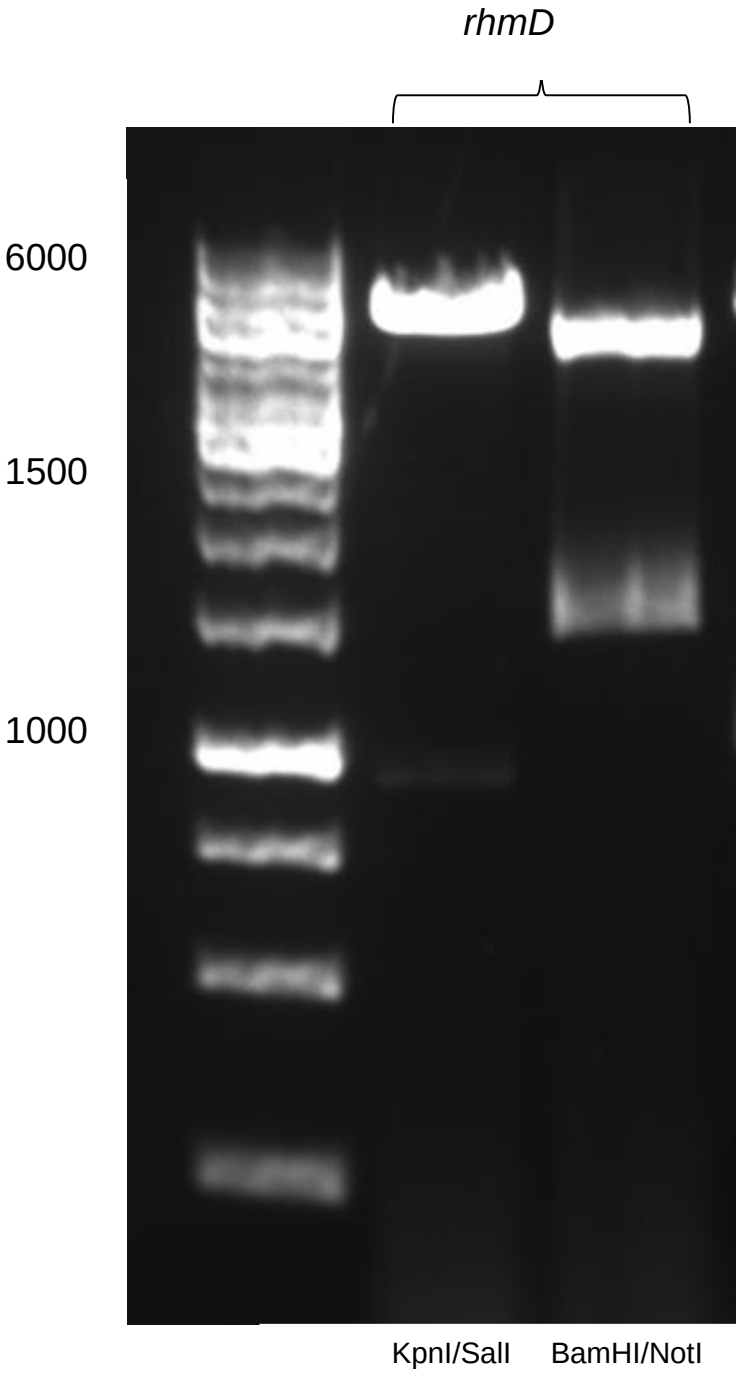

Figure 11 Diagnostic Plasmid digest for *rhmD*. The *rhmD*5' and 3' fragments were cloned into the pLPBLP vector backbone using specific restriction enzymes KpnI/HindIII and BamHI/NotI, respectively. The digests show the 5' and 3' inserts for both plasmids to show the cloning was successful.